UNIVERSITAT ROVIRA I VIRGILI
YTTERBIUM AND ERBIUM DOPEP RbTi1-xMxOPO4 (M=Nb or Ta) CRYSTALS. NEW LASER AND NONLINEAR BIFUNCTIONAL MATERIALS
Alexandra Peña Revellez
ISBN: 978-84-691-0370-8 /DL:T.2188-2007

Ytterbium and erbium doped $RbTi_{1-x}M_xOPO_4$ (M = Nb or Ta) crystals. New laser and nonlinear bifunctional materials.

Alexandra Peña Revellez

Bifunctional laser and nonlinear optical crystals, in which the laser effect and the nonlinear optical phenomena take place simultaneously inside the same crystal, are attractive materials for the development of new laser sources in the visible spectral range. These crystals have suitable sites for laser active ions, and when doped with Yb^{3+}, they can combine the infrared laser emission at 1 μm with the second harmonic generation properties of the host to generate visible laser radiation by self-frequency doubling.

This thesis deals with the growth and characterization of the nonlinear crystal, $RbTiOPO_4$, codoped with either niobium or tantalum and active ions such as ytterbium and erbium, to evaluate the potentiality of the obtained crystals as self-frequency doubling materials.

The linear and nonlinear properties of $RbTi_{1-x}Nb_xOPO_4$ and $RbTi_{1-x}Ta_xOPO_4$ indicate that they can be used as nonlinear hosts. Moreover as laser action at around 1 μm has been achieved in Yb^{3+} doped $RbTi_{1-x}Nb_xOPO_4$, self-frequency doubling could be possible, at least in this crystal.

Ytterbium and erbium doped $RbTi_{1-x}M_xOPO_4$ (M = Nb or Ta) crystals. New laser and nonlinear bifunctional materials. A. Peña Revellez

UNIVERSITAT ROVIRA I VIRGILI

Ytterbium and erbium doped $RbTi_{1-x}M_xOPO_4$ (M = Nb or Ta) crystals. New laser and nonlinear bifunctional materials.

Alexandra Peña Revellez

Supervised by:
Prof. Dr. Magdalena Aguiló
Prof. Dr. Francesc Díaz

Física i Cristal.lografia de Materials
FiCMA

Tarragona, 2007

UNIVERSITAT ROVIRA I VIRGILI
YTTERBIUM AND ERBIUM DOPEP RbTi1-xMxOPO4 (M=Nb or Ta) CRYSTALS. NEW LASER AND NONLINEAR BIFUNCTIONAL MATERIALS
Alexandra Peña Revellez
ISBN: 978-84-691-0370-8 /DL:T.2188-2007

Ytterbium and erbium doped $RbTi_{1-x}M_xOPO_4$ (M = Nb or Ta) crystals. New laser and nonlinear bifunctional materials.

Alexandra Peña Revellez

Doctoral thesis supervised by:

Prof. Magdalena Aguiló

Prof. Francesc Díaz

Física i Cristal·lografia de Materials (FiCMA)
Departament de Química Física i Inorgànica
Universitat Rovira i Virgili
Tarragona, 2007

UNIVERSITAT ROVIRA I VIRGILI
YTTERBIUM AND ERBIUM DOPEP RbTi1-xMxOPO4 (M=Nb or Ta) CRYSTALS. NEW LASER AND NONLINEAR BIFUNCTIONAL MATERIALS
Alexandra Peña Revellez
ISBN: 978-84-691-0370-8 /DL:T.2188-2007

Ytterbium and erbium doped $RbTi_{1-x}M_xOPO_4$ (M = Nb or Ta) crystals.
New laser and nonlinear bifunctional materials.

Alexandra Peña Revellez

Física i Cristal·lografia de Materials (FiCMA)
Departament de Química Física i Inorgànica
Universitat Rovira i Virgili
C/Marcel·lí Domingo, sn
43007 Tarragona
Spain

UNIVERSITAT ROVIRA I VIRGILI
YTTERBIUM AND ERBIUM DOPEP RbTi1-xMxOPO4 (M=Nb or Ta) CRYSTALS. NEW LASER AND NONLINEAR BIFUNCTIONAL MATERIALS
Alexandra Peña Revellez
ISBN: 978-84-691-0370-8 /DL:T.2188-2007

Ytterbium and erbium doped $RbTi_{1-x}M_xOPO_4$ (M = Nb or Ta) crystals. New laser and nonlinear bifunctional materials.

Alexandra Peña Revellez

Abstract

Bifunctional laser and nonlinear optical crystals, in which the laser effect and the nonlinear optical phenomena take place simultaneously inside the same crystal, are attractive materials for the development of new laser sources in the visible spectral range. These crystals have suitable sites for laser active ions, and when doped with Yb^{3+}, they can combine the infrared laser emission at 1 μm with the second harmonic generation properties of the host to generate visible laser radiation by self-frequency doubling.

The first aim of this doctoral thesis was to enhance the quality and size of Ytterbium doped $RbTi_{1-x}Nb_xOPO_4$ crystals obtained by the Top Seeded Solution Growth-Slow Cooling technique in order to evaluate its potential as a self-frequency doubling laser crystal The next goal was to find a codopand, with the same characteristics of niobium, which increases the ytterbium concentration in $RbTiOPO_4$ without reducing the nonlinear optical response of the host. A third study investigated the possibility of enhancing the erbium fluorescence at around 1.5 μm by doping $RbTi_{1-x}Nb_xOPO_4$ with the Er^{3+}/Yb^{3+} pair, with Yb^{3+} acting as a sensitizing ion of Er^{3+}.

The growth process of $Yb:RbTi_{1-x}Nb_xOPO_4$, $Yb:RbTi_{1-x}Ta_xOPO_4$ and $Er:Yb:RbTi_{1-x}Nb_xOPO_4$ is described, and in the obtained crystals, the linear and nonlinear optical properties as well as the spectroscopic characterization of the dopand ions have been performed. The results show that $RbTi_{1-x}Nb_xOPO_4$ and $RbTi_{1-x}Ta_xOPO_4$ could be used as a nonlinear host, and with the obtained doping level, they could also be used as laser crystals. Self-frequency doubling is therefore possible, at least in $Yb:RbTi_{1-x}Nb_xOPO_4$, were tunable efficient laser generation has been achieved.

Keywords: Top Seeded Solution Growth-Slow Cooling, $RbTiOPO_4$, nonlinear optics, second harmonic generation, laser crystals.

UNIVERSITAT ROVIRA I VIRGILI
YTTERBIUM AND ERBIUM DOPEP RbTi1-xMxOPO4 (M=Nb or Ta) CRYSTALS. NEW LASER AND NONLINEAR BIFUNCTIONAL MATERIALS
Alexandra Peña Revellez
ISBN: 978-84-691-0370-8 /DL:T.2188-2007

"The important thing is not to stop questioning. Curiosity has its own reason for existing. One cannot help but be in awe when he contemplates the mysteries of eternity, of life, of the marvelous structure of reality. It is enough if one tries merely to comprehend a little of this mystery every day. Never lose a holy curiosity."

Albert Einstein

UNIVERSITAT ROVIRA I VIRGILI
YTTERBIUM AND ERBIUM DOPEP RbTi1-xMxOPO4 (M=Nb or Ta) CRYSTALS. NEW LASER AND NONLINEAR BIFUNCTIONAL MATERIALS
Alexandra Peña Revellez
ISBN: 978-84-691-0370-8 /DL:T.2188-2007

Preface

The Ph.D. study contained in this thesis has been carried out at the group of *Física i Cristal·lografia de Materials* (*FiCMA*) in the *Departament de Química Física i Inorgànica* of the *Universitat Rovira i Virgili* in Tarragona, and was supervised by the Professors Magdalena Aguiló Díaz and Francesc Díaz González.

Within the development of this thesis, we have collaborated actively with the following groups: *Laboratoire de Spectrométrie Physique* leaded by Prof. Benoît Boulanger at the *Université Joseph Fourier* (Grenoble, France); the *Max-born Institute for Non-linear Optics and Ultrafast Spectroscopy* coordinated by Dr. Valentin Petrov at (Berlin, Germany) and *Unidad de materiales y dispositivos optoelectrónicos* leaded by Dr. Juan Martínez Pastor at the *Institut de Ciència dels Materials of the Universitat de València* (València, Spain).

This project was possible thanks to financial support from *Departament d'Universitats, Recerca i Societat de la Informació de la Generalitat de Catalunya* under projects 2005SGR-00658 and 2001SGR-317 and from the *Ministerio de Educación y Ciencia* (*MEC*) of the Spanish Government under projects MAT2005-06354-C03-02, MAT2004-20471-E, MAT2002-04603-C05-03 and CIT-020400-2005-14. I would like to thank to the *Ministerio de Educación y Ciencia* (*MEC*) of the Spanish Government for the personal funding BES-2003-1694.

UNIVERSITAT ROVIRA I VIRGILI
YTTERBIUM AND ERBIUM DOPEP RbTi1-xMxOPO4 (M=Nb or Ta) CRYSTALS. NEW LASER AND NONLINEAR BIFUNCTIONAL MATERIALS
Alexandra Peña Revellez
ISBN: 978-84-691-0370-8 /DL:T.2188-2007

To Òscar, my parents, my sister and my nephew,
with great affection.

UNIVERSITAT ROVIRA I VIRGILI
YTTERBIUM AND ERBIUM DOPEP RbTi1-xMxOPO4 (M=Nb or Ta) CRYSTALS. NEW LASER AND NONLINEAR BIFUNCTIONAL MATERIALS
Alexandra Peña Revellez
ISBN: 978-84-691-0370-8 /DL:T.2188-2007

Acknowledgements

First, I would like to thank my advisors, Professor Magdalena Aguiló and Professor Francesc Díaz for giving me the opportunity to perform my Ph.D. in the FiCMA group, for sharing their knowledge and their never-ending enthusiasm with me, and for advising and encouraging me over the years that I've been here. I would especially like to thank Magdalena Aguiló for introducing me to the basis of crystallography during the last University year in such an enjoyable way, and for giving me a deeper knowledge of it during my Ph.D. Thanks to Francesc Díaz for helping me to see that things were sometimes easier than I thought, and for his many constructive scientific arguments which helped to solve everyday problems in the laboratory.

I also want to thank the other members of the FiCMA group for their collaboration during my stay in this research group. I would like to thank Dra. Mª Rosa Solé for introducing me to the amusing world of crystal growth and for showing me how to perform a good crystal growth process, Dr. Jaume Massons for helping me each time I needed him in the optical laboratory, and Dra. Josefina Gavaldà for performing the ionic conductivity measurements of this thesis and for discussing the results with me.

This thesis would also not have been possible without the collaboration of the technicians of this group. I do not have words to thank Agustí Montero for all his help in the laboratory, for showing me how things work, for making me smile even on my worst days and for giving me a present that wakes me up and makes me laugh everyday. I would like to thank Nicolette Bakker for obtaining polished and crack free samples from my crystals without getting wound up and for cheering us up almost everyday, and Pere Fibla for trying to help me each time I've asked him.

Everyday life at FiCMA has been easy with the help and the company of all these workmates, the post and pre-doctoral members of FiCMA, those I've shared office and laboratories with and great times in and out of the work place. Thanks to Dr. Joan J. Carvajal for advising me during the writing of my *DEA*, for introducing me to the KTP family and for being there each time I needed him to solve or understand the obtained results. Thanks to Dra. Cinta

UNIVERSITAT ROVIRA I VIRGILI
YTTERBIUM AND ERBIUM DOPEP RbTi1-xMxOPO4 (M=Nb or Ta) CRYSTALS. NEW LASER AND NONLINEAR BIFUNCTIONAL MATERIALS
Alexandra Peña Revellez
ISBN: 978-84-691-0370-8 /DL:T.2188-2007

Pujol for discussing with me each of the spectroscopic results obtained, for sharing long afternoons with me and for taking me home almost every day, and to Dr. Xavier Mateos for obtaining the laser operation described in this thesis and for revising the last chapter of the thesis. I would also like to thank Dra. Isabel Parreu, who has been almost all the time *by my side*, for listening to me, for her enthusiasm and for being who she is, Montse Galceran for trying to calm me and help me each time I needed it and Western Bolaños for making me laugh and *enjoy* the Catalan language. Thanks to Ana Aznar for always being in a good mood and to Arantxa Vilalta for coming to visit us and bring us to the real world.

I would also like to deeply acknowledge Professor Benoît Boulanger and Associated Professor Patricia Segonds for receiving me at the Laboratoire de Spectrométrie Physique in the Joseph Fourier Université in Grenoble, and for sharing their knowledge on nonlinear optics with me. I thank Patricia Segonds for performing with me the nonlinear characterization included in this thesis as well as for explaining the obtained results to me and discussing them with me, and also for revising the chapter about optical characterization included in this thesis. I would also thank Dr. Bertran Ménaert for all the time that he spent with me at the Laboratoire de Cristallographie (CNRS) in Grenoble, and everybody I met there and at Laboratoire de Spectrométrie, Alain Ibanez, Julien Zaccaro, Jérôme Debray, Yannick Petit, Fabien Gravier, etc., who made my stay there enjoyable. Moreover, I would like to thank Dr. Valentin Petrov for his help with the laser operation measurement at the Max-Born Institute of Nonlinear Optics and Ultrafast Spectroscopy in Berlin.

I would also like to say few words of gratitude to all my friends from Vilafranca, with whom I have had a great time, especially to Laura and Judith, for being there each time I needed them. Also, I thank my closest friends from the University, Lídia, Albert, Xavi, Sílvia and Edu, with whom I've shared the best time in Tarragona, and to Damià and Gemma for coming almost each week to see me and share funny dinners with me.

I want to thank my parents, Fidel Peña and Conchi Revellez, for encouraging me to keep on doing what I was interested in, and my sister and my nephew for sharing all the weekends in my birthplace with me, and for

UNIVERSITAT ROVIRA I VIRGILI
YTTERBIUM AND ERBIUM DOPEP RbTi1-xMxOPO4 (M=Nb or Ta) CRYSTALS. NEW LASER AND NONLINEAR BIFUNCTIONAL MATERIALS
Alexandra Peña Revellez
ISBN: 978-84-691-0370-8 /DL:T.2188-2007

being who they are. Finally, I thank my partner Òscar Silvestre for being my best friend during all these years, for giving me his support in everything I've done. I want to thank him and Frida for sharing their life with me, for relaxing me and for waiting for me at home.

UNIVERSITAT ROVIRA I VIRGILI
YTTERBIUM AND ERBIUM DOPEP RbTi1-xMxOPO4 (M=Nb or Ta) CRYSTALS. NEW LASER AND NONLINEAR BIFUNCTIONAL MATERIALS
Alexandra Peña Revellez
ISBN: 978-84-691-0370-8 /DL:T.2188-2007

UNIVERSITAT ROVIRA I VIRGILI
YTTERBIUM AND ERBIUM DOPEP RbTi1-xMxOPO4 (M=Nb or Ta) CRYSTALS. NEW LASER AND NONLINEAR BIFUNCTIONAL MATERIALS
Alexandra Peña Revellez
ISBN: 978-84-691-0370-8 /DL:T.2188-2007

List of publications

This doctoral thesis is partially based on the work contained in the following papers, referred to by roman numerals in the text:

***Paper I*:** A. Peña, J. J. Carvajal, J. Massons, Jna. Gavaldà, F. Díaz and M. Aguiló, *"Yb:Ta:$RbTiOPO_4$, a new strategy to further increase the lanthanide concentration in crystals of the $KTiOPO_4$"*, *Chemistry of Materials* **19**, *4069* (2007)

***Paper II*:** A. Peña, J. J. Carvajal, M. C. Pujol, X. Mateos, V. Petrov, P. Segonds, B. Boulanger, F. Díaz and M. Aguiló, *"Yb^{3+} spectroscopy in (Nb or Ta):$RbTiOPO_4$ single crystals for laser applications"*, *submitted to Optics Express*

***Paper III*:** X. Mateos, V. Petrov, A. Peña, J. J. Carvajal, M. Aguiló, F. Díaz, P. Segonds and B. Boulanger, *"Laser operation of Yb^{3+} in the acentric $RbTiOPO_4$ codoped with Nb^{5+}"*, *Optics Letters* **32**, *1929* (2007)

***Paper IV*:** J. Canet-Ferrer, L. Martínez-Carrón, J. Martínez-Pastor, J. L. Valdés, A. Peña, J. J. Carvajal and F. Díaz, *"Scanning probe microscopies applied to the study of the domain wall in a ferroelectric crystal"*, *Journal of Microscopy* **226**, *133* (2007)

***Paper V*:** J. J. Carvajal, P. Segonds, A. Peña, J. Zaccaro, B. Boulanger, F. Díaz and M. Aguiló, *"Structural and optical properties of $RbTiOPO_4$:Nb"*, *Journal of Physics Condensed Matter* **19**, *16214* (2007)

UNIVERSITAT ROVIRA I VIRGILI
YTTERBIUM AND ERBIUM DOPEP RbTi1-xMxOPO4 (M=Nb or Ta) CRYSTALS. NEW LASER AND NONLINEAR BIFUNCTIONAL MATERIALS
Alexandra Peña Revellez
ISBN: 978-84-691-0370-8 /DL:T.2188-2007

Other publications by the author not included in this thesis.

Paper AI: A. Peña, S. Di Finizio, T. Trifonov, J. J. Carvajal, M. Aguiló, J. Pallarès, A. Rodríguez, R. Alcubilla, L. F. Marsal, F. Díaz and J. Martorell, *"A two-dimensional $KTiOPO_4$ photonic crystal grown using a macroporous silicon template"*, *Advanced Materials* **18**, *2220* (2006)

Paper AII: A. Peña, R. Solé, Jna. Gavaldà, J. Massons, F. Díaz and M. Aguiló, *"Primary crystallization region of $NaAl(MoO_4)_2$, Cr^{3+} doping, crystal growth, and characterization"*, *Chemistry of Materials* **18**, *442* (2006)

UNIVERSITAT ROVIRA I VIRGILI
YTTERBIUM AND ERBIUM DOPEP RbTi1-xMxOPO4 (M=Nb or Ta) CRYSTALS. NEW LASER AND NONLINEAR BIFUNCTIONAL MATERIALS
Alexandra Peña Revellez
ISBN: 978-84-691-0370-8 /DL:T.2188-2007

Table of contents

UNIVERSITAT ROVIRA I VIRGILI
YTTERBIUM AND ERBIUM DOPEP RbTi1-xMxOPO4 (M=Nb or Ta) CRYSTALS. NEW LASER AND NONLINEAR BIFUNCTIONAL MATERIALS
Alexandra Peña Revellez
ISBN: 978-84-691-0370-8 /DL:T.2188-2007

UNIVERSITAT ROVIRA I VIRGILI
YTTERBIUM AND ERBIUM DOPEP RbTi1-xMxOPO4 (M=Nb or Ta) CRYSTALS. NEW LASER AND NONLINEAR BIFUNCTIONAL MATERIALS
Alexandra Peña Revellez
ISBN: 978-84-691-0370-8 /DL:T.2188-2007

UNIVERSITAT ROVIRA I VIRGILI
YTTERBIUM AND ERBIUM DOPEP RbTi1-xMxOPO4 (M=Nb or Ta) CRYSTALS. NEW LASER AND NONLINEAR BIFUNCTIONAL MATERIALS
Alexandra Peña Revellez
ISBN: 978-84-691-0370-8 /DL:T.2188-2007

UNIVERSITAT ROVIRA I VIRGILI
YTTERBIUM AND ERBIUM DOPEP RbTi1-xMxOPO4 (M=Nb or Ta) CRYSTALS. NEW LASER AND NONLINEAR BIFUNCTIONAL MATERIALS
Alexandra Peña Revellez
ISBN: 978-84-691-0370-8 /DL:T.2188-2007

Chapter 1

Introduction

In 1958 the possibility of generating and amplifying electromagnetic oscillations over the optical and near-optical range by stimulated emission was analyzed by Schalow and Townes.[1] Almost two years later, in 1960, this goal was achieved by Maiman,[2] who published the first paper about a laser action in Cr^{3+}:Al_2O_3, emitting in the red region of the visible spectrum. The high values of energy achieved in a coherent radiation beam allowed the experimental demonstration of the nonlinear phenomena in electromagnetic propagation inside a material, as Franken *et al.*[3] reported one year later with the first demonstration of laser action in ruby. Since nonlinear effects need powerful light sources, the development in the last years of high-power semiconductor diode lasers opened the possibility of diode-pumping nonlinear new materials to generate nonlinear optical processes and convert, for instance, IR wavelengths into the visible (blue-green) regions of the spectrum.

UNIVERSITAT ROVIRA I VIRGILI
YTTERBIUM AND ERBIUM DOPEP RbTi1-xMxOPO4 (M=Nb or Ta) CRYSTALS. NEW LASER AND NONLINEAR BIFUNCTIONAL MATERIALS
Alexandra Peña Revellez
ISBN: 978-84-691-0370-8 /DL:T.2188-2007

1.1 Nonlinear crystals

Nonlinear crystals can show different optical nonlinearities, mainly χ^2 or χ^3, resulting from a nonlinear polarization, which is achieved by applying high amplitude fields $(P = P_0 + \varepsilon_0(\chi^1 \cdot E + \chi^2 \cdot E^2 + ... + \chi^n \cdot E^n + ...) = P^L + P^{NL})$. χ^2 nonlinear crystal materials, non-centrosymmetric materials, are mainly used in frequency doublers and optical parametric oscillators, and χ^3 nonlinearities lead to processes such as the Kerr effect and Raman scattering.

To study nonlinear crystals and their suitability for use in nonlinear optical devices, one should determine basic nonlinear parameters such as phase-matching directions and the magnitude of the effective nonlinear coefficients (d_{eff}). The first stages of study, when sample sizes are not large enough to perform direct measurement of phase-matching, should be perform with powdered samples in the method described by Kurtz and Perry,[4] which detects the second harmonic generation efficiency. At further steps, when samples reaches millimeter sizes, the phase matching directions can be determined, by using a crystal with an ellipsoidal[5] or spherical[6] shape. The phase-matching relations can also be calculated using the refractive indices, measured with an accuracy of 10^{-4} in the whole transparency window, determined by the minimum deviation angle using prisms.[7] Also the coefficients determination of the second-order electric susceptibility tensor d^2, which can be measured by the Marker-fringe technique[8] or with phase-matched interactions,[9] are very important for the description of a new nonlinear crystal. For this purpose, the minimum sample size required is about two or three millimeters.

Nonlinear crystals have several applications in nonlinear optical devices, but none of these crystals can be used in all the different potential applications.

For example, a huge number of inorganic crystals have been used to achieve second harmonic generation (SHG), where two identical photons from a single pump beam adds their frequency and leads to a single photon with twice the frequency, of Neodymium solid state lasers; KH_2PO_4 (KDP), $NH_4H_2PO_4$ (ADP), CsH_2AsO_4 (CDA), β-BaB_2O_4 (BBO), LiB_3O_5 (LBO), $KTiOPO_4$ (KTP), $KNbO_3$,

5% MgO:$LiNbO_3$ (Mg:LNB), $LiIO_3$, and some of their characteristics are listed in Table 1.1. $KTiOPO_4$ (KTP), among all these inorganic crystals, is of special interest because it possesses very large nonlinearity, large angular and temperature bandwidths for SHG of 1.06 μm. Moreover, some of the crystals listed above, such as Mg:LNB or KTP, have been used inside an infrared laser cavity, intracavity SHG (ICSHG), to increase the efficiency of conversion to the second harmonic. The first demonstration for the generation of green light by intracavity frequency doubling of neodymium lasers was achieved by Smith *et al.*[10] in 1965 with $LiNbO_3$ (LNB), but in the mid- 1980s the interest in this field grew due to the development of high-power diode lasers which pumped efficiently solid-state lasers and demonstrated that milliwatt beams of green light could be generated.[11] Also, blue light generation has been achieved by using ICSHG of a 946 nm laser.[12] Nonlinear crystals have also been used for frequency doubling of non Neodymium solid state lasers, to double ruby (Cr:Al_2O_3) laser radiation (λ = 694.3 nm), KDP, DKDP, ADP, RDA, RDP, $LiIO_3$ and KB_5 ($KB_5O_8 \cdot 4H_2O$) have been used.[13]

For example, it is also possible to obtain radiation with a tuneable frequency from nonlinear crystals by optical parametric oscillation (OPO). Parametric oscillation generates two tuneable output beams from a single input beam. The generated output beams are of lower frequency than the input one. The first OPO was demonstrated in 1965 and operated around 1 μm.[14] Nowadays, the available tunability obtained from optical parametric oscillation, operating in either the continuous-wave or pulsed regimes, ranges across the EM spectrum from the UV (330 nm) to middle IR (16.4 μm). In the spectral range between 0.3-5 μm, the inorganic crystals used for OPO, most of them pumped by a Nd:YAG or Nd^{3+} phosphate glass lasers, have been KDP, DKDP, ADP, CDA, $LiIO_3$, BBO, BNN, α-HIO_3, $KNbO_3$. Beyond 5 μm, in the mid IR region, crystals such as Ag_3AsS_3, $AgGaS_2$, $AgGaSe_2$, $ZnGeP_2$ and CdSe have been used.[13]

The list of applications for nonlinear crystals mentioned above is not exhaustive, but does represent some of the most relevant examples.

UNIVERSITAT ROVIRA I VIRGILI
YTTERBIUM AND ERBIUM DOPEP RbTi1-xMxOPO4 (M=Nb or Ta) CRYSTALS. NEW LASER AND NONLINEAR BIFUNCTIONAL MATERIALS
Alexandra Peña Revellez
ISBN: 978-84-691-0370-8 /DL:T.2188-2007

Table 1.1. *Second Harmonic Generation of Neodymium Lasers Radiation in Inorganic Crystals. Data found in International tables for crystallography.*[15]

	KDP	**ADP**	**CDA**	**BBO**	**Mg:LNB**	**$LiIO_3$**	**LBO**	**KTP**	**$KNbO_3$**
Point group	$\bar{4}\,2m$	$\bar{4}\,2m$	$\bar{4}\,2m$	$3m$	$3m$	$6mm$	$mm2$	$mm2$	$mm2$
Transparency (μm)	0.18-1.8	0.184-1.5	0.27-1.66	0.198-2.6	0.35-5	0.31-5 || ***c*** 0.34-4 $\perp$ ***c***	0.16-2.3	0.35-4.5	0.4-5.5
λ_{NCPM} (μm); **Type I**, **Type II**	0.519, -	0.524, -	1.045, -	0.409, -		0.756,-	0.554, - [3] 1.212, - [1] -, 1.19 [2]	-, 0.990 [2] -, 1.081 [1]	0.860, - [1] 0.982, - [2]
T_{PM} (K)			385		380		421		456
PM Type; θ (°),φ (°)	II 54, -	II 62, -	I 90, -	I 23, -	I 90, -	I 30, -	I [1] 90, 0	II [1,2] 90, 23	I [2] 90, 90
d_{eff} (pm V^{-1})	0.35	0.39	0.30	1.9	4.7	1.8	0.85	2.4	-13
Angular bandwidth (mrad cm)	2.3	2.2	51	0.53	33	0.34	72	9	13
Walk-off angles; ρ^{ω} (°),$\rho^{2\omega}$ (°)	1.3, 1.4	1.2, 1.5	0,0	0, 3.2	0,0	0, 4.3	0, 0	0.20, 0.27	0, 0
Thermal bandwidth (K cm)	12	2.1	3.3	51	0.75	23	3.9	17	0.3
Spectral bandwidth (nm cm)	5.6	26	2.5	2	0.31	0.82	3.6	0.46	0.12
Surface optical damage threshold (GW cm^{-2})	5 (1 ns) >8 (0.6 ns at 0.53 μm)	6 (15 ns) >8 (0.6 ns at 0.53 μm)	0.25 (12 ns)	13.5 (1 ns) 23 (14 ns) 32 (8 ns at 0.53 μm)		2 (1 ns) 1 (0.1 ns at 0.53 μm)	25 (0.1 ns) 14 (12 ns at 0.78 μm)	9-20 (1 ns) >2 (10 ns at 0.5 μm)	>1 (10 ns)

[1] along ***a***, [2] along ***b***, [3] along ***c***

UNIVERSITAT ROVIRA I VIRGILI
YTTERBIUM AND ERBIUM DOPEP RbTi1-xMxOPO4 (M=Nb or Ta) CRYSTALS. NEW LASER AND NONLINEAR BIFUNCTIONAL MATERIALS
Alexandra Peña Revellez
ISBN: 978-84-691-0370-8 /DL:T.2188-2007

1.2 Self frequency doubling crystals

Nowadays, there is a great interest in obtaining compact solid state visible laser sources that could be used for applications such as high density optical data storage, underwater communications, colour printing and medicine. Achieving the specific wavelength for each desired application is of a great importance in the study of nonlinear optical materials that can incorporate active ions and that can be pumped by diode lasers. In these kinds of bi-functional materials, the nonlinear optical phenomena and the laser effect instantaneously take place inside the crystal. The nonlinear optical process originates in non–centrosymmetric crystals from the second order nonlinear polarization (χ^2). The best known device illustrating this phenomenon is the self-frequency doubling (SFD) laser for visible light generation.

The preparation of materials with good nonlinear optical properties and sufficient concentrations of lanthanide ions, such as Nd^{3+} and Yb^{3+} which have the laser emissions at around 1 μm, has not been an easy task. Incorporating lanthanide ions as dopands in nonlinear optical materials causes difficult crystal growth and degrades the materials optical qualities.[12] Proper selection of materials demonstrates some important features that should be accomplished in materials to be used in self frequency solid state laser devices. These materials should show high thermal conductivity, high quantum efficiency, small Stoke's shift, should be efficient (having a great capacity for accepting the active ions excitation by absorbing at the pump wavelength with a high gain cross-section) and phase-matchable without significant losses.[16]

Nd^{3+} as well as Yb^{3+} have been the two active ions commonly used in self-frequency doubling lasers, as well as in solid state lasers operating at 1 μm. Initially, Nd^{3+} was the most used, but nowadays there is increasing interest in replacing Nd^{3+} with Yb^{3+}, because Yb^{3+} solid state lasers show some advantages relative to Nd^{3+}. These advantages, such as no excited state absorption, no concentration quenching and no up-conversion, are due to its simple level scheme which is constituted by the ground level ($^2F_{7/2}$) and the excited one ($^2F_{5/2}$). Moreover another great advantage of Yb^{3+} versus Nd^{3+} is that the first one has no absorption in the green wavelengths, which is a particularly

UNIVERSITAT ROVIRA I VIRGILI
YTTERBIUM AND ERBIUM DOPEP RbTi1-xMxOPO4 (M=Nb or Ta) CRYSTALS. NEW LASER AND NONLINEAR BIFUNCTIONAL MATERIALS
Alexandra Peña Revellez
ISBN: 978-84-691-0370-8 /DL:T.2188-2007

attractive characteristic for a self-frequency doubling laser (SFD). But the quasi-three-level laser operation is a significant disadvantage for Yb^{3+} solid state lasers because a high pump intensity is needed. Yb^{3+} solid state lasers have sparked intense interest since the development of high power InGaAs diode lasers, because the position of the Yb^{3+} absorption lines are well matched for the InGaAs pumping (near 980 nm).

A continuous wave self-frequency doubling (SFD) laser action in the green was first demonstrated from a neodymium doped Lithium Niobate (Nd:LNB) crystal in 1986.[17] However, prior to this SFD in a continuous mode, there were two demonstrations of SFD in a pulsed mode which were also in LNB, in 1969 SFD in Tm:LNB was reported and then in 1979 using Nd:LNB.[18,19] Since these first achievements, several new nonlinear laser crystals have been tested for SFD, most of them borate crystals and LNB doped with Nd^{3+} and Yb^{3+}. In Nd^{3+} doped $YAl_3(BO_3)_4$ (YAB), $GdAl_3(BO_3)_4$ (GAB), $GdCa_4O(BO_3)_3$ (GdCOB), $YCa_4O(BO_3)_3$ (YCOB) and $LiNbO_3$ (LNB) efficient green and red laser radiation by SFD has been obtained from the $^4F_{3/2} \rightarrow {}^4I_{11/2}$ and $^4F_{3/2} \rightarrow {}^4I_{13/2}$ laser channels respectively. These results have been obtained using conventional birefringence phase matching (BPM) in all the crystals tested. With regards to doping materials with Yb^{3+}, generate green laser radiation in all the crystals by BPM, and in LNB have been obtained by BPM and also by quasi phase matching (QPM). In BPM the perfect matching ($\Delta k = 0$) between the nonlinear polarization and the radiative field is accomplished by index matching, which in a dispersive medium is obtained in a propagation direction when the birefringence compensates the dispersion; allowing the generated field to grow continuously. In QPM, perfect index matching is not possible, but it is possible to increase the energy of the generated wave continuously during the propagation by introducing a periodic change in the sign of the nonlinear electric susceptibility (χ^2_{eff}).

In the case of YAB, the Yb^{3+} broad emission bands caused the IR tuning range to shift from light generation in the green to the yellow range by SFD. These crystals are not the only SFD crystals, but are the most relevant ones to our knowledge; moreover Table 1.2 shows the main crystalline lasers with self-

frequency conversion. Other nonlinear crystals have been doped with Nd^{3+}, such as BiB_3O_6 (BIBO), and with Yb^{3+}, such as $LaCa_4(BO_3)_3O$ (LaCOB), KGP ($KGd(PO_3)_4$) and Nb:RTP ($RbTi_{1-x}Nb_xOPO_4$), and are candidates to be used in self-frequency conversion lasers. To our knowledge Yb^{3+} doped GAB,[20] KGP[21] and Nb:RTP[22] have recently achieved the CW lasing operation, but Nd^{3+} concentration in BIBO is too low to obtain laser oscillation.[23]

Table 1.2. *Self-frequency doubling lasers.*

Active ion	Host	Conversion efficiencies	laser source	Process
Tm^{3+}, Ho^{3+}	*LNB*[18]		Xenon flash lamp	BPM
Nd^{3+}	*LNB*[19,24]	0.1%[24]	Ti:sapphire	QPM
	YAB[25-32]	14%[30] 20%[30]	Diode Ti:sapphire	BPM
	LNB:Mg[17,33-36]	7.6%[17]	Dye	BPM
	LNB:Sc[37]	0.2%	Ti:sapphire	BPM
	LSB[38-39]	26%[38]	diode	BPM
	GdCOB[40-43]	14.4%[42]	Ti:sapphire	BPM
	LBG[44]	0.15%	Ti:sapphire	BPM
	BNN[45-46]	0.13%[46]	diode	BPM
	YCOB[47-48]	6.2%(green)[47] 1.68%(red)[48]	diode	BPM
	GAB[49-50]	0.5%[49]	diode	BPM
	LaCOB[51]	5%	dye	BPM
Yb^{3+}	*YCOB*[52]	< 0.1%	Ti:sapphire	BPM
	GdCOB[53-54]	< 0.1%[54]	diode	BPM
	LNB:Mg[55-58]	30%[55,57-58] 15%[56,58]	Ti:sapphire	BPM QPM
	YAB[59-63]	10%[60]	diode	BPM

UNIVERSITAT ROVIRA I VIRGILI
YTTERBIUM AND ERBIUM DOPEP RbTi1-xMxOPO4 (M=Nb or Ta) CRYSTALS. NEW LASER AND NONLINEAR BIFUNCTIONAL MATERIALS
Alexandra Peña Revellez
ISBN: 978-84-691-0370-8 /DL:T.2188-2007

1.3 RE^{3+} doped crystals of the $KTiOPO_4$ family

The first paper reporting the synthesis of $KTiOPO_4$ (KTP) was in 1890,[64] but no detailed analysis of the crystal structural was done until 1974.[65] Two years later, KTP was described as a nonlinear optical material,[66] and since then it has been employed for nonlinear processes such as for frequency doubling of 1064 nm Nd:YAG lasers using type II BPM[67-68] and because it is ferroelectric, periodically-poled KTP has been also used for QPM.[69]

KTP belongs to a structural family of great diversity and versatility, $ABOXO_4$, with A = K, Rb, Na, Cs, Tl, NH_4; B = Ti, Sn, Sb, Zr, Ge, Al, Cr, Fe, V, Nb, Ta and X = P, As or Si. They crystallize in the orthorhombic system; belong to the mm2 symmetry group, which is non-centrosymmetric, and to the $Pna2_1$ space group. The crystallographic axes ***a***, ***b*** and ***c*** are parallel to the optical axes ***x***, ***y***, ***z***, for which $n_x<n_y<n_z$ is fulfilled, and ***c*** is the polar axis of the structure.

All the atoms in KTP's structural family are in general positions and for each of the different atoms there exists two non-equivalent positions, neither related by symmetry nor by translation, in the unit cell (Figure 1.1). KTP's structure consists of a rigid extended helical network of distorted BO_6 octahedra bridged by slightly distorted XO_4 tetrahedra, and a mobile framework of A atoms. A large number of KTP's isostructural compounds had been studied[70-71] and some general rules can be extracted and related with the ferroelectric and nonlinear optical properties of this family of compounds. Even though the origin of the high nonlinearity is still ambiguous, it should be noted that the early results performed by Zumsteg *et al.*,[66] which conjectured that the short bonds of the TiO_6 groups are responsible for the high nonlinearity, have been recently supported.[72] Moreover, another conclusion about the origin of the nonlinearity in this family of compounds was extracted by the use of chemical bond calculations,[73] which attributed the nonlinearity to the K-O bonds and PO_4 groups. So, the choice of A, B or X atoms must be carefully made if no decrease in the nonlinearity is wanted.

UNIVERSITAT ROVIRA I VIRGILI
YTTERBIUM AND ERBIUM DOPEP RbTi1-xMxOPO4 (M=Nb or Ta) CRYSTALS. NEW LASER AND NONLINEAR BIFUNCTIONAL MATERIALS
Alexandra Peña Revellez
ISBN: 978-84-691-0370-8 /DL:T.2188-2007

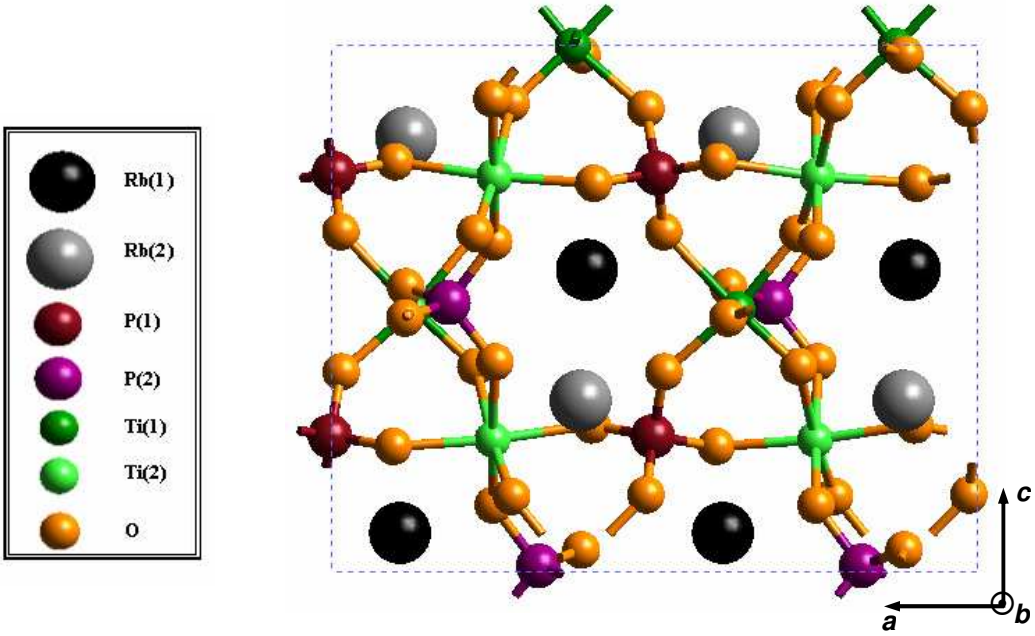

Figure 1.1. RTP unit cell, where there are the two non equivalent positions for Rb, P and Ti and O.

As KTP and related isostructural crystals, have already shown exceptional properties to be used for several nonlinear applications,[71] great efforts have been made to dope KTP with RE^{3+} (or Ln^{3+}) ions to obtain a self-frequency doubling (SFD) laser in the visible spectral range. A variety of techniques have been used to dope KTP and its isostructurals with RE^{3+} ions, including: TSSG-SC technique, electron beam evaporation, laser ablation, ion beam mixing and ion implantation, pulsed laser deposition, and hydrothermal or solid state syntheses.

All the attempts to dope KTP with RE^{3+} ions by the TSSG-SC technique have returned less than encouraging results, as the RE^{3+} concentration obtained, 5×10^{17} - 6×10^{18} ions/cm^3, is far from threshold needed to obtain efficient fluorescence.[74-76] Moreover, the crystallization region of KTP became narrower and new phases appeared ($LnPO_4$ and $K_3Ln(PO_4)_2$), while the distribution coefficient of the RE^{3+} ions (K_{RE}) is quite low and depends on the RE^{3+} ionic radius (see Figure 1.2). But it is also shown[74] that the RE^{3+} ions incorporation could be enhanced by co-doping KTP with Nb^{5+} and Rb^+.

Codoping, to try to increase the RE^{3+} concentration, is better when the ionic radius of the codopand ion is as close as possible to that of the substituted atom, and with a higher ionic radius.

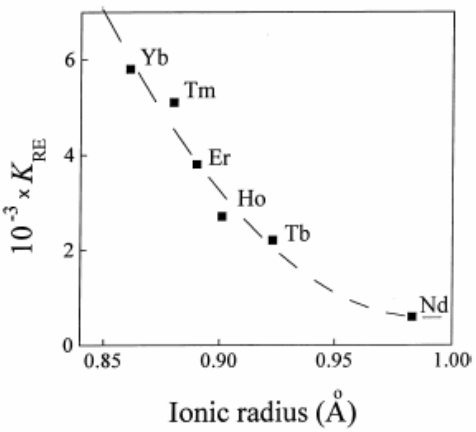

Figure 1.2. Distribution coefficient of RE^{3+} (K_{RE}) in KTP single crystals grown in its self flux by TSSG-SC technique.[76]

Although, RE^{3+} ions can be incorporated in Ti^{4+} (r_{ionic} = 0.605 Å) sites or K^+ (r_{ionic} = 1.51 Å) sites, we assume that they are incorporated in Ti^{4+} sites since increasing the RE^{3+} ionic radius ($r_{Nd^{3+}}$ = 0.983 Å; $r_{Tb^{3+}}$ = 0.923 Å; $r_{Ho^{3+}}$ = 0.901 Å; $r_{Er^{3+}}$ = 0.890 Å; $r_{Tm^{3+}}$ = 0.880 Å; $r_{Yb^{3+}}$ = 0.861 Å) decreases the distribution coefficient, as shown in Figure 1.2.

By electron-beam evaporation, the Er^{3+} concentration achieved in KTP was about 2.6×10^{20} ions/cm^3,[77] while the concentration of RE^{3+} reached by using thermal diffusion of Ln_2O_3 layers deposited by laser ablation on KTP surfaces was about 10^{21} ions/cm^3.[78] This technique has two main limitations; firstly the thermal diffusion temperature could not be raised above 1123 K (in order to avoid surface degradation due to K^+ losses) and secondly, $LnPO_4$ was formed, which stops the diffusion process. By ion implantation and ion beam mixing, Er^{3+}, Yb^{3+} and Tm^{3+} impurities have been incorporated into the KTP lattice.[79] As an attractive alternative to incorporate RE^{3+} ions into KTP to these methods it should be mentioned pulsed laser deposition, with which transparent and bright surfaces with Er^{3+} up to 3 at. % have been obtained,[80] but the Er^{3+} distribution is not homogeneous along the entire surface.

Attempts at RE^{3+} doping KTP isostructural crystals have also been performed. Ln:X:RTA, where Ln = Yb or Er and X = Nb, F, S, Se, Re, Mo, W, crystals grown by hydrothermal and solid state synthesis,[81] increased the birefringence, obtaining a blue shift in the non critical phase matching

wavelength (λ_{NCPM}) of KTP. In Er:RTP: grown by the TSSG-SC technique, the concentration achieved of Er^{3+} was not enough to obtain efficient luminescence, although the concentration was higher than that obtained in KTP grown by the same technique.[75]

In the last years, great results have been achieved in the enhancement of RE^{3+} concentration in $RbTi_{1-x}Nb_xOPO_4$ single crystals grown by the TSSG-SC technique in *FiCMA*'s laboratory. Concentrations up to ≈ 2×10^{20} and 0.65×10^{20} ions/cm^3 were achieved for Yb^{3+} and Er^{3+} respectively, which allowed performing accurate spectroscopic characterization[82] and checking the SHG efficiency by the powder method.[83]

1.4 Ferroelectricity

KTP and isostructural crystals are dielectric; they have no free electrons at room temperature. Normally a dielectric material becomes polarised when an electric field is applied leading to dipole formation, but KTP also possess a spontaneous polarization, P_s, without applying an external field. If this P_s, with no action of an external electric field, has two or more different orientations which are reversible by applying an external field, the crystal belongs to the ferroelectric group. Ferroelectricity indicates that inside the crystal, the calculated centre of positive charges does not match the centre of the negative charges. P_s is temperature dependent, $P_s \sim \sqrt{T_c - T}$ (according to the Curie-Weiss law), and the crystal undergoes a phase transition at the T_c (Curie temperature) becoming a centrosymmetric structure.

The ferroelectric nature of KTP was suggested in 1980 due to the observation of the complete and reversible losses in powder SHG intensity at elevated temperatures.[84] The SHG intensities were constant while increasing the temperature until the T_c was reached, becoming zero when this value was crossed. So, KTP undergoes a phase transition at T_c = 1207 K from a ferroelectric phase ($Pna2_1$) to a paraelectric phase (*Pnan*) leading to a centrosymmetric structure.

UNIVERSITAT ROVIRA I VIRGILI
YTTERBIUM AND ERBIUM DOPEP RbTi1-xMxOPO4 (M=Nb or Ta) CRYSTALS. NEW LASER AND NONLINEAR BIFUNCTIONAL MATERIALS
Alexandra Peña Revellez
ISBN: 978-84-691-0370-8 /DL:T.2188-2007

Ferroelectric crystals have regions where the spontaneous polarisation is oriented along the same direction, called domains. In KTP P_s is aligned along ***c*** axis, depending on the synthesis method and the conditions used, samples could be single-domain or multi-domain. Ferroelectric inversion domains normally can not been observed by using polarized light optical microscopy because there are no changes in the birefringence across antiparallel domain walls. Different techniques have been employed to visualize ferroelectric domain structures, such as those based upon piezoelectric,[85] electro-optic,[85-86] nonlinear optical, and pyroelectric[85,87] properties of KTP. Moreover, selective etching of domains with opposing directions of P_s was utilized for optical and electron microscopy studies,[86] X-ray diffraction[88] and also a few scanning probe microscopy (SPM) techniques.[89] Recently, by Scanning Near-Field Optical Microscopy (SNOM), which measures synchronized optical signals and topography, the domain walls of an RTP sample grown by the TSSG-SC technique have been studied (see *paper IV*).

KTP, as well as other ferroelectric materials such as LNB, have been periodically poled (for the first time in 1993[90]), which means that a ferroelectric domain reversal is created, to generate optical nonlinear frequency conversion by quasi-phasematching (QPM). The main advantage of QPM versus BPM, in KTP crystals, is that by QPM allows the employment of a larger effective nonlinear coefficient, d_{33}, and a subsequently higher conversion efficiency.

1.5 Doctoral Thesis Aims

KDP and ADP were the first nonlinear materials which were used in frequency doubling. Although they can be easily grown in large crystals, their nonlinear coefficients are small, their transparency in the IR range is quite narrow and they are very hygroscopic. Borates, such as BBO and LBO, have a wider transparency range but their nonlinear coefficients are of the same order of magnitude. KTP, $KNbO_3$, LNB, and $LiIO_3$ have larger nonlinear optical coefficients and wider transparency ranges. In the last decade, KTP has been widely used for frequency doubling of the 1.06 μm radiation from Nd:YAG

UNIVERSITAT ROVIRA I VIRGILI
YTTERBIUM AND ERBIUM DOPEP RbTi1-xMxOPO4 (M=Nb or Ta) CRYSTALS. NEW LASER AND NONLINEAR BIFUNCTIONAL MATERIALS
Alexandra Peña Revellez
ISBN: 978-84-691-0370-8 /DL:T.2188-2007

lasers, because it shows very large thermal and angular phase-matching bandwidths for SHG of this wavelength.

Doping KTP, or isostructural crystals, with RE^{3+} ions, as mentioned in section 1.3, will convert them into bifunctional materials, where the laser effect and the nonlinear optical phenomena occur within the same host, leading to a compactness of devices. Attempts at KTP doping with RE^{3+} have been unsuccessful but it seems that the RE^{3+} concentrations achieved in $RbTi_{1-x}Nb_xOPO_4$ are promising enough to dream obtaining a new SFD laser.[91]

The main objective of this thesis was to enlarge the size of the Er^{3+} and Yb^{3+} doped $RbTi_{1-x}Nb_xOPO_4$ crystals previously obtained by the TSSG-SC technique by optimizing the crystal growth conditions.

The TSSG-SC technique was used because RTP crystals decompose before melting. The bulk crystals obtained are already doped, as dopands are added to the initial growth solutions. As a result, no post processing, such as thermal diffusion or ionic implantation, is needed to dope the crystals, avoiding the related problems of these techniques as explained in section 1.3.

$RbTi_{1-x}Nb_xOPO_4$ has already shown its possibility to be doped with Yb^{3+} to obtain efficient fluorescence.[91] The advantages of using Yb^{3+} in solid state lasers operating at 1 μm as well as in self-frequency doubling lasers were discussed in section 1.2. We have sought to improve the growth conditions with Yb^{3+} in order to obtain bigger defect free crystals, because it is the smallest of its family and closest to Ti^{4+} ionic radius. Moreover, efforts have been made to increase the Yb^{3+} concentration, either by using a different charge compensator than Nb^{5+} or by introducing small impurities of other ions in the growth solution.

Ta^{5+} was the ion chosen to balance the charge in the Ti^{4+} substitution by Yb^{3+}. As shown in Ta:KTP,[92] we expected an optical birefringence (n_z-$n_{y,x}$) increase, pushing the NCPM limit for frequency doubling to shorter wavelengths. But a high Ta^{5+} concentration leads to a decrease in the nonlinearity, so care must be taken in choosing the right amount of Ta^{5+} substitution. To find out which is the right Ta^{5+} substitution for obtaining a high enough Yb^{3+} concentration, crystal growth and optical characterization have been completed throughout this thesis.

UNIVERSITAT ROVIRA I VIRGILI
YTTERBIUM AND ERBIUM DOPEP RbTi1-xMxOPO4 (M=Nb or Ta) CRYSTALS. NEW LASER AND NONLINEAR BIFUNCTIONAL MATERIALS
Alexandra Peña Revellez
ISBN: 978-84-691-0370-8 /DL:T.2188-2007

Also we have studied the spectroscopy of the RE^{3+} pair, Yb^{3+} and Er^{3+}, in $RbTi_{1-x}Nb_xOPO_4$. This pair was chosen because we already know the crystallization region of $Er:RbTi_{1-x}Nb_xOPO_4$ and $Yb:RbTi_{1-x}Nb_xOPO_4$[93] and which was the best point in this crystallization region to obtain a larger RE^{3+} concentration. Furthermore, by using Yb^{3+} as a sensitizer for the $^4I_{11/2}$ Er^{3+} multiplet, the drawback of Er^{3+}, which mainly relies on having a low absorption cross section, would be avoided and laser action around 1.55 μm could be achieved by diode-pumped laser crystals. This 1.55 μm Er^{3+} laser would have applications in optical communication technology and in eye-safe lasers.[94]

Nonlinear optical properties, such as the conversion efficiency and the non critical phase-matching (NCPM limit for frequency doubling along the ***a*** and ***b*** crystallographic axes, were determined for $RbTi_{1-x}Nb_xOPO_4$ samples doped with Yb^{3+} and/or Er^{3+}. The theoretical phase matching curve of Type II SHG for $Yb:RbTi_{1-x}Nb_xOPO_4$ was also calculated.

With the help of the spectroscopic characterization of $Yb:RbTi_{1-x}Nb_xOPO_4$, the laser action achieved for the first time in this material and the theoretical phase matching curve, predictions about the angle where the SFD laser action would take place have been completed.

UNIVERSITAT ROVIRA I VIRGILI
YTTERBIUM AND ERBIUM DOPEP RbTi1-xMxOPO4 (M=Nb or Ta) CRYSTALS. NEW LASER AND NONLINEAR BIFUNCTIONAL MATERIALS
Alexandra Peña Revellez
ISBN: 978-84-691-0370-8 /DL:T.2188-2007

Chapter 2

Experimental techniques

In this chapter, all the main experimental techniques used for the realization of this thesis are summarised. A brief description of each technique and their theoretical fundamentals are given. Furthermore, schematic views and illustrations of some of the experimental equipment are shown.

All the equipments were available at *FiCMA's* laboratories and at the *Servei de Recursos Científics i Tècnics* of the *Universitat Rovira i Virgili*, at the *Serveis de Recursos Cientifico-Tècnics* of the *Universitat de Barcelona*, at the *Institut de Ciència dels Materials* of the *Universitat de València*, at the *Laboratoire de Spectrométrie Physique* of the *Université Joseph Fourier* (Grenoble, France) and at the Max-Born-Institute for Nonlinear Optics and Ultrafast Spectroscopy (Berlin, Germany).

UNIVERSITAT ROVIRA I VIRGILI
YTTERBIUM AND ERBIUM DOPEP RbTi1-xMxOPO4 (M=Nb or Ta) CRYSTALS. NEW LASER AND NONLINEAR BIFUNCTIONAL MATERIALS
Alexandra Peña Revellez
ISBN: 978-84-691-0370-8 /DL:T.2188-2007

2.1 Crystal growth

We already know that the crystals which are going to be the basis of this thesis melt incongruently, decomposing at temperatures below their melting points (at 1343 K in the case of RTP[95]). Because of this, the growth method chosen was a high temperature flux technique. It relies on forming a homogeneous solution of the components in an appropriate solvent, determining the saturation temperature (T_s) and finally applying a slow decrease of the solution temperature in order to obtain the crystal growth.

2.1.1 Spontaneous nucleation

We decided to grow Yb:$RbTi_{1-x}Ta_xOPO_4$ crystals in its self flux, to determine the maximum TiO_2 substitution with Yb_2O_3, Ta_2O_5 or Yb_2O_3 + Ta_2O_5 allowed without losing the desired orthorhombic phase.

In order to determine the Yb:$RbTi_{1-x}Ta_xOPO_4$ crystallization region, crystals of micrometer sizes were grown by spontaneous nucleation on a Pt wire from different flux compositions, in the ternary system Rb_2O-P_2O_5-TiO_2 with small concentrations of Yb_2O_3 or Ta_2O_5 or both together. The crystalline phase of the crystals obtained in each of the studied compositions was determined, allowing limitation of the crystallization region.

The growth experiments were performed in a vertical tubular single-zone furnace (Figure 2.1) heated by a Kanthal AF resistance (1 mm Ø wire) and the temperature was controlled by a Eurotherm 818P controlled/programmer which was connected to an S-type thermocouple Pt/Pt-Rh 10% placed near to the central zone of the resistance and to a thyristor that controls the power of the furnace. The characterization of the thermal axial gradient of the furnace as well as the thermal axial gradient of the growth solution was measured prior to beginning the crystal growth process. The first determination gives an estimation of the best position of the Pt crucible inside the furnace and the second accurately measures to ensure that the surface of the solution is colder than the bottom.

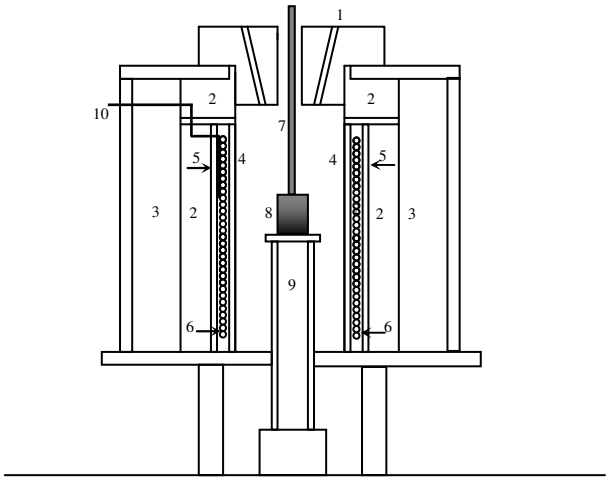

1. Top of furnace
2. Alumina insulator
3. Thermal wool insulator
4. Internal alumina cylinder
5. External alumina cylinder
6. Resistance heating coil
7. Pt wire
8. Pt crucible
9. Crucible base
10. Thermocouple

Figure 2.1. Scheme of the vertical tubular single-zone furnace.

Solutions weighing between 20 and 30 g were prepared by mixing the precursor oxides (Rb_2O, P_2O_5, TiO_2, Yb_2O_3 and Ta_2O_5) in the desired ratios in a 25 cm^3 Pt crucible, and then homogenizing the components by keeping the solution temperature around 75 K above the saturation temperature (T_s). This temperature was determined by observing the growth or the dissolution of small crystals on a Pt wire placed inside the solution, and then applying a slow cooling rate to obtain the needed crystals. After removing the crystals on the Pt wire from the solution, they were cleaned and then the crystallized phase was characterized by X-ray powder diffraction, and their shape was visualized by optical microscopy.

2.1.2 Top Seeded Solution Growth-Slow Cooling technique

The technique used to grow the single crystals was the Top Seeded Solution Growth-Slow Cooling (TSSG-SC) technique, a flux growth technique commonly used to grow crystals from high temperature solutions. In TSSG-SC, the crystal growth begins on a crystal seed which is in contact with the solution surface, and during the growth process the crystal is completely submerged in the flux, allowing the crystal facets to freely grow. The solution is slowly cooled after determining the crystallization temperature, which is measured by observing the growth or dissolution of the seed in contact with the solution

UNIVERSITAT ROVIRA I VIRGILI
YTTERBIUM AND ERBIUM DOPEP RbTi1-xMxOPO4 (M=Nb or Ta) CRYSTALS. NEW LASER AND NONLINEAR BIFUNCTIONAL MATERIALS
Alexandra Peña Revellez
ISBN: 978-84-691-0370-8 /DL:T.2188-2007

surface. By applying this slow cooling of the solution, the crystal growth process begins from the seed when the solution becomes supersaturated and continues while the solution temperature steadily decreases. The possibility of secondary nucleation, during the crystal growth, was avoided by placing the seed crystal at the coldest point of the solution. Moreover to obtain inclusion-free single crystals, a good convection flow was present in the solution. This free convection flow, caused by the axial temperature gradient, is compensated by the forced flow of the rotating crystal.

All the growth experiments were performed in vertical tubular single-zone furnaces (Figure 2.1), and as explained in the previous section, the axial thermal gradient of the furnace and of the solution were determined before the crystal growth began, in order to locate the Pt crucible in the right position inside the furnace to have a low temperature gradient inside the growth solution. As the axial thermal gradient is different in an empty furnace than in the solution inside the Pt crucible, an alumina column, which supports the Pt crucible, is used to place the crucible in the right zone of the furnace.

To place and rotate the crystal seed vertically inside the growth solutions a mechanical part was added above the furnace. This mechanical part of the crystal growth system (Figure 2.2) comprises an extremily rigid and stable vertical metal structure, which supports a hanging, vertically displacing and rotating an alumina rod. At the end part of this alumina rod it is laced with Pt wire a Pt holder, were the seed crystal is attached. A Mitutoyo micrometer (accuracy of 0.01 mm) is used to measure the position of the seed crystal, which is critical in order to determine the crystallization temperature from the growth or dissolution of the seed.

Depending on the dimensions of the furnace used to perform the different growth experiments, 25 cm^3 conical Pt crucibles, or cylindrical 125 cm^3 or 250 cm^3 crucibles were used. Solutions weighing between ≈ 300 and 30 g were prepared by mixing the desired ratios of the precursor oxides: Rb_2O, P_2O_5 and TiO_2, and small amounts of Nb_2O_5, Yb_2O_3 and Er_2O_3 or Ta_2O_5 and Yb_2O_3. The crystals were grown in either self flux or tungsten flux, with an excess of Rb_2O and P_2O_5 as a solvent, and then subjected to cooling programs and growth conditions described in chapter 3.

UNIVERSITAT ROVIRA I VIRGILI
YTTERBIUM AND ERBIUM DOPEP RbTi1-xMxOPO4 (M=Nb or Ta) CRYSTALS. NEW LASER AND NONLINEAR BIFUNCTIONAL MATERIALS
Alexandra Peña Revellez
ISBN: 978-84-691-0370-8 /DL:T.2188-2007

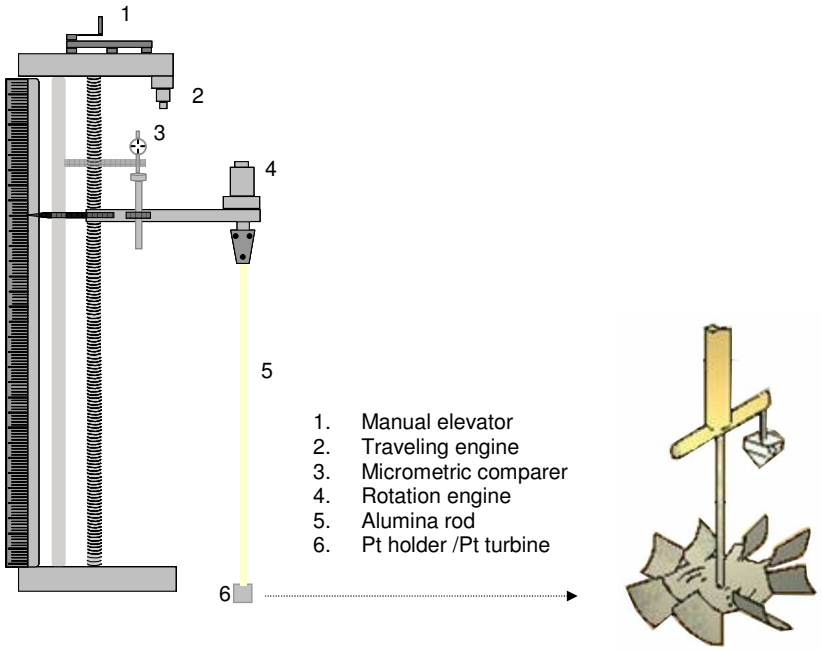

Figure 2.2. Scheme of the mechanical part of the growth device (left hand) and Pt turbine used to increase the mass transport in the solution.

2.2 Sample preparation

In the characterization of anisotropic optical materials, care must be taken in the sample preparation, as each property should be evaluated as a function of the direction. In RTP, the crystallographic directions, ***a***, ***b*** and ***c*** are parallel to the principal optical axes, ***X***, ***Y*** and ***Z***, for which $n_x<n_y<n_z$ is fulfilled. The orientation of the samples was carefully aligned for structural and optical studies.

On the grown crystals it appears faces perpendicular to ***a*** direction which will be used as a reference in order to prepare slices of the needed thickness parallel to the (100) faces. Since the as-grown crystals do not contain natural faces perpendicular to direction ***c***, a polished plane normal to the [001] direction is obtained by placing the (201) and $(\bar{2}01)$ faces inside a piece of aluminium cut at 62.4°, which matches with the angle between these two faces. The ***c***-oriented plate was obtained by cutting one slice parallel to the plane.

UNIVERSITAT ROVIRA I VIRGILI
YTTERBIUM AND ERBIUM DOPEP RbTi1-xMxOPO4 (M=Nb or Ta) CRYSTALS. NEW LASER AND NONLINEAR BIFUNCTIONAL MATERIALS
Alexandra Peña Revellez
ISBN: 978-84-691-0370-8 /DL:T.2188-2007

The ***c***-oriented plates were supported on a goniometric head, to facilitate the further correction of possible disorientation, and the orientation was verified by texture analysis using a D5000 Siemens diffractometer.

Plates oriented perpendicular to the ***b***-direction are prepared by cutting at 90º of the natural (100) face and the polished plane normal to the [001] direction, obtained as described above.

Cube-shaped samples were also obtained, from crystals of sufficient size and quality to prepare single cubes, in order to obtain a single sample containing the three axes, so the desired characterizations performed along the three crystallographic directions, ***a***, ***b*** and ***c*** (which matches with the principal optical axes, ***X***, ***Y*** and ***Z***) could be done in a single sample.

The samples were cut with a diamond wire Logitech model 15 saw. Diamond wires were use instead of diamond disks, to induce less mechanical stress in order to avoid fractures. Furthermore, the load applied to the sample was limited to the minimum needed to cut the sample.

A Logitech PM5 polisher was used to polish the samples. The rotation and the pressure applied to the samples was controlled by an oscillatory arm depending on the sample hardness. The samples were lapped with 9 μm alumina abrasive powders and then polished to the desired quality with a silicon colloidal solution (SF1). Parameters such as roughness (*rms*), flatness (curvature radius) and parallelism were used to control the final polished quality. An average roughness value and flatness value were obtained with a confocal microscope (see section 2.5.3). Parallelism was measured with an autocollimator.

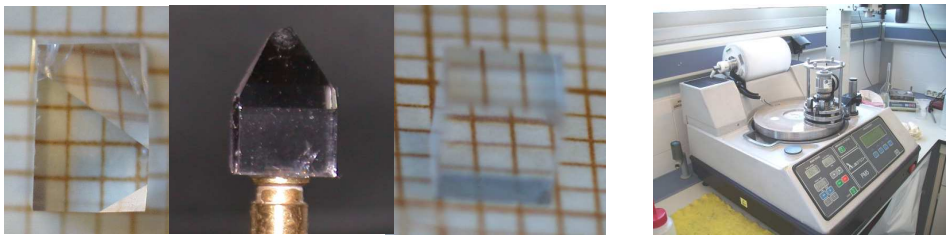

Figure 2.3. Different polished samples used to perform some of the characterizations showed in this thesis (left hand), and the Logitech PM5 polisher (right hand).

UNIVERSITAT ROVIRA I VIRGILI
YTTERBIUM AND ERBIUM DOPEP RbTi1-xMxOPO4 (M=Nb or Ta) CRYSTALS. NEW LASER AND NONLINEAR BIFUNCTIONAL MATERIALS
Alexandra Peña Revellez
ISBN: 978-84-691-0370-8 /DL:T.2188-2007

All the samples were completely prepared at the *FiCMA* group, where all the equipment described above: diamond wire saws, the polisher, the confocal microscope and the autocollimator, are available. Figure 2.3 shows some of the samples obtained as well as the Logitech polisher.

2.3 X-ray diffraction techniques

The X-rays applied to the study of crystals gave a great boost to the crystallography. Thanks to the use of the X-rays, the distance between adjacent lattice planes as well as the atomic positions in a crystal were measured leading to the determination of crystalline structures.

W. L. Bragg observed that X-rays were really diffracted by crystals. The scattered radiation from the crystals showed that the crystals act as individual atoms periodically aligned on planes. These planes act as reflecting mirrors and the "reflected" waves by these lattice planes interfere constructively only if

$$\lambda = 2d_{hkl}\sin\theta \qquad \text{eq. 2.1}$$

where λ is the wavelength of the radiation used; d_{hkl} is the spacing distance between two consecutive lattice planes, and θ is the incident angle of the X-ray beam.[96] This equation is known as the Bragg's Law.

When a monochromatic X-ray beam is directed at a powdered crystalline sample, the complete diffraction pattern will be observed for any orientation of the crystalline powder with respect to the X-ray beam which fulfils the Bragg's law.[96]

Powder diffraction is a non-destructive tool for identifying crystalline phases and analyzing mixtures. The recorded diffraction patterns are compared with the patterns compiled by the Joint Committee for Powder Diffraction Standards (JCPDS).[96] Moreover, the determination of phase diagrams, phase transitions and the cell parameters evolution as a function of the temperature, pressure, or dopant concentration, could be also studied by the use of this technique. The FULLPROF program,[97] which is based in the Rietveld method,[98] gives the possibility to delineate precise cell-parameters, atomic coordinates, and temperature factors by adjusting parameters with an experimental powder diffraction pattern.

UNIVERSITAT ROVIRA I VIRGILI
YTTERBIUM AND ERBIUM DOPEP RbTi1-xMxOPO4 (M=Nb or Ta) CRYSTALS. NEW LASER AND NONLINEAR BIFUNCTIONAL MATERIALS
Alexandra Peña Revellez
ISBN: 978-84-691-0370-8 /DL:T.2188-2007

To record the powder patterns used in this thesis, a Siemens D-5000 powder diffractometer with a Bragg-Brentano parafocusing geometry and θ-θ configuration using a Cu source ($\lambda_{K\alpha}$ = 1.540560 Å), available at the *Servei de Recursos Científics i Tècnics* of the *Universitat Rovira i Virgili*, was used. In this system, the source, the sample and the detector occupy three consecutive positions on a circumference. The position of the source and the detector vary synchronously, always symmetrically while keeping the sample fixed. The discrete patterns of reflection for the families of planes parallel to the sample surface were obtained by varying the 2θ angle of the source and the detector.

Although powder diffraction is a powerful technique, resolving structures by using this technique is quite difficult as the three-dimensional crystallographic information is lost.

Texture analysis was used to verify the orientation of the **c**-oriented plates (see section 2.2). These analyses were performed in a D5000 Siemens diffractometer with Bragg-Brentano parafocusing geometry and a horizontal θ-2θ goniometer with an open Eulerian cradle (available at the *Servei de Recursos Científics i Tècnics* of the *Universitat Rovira i Virgili*). The orientation of the obtained sample crystal plane is defined by three angles with respect to the diffraction plane: the Bragg diffraction angle (θ), the rotation angle around the axis of intersection between the sample and the diffraction plane (χ), and the rotation angle around the normal axis to the sample plane (φ). Our measure comprises a stereographic projection perpendicular to the [001] direction that shows the variation of the pole density with pole orientation for (004) crystal planes, known as pole figure. The measurements comprise an increase of the χ angle from 0 to 10º with a $\Delta\chi$ = 1º and the φ angle was increased from 0 to 360º with a $\Delta\varphi$ = 3º and 3s of counting time, for the theoretical 2θ angle of the diffraction of the (004) reflection (33.96º), using $\lambda_{K\alpha}$ = 1.540560 Å. The obtained pole figure and the 2θ-scan obtained fixing the χ and φ obtained from the pole figure are shown in Figure 2.4.

UNIVERSITAT ROVIRA I VIRGILI
YTTERBIUM AND ERBIUM DOPEP RbTi1-xMxOPO4 (M=Nb or Ta) CRYSTALS. NEW LASER AND NONLINEAR BIFUNCTIONAL MATERIALS
Alexandra Peña Revellez
ISBN: 978-84-691-0370-8 /DL:T.2188-2007

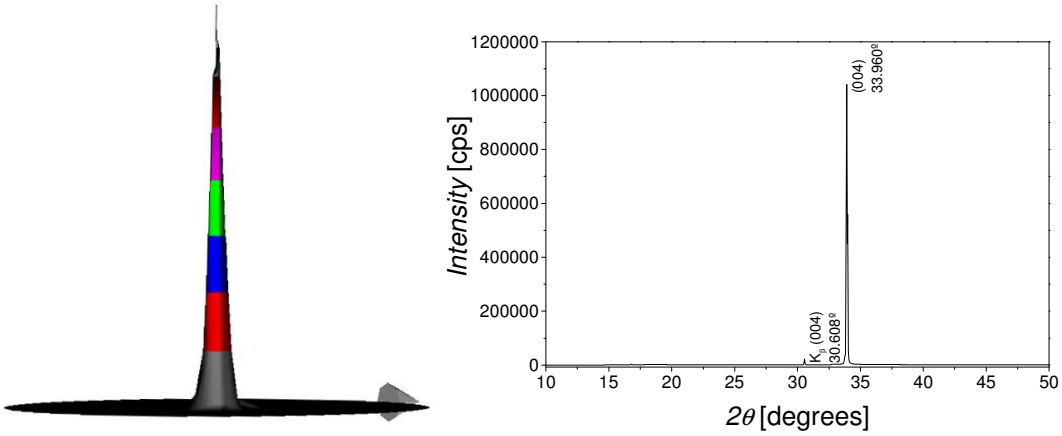

Figure 2.4. Pole figure corresponding to the (004) reflection with a 2θ = 33.96º (left hand) and 2θ-scan for (χ,φ) = 0º, 307º (right hand).

2.4 Electron Probe Microanalyses

The chemical composition of the crystals and the dopant concentrations in these crystals were analyzed by Electron probe microanalysis (EPMA) in a Cameca SX-50 microprobe analyzer available at the *Servei de Recursos Científico-Tècnics* of the *Universitat de Barcelona*.

Electron probe microanalysis is a nondestructive technique which uses a focused electron beam to produce characteristic X-rays from samples. The electron beam is generated at an intensity of 30 nA or 100 nA, depending on the concentration of the element to be determined, at an accelerating voltage of 20 kV. The X-rays produced by the samples were detected and characterized by a wavelength-dispersive spectrometer (WDS). The spectrometer crystals commonly used are: lithium fluoride 200 (LIF) (which is an ionic solid with $2d$ = 4.028 Å), pentaerythritol 002 (PET) (an organic crystal with $2d$ = 8.742 Å), thallium acid phthalate 1011 (TAP) (an organic crystal with $2d$ = 25.75 Å), and PC1 (W/Si multilayered pseudo-crystal with $2d$ = 60 Å). The wavelengths covered by these spectrometer crystals range from 1 to 24 Å.

UNIVERSITAT ROVIRA I VIRGILI
YTTERBIUM AND ERBIUM DOPEP RbTi1-xMxOPO4 (M=Nb or Ta) CRYSTALS. NEW LASER AND NONLINEAR BIFUNCTIONAL MATERIALS
Alexandra Peña Revellez
ISBN: 978-84-691-0370-8 /DL:T.2188-2007

The X-ray intensity of the sample is compared with that of the standard sample, which contains known concentrations, to determine the chemical composition of the studied samples. Details of the conditions for the measurements and the standards used for each element are given in Table 2.1 and in *papers I and II*. The corrected intensity ratio of an element's X-ray line is not directly proportional to its concentration. The ratios are affected by absorption, fluorescence and atomic number, and these factors must be corrected. This correction was done with PAP.[99]

Table 2.1. *Measurement conditions used in EPMA analysis.*

Element	***Line***	***Time*** (s)	***Spectrometer crystal***	***Standard***	***Detection limit*** (wt%)	***Experimental error*** (%)
Rb	L_α	10	TAP	$RbTiOPO_4$	0.05	1
Ti	K_α	10	PET	$RbTiOPO_4$	0.02	1
P	K_α	10	PET	$RbTiOPO_4$	0.02	1
O	K_α	10	PC1	$RbTiOPO_4$	0.15	3
W	M_α	60	TAP	$KYb(WO_4)_2$	0.03	3
Nb	L_α	60	PET	Nb	0.06	3
Ta	L_α	60	LiF	Ta	0.06	3
Yb	L_α	60	LiF	YbF_3	0.09	3
Er	L_α	60	LiF	REE1	0.02	4

All the samples were prepared in the same way, by putting a small piece of crystal in a cylindrical container, where we add a polyester resin with the proper catalyst, and let it cure. Both surfaces of the solid cylindrical sample (which contains the small crystal to be analyzed), are lapped with a SiC disk and then the surface containing the crystal is polished to optical quality with diamond powder of 3 and 1 μm. Crystals inclusion, lapping, and final polishing processes (with a Struers DAP-7 polisher) were performed at *FiCMA*. The samples, cleaned with alcohol, were coated with a fine C layer (which is a conductor and avoids electrical overcharge of the samples by the electron beam

UNIVERSITAT ROVIRA I VIRGILI
YTTERBIUM AND ERBIUM DOPEP RbTi1-xMxOPO4 (M=Nb or Ta) CRYSTALS. NEW LASER AND NONLINEAR BIFUNCTIONAL MATERIALS
Alexandra Peña Revellez
ISBN: 978-84-691-0370-8 /DL:T.2188-2007

of the microprobe analyzer) before beginning to measure the dopant concentration analysis.

All the measurements have an experimental error (ε), which is especially measured for all the minority elements determined. These errors are calculated by using the following expression

$$\varepsilon = \sqrt{\frac{I_p/t_p + I_b/t_b}{(I_p - I_b)^2} + \frac{I_p^s/t_p^s + I_b^s/t_b^s}{(I_p^s - I_b^s)^2}} \times 100 \qquad \text{eq. 2.2}$$

where I_p and I_b are the intensities of the peaks and the background of the sample in counts per second (c/s), respectively; t_p and t_b are the integration times of the peak and the background of the sample in seconds (s), and the super index, s, denotes the intensities (sample and background) and the integration times (sample and background) for the standards.

The detection limit for the minority elements was also determined with the expression:

$$DL = \left[\frac{C^s}{(I_p^s - I_b^s)}\right] 3\sqrt{2}\left(\frac{I_b}{t_b}\right)^{1/2} \qquad \text{eq. 2.3}$$

where C^s is the concentration of the minority element in the standard expression of weight % (wt %).

2.5 Microscopy techniques

All the techniques described have been used to perform initial observations of the obtained crystals, such as reflection optical microscopy, and more detailed views of the surfaces of the crystals were obtained, with scanning electron microscopy (SEM). Confocal microscopy was used to evaluate the quality of the polished samples and AFM and SNOM were used to visualize and quantify the selective etching processes in the different ferroelectric domains (C^- and C^+) present in the grown crystals.

UNIVERSITAT ROVIRA I VIRGILI
YTTERBIUM AND ERBIUM DOPEP RbTi1-xMxOPO4 (M=Nb or Ta) CRYSTALS. NEW LASER AND NONLINEAR BIFUNCTIONAL MATERIALS
Alexandra Peña Revellez
ISBN: 978-84-691-0370-8 /DL:T.2188-2007

2.5.1 Reflection Optical Microscopy

Reflection optical microscopy, which allows visualization of the obtained crystals, gives preliminary information about their crystalline habit, and is based on the normal incidence of visible light on the sample surface and the simultaneous normal visualization, of the sample, through the objective. The reflected, unobscured image, that is highly illuminated, is given by the specific configuration of the incident and the reflected paths. The high contrast obtained makes for the easy observation of the fine details of the sample surface, without any previous preparation of the sample. The equipment used, that is available at *FiCMA*, is an Olympus BH-2 and Olympus TL-2 microscopes.

2.5.2 Scanning Electron Microscopy

Scanning electron microscopy (SEM) is one of the most often used techniques in several research fields today, mainly due to the fact that SEM can focus on a wide range of specimen surfaces, because of its large depth of field, and it can also be used to observe fine details, because of its high resolution. Another key feature is that samples, going to be studied by SEM, are easy to prepare since the only requirement is that they should be conductive. In the case of non-conductive samples, analytes are coated with a fine layer of a conductive metal such as carbon or gold.

In this technique, the surface of the sample is scanned with an electron beam with a fine focal spot size (from 1 to 5 nm), and this beam is scattered, when it impinges on the sample, by the atomic layers near the sample surface, leading to energy loss. The quanta generated (secondary electrons, backscattered electrons, X-rays, etc.) carry information that describes the nature of the sample (topography, the sample atomic number, the elements distribution, etc.). All this information is converted into a video signal displayed on a screen. This technique can obtain magnifications between 10 and 300000.

SEM studies were performed with a Jeol JSM 6400 electron microscope and the samples were coated with a Bal-Tec SCD004 sputter coating. Experiments were performed at *Servei de Recursos Científics i Tècnics* of the *Universitat Rovira i Virgili*.

UNIVERSITAT ROVIRA I VIRGILI
YTTERBIUM AND ERBIUM DOPEP RbTi1-xMxOPO4 (M=Nb or Ta) CRYSTALS. NEW LASER AND NONLINEAR BIFUNCTIONAL MATERIALS
Alexandra Peña Revellez
ISBN: 978-84-691-0370-8 /DL:T.2188-2007

2.5.3 Confocal Microscopy

Sample images that are blurred with conventional microscopy, turn to sharp images when viewed with a confocal microscope. This enhancement of the quality of the images is achieved by excluding most of the light from the sample that is not from the microscope's focal plane. Furthermore, the sharp images obtained by confocal microscopy allow three-dimensional reconstructions of a sample volume by assembling a series of thin slices taken along the vertical axis.

Confocal microscopy differs from fluorescence microscopy, in which the sample is illuminated with light of an appropriate wavelength and an image is formed from the resulting fluorescence light, that it illuminates only one point of the sample. This point coincides with the focal point of the lens, where the excitation light is the most intense. As only one point of the sample is illuminated the fluorescence of this individual point is the only measured, reducing the background haze in the resulting image but enlarging the collection time to make an accurate measurement. There is never a complete image of the sample because at any instant only one point is observed. So, visualization is accommodated by attaching the detector to a computer, which builds up the image one pixel at a time. The restricted illumination of the sample is managed by adding a pinhole at the point where the focal point of the objective lens of the microscope forms the image. These two points are known as "conjugate points", being the pinhole conjugate to the focal point of the lens (a confocal pinhole).

In this case the confocal microscope used, to evaluate the roughness and the flatness of the sample surface obtained in the polishing process, is a Sensofar Plμ 2300 illuminated with blue laser light at λ = 470 nm available at the *FiCMA*.

2.5.4 Atomic Force Microscopy

Atomic force microscope (AFM) is one type of scanned-proximity probe microscopes, where a small probe is scanned across the sample to obtain information about the sample's surface. With the probe tip placed very close to the sample, the local attractive/repulsive forces are measured. The small

UNIVERSITAT ROVIRA I VIRGILI
YTTERBIUM AND ERBIUM DOPEP RbTi1-xMxOPO4 (M=Nb or Ta) CRYSTALS. NEW LASER AND NONLINEAR BIFUNCTIONAL MATERIALS
Alexandra Peña Revellez
ISBN: 978-84-691-0370-8 /DL:T.2188-2007

separation between the probe and the sample enables measurements to be taken in a very small area.

The resolution in atomic force microscopy is different from radiation based microscopies, where the resolution is determined by the diffraction effects. In AFM, the resolution is determined by the size of the probe and could be fractions of a nanometer.

There are different image modes in AFM, and we briefly introduce the contact mode and the tapping mode. In the contact mode, the probe located at the end of the cantilever lightly touches the sample, the piezo-electric scanners maintain the probe at a constant force, and the microscope measures the vertical deflection of the cantilever that indicates the local height from the sample. In the tapping mode the probe is kept at a fixed height from the sample surface and the microscope derives topographic images from measurements of attractive forces.

To obtain AFM images, the sample does not need to be coated, because AFM provides extraordinary topographic contrast and direct height measurements.

We used a commercially avalaible AFM from Nanotec Electronica working in a tapping mode available at the *Institut de Ciència dels Materials* of the *Universitat de València*, and also a PicoPlus from ScienTec avalaible at the *Servei de Recursos Científics i Tècnics* of the *Universitat Rovira i Virgili*.

2.5.5 Scanning Near-Field Optical Microscopy

Scanning near-field optical microscopy (NSOM or SNOM) has been described as a bridge between atomic force microscopy (AFM) and optical microscopy, being capable of measuring the topography and optical signals at the same time with optical resolutions of < 50 nm.

The imaging mechanism of SNOM is based on using a very small light source, smaller than the wavelength of light which is very close to the surface of the sample, to scan the sample in order to generate a point-by-point image of the light intensity variations in the sample.

UNIVERSITAT ROVIRA I VIRGILI
YTTERBIUM AND ERBIUM DOPEP RbTi1-xMxOPO4 (M=Nb or Ta) CRYSTALS. NEW LASER AND NONLINEAR BIFUNCTIONAL MATERIALS
Alexandra Peña Revellez
ISBN: 978-84-691-0370-8 /DL:T.2188-2007

The probe, an optical fiber tip with a small opening at the end, must be very close to the surface of the sample, much closer than the wavelength of the light.

The *"Near Field"* optical signal is strongly dependent on the distance between the probe and the sample surface: slight distance changes considerably change the recorded optical signal. So, it is important to keep the optical probe at a constant distance from the surface of the sample while recording the images. The distance control most commonly used in SNOMs is based on optical detection of shear forces acting on the probe.

There are multiple modes of operation for SNOM, depending on the sample being imaged: Transmission mode, where the light source travels through the probe aperture and transmits through the sample, requires transparent samples. Reflection mode, where the light source travels though the probe aperture and reflects from the surface, utilizes opaque samples. The collection mode consist of a large external light source illuminating the sample, and a probe that collects the reflected light. Finally, the illumination/collection mode consist of a probe that illuminates the sample and then collects the reflected light.

In our case, we used a SNOM (attoSNOMIII from Attocube Systems AG), available at the *Institut de Ciència dels Materials* of the *Universitat de València*. The basis of the working mode used is described in *paper IV*.

2.6 Differential Thermal Analysis

The thermal analysis of a substance implies studying the behaviour of several physical properties as a function of the temperature. When heating or cooling a material, the chemical composition and the crystal structure of the material undergo changes, such as fusion, melting, crystallization, oxidation, decomposition, reactions or phase transition. These changes can be observed by using thermal analysis.

Differential Thermal Analysis (DTA) measures the temperature, the direction and the magnitude of thermal transitions induced by heating or cooling a material, by comparing the sample temperature with an inert reference material under the same conditions. The temperature difference

UNIVERSITAT ROVIRA I VIRGILI
YTTERBIUM AND ERBIUM DOPEP RbTi1-xMxOPO4 (M=Nb or Ta) CRYSTALS. NEW LASER AND NONLINEAR BIFUNCTIONAL MATERIALS
Alexandra Peña Revellez
ISBN: 978-84-691-0370-8 /DL:T.2188-2007

determined as a function of time or temperature under a controlled atmosphere provides information about the transition temperatures, and about thermodynamics and kinetics of reactions.

Thermogravimetric analysis (TGA) determines the weight gain or loss of a determined phase due to gas release or absorption as a function of temperature under a controlled atmosphere, and is a useful technique for determining the sample purity, its water and carbonate content, and its organic content. This technique it is also useful for studying decomposition reactions.

In the combined DTA-TGA system, both thermal and mass changes are measured at the same time. These analyses were performed by using an SDT 2960 analysis instrument from TA Instruments. The performed measurements differentiate between endothermic or exothermic transitions with associated weight loss (e.g. fusion or crystallization) or with no weight loss (e.g. degradation).

2.7 Ionic conductivity

The alternating current (ac) conductivity in ionic materials shows dispersion behaviour through a dependence of the electrical conductivity (σ) on an angular frequency (ω) of the form

$$\sigma(\omega) = \sigma_0 + A\omega^s \qquad \text{eq. 2.4}$$

where σ_0 is the low frequency conductivity (or dc conductivity) and the super index *s* takes values between 0 and 1 ($0<s<1$).

In our case, we measured the ac ionic conductivity along the ***c*** crystallographic direction, where there exists a high mobility of Rb^+ ions along channels parallel to this direction, in samples (coated with a fine, 120 nm, Au layer acting as electrodes) of a thickness of ≈ 0.90 mm. The samples were linked into an ac impedance bridge circuit based on a Hewlett-Packard Model 4284A LCR meter operating between 20 Hz and 1 MHz frequency, which is available at *FiCMA*.

2.8 Raman spectroscopy

Raman scattering gives information about the vibrational energy levels of molecules, providing information on the structure of a material, allowing identification of solid, liquid or gaseous substances. In addition, Raman scattering requires minimal sample preparation and the technique is non-contact and non-destructive. Raman scattering and infrared absorption provide complementary information, and by merging both techniques, the characterization of the vibrational, rotational, and other low-frequency modes of molecules, such as the lattice vibrations of crystals, are completely described.

Raman scattering relies on inelastic scattering (the energies of the incident and scattered photons are different) of monochromatic light, that leads the energy of the scattered photons to be shifted down or up for the Stokes or anti-Stokes lines, respectively. This shift in the energy is related to the vibrational energy spacing in the ground electronic state of the molecule: the positions of the Stokes and anti-Stokes lines are a direct measurement of the vibrational energies of the molecule. The Stokes and anti-Stoke lines are displaced the same distance from the Rayleigh line; in each case one vibrational energy quantum is gained or lost, but the anti-Stokes line is much less intense than the Stokes line. Because only molecules that were in the first vibrational level of the excited state would lead to anti-Stokes lines, and at room temperature there are few molecules in the aforementioned level. The most intense Stokes line is measured in Raman scattering.

A high power monochromatic excitation source is needed in spontaneous Raman scattering, to separate the weak inelastically scattered light from the intense Rayleigh scattered light. So, typically, the sample is illuminated with a laser beam in the visible, near IR, or near UV range. By combining Raman scattering and a conventional optical microscope, Raman microstructural investigations on the micrometer scale are possible. The experimental set-up used consisted of a Jobin-Ybon T64000 spectrometer with excitation in the visible by a cw argon laser (Coherent INNOVA 300, λ = 514 nm). Behind a triple-monochromator (1800g/mm), the light was detected by a two-dimensional CCD matrix with liquid N_2. A pre-monochromator eliminated the

UNIVERSITAT ROVIRA I VIRGILI
YTTERBIUM AND ERBIUM DOPEP RbTi1-xMxOPO4 (M=Nb or Ta) CRYSTALS. NEW LASER AND NONLINEAR BIFUNCTIONAL MATERIALS
Alexandra Peña Revellez
ISBN: 978-84-691-0370-8 /DL:T.2188-2007

plasma discharge lines of the argon laser. A microscope (Olympus BH2) with high resolution was used to locate the laser spot in the sample. The laser power incident on the sample was about 3.9 mW. We chose a backward scattering scheme to increase the signal-to-noise ratio. This equipment is available at the *Servei de Recursos Científico-Tècnics* of the *Universitat de Barcelona*.

2.9 Linear optical characterization

When dealing with a nonlinear optical material, it is important to accurately measure the refractive indexes in order to make reliable predictions of the phase-matching directions.

When an electric field (E) of angular frequency ω is incident on an isotropic dielectric medium, an electric polarization (P) is generated and is parallel to the electric field. The relation between the electric field and the electric polarization is given by

$$P(\omega) = \varepsilon_0 \chi E(\omega) \qquad \text{eq. 2.5}$$

where χ, that is related with the dielectric constant ($\varepsilon = \varepsilon_0(1+\chi) = \varepsilon_0\varepsilon_r$), is the electric susceptibility, which is only a constant in an isotropic dielectric medium, but is a second rank tensor (χ_{ij}) in anisotropic dielectric media, where usually the polarization field is not parallel to the electric field

$$P_i(\omega) = \sum_j \varepsilon_0 \chi_{ij} E_j(\omega) \qquad \text{eq. 2.6}$$

Since the optical susceptibility is a second rank tensor (χ_{ij}), the refractive index in an anisotropic dielectric medium can also be represented as a second order tensor (n_{ij})

$$n_{ij} = \sqrt{1+\chi_{ij}} = \sqrt{\varepsilon_{rij}} = \begin{pmatrix} n_{11} & n_{12} & n_{13} \\ n_{21} & n_{22} & n_{23} \\ n_{31} & n_{32} & n_{33} \end{pmatrix} \qquad \text{eq. 2.7}$$

The symmetric nature of this tensor was demonstrated by the Onsanger theorem.[100] So, only six values (n_{11}, n_{22}, n_{33}, n_{12}, n_{13}, n_{23}) are needed to determine the refractive index tensor. And a symmetric matrix can be diagonalised by calculating the eigenvalues by using the principal axes as eigenvectors. So, the

UNIVERSITAT ROVIRA I VIRGILI
YTTERBIUM AND ERBIUM DOPEP RbTi1-xMxOPO4 (M=Nb or Ta) CRYSTALS. NEW LASER AND NONLINEAR BIFUNCTIONAL MATERIALS
Alexandra Peña Revellez
ISBN: 978-84-691-0370-8 /DL:T.2188-2007

refractive index tensor is described as a diagonal matrix, representing each value a principal direction

$$n_{ij} = \begin{pmatrix} n_{11} & 0 & 0 \\ 0 & n_{22} & 0 \\ 0 & 0 & n_{33} \end{pmatrix} \qquad \text{eq. 2.8}$$

And, this diagonalised tensor can be geometrical visualized through the Fresnel ellipsoid that it can be expressed as

$$\frac{x^2}{n_{11}^2} + \frac{y^2}{n_{22}^2} + \frac{z^2}{n_{33}^2} = 1 \qquad \text{eq. 2.9}$$

The ellipsoid represents the refractive index value for any spatial direction and is called the optical ellipsoid, which intercepts the principal axis ***X***, ***Y*** and ***Z*** at $\pm n_x$, $\pm n_y$ and $\pm n_z$.

The crystal symmetry gives additional information over the symmetric form of the second order tensor and helps to experimentally localize the principal axes by the Neumann principle. For the orthorhombic, $Pna2_1$, RTP crystals the refractive indices (n_x; n_y; n_z) along the principal directions (***X***, ***Y*** and ***Z***) are different, coinciding the principal directions with the crystallographic axes ***a***, ***b*** and ***c***.

The refractive indices were measured by using the minimum deviation angle method,[7,101] slightly modified (semi-prism with an angular directrix $\alpha/2$ were used). A monochromatic light beam passing through a prism of angular directrix α and refractive index n is deviated from its incident path at a certain angle δ. The deviation angle is minimal (δ_{min}) for a particular incident angle, when the incident and the reflected beams coincide in their paths, and then the refractive index is:

$$n = \frac{\sin(\alpha + \delta_{\min}/2)}{\sin(\alpha/2)} \qquad \text{eq. 2.10}$$

We cut and polished two semi-prisms from $RbTi_{1-x}Nb_xOPO_4$ with an angle of about 22.5º between the faces, one of which was a principal plane: ***X***-***Z*** and ***Y***-***Z***, respectively. The measurements, which were performed in the experimental set up shown in Figure 2.5, consists of illuminating the first face of the prism by an unpolarized laser beam under normal incidence, and then the prism was

UNIVERSITAT ROVIRA I VIRGILI
YTTERBIUM AND ERBIUM DOPEP RbTi1-xMxOPO4 (M=Nb or Ta) CRYSTALS. NEW LASER AND NONLINEAR BIFUNCTIONAL MATERIALS
Alexandra Peña Revellez
ISBN: 978-84-691-0370-8 /DL:T.2188-2007

rotated until incidence on the second face (the principal plane) was normal. The minimum deviation angle (δ_{min}), for different wavelengths, was measured.

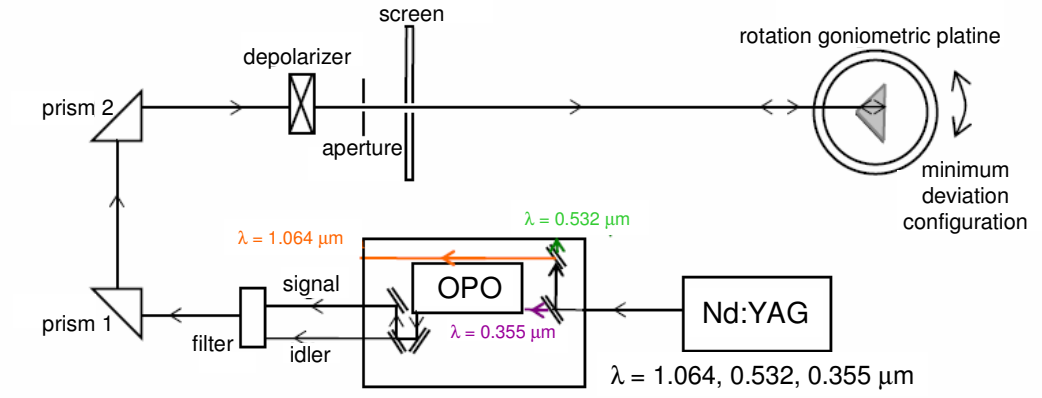

Figure 2.5. Experimental set-up for the measurements of refractive indices measurements.

The thermal dependence of the $RbTi_{1-x}Nb_xOPO_4$ principal refractive indices, at 632.8 nm, was analyzed using a prism coupler (Metricon model 2010) that scans the incidence angle to determine the critical angle for total internal reflection (TIR). The temperature range studied goes from room temperature (298 K) to 393 K, covering the temperature range subjected on the crystals during laser operation. To ensure good coupling of the studied samples with the prism, we used very thin (< 1 mm) polished plate-shaped samples.

2.10 Nonlinear optical characterization

Moreover to determine the $RbTi_{1-x}Nb_xOPO_4$ refractive indices and their thermal evolution, we determined if its nonlinear optical properties are comparable to those from KTP or RTP. So, we are going to explain the experimental set-up used to determine the second harmonic generation efficiency in powder samples and in single crystals, and the phase matching directions.

UNIVERSITAT ROVIRA I VIRGILI
YTTERBIUM AND ERBIUM DOPEP RbTi1-xMxOPO4 (M=Nb or Ta) CRYSTALS. NEW LASER AND NONLINEAR BIFUNCTIONAL MATERIALS
Alexandra Peña Revellez
ISBN: 978-84-691-0370-8 /DL:T.2188-2007

2.10.1 Second Harmonic Generation efficiency

Powder Samples

In powdered samples it is possible to determine the averaged nonlinear efficiency, as demonstrated by Kurtz and Perry in 1968.[4] They demonstrated that second harmonic generation (SHG) studies could be performed on crystalline powders, and that the second-harmonic intensity of powdered samples depends on four parameters: the angle between detector and the direction of the incident light beam (θ), the thickness of the cell containing the powder sample (L), the average particle size ($\hat{r}$) and the laser beam diameter (D). The consideration that all the crystallographic orientations are equally represented in the powder, which will give an averaged nonlinear intensity of the studied material is accomplished when the average particle size is smaller than the thickness of the cell containing the powdered sample and smaller than the diameter of the laser beam ($\hat{r} \langle\langle L \langle\langle D$). Moreover to this consideration, the powdered sample particles should have almost identical size, should be randomly oriented and densely packed to obtain a reliable measurement of an average of the nonlinear intensity. So, to try to obtain a good measurement of the nonlinear measurements we powdered and graded with standard sieves small crystals of doped RTP to obtain a uniform particle size between 5 and 20 μm. The obtained powdered sample was uniformly packed in a 2 mm-thick quartz cell.

The experimental set-up used to make the measurements (available at *FiCMA*) is depicted in Figure 2.6. The sample is irradiated by a Nd:YAG laser emitting at 1064 μm, and the fundamental power, at this wavelength, reflected by the sample was measured using a Silicon PIN. The doubled beam generated by the sample was focused with a lens to a Silicon PIN and an interferometric filter to eliminate the non-doubled portion of the incident power. The ratio between the intensity of the maxima obtained from the fundamental power and that obtained from the doubled beams generated, averaging ≈ 100 laser shots, gave an estimation of the second harmonic generation efficiency of the samples. As a standard, to evaluate the second harmonic generation efficiency of the

UNIVERSITAT ROVIRA I VIRGILI
YTTERBIUM AND ERBIUM DOPEP RbTi1-xMxOPO4 (M=Nb or Ta) CRYSTALS. NEW LASER AND NONLINEAR BIFUNCTIONAL MATERIALS
Alexandra Peña Revellez
ISBN: 978-84-691-0370-8 /DL:T.2188-2007

studied samples, we used the efficiency measured in a KTP powdered sample, the nonlinearity of which is well establish in the literature.[13]

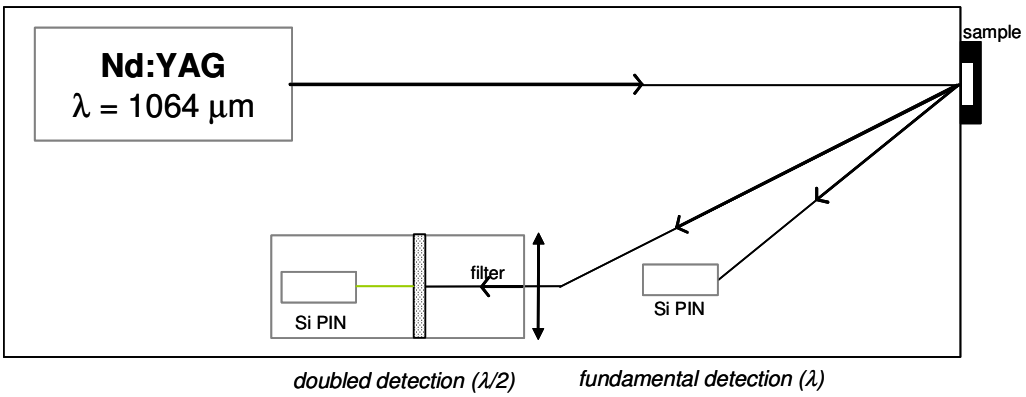

Figure 2.6. Experimental set-up used to measure SHG efficiency in powdered samples.

Single Crystal Samples

The second harmonic conversion efficiency is defined as the ratio between the intensity of the doubled beam and the intensity of the fundamental beam

$$\eta_{SHG}(L) = I^{2\omega}(L) \Big/ I^{\omega}(0) \qquad \text{eq. 2.11}$$

along the principal axes of the index surface (where there is no walk-off angle) $I(2\omega,L) \propto L^2$. In order to compare the second harmonic conversion efficiency obtained in RTP doped samples (θ = 90°; φ = 90°) with the one obtained in a KTP sample (θ = 90°; φ = 23°), the length (L) of both samples should be comparable. In our case, the samples have a length of ≈ 2.5 mm, and the intensity of the fundamental beam ($I(\omega,0)$) and the intensity of the doubled generated beam, were detected by a silicon PIN and displayed on an oscilloscope. Before evaluating the obtained signals, collected at different wavelengths, they were corrected because the sensitivity of the Si PIN is different depending on the wavelength.

The measures of the second harmonic conversion efficiency in doped RTP single crystal samples were performed by using the same experimental set-up used in the measurement of the type II SHG angular non critical phase-

UNIVERSITAT ROVIRA I VIRGILI
YTTERBIUM AND ERBIUM DOPEP RbTi1-xMxOPO4 (M=Nb or Ta) CRYSTALS. NEW LASER AND NONLINEAR BIFUNCTIONAL MATERIALS
Alexandra Peña Revellez
ISBN: 978-84-691-0370-8 /DL:T.2188-2007

matching fundamental wavelength, which is described and shown in Figure 2.7.

2.10.2 Determination of the phase-matching directions

The power of the doubled wave $P(\theta,\varphi,\omega_3,L)$ generated by a sum-frequency generation (SFG) process, for collinear waves, is highly dependent on the phase mismatch ($\Delta\kappa$) according to

$$P(\theta,\varphi,\omega_3,L) \propto P(\theta,\varphi,\omega_1,0)P(\theta,\varphi,\omega_2,0)\chi^{(2)}_{eff}(\theta,\varphi,\omega_3)L^2\sin c^2(\Delta\kappa/2) \qquad \text{eq. 2.12}$$

being $\Delta\kappa$ the phase-mismatch between the nonlinear polarisation $P^{NL}(\omega_1,\theta,\varphi)$ and the electromagnetic field $E(\omega_1,\theta,\varphi)$ inside a crystal, according to the equation

$$\Delta\kappa = \frac{n^{\pm}(\omega_3,\theta,\varphi)\omega_3}{c} - \left(\frac{n^{\pm}(\omega_1,\theta,\varphi)\omega_1}{c} + \frac{n^{\pm}(\omega_2,\theta,\varphi)\omega_2}{c}\right) \qquad \text{eq. 2.13}$$

being $n^{\pm}$ the two possible values that can take the refractive index in a given direction of propagation.

$P^{2\omega}$ increases as a quadratic function of L, only when light propagates along a phase matching direction, when the phase mismatch is null ($\Delta\kappa = 0$), when there is a perfect matching between the nonlinear polarization and the electromagnetic field. The phase-matching condition ($\Delta\kappa = 0$) in the case of collinear waves depending on (θ,φ) for a sum-frequency doubling process is given by:

$$n^{\pm}(\omega_3,\theta,\varphi)\omega_3 = n^{\pm}(\omega_1,\theta,\varphi)\omega_1 + n^{\pm}(\omega_2,\theta,\varphi)\omega_2 \text{ ; with } \omega_3 = \omega_1 + \omega_2 \qquad \text{eq.2.14}$$

In the case of second harmonic generation (which is a particular case of SFG), $\omega_3 = 2\omega$ and $\omega_1, \omega_2 = \omega$, the phase-matching condition is given by

$$n^{\pm}(2\omega,\theta,\varphi)2\omega = n^{\pm}(\omega,\theta,\varphi)\omega + n^{\pm}(\omega,\theta,\varphi)\omega \qquad \text{eq.2.15}$$

And the phase-matching interactions, under normal dispersion, should fulfill the condition: $n^{\pm}_{2\omega} \rangle n^{\pm}_{\omega}$.

UNIVERSITAT ROVIRA I VIRGILI
YTTERBIUM AND ERBIUM DOPEP RbTi1-xMxOPO4 (M=Nb or Ta) CRYSTALS. NEW LASER AND NONLINEAR BIFUNCTIONAL MATERIALS
Alexandra Peña Revellez
ISBN: 978-84-691-0370-8 /DL:T.2188-2007

Although there are two types of collinear phase-matching, we are going to explain type II. In this type of collinear phase-matching, the fundamental waves have orthogonal polarizations

$$n^{-}(2\omega,\theta,\varphi)2\omega = n^{+}(\omega,\theta,\varphi)\omega + n^{-}(\omega,\theta,\varphi)\omega \qquad \text{eq.2.16}$$

The allowed phase-matching directions in acentric biaxial crystals for type II SHG are obtained by considering the intersections of the index surfaces at the fundamental and harmonic frequencies. The representation of index surfaces for a positive biaxial crystal ($n_x < n_y < n_z$) is shown in Figure 2.7.[15]

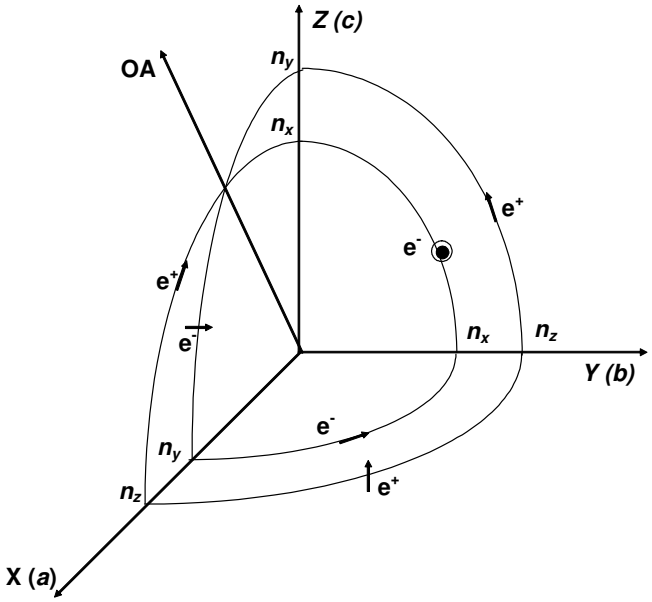

Figure 2.7. Index surfaces of the positive biaxial class. e^+ and e^- are the electric field vectors relative to the external (+) or internal (-) sheets for propagation in the principal planes. OA is the optic axis.

The experimental measurements to determine type II non critical phase-matching fundamental wavelenghts (λ_{NCPM}) in the ***ab*** plane, were performed in cube-shaped samples placed at the center of a three Euler goniometric device. The polished faces of the samples were perpendicular to the ***a*** and ***b*** crystallographic directions (***x*** and ***y*** optical axis, respectively) and only normal incidences were studied. To ensure type II SHG, an achromatic half-wave plate was set to 22.5º and placed between the laser source and the sample (see

UNIVERSITAT ROVIRA I VIRGILI
YTTERBIUM AND ERBIUM DOPEP RbTi1-xMxOPO4 (M=Nb or Ta) CRYSTALS. NEW LASER AND NONLINEAR BIFUNCTIONAL MATERIALS
Alexandra Peña Revellez
ISBN: 978-84-691-0370-8 /DL:T.2188-2007

Figure 2.8), and the λ_{NCPM} (when the conversion efficiency is maximum) was checked for each of the studied samples and at θ = 90°; φ = 0° and θ= 90°; φ = 90°. The equipment used was avalaible at the *Laboratoire de Spectrométrie Physique* of the *Université Joseph Fourier*.

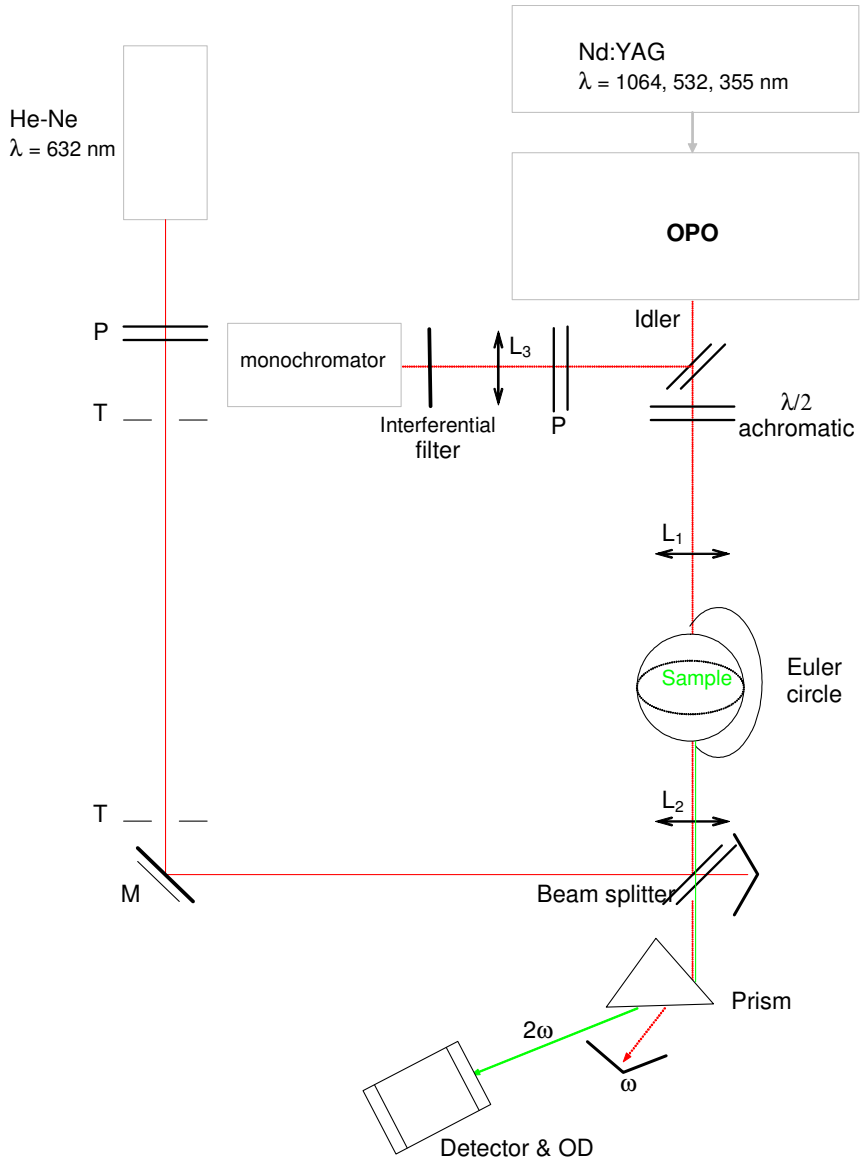

Figure 2.8. Experimental set-up used to measure the angular non critical phase-matching wavelengths on $RbTiOPO_4$ doped samples.

UNIVERSITAT ROVIRA I VIRGILI
YTTERBIUM AND ERBIUM DOPEP RbTi1-xMxOPO4 (M=Nb or Ta) CRYSTALS. NEW LASER AND NONLINEAR BIFUNCTIONAL MATERIALS
Alexandra Peña Revellez
ISBN: 978-84-691-0370-8 /DL:T.2188-2007

2.11 Spectroscopic characterizations

In this section we will analyse the fundamentals of the spectroscopic techniques used in this thesis.

2.11.1 Absorption and transmission measurements

The amount of absorbed light when an electromagnetic wave passes through a material depends on the wavelength of light, and to measure the decrease in intensity of the wave when passing through the material we used the absorption coefficient ($\alpha(cm^{-1})$), and to determine this parameter we used the Beer's law which relates I to I_0 (incident light intensity) via the equation

$$I = I_0 e^{-\alpha d} \qquad \text{eq.2.17}$$

where d (cm) is the thickness of the sample.

To measure the absorption, which is reflected in the variation of the intensity of the electromagnetic radiation, we can measure the optical density (OD) with a doubled ray spectrophotometer

$$OD = -\log(I / I_0) \qquad \text{eq.2.18}$$

And by combining these two equations, we can correlate the absorption coefficient (α) with the optical density (OD)

$$\alpha = OD\left(\frac{1}{d \log e}\right) \qquad \text{eq.2.19}$$

Moreover, the absorption coefficient (α) can be correlated with the absorption cross-section ($\sigma_{abs}(cm^2)$) of every absorbing ion as

$$\sigma = \frac{\alpha}{N} \qquad \text{eq.2.20}$$

where N (ions/cm^3) is the density of absorbent centers.

The absorption measures were done in a Varian Cary 500 Scan spectrophotometer, which is available at *FiCMA*. The main features of this equipment are that it is a double ray spectrophotometer with an effective spectral range from 0.175 to 3.3 μm and that can measure optical densities

UNIVERSITAT ROVIRA I VIRGILI
YTTERBIUM AND ERBIUM DOPEP RbTi1-xMxOPO4 (M=Nb or Ta) CRYSTALS. NEW LASER AND NONLINEAR BIFUNCTIONAL MATERIALS
Alexandra Peña Revellez
ISBN: 978-84-691-0370-8 /DL:T.2188-2007

from 0 to 10. It has two monochromators that can separate 1200 lines/mm in the UV-visible region and 300 lines/mm in the IR region. Its light source is a Deuterium lamp (in the UV region) and a quartz halogen lamp (in the visible-IR region). The UV-visible light is detected by a photomultiplier and the IR light by a lead sulphide detector. As we expected absorption dichroism, we used a Glan-Thompson polarizer positioned before the sample, and the aperture diameter was appropriately set for each sample in order to avoid crystal-edge obscurations. To measure the absorption at low temperatures (6K), we used a Leybold helium closed circuit cryostat with a temperature controller that stabilizes the temperature in the 6 to 100 K range with a precision of ± 3 K and in the 200 to 300 K range with a precision of ± 5 K.

The transmission measurements, between 0.3 and 3 μm, were performed in the same spectrophotometer described above, and between 3 and 10 μm in a FT-IR-680 Plus Fourier transformed infrared spectrophotometer, available at the *Servei de Recursos Científics i Tècnics* of the *Universitat Rovira i Virgili*.

2.11.2 Luminescence measurements

The result of a radiative transition of an electron from an excited or higher energy level to a lower energy level is optical emission (or luminescence). The luminescence spectra are determined by fixing the excitation wavelength and changing the detection wavelength.

The excitation wavelength, in the fluorescence measurements, was provided by a 200 mW InGaAs diode laser emitting at 0.94 μm, which was modulated at 1 kHz. The luminescence was recorded in 90º geometry to minimize the influence of the laser pump and it was dispersed by a doubled monochromator (Jobin Ybon-Spex HR460) with o focal length of 460 mm and detected by a cooled Hamamatsu NIR R5509-72 photomultiplier which was connected to a lock-in amplifier. This lock-in amplifier (EG&G 7265 DSP) processes the obtained signals. Figure 2.9 illustrates the experimental set-up used to measure luminescence.

UNIVERSITAT ROVIRA I VIRGILI
YTTERBIUM AND ERBIUM DOPEP RbTi1-xMxOPO4 (M=Nb or Ta) CRYSTALS. NEW LASER AND NONLINEAR BIFUNCTIONAL MATERIALS
Alexandra Peña Revellez
ISBN: 978-84-691-0370-8 /DL:T.2188-2007

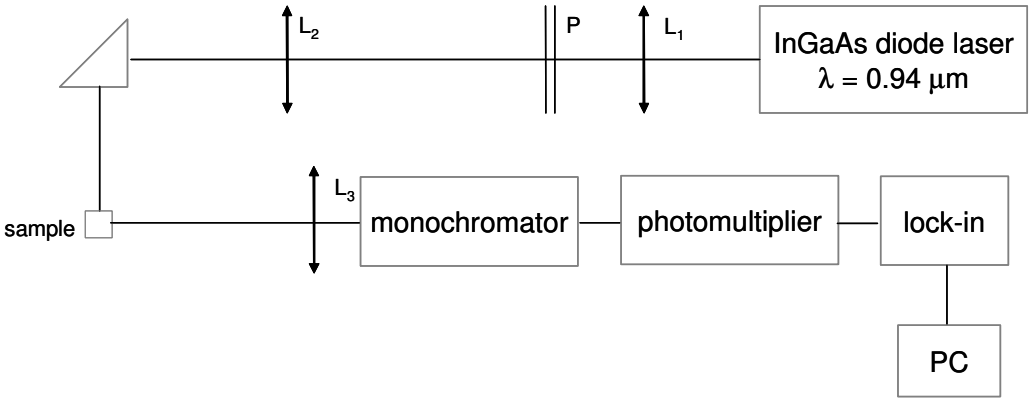

Figure 2.9. Experimental set-up used to measure Yb^{3+} luminescence in $RbTi_{1-x}Nb_xOPO_4$ and $RbTi_{1-x}Ta_xOPO_4$.

2.12 Laser set-up

Ytterbium doped $RbTi_{1-x}Nb_xOPO_4$ laser experiments were made in a standard, astigmatically compensated Z-shaped cavity 150 cm long (Figure 4 in *paper II* and Figure 2 in *paper III*), which is available at the *Max-Born Institute for Non-linear Optics and Ultrafast Spectroscopy*. At the ends of the cavity there were two plane reflectors, a rear mirror (M3) and an output coupler (M4) whose transmission ranged from 1 to 3 % (T_{oc} = 1 and 3 %).

The pump source was a home-made Ti:sapphire laser (λ_{pump} = 972.7 nm, FWHM<1 mm, max. 1.8 W), with the beam focused onto the sample by an anti-reflection lens of f = 6.28 cm, the focus of which had a waist of ≈ 30 μm. The pumping was done in a single-pass. The uncoated $Yb:RbTi_{1-x}Nb_xOPO_4$ sample was attached to a Cu-holder without active cooling and positioned under Brewster angle between the two folding mirrors.

UNIVERSITAT ROVIRA I VIRGILI
YTTERBIUM AND ERBIUM DOPEP RbTi1-xMxOPO4 (M=Nb or Ta) CRYSTALS. NEW LASER AND NONLINEAR BIFUNCTIONAL MATERIALS
Alexandra Peña Revellez
ISBN: 978-84-691-0370-8 /DL:T.2188-2007

Chapter 3

Crystal growth, morphological and structural characterization

Crystal growth is science and technology, and crystals fascinate not only for their appearance but also for their physical properties.

Although crystals were mainly used in jewellery in the 19th century, during the last fifty years, they became the basis for a large number of electronic, optoelectronic and optical devices, and since then there has been an increasing demand of crystals. So, the scientific understanding of crystal growth technology is necessary to cover the demands for crystals to be used in novel technologies. Moreover, the crystal structure and their symmetry are related to interesting physical properties, which should be studied in order to determine if one crystal would be theoretically useful for a specific application.

3.1 Crystallization region of Yb:$RbTi_{1-x}Ta_xOPO_4$

We already know the crystallization region of RTP in its self flux and tungstate fluxes[102] and that it decomposes before melting, at 1343 K,[95] so melt growth methods could not be used to grow RTP single crystals. We grew the doped RTP crystals from high-temperature solutions. One of the most important things while working with high temperature solution growth techniques is to choose an appropriate solvent and determine the properties of the solution used. The knowledge of such properties is particularly important for choosing the best growth conditions.[103]

For determining the crystallization region of Yb:$RbTi_{1-x}Ta_xOPO_4$ we previously investigated the RTP phase diagram in the ternary system Rb_2O-P_2O_5-TiO_2 and the crystallization region of Yb:$RbTi_{1-x}Nb_xOPO_4$,[93] by using an excess of the first two oxides (Rb_2O and P_2O_5) as a solvent, and chose three solution compositions with different ratios of the precursor oxides (Rb_2O-P_2O_5-TiO_2) placed far from the boundary lines between RTP and neighbouring phases, as could be seen in Figure 3.1. The three phase diagrams, which are shown in Figure 1 of *paper I*, were performed by successively replacing TiO_2 by Ta_2O_5 or Yb_2O_3 or both together and keeping constant the ratio between Rb_2O and P_2O_5, as explained in *paper I*. X-ray powder diffraction analysis was performed for each of the crystals obtained to determine the phase in which they crystallize, in order to evaluate the maximum concentration of Ta_2O_5 and Yb_2O_3 added in the initial solution allowed without losing the RTP phase. This concentration, also called the critical concentration, is also added in Figure 3.1, as well as the three different molar compositions used. The right and left position of Ta_2O_5 and Yb_2O_3, respectively, from the initial molar solution composition chosen, is because it seemed to be consistent the relation between the critical amount obtained for tantalum and ytterbium oxides and the distance from the starting point to the border lines of the RTP crystallization region. Before the X-ray powder diffraction analysis, which lead us to identify three different phases, $RbTiOPO_4$, $RbTiPO_5$ and $Rb_2Ti_2(PO_4)_3$, the shape of the obtained crystals was firstly observed by reflection optical microscopy and then by scanning electron microscopy (SEM). Pictures of the three different phases obtained are also shown in *paper I* (Figure 1).

UNIVERSITAT ROVIRA I VIRGILI
YTTERBIUM AND ERBIUM DOPEP RbTi1-xMxOPO4 (M=Nb or Ta) CRYSTALS. NEW LASER AND NONLINEAR BIFUNCTIONAL MATERIALS
Alexandra Peña Revellez
ISBN: 978-84-691-0370-8 /DL:T.2188-2007

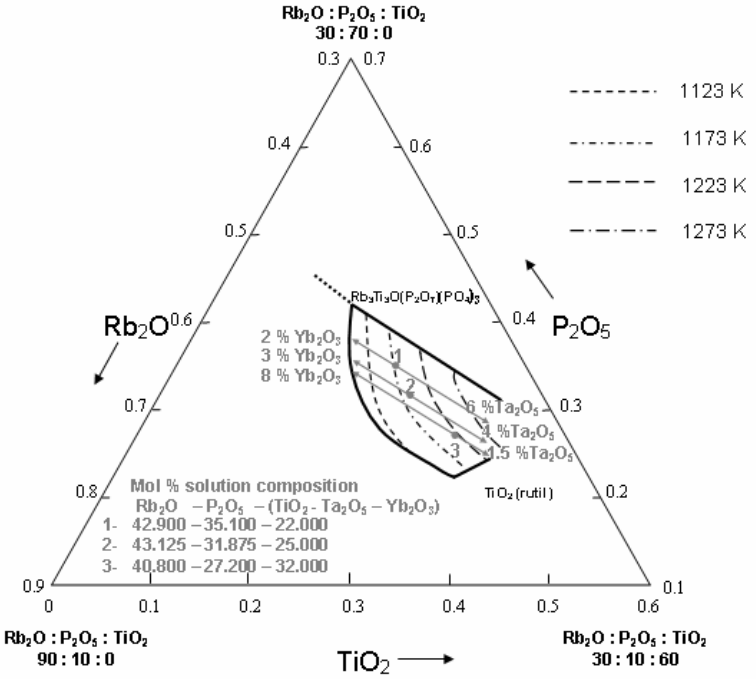

Figure 3.1. RTP crystallization region,[102] showing the three different solution compositions studied and the obtained Ta_2O_5 and Yb_2O_3 critical concentrations.

The stoichiometry and the distribution coefficients (K_i) of some of the crystals obtained were determined by electron probe microanalysis (EPMA). The distribution coefficients for Ti^{4+} (K_{Ti}), Ta^{5+} (K_{Ta}) and Yb^{3+} (K_{Yb}) are listed in Table 1 of *paper I*, being $K_{Ta} > 1$ and $K_{Yb} < 1$. These values are well explained in terms of the differences between the ionic radii in an octahedral environment of Ti^{4+} (r_{Ti}^{4+} = 0.605 Å), Ta^{5+} (r_{Ta}^{5+} = 0.640 Å) and Yb^{3+} (r_{Yb}^{3+} = 0.868 Å).[104] The easiness incorporation of Ta^{5+}, as measured by the concentration of Ta^{5+} in crystals was always higher than the one expected by considering the initial Ta_2O_5 added in the initial solution, and that was also observed in Ta:KTP.[105] We propose that this phenomenon was due to the tendency of tantalum atoms to occupy the two non-equivalent titanium positions of the lattice.

The determination of these crystallization regions lead us to choose the best solution composition to further obtain single crystals of the desired orthorhombic phase with the maximum dopant (Yb^{3+}) concentration. The optimal solution composition, with a high value of K_{Yb} and being not to close to the limit between different phases, was: Rb_2O-P_2O_5-(TiO_2+Ta_2O_5+Yb_2O_3) = 40.800-27.200-(31.040-0.320-0.640).

3.2 Comparative study between the crystallization regions of Yb:$RbTi_{1-x}Ta_xOPO_4$ and Yb:$RbTi_{1-x}Nb_xOPO_4$

The main objective in determining these crystallization regions was to find out if using codopants such as niobium or tantalum enhances of the Ln^{3+} ions (RE^{3+} ions) concentration achieved in KTP[74-76] and RTP[75] grown by TSSG-SC, and which solution composition was the best for this purpose. In 1997 it was pointed out by Solé *et al.* that the Ln^{3+} concentration incorporated in KTP was enhanced by codoping with Nb^{5+} and Rb^{+} and that the value of the Ln^{3+} ions distribution coefficient was larger when the ionic radii of Ln^{3+} ions was smaller,[74] as shown in Figure 1.2. So, with this previous knowledge, it seems that it was better to codope RTP than KTP, since Rb^{+} has a higher ionic radius than K^{+} the crystalline cell is a little bit expanded in RTP, and the incorporation of Nb^{5+} or Ta^{5+} and Ln^{3+} will be easier.

The crystallization regions of Yb:$RbTi_{1-x}Nb_xOPO_4$ were previously determined[93] and the Yb:$RbTi_{1-x}Ta_xOPO_4$ domains have been determined during the course of this thesis, and are shown in *paper I*. In the case of Yb:$RbTi_{1-x}Nb_xOPO_4$, two different solutions compositions were checked which match with two of the three studied for Yb:$RbTi_{1-x}Ta_xOPO_4$. The main differences between the crystallization regions obtained is that as the Ta^{5+} is more easily incorporated into the lattice than Nb^{5+}, the Yb:$RbTi_{1-x}Ta_xOPO_4$ crystallization regions are narrower than those seen with Yb:$RbTi_{1-x}Nb_xOPO_4$. The maximum Nb_2O_5 added in the initial solution, before attaining the RTP high temperature phase ($RbTiPO_5$), was 9 and 5 mol % (of TiO_2+Nb_2O_5 mol %) in the initial solutions with a molar composition of Rb_2O-P_2O_5-TiO_2 = 43.125-31.875-25.000 and 40.800-27.200-32.000 respectively, and the maximum of Ta_2O_5 was 4 and 1.5 mol % (of TiO_2+Ta_2O_5 mol %). So, in both cases, when the solutions are richer in TiO_2 the Nb_2O_5 and Ta_2O_5 critical concentrations are lower but the Yb_2O_3 is higher. Moreover, by checking the K_{Yb} obtained in solutions richer in TiO_2, see Table 3.1, we observed that this value is higher than those obtained in solutions poorer in TiO_2. These observations, as explained in the previous section, lead us to choose the better solution composition to be used to grow bulk single crystals with a higher ytterbium concentration, although the K_{Yb} would not be exactly the same in the small

UNIVERSITAT ROVIRA I VIRGILI
YTTERBIUM AND ERBIUM DOPEP RbTi1-xMxOPO4 (M=Nb or Ta) CRYSTALS. NEW LASER AND NONLINEAR BIFUNCTIONAL MATERIALS
Alexandra Peña Revellez
ISBN: 978-84-691-0370-8 /DL:T.2188-2007

crystals grown by spontaneous nucleation (the ones used in these studies) than in the bulk crystals grown by TSSG-SC technique.

Table 3.1. *Distribution coefficients of Nb^{5+} (K_{Nb}), Ta^{5+} (K_{Ta}) and Yb^{3+} (K_{Yb}) obtained in solutions with different molar composition.*

Crystallization region	***Solution composition*** [mol %] ***Rb_2O-P_2O_5-(TiO_2+(Nb_2O_5 or Ta_2O_5)+Yb_2O_3)***		
$Yb:RbTi_{1-x}Nb_xOPO_4$[93]	43.10-31.90-(24.00+0.50+0.50) K_{Nb}=0.85 K_{Yb}=0.30	40.80-27.20-(30.72+0.64+0.64) K_{Nb}=1.05 K_{Yb}=0.56	
$Yb:RbTi_{1-x}Ta_xOPO_4$	42.90-35.10-(21.34+0.44+0.22) K_{Ta}=1.34 K_{Yb}=0.16	43.10-31.90-(24.25+0.50+0.25) K_{Ta}=2.30 K_{Yb}=0.31	40.80-27.20-(31.04+0.64+0.32) K_{Ta}=1.34 K_{Yb}=0.45

It seems that the ytterbium concentration achieved in RTP by using Ta^{5+} or Nb^{5+} as codopants (see Table 3.1), would be of the same order, ≈ 2×10^{20} ions/cm^3.[93] So, it makes sense to grow single crystals of $Yb:RbTi_{1-x}Ta_xOPO_4$, and the growth experiments are explained in next section.

3.3 Crystal growth of $RbTi_{1-x}Ta_xOPO_4$ doped with Yb^{3+} in self flux

The experimental conditions as well as the results of the crystal growth experiments of $Yb:RbTi_{1-x}Ta_xOPO_4$ are explained in *paper I* and *paper II* of this thesis. But, in this section we are going to make a general discussion of the main results obtained until now.

All the crystal growth experiments were made in solutions, weighting ≈ 30 g, with the same molar composition (Rb_2O-P_2O_5-(TiO_2+Ta_2O_5+Yb_2O_3) = 40.80-27.20-(31.04-0.32-0.64)), which were prepared by mixing the precursor oxides in the desired ratios in a small conical crucible (25 cm^3). The seed used in the first experiment was a crystal obtained from spontaneous nucleation onto a Pt wire, which shows the plate-like habit, previously shown in Nb:KTP[106] and Nb:RTP.[82] And the dimensions of the crystal obtained from this seed are listed in Table 4 of *paper I*. The fact that the growth rate along ***b*** and ***c*** direction is faster than the rate obtained along the ***a*** crystallographic direction means

UNIVERSITAT ROVIRA I VIRGILI
YTTERBIUM AND ERBIUM DOPEP RbTi1-xMxOPO4 (M=Nb or Ta) CRYSTALS. NEW LASER AND NONLINEAR BIFUNCTIONAL MATERIALS
Alexandra Peña Revellez
ISBN: 978-84-691-0370-8 /DL:T.2188-2007

that the seed width (***a***) will limit the width along this direction, which is clearly seen in all the crystals listed in the aforementioned table of *paper I*.

All the crystal growth experiments were performed centered and without additional stirring, only the normal stirring produced by the rotation of the as grown crystal was used (the rotation speed was set to 60 or 80 rpm). All the crystals were grown from ***c*** oriented seeds, which were laced with Pt wire in a Pt holder placed at the end of an alumina rod. The seed was about 5 mm long in the axial direction and varied in thickness (from 1.8 to 3 mm) in the radial direction of rotation. Although the growth rate increases by using faster cooling ramps, the quality of the crystals improves considerably by applying slower cooling ramps. All the crystal growth processes lasted until spurious nucleation appears on the surface of the solution, when the crystal was slowly remove from the solution and kept some millimeters above the solution surface during the cooling process of the furnace, which was cooled to room temperature by applying a cooling ramp of 15 K/h. This slow cooling ramp was used to avoid any additional thermal stress in the crystals which could induce cracks.

Table 3.2 summarizes the relevant data associated with the Yb:$RbTi_{1-x}Ta_xOPO_4$ crystals obtained. The Yb^{3+} concentration obtained was ≈ 1.6×10^{20} ions/cm^3. Figure 3.2 shows some of the obtained crystals and a morphological scheme with the crystallographic directions and the different faces shown in the obtained crystals are labeled. As can be seen in the first photo of this figure, the crystals have a pale blue color related to the presence of Ti^{3+} in the obtained crystals. This color disappears when annealing the crystals at around 800 K during 5 h, obtaining transparent crystals as shown in the last two pictures. All the obtained crystals show a crack coming from the seed, even in those obtained by growth by over a slower cooling rate. As all the seeds used were of the same composition of the as grown crystals to avoid cracks caused by the lattice mismatch between the seed and the crystal, the presence of these cracks could be related to the presence of defects in the seeds which propagate in the nascent crystals, or even because ***c*** oriented seeds are not the best to grow these crystals. To see if using a seed with a different orientation the crack coming from the seed was avoided, we performed a crystal growth with a seed oriented along the [201] direction. The crystal obtained was

UNIVERSITAT ROVIRA I VIRGILI
YTTERBIUM AND ERBIUM DOPEP RbTi1-xMxOPO4 (M=Nb or Ta) CRYSTALS. NEW LASER AND NONLINEAR BIFUNCTIONAL MATERIALS
Alexandra Peña Revellez
ISBN: 978-84-691-0370-8 /DL:T.2188-2007

of a very bad quality (with attached crystals on the (100) and $(\bar{1}00)$ faces and cracks) because it seems that although using the cooling ramp with which the better quality crystals were obtained, the crystal growth rate obtained was higher (3 fold). With seeds oriented along this direction, single crystals of Yb:$RbTi_{1-x}Nb_xOPO_4$, grown in tungsten flux, were obtained with no crack coming from the seed (see section 3.5).

Table 3.2. *Growth data associated for Yb:$RbTi_{1-x}Ta_xOPO_4$ single crystals grown in initial solution composition Rb_2O-P_2O_5-(TiO_2+Ta_2O_5+Yb_2O_3) = 40.80-27.20-(31.04-0.32-0.64) mol % of ≈ 30 g.*

A	***B***	***C***	***D***	***E***	***F***	***G***	***H***
1	***c***	1209.5	4 16.5	1 0.1	1.84×4.24×3.97	0.06	good
2	***c***	1208	4 27.2	1 0.2	2.46×8.47×7.09	0.34	crack, inclusions
3	***c***	1208	23.2	0.2	2.49×6.58×4.95	0.17	crack, inclusions
4	***c***	1211.5	30	0.2	2.71×10.39×8.30	0.50	cracks
5	***c***	1212.5	22.6	0.1	2.34×7.83×5.75	0.19	inclusions
6	***c***	1205	1 17.6	1 0.1	2.50×3.53×4.00	0.10	good
7	***c***	1207	1 20	1 0.1	3.19×5.73×5.50	0.18	good
8	***c***	1201.6	1 18.6	1 0.1	2.62×7.11×6.69	0.27	inclusions
9	***c***	1196.1	1 22	1 0.1	3.01×6.87×7.01	0.28	good
10	**[201]**	1203.6	1 17	1 0.1	1.83×12.40×9.08	0.61	bad

A: *Growth experiment,* ***B:*** *Seed orientation,* ***C:*** *Saturation temperature* (K), ***D:*** *Cooling range* (K), ***E:*** *Cooling ramp* (K/h), ***F:*** *Crystal dimensions* (***a***×***b***×***c***) (mm), ***G:*** *Crystal weight* (g), ***H:*** *Crystal quality.*

UNIVERSITAT ROVIRA I VIRGILI
YTTERBIUM AND ERBIUM DOPEP RbTi1-xMxOPO4 (M=Nb or Ta) CRYSTALS. NEW LASER AND NONLINEAR BIFUNCTIONAL MATERIALS
Alexandra Peña Revellez
ISBN: 978-84-691-0370-8 /DL:T.2188-2007

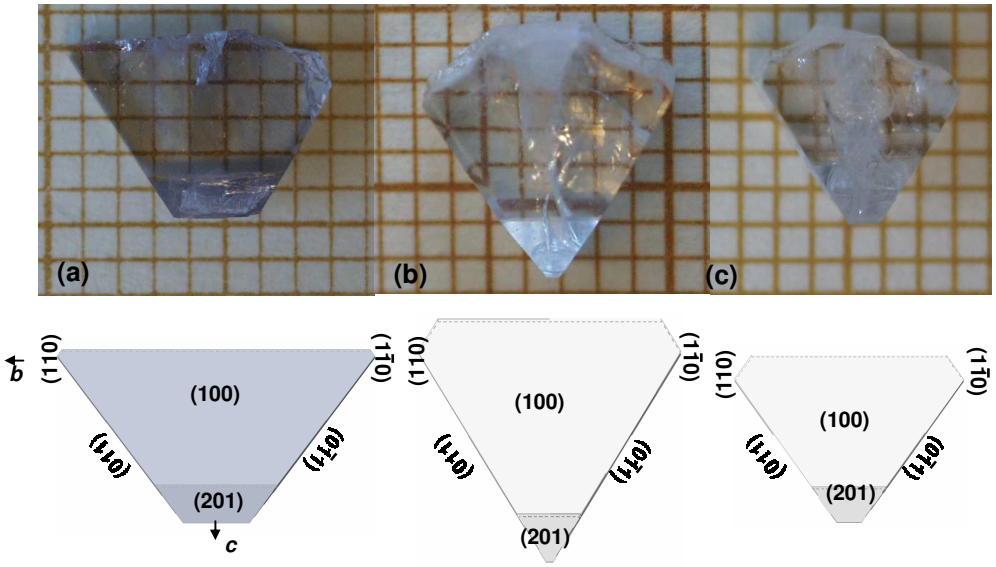

Figure 3.2. Yb:$RbTi_{1-x}Ta_xOPO_4$ crystals obtained from ***c*** oriented seeds. Crystal before annealing (a) and after annealing (b,c), and under each of this photos are the morphological schemes in projection parallel to ***a*** direction.

3.4 Crystal growth of $RbTi_{1-x}Nb_xOPO_4$ doped with Ln^{3+} ions in self flux

Crystal growth of Yb:$RbTi_{1-x}Nb_xOPO_4$, Er:$RbTi_{1-x}Nb_xOPO_4$ and Er:Yb:$RbTi_{1-x}Nb_xOPO_4$ were performed, by the TSSG-SC technique, in order to optimize the growth conditions of the Ln^{3+} mono-doped samples and to study the growth conditions of the Ln^{3+} co-doped samples. The composition of the initial solutions used to grow the crystals were determined in the study of the change of the crystallization region while codoping RTP with Nb^{5+} and Yb^{3+} and with Nb^{5+} and Er^{3+}.[93] In the case of rare earth single doping, Yb^{3+} or Er^{3+} $RbTi_{1-x}Nb_xOPO_4$, this molar % composition was: Rb_2O-P_2O_5-(TiO_2+Nb_2O_5+Yb_2O_3 or Er_2O_3) = 40.80-27.20-(30.40-0.96-0.64), and in the case of the codoped Er^{3+}/Yb^{3+} samples it was: Rb_2O-P_2O_5-(TiO_2+Nb_2O_5+Yb_2O_3+Er_2O_3) = 40.80-27.200-((30.080-X)-0.960-0.960-X), with X ranging from 0.032 up to 0.32 mol %. No more than 0.32 mol % of Er_2O_3, in the Er^{3+}/Yb^{3+} codoped samples, can be added to the initial solution because of the nucleation of the $ErPO_4$ phase.

UNIVERSITAT ROVIRA I VIRGILI
YTTERBIUM AND ERBIUM DOPEP RbTi1-xMxOPO4 (M=Nb or Ta) CRYSTALS. NEW LASER AND NONLINEAR BIFUNCTIONAL MATERIALS
Alexandra Peña Revellez
ISBN: 978-84-691-0370-8 /DL:T.2188-2007

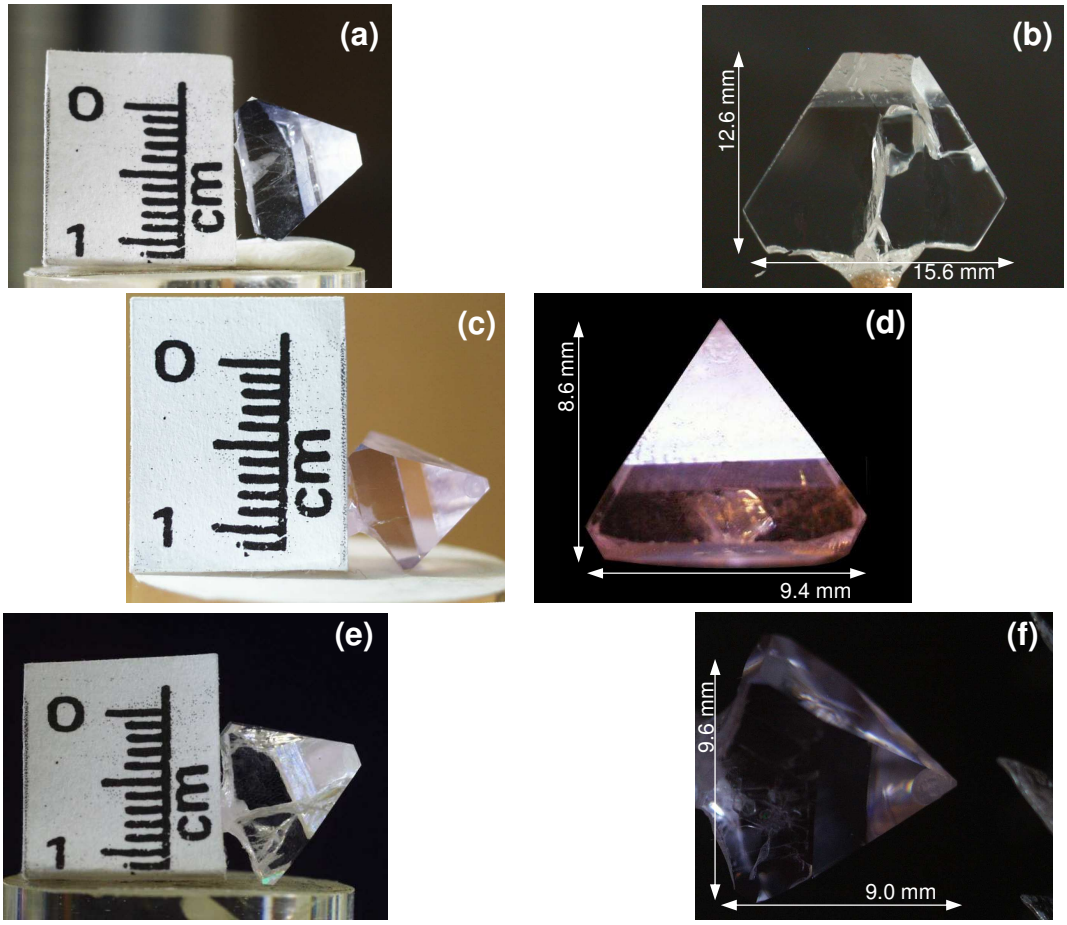

Figure 3.3. Yb:$RbTi_{1-x}Nb_xOPO_4$ crystals (a,b), Er:$RbTi_{1-x}Nb_xOPO_4$ crystals (c,d), and Er:Yb:$RbTi_{1-x}Nb_xOPO_4$ (e,f) obtained from ***c*** oriented seeds.

All these crystal growth experiments were performed in 125 cm^3 Pt crucibles and by using crystal seeds of about the same concentration of the crystal to be grown to avoid cracks caused by the possible lattice mismatch between the growing crystal and the seed crystal used, as explained in the previous section. The ***c*** oriented seeds, polished and crack free, have a width in ***a*** direction ranging from 4 to 7 mm, forcing crystal growth along this direction, and were located 5 mm offset from the rotation axis and attached to a special growth device, consisting of a Pt turbine (see right hand side scheme of Figure 2.2) to facilitate the stirring of the solution, enhancing the mass transport of the crystallization units to the seed/crystal surface. Figure 3.3 contains

UNIVERSITAT ROVIRA I VIRGILI
YTTERBIUM AND ERBIUM DOPEP RbTi1-xMxOPO4 (M=Nb or Ta) CRYSTALS. NEW LASER AND NONLINEAR BIFUNCTIONAL MATERIALS
Alexandra Peña Revellez
ISBN: 978-84-691-0370-8 /DL:T.2188-2007

photographs of the crystals, and the growth data associated to the best crystals obtained is listed in Table 3.3.

Table 3.3. *Growth data associated for Yb:RbTi$_{1-x}$Nb$_x$OPO$_4$, Er:RbTi$_{1-x}$Nb$_x$OPO$_4$ and Er:Yb:RbTi$_{1-x}$Nb$_x$OPO$_4$ single crystals obtained by the TSSG-SC technique.*

A	***B***	***C***	***D***	***E***	***F***	***G***	***H***	***I***
1	0.0 /2.0	1195.5	0.25	4.8	1 4 9.5	1 0.05 0.02	5.12×10.12×8.19	0.84
2	0.0/2.0	1187.5	0.24	5.2	1 6 10	1 0.05 0.03	5.95×16.04×16.69	2.60
3	2.0/0.0	1152.3	0.22	6.0	1 4 9.9	0.1 0.05 0.02	6.48×9.35×8.79	0.94
4	2.0/0.0	1149.8	0.22	6.0	1 4 9.5	0.1 0.05 0.02	6.27×8.26×7.69	0.63
5	0.1 /3.0	1195.5	0.28	6.4	1 6 8.4	1 0.05 0.03	7.20×9.11×9.29	1.13
6	0.5 /3.0	1184	0.28	4.0	1 6 7.5	1 0.05 0.03	4.60×8.95×9.80	0.67
7	0.8 /3.0	1175.5	0.15	4.5	1 14.5	1 0.05	5.89×9.62×9.00	1.00
8	1.0 /3.0	1167,5	0.28	7.0	1 4 8.1	0.1 0.05 0.02	7.42×6.83×7.33	0.71

A: *Growth experiment,* ***B:*** *Er$_2$O$_3$/Yb$_2$O$_3$ mol % in relation with (TiO$_2$+Nb$_2$O$_5$+Ln$_2$O$_3$) mol % added to the initial solution,* ***C:*** *Saturation temperature* (K), ***D:*** *Axial gradient* (K/mm), ***E:*** *Seed width in* ***a*** *direction* (mm), ***F:*** *Cooling range* (K), ***G:*** *Cooling ramp* (K/h), ***H:*** *Crystal dimensions* (***a***×***b***×***c***) (mm), ***I:*** *Crystal weight* (g).

UNIVERSITAT ROVIRA I VIRGILI
YTTERBIUM AND ERBIUM DOPEP RbTi1-xMxOPO4 (M=Nb or Ta) CRYSTALS. NEW LASER AND NONLINEAR BIFUNCTIONAL MATERIALS
Alexandra Peña Revellez
ISBN: 978-84-691-0370-8 /DL:T.2188-2007

Although we have obtained crystals of sufficient quality and size to perform all the characterizations that are described in the following sections, applying this technique has not been an easy task. To see if the crystal growth process improves by using tungsten flux, we performed some preliminary growth in fluxes containing different molar percentage of tungsten (see next section).

3.5 Crystal growth of $RbTi_{1-x}Nb_xOPO_4$ doped with Yb^{3+} in tungsten flux

As shown, and explained in *paper II*, RTP crystallization region becomes narrower and shows a displacement to Rb_2O rich regions in tungsten-containing fluxes,[102] single crystals of $Yb:RbTi_{1-x}Nb_xOPO_4$ could not be grown from the same solution compositions used when grown in self-fluxes.

Some different solution compositions were checked in solutions with a 10 mol % WO_3 and only one was checked in a flux containing a 20 mol % WO_3. All the crystals grown from the different solution compositions with a 10 mol % WO_3 (Rb_2O-P_2O_5-(TiO_2+Nb_2O_5+Yb_2O_3)-WO_3 = 43.875-23.625-(21.375-0.675-0.450)-10.000; 43.200-28.800-(17.100-0.540-0.360)-10.000; 45.018-28.782-(15.390-0.486-0.324)-10.000 persistently shows a crack coming from the seed, the growth rate was on the order of the rates obtained in self-fluxes, and the ytterbium incorporation in the crystals was slightly lower. Although the Yb^{3+} concentration achieved in the crystals obtained from the solution containing a 20 % WO_3 was lower than the one obtained in crystals grown in self-fluxes, and the growth rate was also of the order of the ones obtained in self-fluxes, it seems that the crack coming from the seed was completely avoided in the crystals grown from ***c*** oriented seeds and also from seeds oriented along the [201] direction. To perform these preliminary growths, some parameters, like the axial temperature gradient or the cooling rate applied during the crystal growth process, were not optimized and some inclusions appeared in the as grown crystal, as could be seen in Figure 3.4. Further crystal growth should be performed in order to enhance the quality and ensure that crack free and big size crystals (with enough Yb^{3+} concentration to ensure efficient fluorescence) could be obtained from solutions containing 20 % WO_3.

UNIVERSITAT ROVIRA I VIRGILI
YTTERBIUM AND ERBIUM DOPEP RbTi1-xMxOPO4 (M=Nb or Ta) CRYSTALS. NEW LASER AND NONLINEAR BIFUNCTIONAL MATERIALS
Alexandra Peña Revellez
ISBN: 978-84-691-0370-8 /DL:T.2188-2007

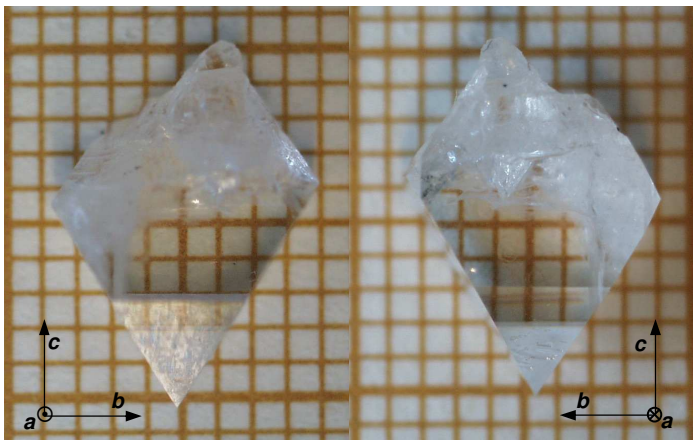

Figure 3.4. Yb:$RbTi_{1-x}Nb_xOPO_4$ crystal obtained from a seed oriented along the [201] direction from a solution composition: Rb_2O-P_2O_5-(TiO_2+Nb_2O_5+Yb_2O_3)-WO_3 = 43.820-22.580-(12.920-0.408-0.272)-20.000.

3.6 The crystal structure of $RbTiOPO_4$

As said in previous sections, the crystal symmetry of RTP, at room temperature, is orthorhombic and belongs to the non-centrosymmetric space group *Pna2₁*. The lattice parameters of RTP are *a* = 12.974(2) Å, *b* = 6.494(2) Å and *c* = 10.564(2) Å and the primitive cell contains eight formula units and four asymmetric units, each made up of two formula units.[107] This primitive cell is shown in Figure 3.5 in a projection parallel to the [010] direction, where there are shown the two non equivalent positions for each different atom. In Table 3.4 there are listed the atomic coordinates of all the atoms.

The structure of RTP and isostructural materials ($ABOXO_4$), is described as a network of chains of distorted BO_6 octahedra (in that case TiO_6) bridged by slightly distorted XO_4 tetrahedra (in that case PO_4), and a mobile framework of A atoms (Rb). In Figure 3.5 it is shown that the TiO_6 octahedra are linked by PO_4 tetrahedra with periodic bond chains in the ***a*** direction and also along the ***ac*** diagonal. $TiO_6(1)$ and $TiO_6(2)$ octahedra alternate along the ***c*** direction, forming helicoidal chains of linked TiO_6 octahedra.

UNIVERSITAT ROVIRA I VIRGILI
YTTERBIUM AND ERBIUM DOPEP RbTi1-xMxOPO4 (M=Nb or Ta) CRYSTALS. NEW LASER AND NONLINEAR BIFUNCTIONAL MATERIALS
Alexandra Peña Revellez
ISBN: 978-84-691-0370-8 /DL:T.2188-2007

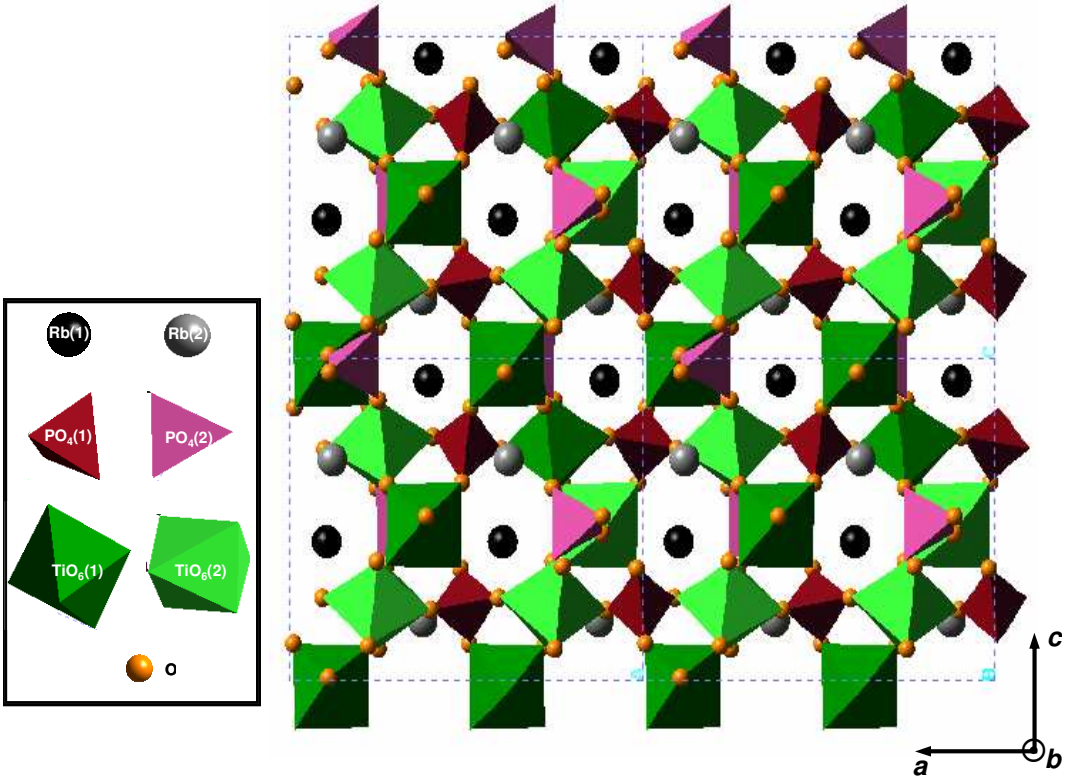

Figure 3.5. View of a projection parallel to [010] direction of the RTP structure.

Table 3.4. *Atomic coordinates and equivalent isotropic displacement parameters of $RbTiOPO_4$ from X-ray single-crystal diffraction.*[107]

Cell parameters				
a **= 12.974(2) Å,** ***b*** **= 6.494(2) Å,** ***c*** **= 10.564(2) Å,** ***V*** **= 890.0(7) Å^3;** ***Pna2$_1$***				
atom	***x***	***y***	***z***	U_{iso}**(Å^2)**
Ti(1)	0.37284(6)	0.4998(1)	0.00081(9)	0.0066(3)
Ti(2)	0.24836(7)	0.2678(1)	0.74858(9)	0.0067(3)
P(1)	0.4997(1)	0.3332(2)	0.7422(1)	0.0070(4)
P(2)	0.18035(9)	0.5014(2)	0.4884(1)	0.0079(4)
Rb(1)	0.38504(4)	0.78347(8)	0.67465(7)	0.0205(2)
Rb(2)	0.10537(4)	0.69184(9)	0.92598(8)	0.0176(2)
O(1)	0.4862(3)	0.4786(7)	0.8535(4)	0.008(1)
O(2)	0.5141(3)	0.4604(7)	0.6199(3)	0.009(1)
O(3)	0.4024(2)	0.2026(5)	0.7207(3)	0.009(1)
O(4)	0.5949(3)	0.1943(6)	0.7616(4)	0.011(1)
O(5)	0.1141(3)	0.3109(6)	0.4583(3)	0.009(1)
O(6)	0.1128(3)	0.6894(6)	0.5174(4)	0.012(1)
O(7)	0.2505(3)	0.5423(6)	0.3729(3)	0.009(1)
O(8)	0.2522(3)	0.4576(6)	0.6010(4)	0.011(1)
OT(1)	0.2218(3)	0.9607(6)	0.3564(4)	0.008(1)
OT(2)	0.2226(3)	0.0437(7)	0.6097(3)	0.009(1)

UNIVERSITAT ROVIRA I VIRGILI
YTTERBIUM AND ERBIUM DOPEP RbTi1-xMxOPO4 (M=Nb or Ta) CRYSTALS. NEW LASER AND NONLINEAR BIFUNCTIONAL MATERIALS
Alexandra Peña Revellez
ISBN: 978-84-691-0370-8 /DL:T.2188-2007

The open nature of the three-dimensional network formed by the TiO_6 octahedra and the PO_4 tetrahedra, in RTP, allows Rb^+ cations to diffuse easily parallel to [001] direction, resulting in a high ionic conductivity along this direction. These Rb^+ cations occupy positions related by the 2_1 screw axis, as shown in Figure 3.6.

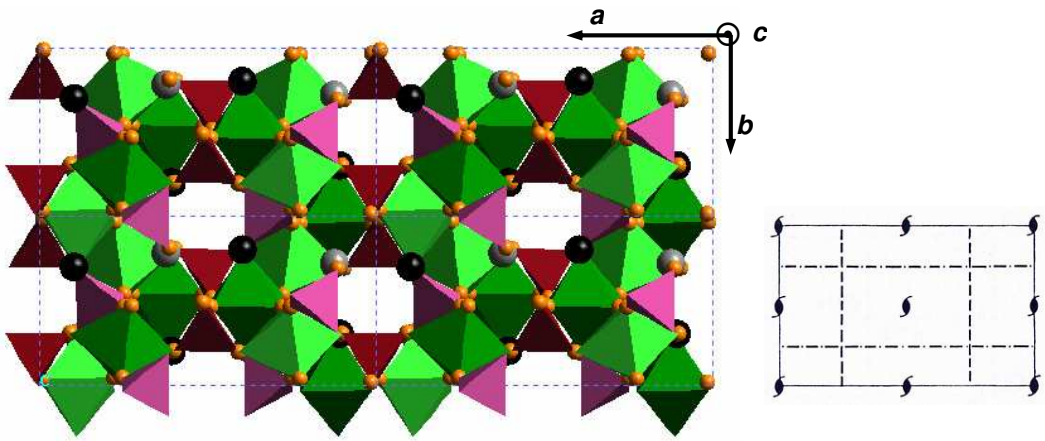

Figure 3.6. View of a projection parallel to [001] direction of the RTP structure (left hand side) and representation of the symmetry elements of the *Pna2₁* space group (right hand side).

3.7 Evolution of the cell parameters as increasing Yb^{3+} concentration in $RbTi_{1-x}Ta_xOPO_4$

The evolution of the cell parameters, *a*, *b*, *c* and the volume of $Yb:RbTi_{1-x}Ta_xOPO_4$ as increasing the Yb at % in crystals has been studied. Due to the low Yb_2O_3 concentration added in solution, with a composition of Rb_2O-P_2O_5-(TiO_2+Ta_2O_5+Yb_2O_3) = 40.80-27.20-((31.68-X)-0.32-X), before loosing the RTP phase, this variation has been studied for a maximum of a 2.22 at % of Yb in crystals. The values obtained as increasing the Yb at % are listed in Table 3.5.

All the cell parameters and the cell volume show the same behaviour, all of them increase while increasing the Yb at % in crystals, showing a positive linear tendency in the studied range (Figure 3.7). The tendency to increase its cell parameters and volume, as the Yb^{3+} concentration increases, is consistent with an expansion of the structure as expected because the Yb^{3+} ionic radius is bigger than that of Ti^{4+}, as explained in section 3.1.

UNIVERSITAT ROVIRA I VIRGILI
YTTERBIUM AND ERBIUM DOPEP RbTi1-xMxOPO4 (M=Nb or Ta) CRYSTALS. NEW LASER AND NONLINEAR BIFUNCTIONAL MATERIALS
Alexandra Peña Revellez
ISBN: 978-84-691-0370-8 /DL:T.2188-2007

Table 3.5. *Cell parameters and volume for Yb:$RbTi_{1-x}Ta_xOPO_4$ crystals as increasing the Yb at %.*

Yb [at %]	*a* [Å]	*b* [Å]	*c* [Å]	*V* [Å]
0	12.9602(2)	6.5016(1)	10.5636(2)	890.11(3)
1.43	12.9648(4)	6.5035(2)	10.5650(4)	890.81(5)
1.76	12.9693(5)	6.5053(2)	10.5674(4)	891.56(5)
2.22	12.9710(5)	6.5060(2)	10.5683(4)	891.86(6)

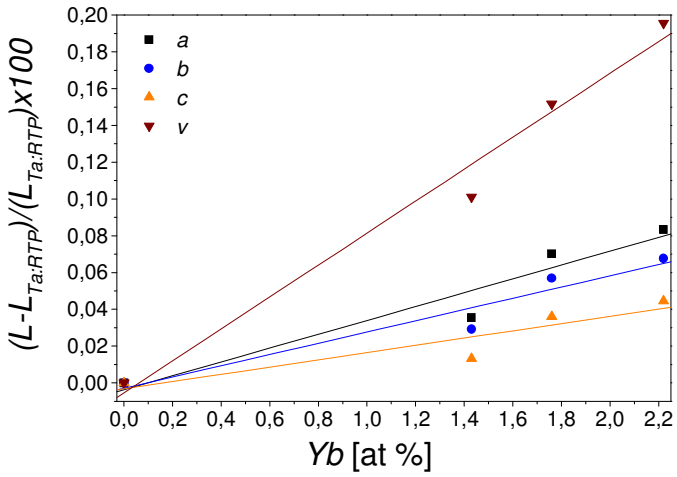

Figure 3.7. Relative evolution of the cell parameters and unit cell volume of $RbTi_{1-x-y}Ta_xYb_yOPO_4$ as a function of Yb at % incorporated into the crystal.

3.8 Phase transitions and thermal expansion of $RbTi_{1-x}Ta_xOPO_4$

The phase transitions were studied between room temperature and 1373 K by X-ray powder diffraction analysis and until 1500 K by differential thermal analysis (DTA).

From the X-ray patterns obtained, we can identify the different phases present at each temperature, shown in Figure 3.8. From room temperature to 1273 K, there is only one phase, $RbTiOPO_4$, which does not disappear completely until 1373 K, but at 1323 K and 1373 $RbTiOPO_4$ was present only as a minor phase with the cubic phase, $RbTiPO_5$, comprising the majority. The

UNIVERSITAT ROVIRA I VIRGILI
YTTERBIUM AND ERBIUM DOPEP RbTi1-xMxOPO4 (M=Nb or Ta) CRYSTALS. NEW LASER AND NONLINEAR BIFUNCTIONAL MATERIALS
Alexandra Peña Revellez
ISBN: 978-84-691-0370-8 /DL:T.2188-2007

phase transition between the orthorhombic phase and the cubic ($T_{o\rightarrow c}$) is between 1273 K and 1323 K. This phase transition is shown to be irreversible as in all the patterns recorded in the cooling program, $RbTiOPO_4$ was not present. Additionally, to the cubic phase which appeared at 1323 K, at 1373 K it appears the TiO_2 in the rutile phase, as a result of the decomposition of the cubic phase in Rb_2O and P_2O_5 (that evaporate) and TiO_2 (that remains in solid state). These results are comparable to the ones obtained for $RbTi_{1-x}Nb_xOPO_4$.[108]

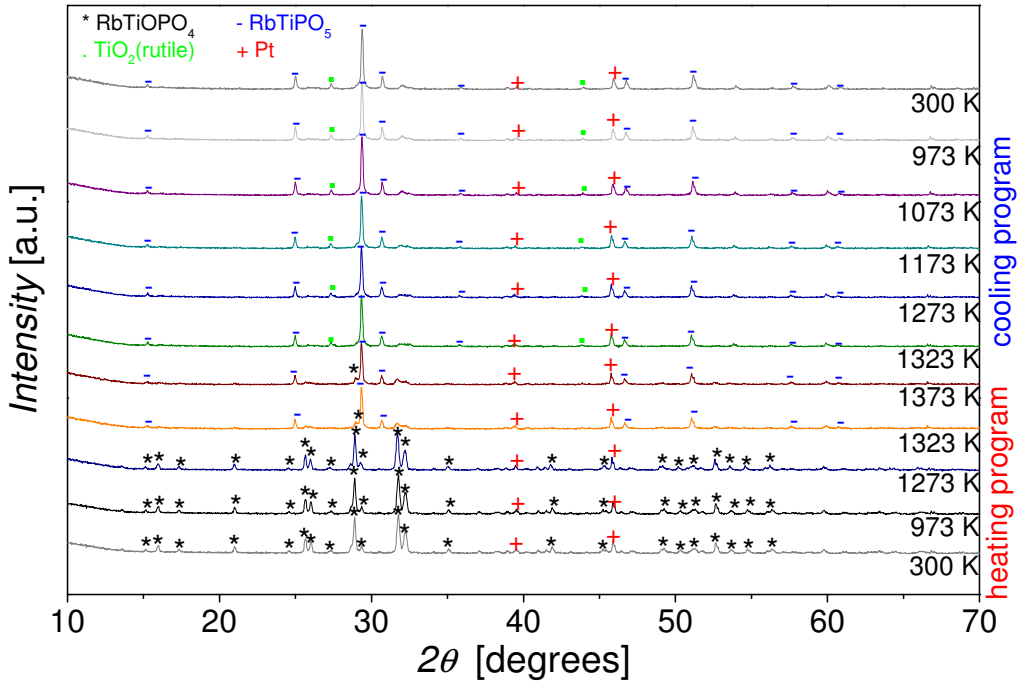

Figure 3.8. Selected X-ray powder patterns at different temperature showing the phase transitions of $RbTi_{0.91}Ta_{0.09}OPO_4$.

To obtain a precise measurement of the transition temperature between the orthorhombic and the cubic phase ($T_{o\rightarrow c}$) and the temperature decomposition of this last phase we performed DTA analysis of a RTP tantalum doped sample, and we determined that $T_{o\rightarrow c}$ was 1371 K and the decomposition temperature (T_d) was 1490 K, and at this temperature there was a slight weight decrease due to the evaporation of Rb_2O and P_2O_5. The obtained thermogram is shown in Figure 3.9.

UNIVERSITAT ROVIRA I VIRGILI
YTTERBIUM AND ERBIUM DOPEP RbTi1-xMxOPO4 (M=Nb or Ta) CRYSTALS. NEW LASER AND NONLINEAR BIFUNCTIONAL MATERIALS
Alexandra Peña Revellez
ISBN: 978-84-691-0370-8 /DL:T.2188-2007

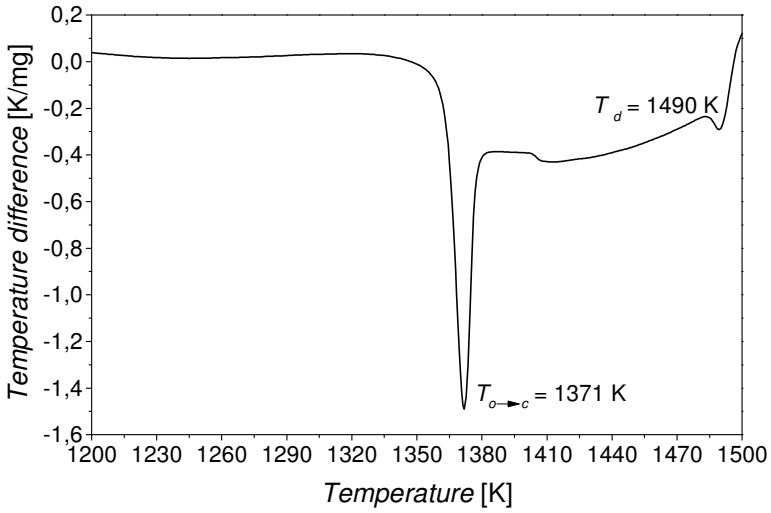

Figure 3.9. Differential thermal analysis (DTA) of $RbTi_{0.96}Ta_{0.04}OPO_4$.

Furthermore, to this thermogram we also checked how the phase transition temperature evolves as the Yb^{3+} concentration increases in $RbTi_{1-x}Ta_xOPO_4$ samples. These temperatures are listed in Table 3.6. As shown in this Table, while increasing the Yb^{3+} concentration the $T_{o\rightarrow c}$ decreases, the thermal stability of the orthorhombic phase is smaller in doped samples.

Table 3.6. *Orthorhombic to cubic phase transition temperature in $RbTi_{1-x-y}Ta_xYb_yOPO_4$ crystals.*

	$T_{o\rightarrow c}$ [K]
$\boldsymbol{RbTi_{0.961}Ta_{0.039}OPO_4}$	1371
$\boldsymbol{RbTi_{0.953}Ta_{0.035}Yb_{0.012}OPO_4}$	1370
$\boldsymbol{RbTi_{0.949}Ta_{0.033}Yb_{0.018}OPO_4}$	1368
$\boldsymbol{RbTi_{0.950}Ta_{0.027}Yb_{0.022}OPO_4}$	1367

The temperature of the phase transition between the ferroelectric phase (*Pna2₁*) and the paraelectric phase (*Pnan*), the Curie temperature (T_c), has not been determined by the X-ray patterns obtained to study the phase transitions

neither by the DTA analyses, because this transition does not imply heat absorption or release. In $RTi_{1-x}Nb_xOPO_4$,[108] the T_c decreases by increasing the Nb^{5+} concentration, and these temperatures were extracted from the study of the change in the slope of the evolution with the temperature of the *c* cell parameter. In $KTi_{1-x}Nb_xOPO_4$, this temperature also decreases when increasing the Nb^{5+} concentration in crystals.[109] In our case we determined this temperature by analyzing the evolution of the cell parameter *c* with the temperature by applying the FULLPROF program[97] and the Rietveld method[98] to the X-ray powder patterns recorded at different temperatures, as it was previously done for $RbTi_{1-x}Nb_xOPO_4$.[108] It seems that the change in the slope of the evolution with the temperature of the *c* cell parameter shown between 898 and 998 K (see Figure 3.10) in $RbTi_{0.96}Ta_{0.04}OPO_4$ crystal, could be attributed to the transition from the ferroelectric phase to the paraelectric phase. This temperature is close to the one obtained previously in a $KTi_{0.95}Ta_{0.05}OPO_4$ crystal.[105] In the case of $RbTi_{0.91}Ta_{0.09}OPO_4$, no noticeable change was seen in the slope, so we could not determine the T_c temperature, but we supposed that the value would not been far from 800 K, which was the one determined for $KTi_{0.90}Ta_{0.10}OPO_4$.[105]

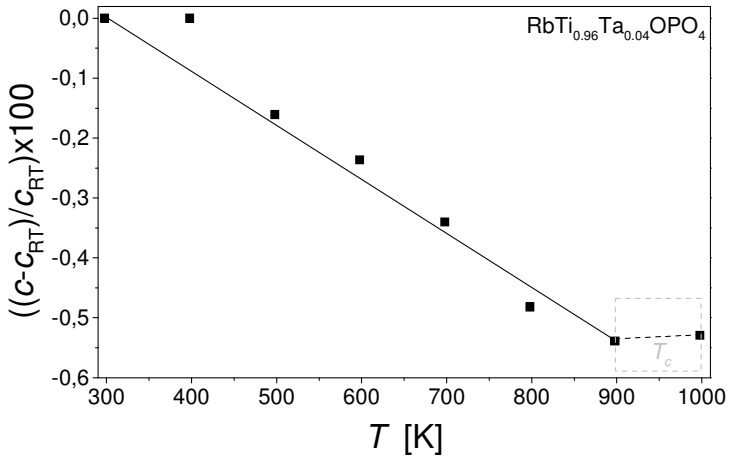

Figure 3.10. Evolution of the *c* cell parameter in $RbTi_{0.96}Ta_{0.04}OPO_4$ crystals with temperature.

The evolution of the other cell parameters, *a*, *b* and the cell volume (*V*) with the temperature were also analyzed in the same way as the parameter *c*,

UNIVERSITAT ROVIRA I VIRGILI
YTTERBIUM AND ERBIUM DOPEP RbTi1-xMxOPO4 (M=Nb or Ta) CRYSTALS. NEW LASER AND NONLINEAR BIFUNCTIONAL MATERIALS
Alexandra Peña Revellez
ISBN: 978-84-691-0370-8 /DL:T.2188-2007

by applying the FULLPROF program[97] and the Rietveld method.[98] The linear relationship between the average change in each parameter and the temperature (from room temperature to 798 K) for $RbTi_{0.96}Ta_{0.04}OPO_4$ and $RbTi_{0.91}Ta_{0.09}OPO_4$ crystals were determined. The evolution was plotted only to 798 K to ensure that we are below the T_c. Figure 3.11 shows that the cell parameters and the cell volume behave in the same way in both crystals: *a*, *b* and cell volume tends to increase while increasing the temperature and *c* (as previously shown in Figure 3.10) tends to decrease. The same behaviour was observed in KTP,[110] RTP,[111] and $RTi_{1-x}Nb_xOPO_4$.[108]

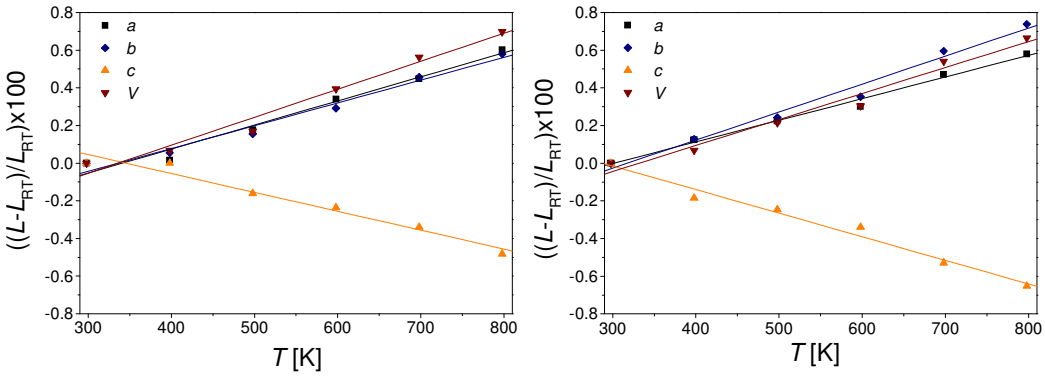

Figure 3.11. Relative thermal evolution of the cell parameters and cell volume of $RbTi_{0.96}Ta_{0.04}OPO_4$ (left hand side) and $RbTi_{0.91}Ta_{0.09}OPO_4$ (right hand side) crystals.

From the slope of the linear relationships of each parameter ($\Delta L/L$) with the temperature we calculated the linear thermal coefficients (α_{ij}) for $RbTi_{1-x}Ta_xOPO_4$ crystals with x = 0.04 and 0.09, which are listed in Table 3.7. In this table there are also listed the α_{ij} of RTP[112] and $RTi_{1-x}Nb_xOPO_4$,[108] and it could be extracted from the thermal expansion coefficients of $RbTi_{0.96}Ta_{0.04}OPO_4$ that are smaller than the values of RTP and the $RbTi_{0.95}Nb_{0.05}OPO_4$; the thermal anisotropy is also lower. This result was promising since it implies that $RbTi_{1-x}Ta_xOPO_4$ (with a lower Ta^{5+} concentration), which shows thermal isotropy in the ***ab*** plane, will suffer lower thermal stress when used as a laser host material. Although α_{11} decreases as the Ta^{5+} concentration increases, the absolute values of α_{22} and α_{33} clearly increase. This behaviour is completely different from the one showed for $RbTi_{1-x}Nb_xOPO_4$, where the α_{ij} remains

UNIVERSITAT ROVIRA I VIRGILI
YTTERBIUM AND ERBIUM DOPEP RbTi1-xMxOPO4 (M=Nb or Ta) CRYSTALS. NEW LASER AND NONLINEAR BIFUNCTIONAL MATERIALS
Alexandra Peña Revellez
ISBN: 978-84-691-0370-8 /DL:T.2188-2007

essentially invariable (only a slight decrease is shown) when increasing the Nb^{5+} concentration.

Table 3.7. *Linear thermal expansion coefficients* α_{ij} for RTP,[112] $RbTi_{1-x}Nb_xOPO_4$,[108] and $RbTi_{1-x}Ta_xOPO_4$.

Crystals	α_{11} [$\times 10^{-6}$ K^{-1}]	α_{22} [$\times 10^{-6}$ K^{-1}]	α_{33} [$\times 10^{-6}$ K^{-1}]
$RbTiOPO_4$ [111]	13.5(6)	18.4(6)	-10.5(3)
$RbTi_{0.95}Nb_{0.05}OPO_4$ [108]	11.7(2)	16.7(3)	-10.2(8)
$RbTi_{0.91}Nb_{0.09}OPO_4$ [108]	11.9(3)	16.1(3)	-9.7(3)
$RbTi_{0.96}Ta_{0.04}OPO_4$	12.5(7)	12.8(8)	-9.8(7)
$RbTi_{0.91}Ta_{0.09}OPO_4$	10.9(5)	14.9(7)	-12.6(6)

3.9 Ionic conductivity

Previous studies have shown that the electric-field poling at room temperature and monitoring procedures of self flux growth RTP is easier and more predictable than KTP, and moreover the effective nonlinearity in PPRTP is comparable to that of PPKTP.[112] This is due to the low conductivity of RTP (≈ 10^{-9} S/cm), which is two or three orders of magnitude lower than that of KTP (between 10^{-6}-10^{-7} S/cm). This lower conductivity along the ***c*** direction is because the Rb^+ ions have a larger ionic radius than K^+ and their mobility along the existing channels along this direction is reduced. A first characterization to perform, not only in the RTP grown in self flux and tungsten containing-fluxes but also in $RbTi_{1-x}Nb_xOPO_4$ and Yb:$RbTi_{1-x}Nb_xOPO_4$ crystals grown in our laboratory, to see whether the electric-field poling will be easier or more difficult than in RTP, was determine their ionic conductivity. As shown in Figure 3.12, the RTP grown in self flux and in solutions containing up to 20 % WO_3 shows almost the same ionic conductivity, but pre-poling experiments show that domain switching is more difficult in the slab oriented perpendicular to ***c*** obtained from a crystal grown in solutions containing 20 % WO_3 than in the slab obtained for a RTP crystal grown in its self flux. The same behaviour was observed in Sc:KTP and Cr:KTP, by using Sc^{3+} and Cr^{3+} to reduce the KTP ionic

UNIVERSITAT ROVIRA I VIRGILI
YTTERBIUM AND ERBIUM DOPEP RbTi1-xMxOPO4 (M=Nb or Ta) CRYSTALS. NEW LASER AND NONLINEAR BIFUNCTIONAL MATERIALS
Alexandra Peña Revellez
ISBN: 978-84-691-0370-8 /DL:T.2188-2007

conductivity.[113] The ionic conductivity of $RbTi_{1-x}Nb_xOPO_4$ is of the order of KTP, because the Nb^{5+} doping creates Rb^+ vacancies as was found by resolving its structure by X-ray single diffraction,[114] which allows a higher mobility in the channels along the ***c*** direction. Contrary to this last result, the ionic conductivity in the $Yb:RbTi_{1-x}Nb_xOPO_4$ sample was lower from the one obtained for $RbTi_{1-x}Nb_xOPO_4$ and just slightly higher (10^{-8} S/cm) from that of RTP. So, although no pre-poling experiments in the sample had been performed, it will be interesting to perform them to see if the electric-field poling is as easy as in RTP, or the presence of dopants cause difficulty in the domain switching, as was shown in RTP grown in tungsten containing fluxes and in Sc^{3+} and Cr^{3+} doped KTP.

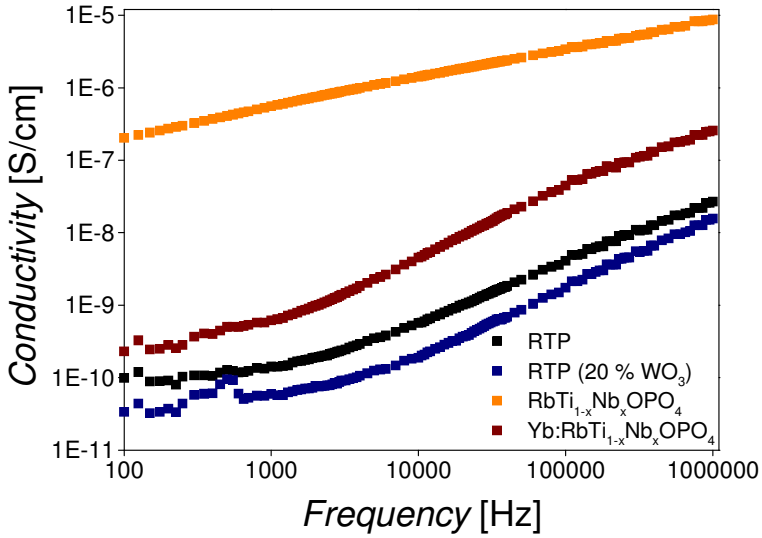

Figure 3.12. Ionic conductivity (σ_{33}) of RTP, RTP grown in a 20 % WO_3 containing flux, $RbTi_{1-x}Nb_xOPO_4$ and $Yb:RbTi_{1-x}Nb_xOPO_4$ obtained at different frequencies.

3.10 Ferroelectric properties

With the motivation of studying whether the RTP crystals grown from its self flux or from tungsten containing fluxes by the TSSG-SC technique present ferroelectric single-domains (C^- or C^+) or multi-domains (C^- and C^+) we cut and polished plates perpendicular to the ***c*** crystallographic direction, from the obtained crystals. The previous knowledge of this information is crucial to

UNIVERSITAT ROVIRA I VIRGILI
YTTERBIUM AND ERBIUM DOPEP RbTi1-xMxOPO4 (M=Nb or Ta) CRYSTALS. NEW LASER AND NONLINEAR BIFUNCTIONAL MATERIALS
Alexandra Peña Revellez
ISBN: 978-84-691-0370-8 /DL:T.2188-2007

perform the periodically poled process of these crystals to obtain a periodic inversion of the ferroelectric domains with the desired periodicity to achieve the desired generated wavelength by quasi-phasematching (QPM). When these crystals present multi-domains a pre-poling process should be applied to obtain single-domain samples before the poling process to achieve the periodic structure.

Different techniques have been used to visualize the ferroelectric domain structures which, as told in section 1.4, are based on piezoelectric, electro-optic, nonlinear optical and pyroelectric properties of KTP and isostructurals. In our case, we studied the ferroelectric domain structures in an RTP sample by previously performing a selective etching (with a mixture of KOH and KNO_3) of the sample domains to visualize them by reflection optical microscopy (Figure 3.13) and the effects of this selective etching have been quantified with the obtained AFM images (see *paper IV*); a step of 40 nm in height was found between the domain wall, due to the different etching rate of the C^- and the C^+ domain surfaces.

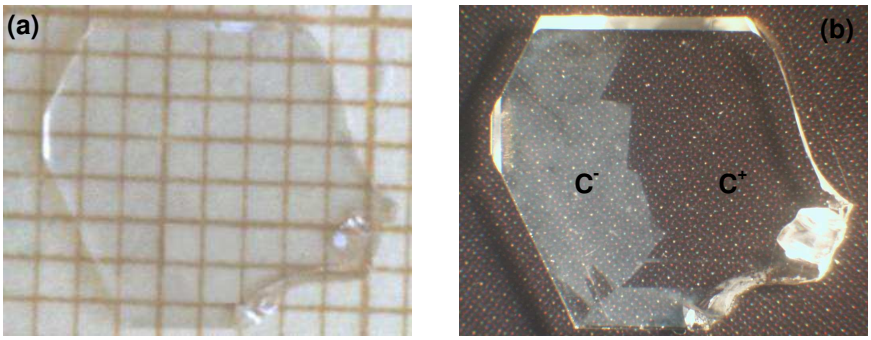

Figure 3.13. Picture of the ***c*** oriented slab, before etching (a) and after etching (b), where it can be distinguish the two domains C^- and C^+.

As the grown crystals (grown in its self flux and in tungsten containing fluxes) seem to contain multi domains, a pre-poling process should be applied before performing the poling process to obtain the periodic structures.

UNIVERSITAT ROVIRA I VIRGILI
YTTERBIUM AND ERBIUM DOPEP RbTi1-xMxOPO4 (M=Nb or Ta) CRYSTALS. NEW LASER AND NONLINEAR BIFUNCTIONAL MATERIALS
Alexandra Peña Revellez
ISBN: 978-84-691-0370-8 /DL:T.2188-2007

3.11 Raman scattering of $RbTi_{1-x}Ta_xOPO_4$

A complete study of polarized Raman scattering of RTP and $RbTi_{1-x}Nb_xOPO_4$ were recently performed (see *paper V*) because no such study was previously done, and to see how the Nb^{5+} presence affects the RTP structure. The main differences between the polarized Raman spectra obtained for RTP and $RbTi_{1-x}Nb_xOPO_4$ were that there is a broadening of the lines in the recorded spectra of $RbTi_{1-x}Nb_xOPO_4$ when compared to those of RTP, that the modes which corresponds to the TiO_6 were the only affected in the spectra of $RbTi_{1-x}Nb_xOPO_4$, because Nb^{5+} substitute Ti^{4+} in the structure, and that the general shift to shorter wavenumbers in $RbTi_{1-x}Nb_xOPO_4$ proves that Ti^{+4} is substituted by a heavier ion; Nb^{5+}.

In this section we will not discuss the results obtained in *paper V*, but we are going to compare the Raman unpolarized spectra recorded for RTP, $RbTi_{1-x}Nb_xOPO_4$ and $RbTi_{1-x}Ta_xOPO_4$ at room temperature in the frequency range between 20-1200 cm^{-1} (see Figure 3.14), to see which differences exist between the spectra and if Ta^{+5} has the same effect in the RTP structure as Nb^{5+}. The Nb^{5+} effect is explained in *paper V* and summarized in the previous paragraph.

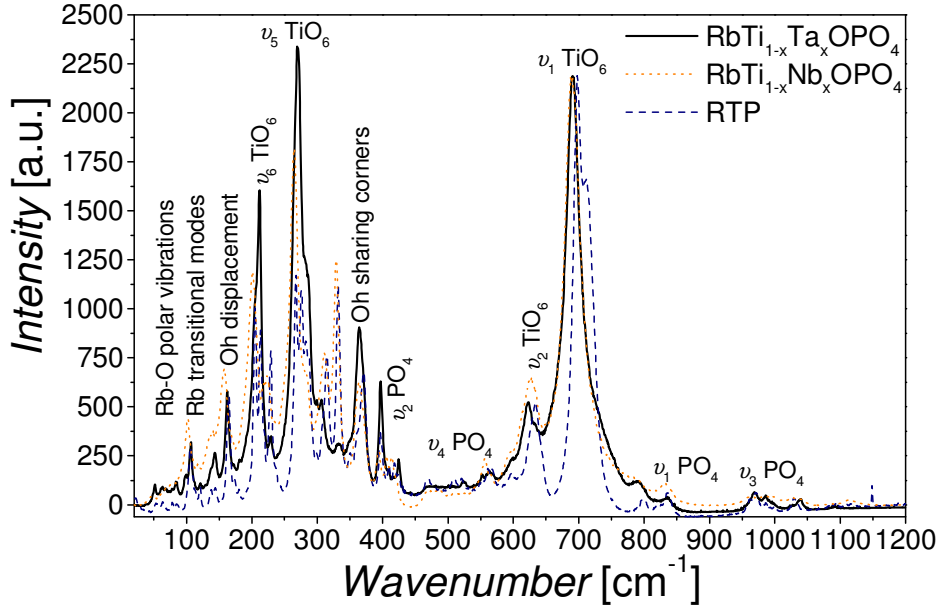

Figure 3.14. Unpolarized Raman spectra of $RbTi_{1-x}Ta_xOPO_4$, $RbTi_{1-x}Nb_xOPO_4$ and RTP at room temperature.

UNIVERSITAT ROVIRA I VIRGILI
YTTERBIUM AND ERBIUM DOPEP RbTi1-xMxOPO4 (M=Nb or Ta) CRYSTALS. NEW LASER AND NONLINEAR BIFUNCTIONAL MATERIALS
Alexandra Peña Revellez
ISBN: 978-84-691-0370-8 /DL:T.2188-2007

In Figure 3.14 it is clear that the presence of Ta^{5+} in RTP leads to a broadening of the lines, just as in the case of $RbTi_{1-x}Nb_xOPO_4$, which have been assigned to a nonhomogeneous structure. Tantalum, just as niobium, is expected to substitute the titanium positions in RTP, and in this case, it is also clear that the shifted bands are the ones related with vibrations involving the TiO_6 octahedra (ν_1 at 691 cm^{-1}, ν_2 at 623 cm^{-1}, ν_4 between 307 and 333 cm^{-1}, ν_5 at 270 cm^{-1} and ν_6 at 212 cm^{-1}). So, the substitution of Ti^{4+} by Ta^{5+} is confirmed, although the $RbTi_{1-x}Ta_xOPO_4$ structure has not been resolved yet. All the bands related with the vibrations of the PO_4 group (ν_1 at 835 cm^{-1}, ν_2 at 424 and 397 cm^{-1}, ν_3 around 1000 and 1100 cm^{-1} and ν_4 between 450 and 560 cm^{-1}) and the ones related to polar vibrations (Rb-O) and Rb transitional modes (between 80 and 160 cm^{-1}) remains in the same position. In the case of $RbTi_{1-x}Nb_xOPO_4$ there exists a shift in the bands related to Rb-O polar vibrations and Rb transitional modes, which were related to the presence of Rb^+ vacancies in the structure. In the case of $RbTi_{1-x}Ta_xOPO_4$, no shift in these bands is observed, so no Rb^+ vacancies are expected, which should be confirmed by resolving the structure. We have shown that Ta^{5+} plays the same role as Nb^{5+} in the RTP structure, substituting only the Ti^{4+} positions, although it is expected that Ta^{+5} would not induce Rb^+ vacancies in the structure.

UNIVERSITAT ROVIRA I VIRGILI
YTTERBIUM AND ERBIUM DOPEP RbTi1-xMxOPO4 (M=Nb or Ta) CRYSTALS. NEW LASER AND NONLINEAR BIFUNCTIONAL MATERIALS
Alexandra Peña Revellez
ISBN: 978-84-691-0370-8 /DL:T.2188-2007

Chapter 4

Optical characterization

It has been shown that the concentration of Ln^{3+} ions obtained is not high enough to get efficient fluorescence in KTP neither in RTP,[76] so it could not be used as a host for solid state lasers. However, by codoping RTP with niobium or tantalum the lanthanide concentration achieved, ≈ 2×10^{20} ions/cm^3, is high enough to produce efficient laser emission. Optical properties, such as the chromatic dispersion, the thermo-optics coefficients and the transparency range of $RbTi_{1-x}Nb_xOPO_4$ and $RbTi_{1-x}Ta_xOPO_4$ have been determined for samples with different concentrations of Ti, Nb and Ta ions, x.

Moreover, as $RbTiOPO_4$ is a well known nonlinear optical crystal, then we want to check if the nonlinear optical properties, of the niobium and tantalum doped RTP, are changed with respect to those of RTP.

UNIVERSITAT ROVIRA I VIRGILI
YTTERBIUM AND ERBIUM DOPEP RbTi1-xMxOPO4 (M=Nb or Ta) CRYSTALS. NEW LASER AND NONLINEAR BIFUNCTIONAL MATERIALS
Alexandra Peña Revellez
ISBN: 978-84-691-0370-8 /DL:T.2188-2007

4.1 Chromatic dispersion and thermo-optic coefficients of the refractive indices

Figure 6 of *paper V* shows the dispersion chromatic curves of $RbTiOPO_4$ (RTP) in the three principal directions, which do not differ from the ones found in the literature.[115] As already said, RTP crystallizes in the orthorhombic system and the axes of the crystallographic frame ***a***, ***b*** and ***c*** correspond to the axes of the dielectric frame ***x***, ***y*** and ***z***, respectively, and it is a positive biaxial crystal, $n_a<n_b<n_c$. This is also the case for $RbTi_{1-x}Nb_xOPO_4$ and $RbTi_{1-x}Ta_xOPO_4$ that we investigated.

Accurate measurements of the $RbTi_{0.96}Nb_{0.04}OPO_4$ three principal refractive indices, n_a, n_b and n_c were performed from 0.45 µm to 1.2 µm along the ***a***, ***b*** and ***c*** principal axes of the crystallographic frame to determine their chromatic dispersion. These dispersion curves are plotted in Figure 4.1 and the data were fitted with a Sellmeier equation using one UV pole and an IR correction term

$$n^2 = A + \frac{B\lambda^2}{\lambda^2 - C} - D\lambda^2 \qquad \text{eq. 6.1}$$

The obtained Sellmeier coefficient; A, B, C (μm^2) and D (μm^{-2}) of each principal refractive index in $RbTi_{0.96}Nb_{0.04}OPO_4$ for the aforementioned range at room temperature are listed in Table 4.1.

Table 4.1. *Sellmeier coefficients of the indices dispersion curves determined at room temperature of* $RbTi_{0.96}Nb_{0.04}OPO_4$.

Sellmeier coefficients	***A***	***B***	***C*** (μm^2)	***D*** (μm^{-2})
$RbTi_{0.96}Nb_{0.04}OPO_4$				
n_a	2.2209	0.8893	0.0495	0.0317
n_b	1.5901	1.6246	0.0355	0.0109
n_c	1.1451	2.3208	0.0351	0.0054

Figure 4.1 illustrates the changes in the birefringence while doping RTP with Nb. The behaviour is the same in KTP.[92] In both cases there is a noticeable increase of n_c which is the responsible of the birefringence enhancement, and

UNIVERSITAT ROVIRA I VIRGILI
YTTERBIUM AND ERBIUM DOPEP RbTi1-xMxOPO4 (M=Nb or Ta) CRYSTALS. NEW LASER AND NONLINEAR BIFUNCTIONAL MATERIALS
Alexandra Peña Revellez
ISBN: 978-84-691-0370-8 /DL:T.2188-2007

in the case of $RbTi_{1-x}Nb_xOPO_4$ there is also a perceptible increase of n_b, while n_a remains almost inalterable in both cases.

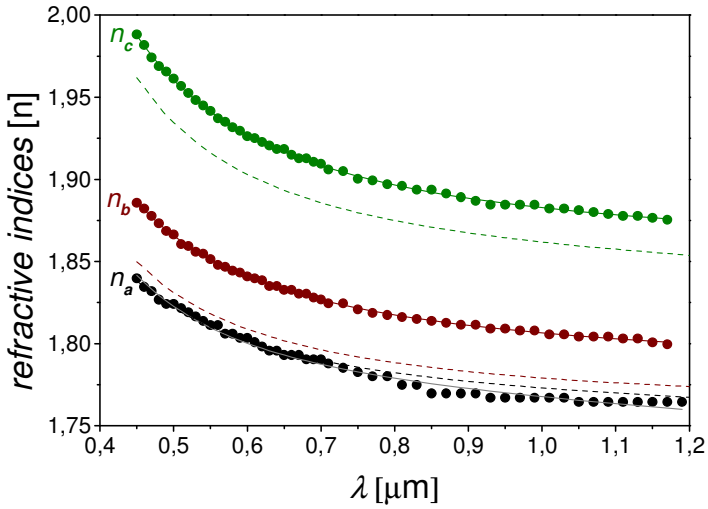

Figure 4.1. Chromatic dispersion curves of $RbTi_{0.96}Nb_{0.04}OPO_4$ (points), and their Sellmeier fitting (eq. 6.1), and RTP curves (dashed lines).

The variation of the three principal refraction indices as a function of the wavelength in $RbTi_{1-x}Ta_xOPO_4$ crystals could not be measure because the size of the obtained samples up to now were not big enough to cut prisms.

We also checked the evolution of the birefringence (n_c-n_a and n_c-n_b) with the at % of Nb^{5+} in $RbTi_{1-x}Nb_xOPO_4$ crystals as shown in Figure 4.2, by measuring the three principal refractive indexes at 632.8 nm. To the aforementioned figure an additional point is added which corresponds to $RbTi_{0.954}Nb_{0.031}Yb_{0.015}OPO_4$, to see whether Yb^{3+} doping affects or not the birefringence of $RbTi_{1-x}Nb_xOPO_4$. It seems that the birefringence, which increases with increasing the Nb content, shows a linear behaviour as a function of the Nb at % in crystals, but we can not affirm such a conclusion before measuring other crystals with different Nd at %. In the case of Nb:KTP, as seven crystals with different Nb concentration were studied, it is clear that there is a linear dependency of n_c-n_a as a function of Nb at %.[92] The obtained birefringence values and the ones previously published for KTP, Nb:KTP and Ta:KTP, are shown in Table 4.2. In this table are also shown the refractive indexes obtained from samples of $Yb:RbTi_{1-x}Nb_xOPO_4$ and $Yb:RbTi_{1-x}Ta_xOPO_4$

UNIVERSITAT ROVIRA I VIRGILI
YTTERBIUM AND ERBIUM DOPEP RbTi1-xMxOPO4 (M=Nb or Ta) CRYSTALS. NEW LASER AND NONLINEAR BIFUNCTIONAL MATERIALS
Alexandra Peña Revellez
ISBN: 978-84-691-0370-8 /DL:T.2188-2007

measured at 632.8 nm. Although we do not know the refractive indices of $RbTi_{1-x}Ta_xOPO_4$, we assume that they will not be far from those obtained for $Yb:RbTi_{1-x}Ta_xOPO_4$, as there are slightly differences in those obtained for $Yb:RbTi_{1-x}Nb_xOPO_4$ and $RbTi_{1-x}Nb_xOPO_4$ crystals with almost the same Nb at %.

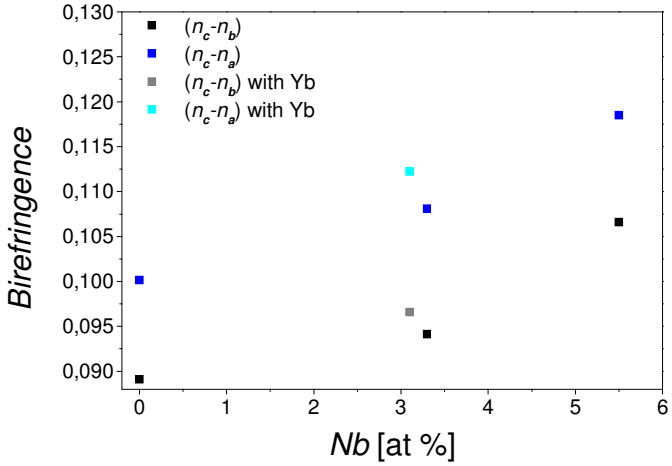

Figure 4.2. Evolution of the crystal birefringence, measured at 632.8 nm at room temperature, with Nb (at %) in crystals.

Table 4.2. *Refractive indices and birefringence* (n_c-n_a *and* n_c-n_b) *at 632.8*

Samples	n_a	n_b	n_c	$n_c - n_a$	$n_c - n_b$
$RbTiOPO_4$	1.7886	1.7997	1.8888	0.1002	0.0891
$RbTi_{0.966}Nb_{0.033}OPO_4$	1.7908	1.8048	1.8989	0.1081	0.0941
$RbTi_{0.945}Nb_{0.055}OPO_4$	1.7938	1.8053	1.9119	0.1181	0.1066
$RbTi_{0.954}Nb_{0.031}Yb_{0.015}OPO_4$	1.7879	1.8035	1.9000	0.1121	0.0965
$RbTi_{0.949}Ta_{0.033}Yb_{0.018}OPO_4$[a]	1.7851	1.8039	1.8992	0.1141	0.0953
$KTiOPO_4$ [92]				*0.1022*	*0.0932*
$KTi_{0.963}Nb_{0.037}OPO_4$ [92]				*0.1138*	*0.1027*
$KTi_{0.970}Nb_{0.030}OPO_4$ [92]				*0.1172*	*0.1059*
$KTi_{0.854}Nb_{0.146}OPO_4$ [92]				*0.1466*	*0.1295*

[a] Value not added in Figure 4.2 as it is codoped with Ta^{5+} not with Nb^{5+}.

Finally, the evolution with the temperature, between 298 and 393 K at λ = 632.8 nm, of the principal refractive indices, n_a, n_b and n_c of

UNIVERSITAT ROVIRA I VIRGILI
YTTERBIUM AND ERBIUM DOPEP RbTi1-xMxOPO4 (M=Nb or Ta) CRYSTALS. NEW LASER AND NONLINEAR BIFUNCTIONAL MATERIALS
Alexandra Peña Revellez
ISBN: 978-84-691-0370-8 /DL:T.2188-2007

$RbTi_{0.97}Nb_{0.03}OPO_4$ were measured and are plotted in Figure 4.3. The values of the thermo-optic coefficients obtained, dn_a/dT, dn_b/dT and dn_c/dT, are added to the graphic. These coefficients are of the same order as Nb:KTP.[116]

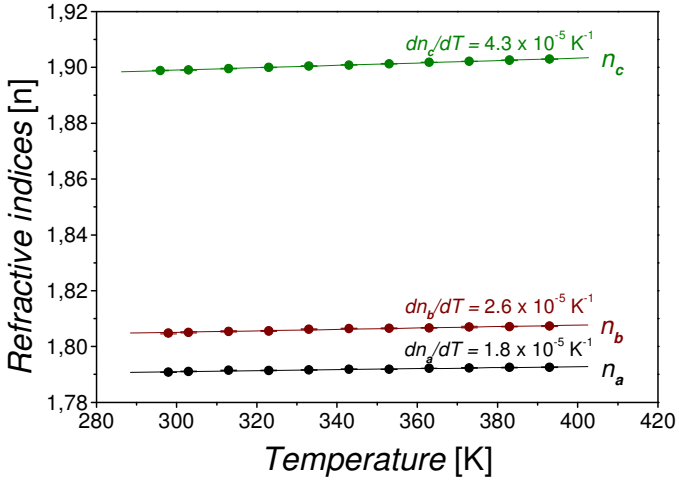

Figure 4.3. Evolution of the principal refractive indices of $RbTi_{0.97}Nb_{0.03}OPO_4$ with the temperature at λ = 632.8 nm.

It is important to know the variation of the refractive indices with the temperature in $RbTi_{1-x}Nb_xOPO_4$, because these changes would induce a variation in the phase-matching directions of the crystal. In addition to these possible changes in the phase-matching directions, it should be said that inside the active laser medium a temperature gradient is present, leading to a variation of the refractive indices and a thermal expansion, causing a thermal lensing effect.

4.2 Transparency window

The transparency range of a crystal (in this case a non linear crystal), to be used as a laser host, should be measured in order to guarantee that the crystal is transparent in the wavelength range where the active ions absorbs and emits as well as in the second harmonic generation range of the active ions luminescence wavelength.

It is well know that the transparency range for bulk crystals of the KTP family extends from 0.35 to 4.5 μm, and that it is enlarged until around 10 μm in thinner samples, on the order of a few hundred microns.[117]

The influence of impurities near the UV absorption edge has been previously reported in this family of materials.[118-119] A band centred around 595 nm appeared in the as-grown $RbTi_{1-x}Nb_xOPO_4$[120] and $RbTi_{1-x}Ta_xOPO_4$ crystals. This band is related to the overlapping contribution of $^2T_2 \rightarrow {}^2E$ transition of Ti^{3+} in Ti(1) and Ti(2) sites of the RTP lattice, and disappears after annealing the crystals at around 800 K during 5 h.

Figure 3 of *paper V* shows the transparency window of RTP crystals (1 mm and 50 µm thick) and of $RbTi_{0.96}Nb_{0.04}OPO_4$ crystal (50 µm thick), and Figure 4 of *paper I* shows the transparency window of $RbTi_{0.96}Ta_{0.04}OPO_4$ and $RbTi_{0.95}Ta_{0.03}Yb_{0.02}OPO_4$ crystals, with a width of the order of 300 µm. The only difference between the transparency window of $RbTi_{0.96}Ta_{0.04}OPO_4$ and $RbTi_{0.95}Ta_{0.03}Yb_{0.02}OPO_4$ is the Yb^{3+} absorption band which appears around 1 µm.

The UV cut-off wavelength is defined as the wavelength at which the optical transmission decays by a factor of 1/e, and it is due to Ti-O electronic transitions in our materials. As shown in Table 5 of *paper I*, the UV cut-off value obtained for both samples display a red shift compared to that of RTP. This red shift was clearer when the absorption coefficient was measured, while no shift could be seen when comparing measured transmissions. This shift on the UV edge to lower energy was smaller than the one observed in $RbTi_{1-x}Nb_xOPO_4$ (see Table 5 of *paper I*), and we can compare this results with the UV cut-off values obtained for $KTaO_3$ (350 nm)[121] and $KTa_{1-x}Nb_xO_3$ (385 nm).[122]

The IR cut-off wavelength of RTP is not affected by the presence of impurities; it only depends on the thickness of the sample, as said before. In Figure 3 of *paper V* is shown the transparency window of a thick (1 mm) and a thin (50 µm) RTP sample and in Figure 4.4 is shown the transparency windows of a thick (1.6 mm) and a thin (300 µm) sample of $RbTi_{0.95}Ta_{0.03}Yb_{0.02}OPO_4$. By comparing these results we conclude that in thick samples, the component responsible for the IR cut-off is the first overtone of the ν_3 fundamental vibrations of the tetrahedral phosphate ion, and in the thinner samples, the modes responsible for closing the IR region are the $(\nu_1+\nu_2)$ combination bands of PO_4^{3-} (300 µm) or the first overtone of the ν_4 fundamental vibrations of PO_4^{3-}

UNIVERSITAT ROVIRA I VIRGILI
YTTERBIUM AND ERBIUM DOPEP RbTi1-xMxOPO4 (M=Nb or Ta) CRYSTALS. NEW LASER AND NONLINEAR BIFUNCTIONAL MATERIALS
Alexandra Peña Revellez
ISBN: 978-84-691-0370-8 /DL:T.2188-2007

(50 µm). The different phosphate bands which appeared in the transparency window are identified, as well as the intense Yb^{3+} absorption band which appears around 1000 nm (1 µm). These bands have been assigned by referring to previous studies performed for KTP.[117,123]

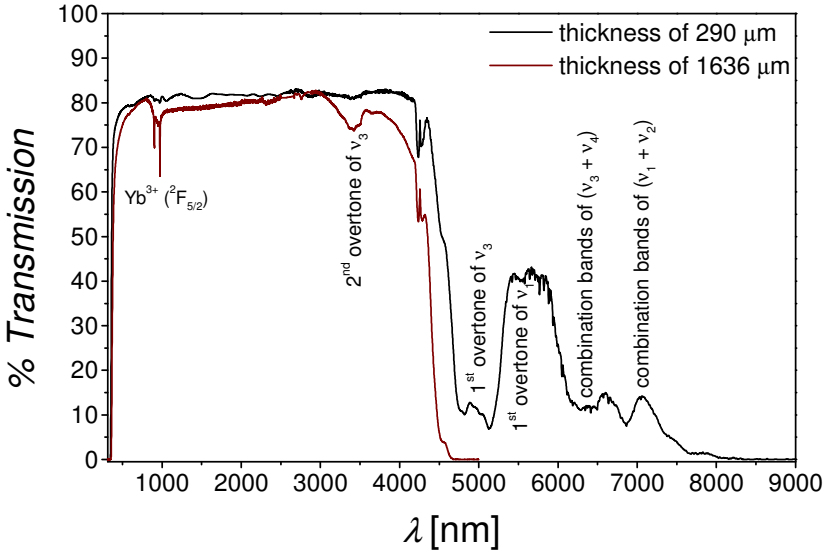

Figure 4.4. Evolution of the IR cut-off as a function of the sample thickness in $RbTi_{0.95}Ta_{0.03}Yb_{0.02}OPO_4$ crystals.

4.3 Second harmonic generation efficiency in powdered samples

The efficiency of the second harmonic generation of powder samples of RTP, $RbTi_{1-x}Nb_xOPO_4$ and $Ln:RbTi_{1-x}Nb_xOPO_4$ have been previously determined.[102,83] So, we only report here the efficiency of the second harmonic generation in powder samples of $RbTi_{1-x}Ta_xOPO_4$ and $Yb:RbTi_{1-x}Ta_xOPO_4$ by using the Kurtz method.[4] We considered this efficiency as the ratio between the power of the pumping beam generated by a Nd:YAG laser (λ = 1064 nm) and the doubled generated by the sample (λ = 532 nm), and for both samples it was slightly smaller than that of KTP. In powder samples of $RbTi_{0.96}Ta_{0.04}OPO_4$ the ratio, $\eta_{Ta:RTP}/\eta_{KTP}$, is equal to 0.95, and in $RbTi_{0.95}Ta_{0.03}Yb_{0.02}OPO_4$ the ratio, $\eta_{Yb:Ta:RTP}/\eta_{KTP}$, slightly decreases (0.80).

Finally, if we compare the efficiency in powder samples of $Yb:RbTi_{1-x}Ta_xOPO_4$ and $Yb:RbTi_{1-x}Nb_xOPO_4$, we can see that both are of the

UNIVERSITAT ROVIRA I VIRGILI
YTTERBIUM AND ERBIUM DOPEP RbTi1-xMxOPO4 (M=Nb or Ta) CRYSTALS. NEW LASER AND NONLINEAR BIFUNCTIONAL MATERIALS
Alexandra Peña Revellez
ISBN: 978-84-691-0370-8 /DL:T.2188-2007

same order.[83] This might be explained if we suppose that the Yb^{3+} ions (which replace Ti^{4+} in the structure) occupe a more symmetrical position in the RTP structure, and accept that the non-linear optical response decreases with less distorted TiO_6 octahedrons.[70] It has also been said that Ti(1) sites contribute more effectively to the non-linear response, by assuming that Yb^{3+} ions replace Ti(1) sites and tend to decrease the distortion of the TiO_6 octahedrons, the decrease in the SHG efficiency will be explained. Although these results seem to be consistent with the models proposed, further structural characterization is being performed to obtain more information about the relation between the SHG efficiency and the modifications in the structure induced by Ta^{5+} and Yb^{3+}.

4.4 Type II SHG phase-matching conditions in the *ab* plane in bulk crystals

We studied RTP and $RbTi_{1-x}Nb_xOPO_4$ samples undoped and doped with Yb^{3+}, Er^{3+} or Er^{3+}/Yb^{3+} grown in our laboratory. No measurements had been performed with $RbTi_{1-x}Ta_xOPO_4$ nor with Yb:$RbTi_{1-x}Ta_xOPO_4$ samples due to the size of the crystals obtained to now.

All measured samples generate visible light from second harmonic generation (SHG) for propagations in the ***bc*** and ***ac*** planes respectively, by using a laser emitting a tuneable wavelength λ corresponding to the frequency ω. Non critical SHG phase-matching conditions were observed by propagating along ***a*** and ***b*** principal axes respectively, for a fundamental laser beam linearly polarized at 45º. Then the generated doubled beam, emitted at $\lambda/2$ or 2ω according to energy conservation, is polarized parallel to the ***b*** and ***a*** principal axes respectively. So, according to the index surface of a biaxial crystal the condition to get type II SHG, $n^-(\omega)+n^+(\omega)=2n^-(2\omega)$, was accomplished (see section 2.9.1) in the ***ab*** plane for all the studied samples.

Measured non critical angular phase-matching fundamental wavelength (λ_{NCPM}) along ***a*** (θ = 90º; φ = 0º) and ***b*** axes (θ = 90º; φ = 90º) are shown in Table 4.3 and Figure 4.5 for RTP and $RbTi_{1-x}Nb_xOPO_4$ studied samples. They are also listed in Table 6 of *paper V*.

UNIVERSITAT ROVIRA I VIRGILI
YTTERBIUM AND ERBIUM DOPEP RbTi1-xMxOPO4 (M=Nb or Ta) CRYSTALS. NEW LASER AND NONLINEAR BIFUNCTIONAL MATERIALS
Alexandra Peña Revellez
ISBN: 978-84-691-0370-8 /DL:T.2188-2007

Measurements of phase-matching directions in RTP have been previously performed by Guillien *et al.*[124] by the sphere method, and from those data theoretical phase-matching angles as a function of the fundamental wavelength could be calculated in the ***ab*** plane for type II SHG. They are also reported in Figure 4.5 and in Table 4.3 for comparison. Figure 4.5 also shows the calculated phase-matching curve for $RbTi_{0.96}Nb_{0.04}OPO_4$ by using its Sellmeier coefficients (see *paper V*). Unfortunately, it is far from the experimental values obtained. The discrepancy increases as decreasing the φ angles, because maybe the associate error in the experimental measurements of the refractive indices is larger at higher wavelengths. Then we used the theoretical phase-matching curve of RTP to have an idea of the one for Yb^{3+}, Er^{3+} or Er^{3+}/Yb^{3+} doped $RbTi_{1-x}Nb_xOPO_4$ crystals in the ***ab*** plane. It is based on a dashed line following the slope of the RTP curve and relating the non critical angular phase-matching fundamental wavelengths $\lambda_{NCPM}^{a,b}$ of the studied sample. It is shown in Figure 4.5 for $RbTi_{0.954}Nb_{0.031}Yb_{0.015}OPO_4$ and is in agreement with phase-matching measurements performed in the sample crystal cut at 70º from the ***a*** axis in the ***ab*** plane for a fundamental wavelength of 1003 nm.

Table 4.3. *Direct phase-matching measurements performed on slabs of undoped and doped crystals.*

Samples	$\varphi = 0º$ λ_{NCPM}^{a} [nm]	$\varphi = 90º$ λ_{NCPM}^{b} [nm]
$RbTiOPO_4$ [124]	1144	1042
$RbTiOPO_4$ *paper V*	1144±0.5	1030±0.5
$RbTi_{0.955}Nb_{0.045}OPO_4$ *paper V*	1101±0.5	984±0.5
$RbTi_{0.965}Nb_{0.028}Er_{0.007}OPO_4$	1122.4±0.1	989.6±0.1
$RbTi_{0.954}Nb_{0.031}Yb_{0.015}OPO_4$	1118.2±0.1	985.4±0.1
$RbTi_{0.947}Nb_{0.035}Yb_{0.015}Er_{0.003}OPO_4$	1117.2±0.1	983.3±0.1
$RbTi_{0.939}Nb_{0.038}Yb_{0.022}Er_{0.001}OPO_4$	1115.4±0.1	975.3±0.1

UNIVERSITAT ROVIRA I VIRGILI
YTTERBIUM AND ERBIUM DOPEP RbTi1-xMxOPO4 (M=Nb or Ta) CRYSTALS. NEW LASER AND NONLINEAR BIFUNCTIONAL MATERIALS
Alexandra Peña Revellez
ISBN: 978-84-691-0370-8 /DL:T.2188-2007

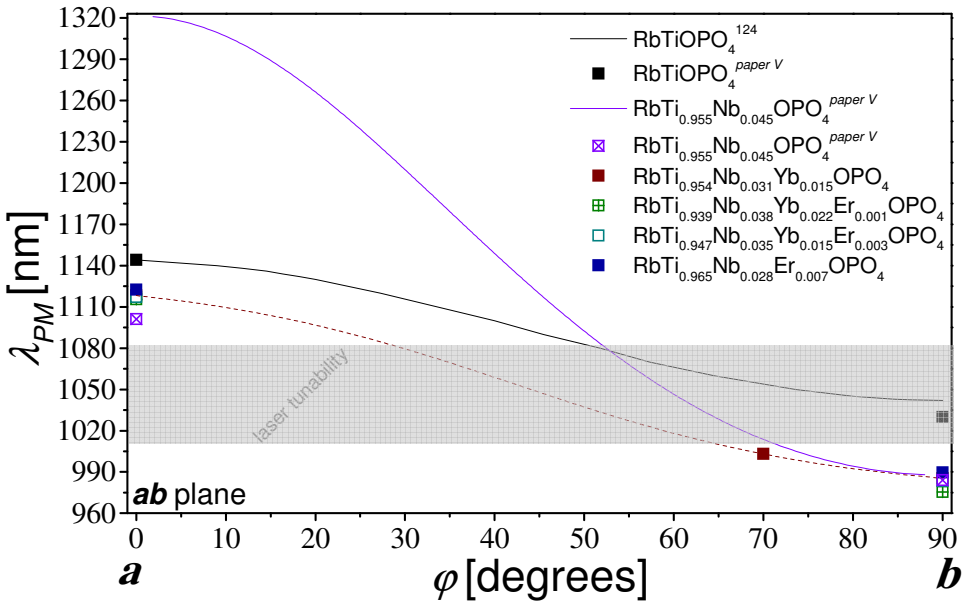

Figure 4.5. Calculated phase-matching curves for type II SHG in RTP[124] and $RbTi_{0.955}Nb_{0.045}OPO_4$ (solid lines). Experimental values for type II SHG angular non-critical phase-matching fundamental wavelength (λ_{NCPM}) for RTP, $RbTi_{1-x}Nb_xOPO_x$ and Yb^{3+}, Er^{3+} or Er^{3+}/Yb^{3+} doped $RbTi_{1-x}Nb_xOPO_x$ samples (squares).

Some general rules could be extracted from Figure 4.5 and Table 4.3. The first one is that $\lambda^{a,b}_{NCPM}$ decreases while increasing the Nb^{5+} content in the studied crystals and Figure 4.6 shows that this decrease is larger along ***b*** than along ***a***. Since we also observe an increase of the birefringence; in the studied samples which increases while increasing the Nb^{5+} content as shown in Figure 4.2, both behaviors could be related, as previously shown in Nb:KTP.[92]

The second rule is that

$$\lambda^{a}_{NCPM} \rangle \lambda^{b}_{NCPM}\ ;\ \lambda^{RTP}_{NCPM} \rangle \lambda^{dopedRTP}_{NCPM}$$

This situation is a favor for great overlap between the fundamental wavelengths leading to type II SHG phase-matching conditions in the ***ab*** plane and the Yb^{3+} luminescence wavelength in Yb^{3+} doped $RbTi_{1-x}Nb_xOPO_4$ crystals. Indeed, the luminescence tunability of $RbTi_{0.954}Nb_{0.031}Yb_{0.015}OPO_4$ is shown in Figure 3 of *paper II* and the tuning range obtained in the laser experiments is shown in Figure 4 of *paper III*. It is ranging between 1009 and 1081 nm and the

UNIVERSITAT ROVIRA I VIRGILI
YTTERBIUM AND ERBIUM DOPEP RbTi1-xMxOPO4 (M=Nb or Ta) CRYSTALS. NEW LASER AND NONLINEAR BIFUNCTIONAL MATERIALS
Alexandra Peña Revellez
ISBN: 978-84-691-0370-8 /DL:T.2188-2007

laser wavelength (λ_{laser}) with a maximum output power corresponds to 1051 nm. It is reported in Figure 4.5 as a grey area.

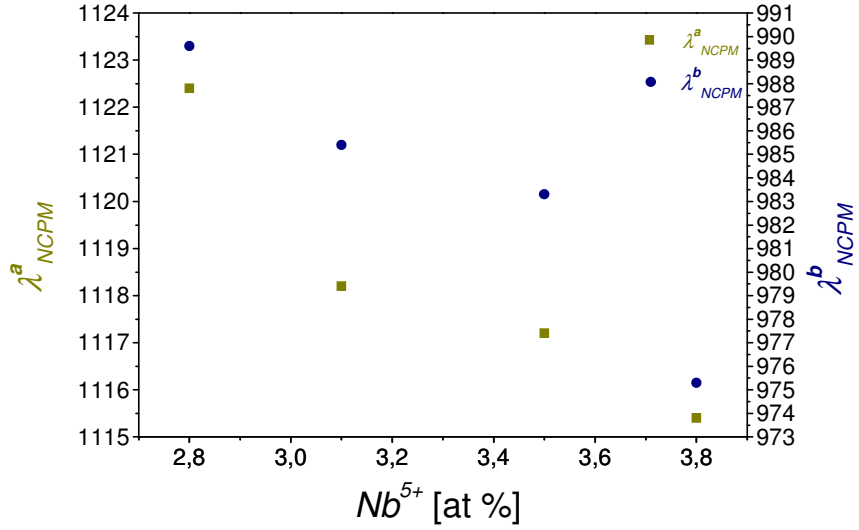

Figure 4.6. Evolution of type II SHG angular non-critical phase-matching fundamental wavelength (λ_{NCPM}) along ***a*** and ***b*** axes with the variation of Nb^{5+} atoms in our studied samples.

We performed preliminary measurements of their type II second harmonic generation efficiency along the ***a*** and ***b*** axes in the ***ab*** plane in crystals of $RbTi_{1-x}Nb_xOPO_4$ doped with Yb^{3+}or Er^{3+} or both together. The SHG efficiency was measured by comparing the intensity of the doubled wave generated by those samples with that generated from a slab of KTP oriented at φ = 23° in the ***ab*** plane, for λ = 1.064 μm. All the samples have comparable length (L ≈ 2.5 mm), to compare directly the results since $I(2\omega,L) \propto L^2P^2(\omega,L)$. We found that the conversion efficiency of the doped samples is lower than that of KTP, with an around 10 % of efficiency referred to KTP oriented at the phase-matching direction given above.

4.5 Self frequency doubling of $RbTi_{0.95}Nb_{0.031}Yb_{0.015}OPO_4$ crystal

We know now that $RbTi_{0.954}Nb_{0.031}Yb_{0.015}OPO_4$ is phase-matchable for type II SHG in the ***ab*** plane for fundamental wavelengths ranging between 1009 and 1081 nm which corresponds to the tuning range obtained in the laser

UNIVERSITAT ROVIRA I VIRGILI
YTTERBIUM AND ERBIUM DOPEP RbTi1-xMxOPO4 (M=Nb or Ta) CRYSTALS. NEW LASER AND NONLINEAR BIFUNCTIONAL MATERIALS
Alexandra Peña Revellez
ISBN: 978-84-691-0370-8 /DL:T.2188-2007

experiments performed with this crystal. Considering the phase-matching estimated curve of $RbTi_{0.954}Nb_{0.031}Yb_{0.015}OPO_4$ the possible orientations of the crystals are ranging between $\varphi \approx 30$ and 65°, as shown in Figure 4.7. Moreover it is shown in Figure 4.7 that self frequency doubling of the wavelength leading to the maximum laser output power in $RbTi_{0.954}Nb_{0.031}Yb_{0.015}OPO_4$, 1051 nm, could be achieved with a sample cut as a slab in the ***ab*** plane and oriented at $\varphi \approx 45°$. A slab oriented at $\varphi = 45°$ has shown type II SHG for a fundamental wavelength of 1047±0.1 nm, which corroborates our approach (see Figure 4.7).

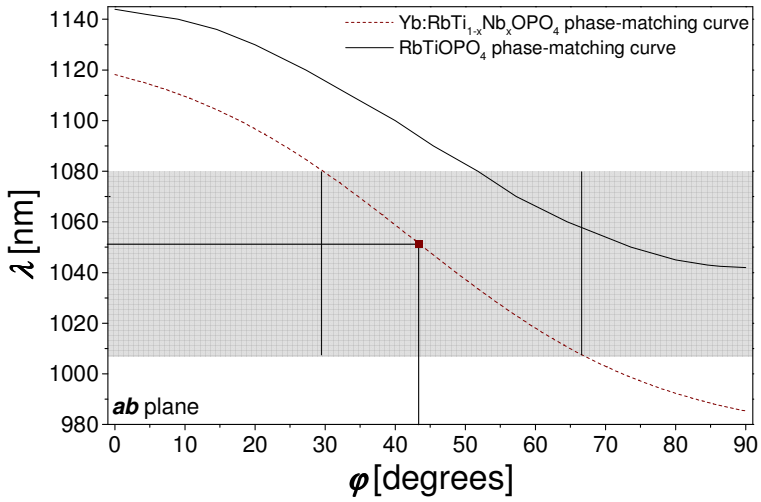

Figure 4.7. Phase-matching curves for type II SHG in $RbTiOPO_4$[124] (solid line) and in $RbTi_{0.954}Nb_{0.031}Yb_{0.015}OPO_4$ (dashed line).

Although no experimental results were performed yet to check type II SHG in ***ac*** or ***bc*** planes, theoretical calculations allowed us to determine that no phase-matching possibility, in the tuning laser range of Yb^{3+}, can be found in the ***ac*** plane, but is possible in the ***bc*** plane, as shown in Figure 4.8. This figure shows, as Figure 4.7, the tuning range obtained in the laser experiments with $RbTi_{0.954}Nb_{0.031}Yb_{0.015}OPO_4$. The red point indicates the wavelength at which maximum output laser was achieved.

UNIVERSITAT ROVIRA I VIRGILI
YTTERBIUM AND ERBIUM DOPEP RbTi1-xMxOPO4 (M=Nb or Ta) CRYSTALS. NEW LASER AND NONLINEAR BIFUNCTIONAL MATERIALS
Alexandra Peña Revellez
ISBN: 978-84-691-0370-8 /DL:T.2188-2007

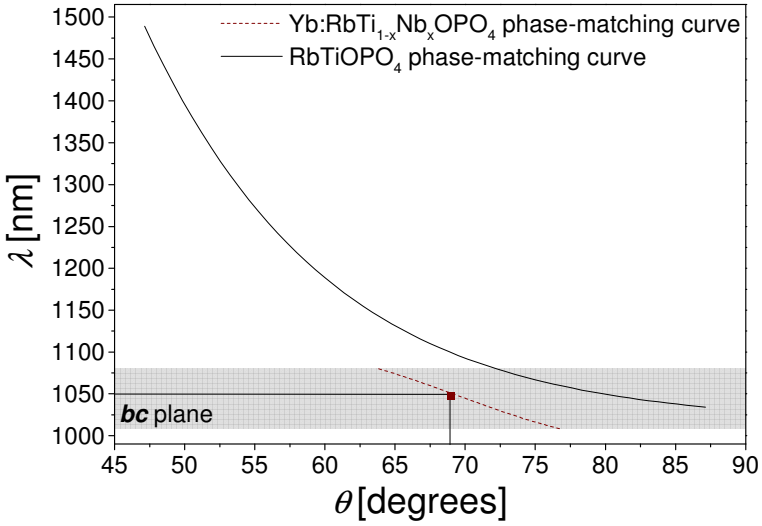

Figure 4.8. Calculated phase-matching curve in the ***bc*** plane for type II SHG in $RbTiOPO_4$[124], and theoretical phase-matching for $RbTi_{0.954}Nb_{0.031}Yb_{0.015}OPO_4$.

So, after this preliminary study, we propose preparing one crystal, of $RbTi_{0.954}Nb_{0.031}Yb_{0.015}OPO_4$, cut as a sphere, to help in the study of all the self frequency doubling directions.

As we are interested in evaluate the potential use of $RbTi_{1-x}Nb_xOPO_4$ doped with lanthanide ions, especially Yb^{3+}, as self frequency doubling crystals we perform preliminary measurements of their type II second harmonic generation efficiency of $RbTi_{0.954}Nb_{0.031}Yb_{0.015}OPO_4$ oriented at φ = 45º in the ***ab*** plane by comparing the intensity of the doubled wave generated by this sample with that generated from the slab of KTP oriented at φ = 23º in the ***ab*** plane, for λ = 1.064 μm. The conversion efficiency of $RbTi_{0.954}Nb_{0.031}Yb_{0.015}OPO_4$ is lower than that of KTP (with an around 10 % of efficiency referred to KTP oriented at the phase-matching direction given above). However it is a promising candidate to be applied as a self frequency doubling crystal, as it has already been utilized to achieve laser generation of Yb^{3+} (see *paper II* and *paper III*). To our knowledge, this is the first example of laser generation from Yb^{3+} in a nonlinear crystal of the KTP family, which is discussed in chapter 6.

UNIVERSITAT ROVIRA I VIRGILI
YTTERBIUM AND ERBIUM DOPEP RbTi1-xMxOPO4 (M=Nb or Ta) CRYSTALS. NEW LASER AND NONLINEAR BIFUNCTIONAL MATERIALS
Alexandra Peña Revellez
ISBN: 978-84-691-0370-8 /DL:T.2188-2007

UNIVERSITAT ROVIRA I VIRGILI
YTTERBIUM AND ERBIUM DOPEP RbTi1-xMxOPO4 (M=Nb or Ta) CRYSTALS. NEW LASER AND NONLINEAR BIFUNCTIONAL MATERIALS
Alexandra Peña Revellez
ISBN: 978-84-691-0370-8 /DL:T.2188-2007

Chapter 5

Spectroscopic characterization of the active ions

The spectroscopic active ions studied in this thesis are ytterbium and erbium, which are lanthanide ions with huge applications in laser technology. The spectroscopic properties of the ions belonging to the lanthanide family are determined by their special electronic configuration.[125] They all belong to the *f*-block elements, characterized by progressively filling the 4*f* electron shell, which is efficiently shielded by the filled 5s and 5p outer shells that remain completely filled in the trivalent oxidation state; the most stable oxidation state of these ions in the studied crystals. As 4*f* electrons are closer to the core and shielded by the 5s and 5p outer shells, the ligand environment has negligible influence on the 4*f* shell of the lanthanide ions. Giving as a result, absorption and emission spectra characterized by sharp lines, and almost invariable level schemes in different hosts. It is clear that lanthanide ions in crystals largely behave like free ions. The effect of the crystal field is treated, normally, as a perturbation of the free ions. Although it is weak, the crystal field splits each of the free-ion energy levels (manifolds) into many closely spaced levels, which is called Stark splitting. The optical transitions of Ln^{3+} are due to intraconfigurational *4f-4f* transitions. These sharp transitions are induced electric-dipolar transitions as a consequence of the interaction of Ln^{3+} ions with the electric field of the electromagnetic radiation, through the electric dipole orientation. Information from the optical spectra of these ions can be extracted such as the electronic structure of the 4*f* shell, related with the energetic position of the peaks, the local site symmetry of the lanthanide structural position and the shape of the coordination polyhedron, related with the splitting generated by the crystal field, and the interaction between the lanthanide ions and their host environment, related with the intensity of the spectral lines.[126] To evaluate this effect and to determine the absorption cross section (σ_{abs}) and the radiative lifetimes (τ), we performed an exhaustive spectroscopic study of ytterbium in $RbTi_{1-x}Ta_xOPO_4$ crystal and erbium/ytterbium in $RbTi_{1-x}Nb_xOPO_4$ crystal.

UNIVERSITAT ROVIRA I VIRGILI
YTTERBIUM AND ERBIUM DOPEP RbTi1-xMxOPO4 (M=Nb or Ta) CRYSTALS. NEW LASER AND NONLINEAR BIFUNCTIONAL MATERIALS
Alexandra Peña Revellez
ISBN: 978-84-691-0370-8 /DL:T.2188-2007

5.1 Absorption of Yb^{3+} in $RbTi_{1-x}Ta_xOPO_4$

As explained in section 1.2 there are several advantages to using ytterbium over neodymium as a laser active ion in the 1 μm range. These are mainly related to its simple energy level scheme consisting of a ground state ($^2F_{7/2}$) and one excited state ($^2F_{5/2}$). Moreover, while doping nonlinear crystals with ytterbium the reabsorption losses in the green region, the second harmonic wavelength range, are avoided. Furthermore, the highest concentration of a Ln^{3+} ion ever achieved in a crystal of the KTP family grown by TSSG-SC technique, was ≈ 2.0×10^{20}ion/cm^3 in Yb^{3+} doped $RbTi_{1-x}Nb_xOPO_4$ crystals.[93] Yb^{3+} substitutes Ti^{4+} in RTP structure, and its ionic radius ($r_{Yb^{3+}}$ = 0.868 Å) is closer to the titanium ion ($r_{Ti^{4+}}$ = 0.605 Å), by comparing it with the other lanthanide active ions (see section 1.3).[104] It has been said that doping RTP with a d^0 element such as Nb^{5+} enhances the Yb^{3+} concentration, because it expands the structure.[114] Because of all these reasons, we focused our attention on doping RTP with Yb^{3+}, and Ta^{5+} was chosen as a codopand because it is a d^0 element, as Nb^{5+}, and as explained in previous chapters, the Yb^{3+} concentration achieved is on the order achieved in $RbTi_{1-x}Nb_xOPO_4$.

The sample used to perform the optical absorption of Yb^{3+} in $RbTi_{1-x}Ta_xOPO_4$ was a small cube (1.64×1.63×1.81 mm^3), which was obtained from the experience nº7 in Table 3.2, polished and oriented along the three principal optical axes ***x*** (***x*** = ***a***), ***y*** (***y*** = ***b***) and ***z*** (***z*** = ***c***), with an Yb^{3+} concentration of 1.6×10^{20} ions/cm^3.

The position and the number of peaks are independent of light polarization, as Yb^{3+} (C_1 symmetry site) has an odd number of electrons in the 4*f* shell ($4f^{13}$) and no selection rules exist for the induced electric dipole, but the intensity may vary. Because of that, absorption spectra with polarized light ***E//a***, ***E//b*** and ***E//b***, were recorded.

The room temperature absorption spectra recorded (Figure 5.1) show an absorption band related to the $^2F_{7/2} \rightarrow {}^2F_{5/2}$ transition which extends from ≈ 860 to 1050 nm (11600-9500 cm^{-1}). The three spectra are characterized by three main peaks centred at 903, 953 and 973 nm (11074, 10493 and 10277 cm^{-1}, respectively). The absorption cross section (σ_{abs}) values obtained at these maxima strongly depend on the light polarization, which shows the strong

UNIVERSITAT ROVIRA I VIRGILI
YTTERBIUM AND ERBIUM DOPEP RbTi1-xMxOPO4 (M=Nb or Ta) CRYSTALS. NEW LASER AND NONLINEAR BIFUNCTIONAL MATERIALS
Alexandra Peña Revellez
ISBN: 978-84-691-0370-8 /DL:T.2188-2007

trichroism of this crystal. With light polarized along ***b*** and ***a*** the maxima σ_{abs} are 0.82×10^{-20} and 0.30×10^{-20} cm^2 respectively at 973 nm, and along ***c*** the maximum is 0.77×10^{-20} cm^2 at 903 nm. So, with ***E//b*** and ***E//c*** the σ_{abs} values obtained are of the same order, which differs from the results obtained for $RbTi_{0.95}Nb_{0.03}Yb_{0.02}OPO_4$ (see Figure 1 of *Paper II*). The σ_{abs}, with ***E//b***, are 0.82×10^{-20} and 0.25×10^{-20} cm^2, at 973 and 903 nm respectively. These values are a little bit lower, but not too far, than those obtained for non-centrosymmetric ytterbium doped laser crystals as YCOB, showing a σ_{abs} of 0.45×10^{-20} cm^2 at 900.4 and 0.94×10^{-20} cm^2 at 976 nm,[127] and GdCOB, which shows a σ_{abs} of 0.41×10^{-20} cm^2 at 902 and 1.15×10^{-20} cm^2 at 976 nm.[53]

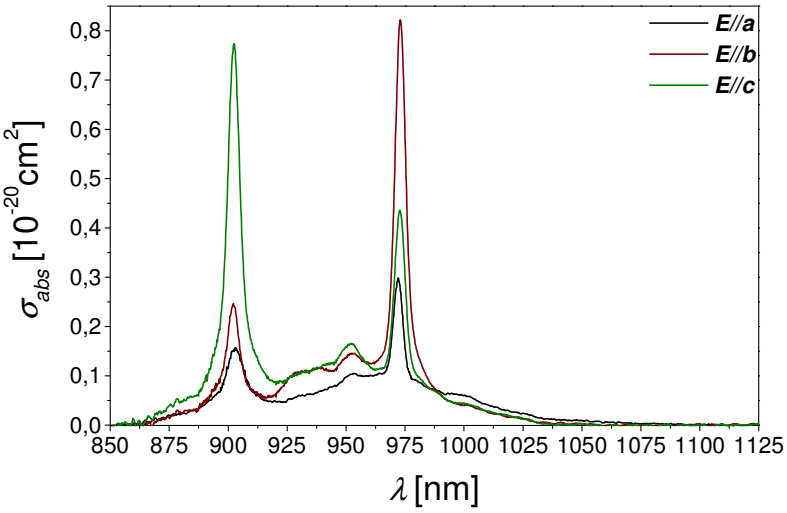

Figure 5.1. Absorption cross sections of $RbTi_{0.95}Ta_{0.03}Yb_{0.02}OPO_4$ determined at room temperature along the three different polarizations.

The recorded absorption spectra at 6K (***E//b*** and ***E//c***) allow us to accurately determine the energies of the three Stark sublevels of the excited state multiplet $^2F_{5/2}$. The bands observed are associated with transitions from the most populated Stark level, at low temperature, of the ground state $^2F_{7/2}(0)$, to the three excited sublevels $^2F_{5/2}(0')$, $^2F_{5/2}(1')$ and $^2F_{5/2}(2')$. The energies associated to these transitions are 10286, 10467 and 11064 cm^{-1} respectively, see inset in Figure 5.2, which does not differ significantly from the ones obtained in $RbTi_{0.95}Nb_{0.03}Yb_{0.02}OPO_4$, as shown in Table 5.1.

UNIVERSITAT ROVIRA I VIRGILI
YTTERBIUM AND ERBIUM DOPEP RbTi1-xMxOPO4 (M=Nb or Ta) CRYSTALS. NEW LASER AND NONLINEAR BIFUNCTIONAL MATERIALS
Alexandra Peña Revellez
ISBN: 978-84-691-0370-8 /DL:T.2188-2007

Table 5.1. *$^2F_{5/2}$ Stark sublevels of Yb^{3+} determined at 6 K in $RbTi_{0.95}Nb_{0.03}Yb_{0.02}OPO_4$ and $RbTi_{0.95}Ta_{0.03}Yb_{0.02}OPO_4$.*

Host	***Energy position*** [cm^{-1}]
$RbTi_{1-x}Nb_xOPO_4$	10289(0'); 10471(1'); 11069(2')
$RbTi_{1-x}Ta_xOPO_4$	10286(0'); 10467(1'); 11064(2')

The evolution of the absorption coefficient, which decreases as increasing the temperature, between 6 and 300 K with ***E//c***, is shown in Figure 2 of *paper II*. The two more energetic transitions ($^2F_{7/2}(0) \rightarrow {}^2F_{5/2}(2')$ and ($^2F_{7/2}(0) \rightarrow {}^2F_{5/2}(1')$ show a blue shift while increasing the temperature. This shift with increasing the temperature is due to dependencies of the spin orbit interaction and crystal field parameters on the lattice constants. The combined effect due to a repulsion between crystal field levels through the phonon field, relative shifts of rare earth ion terms and diminishing of the static crystal field with the lattice temperature expansion, may govern the observed blue shift as increasing the temperature.[128]

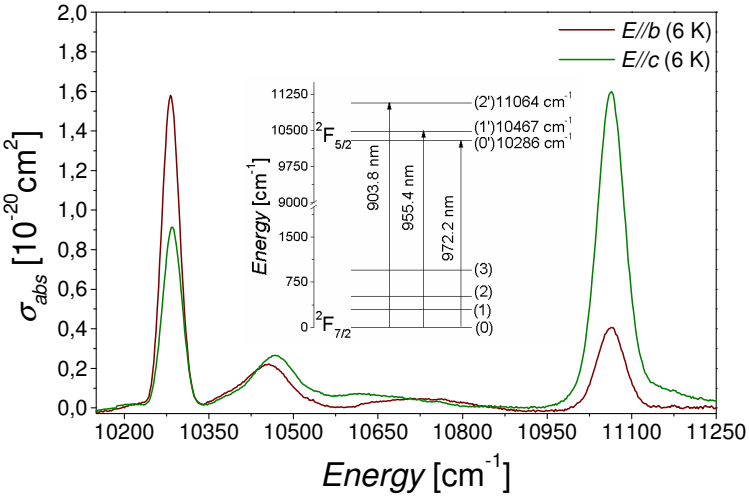

Figure 5.2. Absorption cross sections of $RbTi_{0.95}Ta_{0.03}Yb_{0.02}OPO_4$ determined at low temperature and schematic diagram with the energies of the Stark sublevels of the $^2F_{5/2}$ multiplet.

From the polarized absorption spectra obtained, shown in Figure 5.1, by integrating the absorption intensity we calculated the ytterbium radiative

lifetime (τ_{rad}) by using the chromatic dispersion of $RbTi_{0.96}Nb_{0.04}OPO_4$, shown in section 4.1, and the relationship proposed by Weber

$$\frac{1}{\tau_{rad}} = A_{if} = \left(\frac{g_f}{g_i}\right)\frac{8\pi n^2}{N\lambda^2}\int \alpha(\nu)d\nu \qquad \text{eq. 5.1}$$

The obtained value (τ_{rad} = 2.6 ms), is close to the one obtained for $RbTi_{0.95}Nb_{0.03}Yb_{0.02}OPO_4$, which is shown in *paper II*, so the emission lifetime, although has not been measured until now, should be on the same order as the one obtained for $Yb:RbTi_{1-x}Nb_xOPO_4$.[91] So, Yb^{3+} emission lifetime value is comparable or even much higher than it is in the Yb^{3+} doped non-centrosymmetric laser crystals known until date. These values are shown in Table 3 of *paper II*.

5.2 Emission of Yb^{3+} in $RbTi_{1-x}Ta_xOPO_4$

Unpolarized room and low temperature emission spectra of $RbTi_{0.95}Ta_{0.03}Yb_{0.02}OPO_4$ were performed in a 90° geometry by pumping the sample at 940 nm. The low temperature spectrum (10 K) allows us to determine the emission channels and the Stark sublevels of the ground state multiplet $^2F_{7/2}$. This spectrum, which extends from 955 to 1095 nm, is characterized by four main lines, corresponding to transitions from the lowest excited sublevel $^2F_{5/2}(0')$ to the four ground state sublevels $^2F_{5/2}(3)$, $^2F_{5/2}(2)$, $^2F_{5/2}(1)$ and $^2F_{5/2}(0)$, and another line appears in the room temperature spectrum attributed to a transition between the $^2F_{5/2}$ (1') Stark sublevel of the excited state and the $^2F_{7/2}$ (3) Stark sublevel of the ground state. The energies associated to these transitions (between the excited state to the ground state) do not differ from the ones obtained for Yb^{3+} in $RbTi_{1-x}Nb_xOPO_4$, which are shown in Table 5.2, just as in the case of the energies associated to transitions from the ground to the excited sate, shown in Table 5.1. Figure 5.3 (a) shows the two recorded spectra with the transitions labelled and in 5.3 (b) there is shown the crystal field splitting of Yb^{3+} in $RbTi_{1-x}Ta_xOPO_4$, obtained from the low temperature absorption and emission spectra. So, the broadband emission observed around

UNIVERSITAT ROVIRA I VIRGILI
YTTERBIUM AND ERBIUM DOPEP RbTi1-xMxOPO4 (M=Nb or Ta) CRYSTALS. NEW LASER AND NONLINEAR BIFUNCTIONAL MATERIALS
Alexandra Peña Revellez
ISBN: 978-84-691-0370-8 /DL:T.2188-2007

1000 nm is due to the large splitting of the ytterbium ground state, and would be useful for the generation of ultrashort laser pulses.

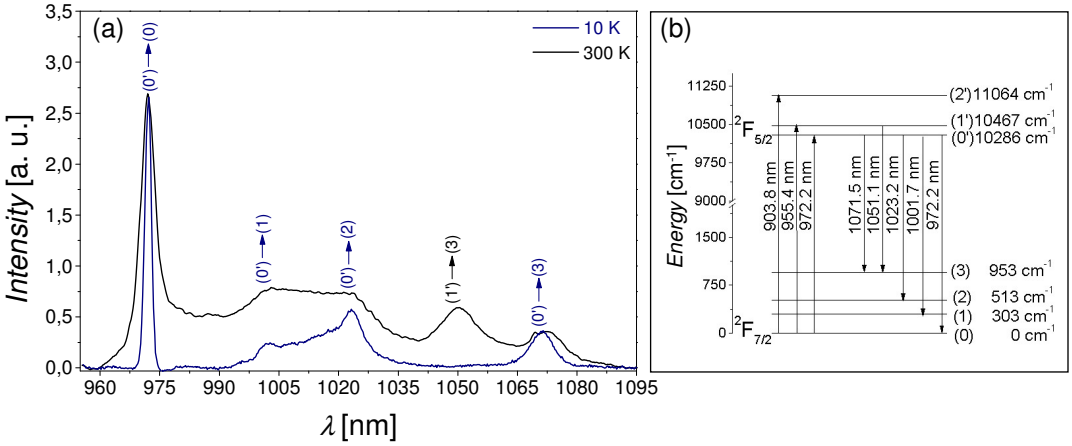

Figure 5.3. (a) Unpolarized emission spectra of $RbTi_{0.95}Ta_{0.03}Yb_{0.02}OPO_4$ recorded at low and room temperature, and (b) Schematic diagram of the Stark sublevels and transitions of Yb^{3+} in $RbTi_{1-x}Ta_xOPO_4$.

Table 5.2. *$^2F_{7/2}$ Stark sublevels of Yb^{3+} determined at 6 K in $RbTi_{0.95}Nb_{0.03}Yb_{0.02}OPO_4$ and $RbTi_{0.95}Ta_{0.03}Yb_{0.02}OPO_4$.*

Host	***Energy position*** [cm^{-1}]
$RbTi_{1-x}Nb_xOPO_4$	0(0); 309(1); 521(2); 956(3)
$RbTi_{1-x}Ta_xOPO_4$	0(0); 303(1); 513(2); 953(3)

The high energies of the Yb^{3+} highest sublevel of the ground state in $RbTi_{1-x}Nb_xOPO_4$ and $RbTi_{1-x}Ta_xOPO_4$, 956 cm^{-1} and 953 cm^{-1} respectively, facilitate the laser operation in a quasi-three level laser, reducing the laser threshold, as it could be seen in Table III of *paper II* and *paper III*.

While recording the temperature evolution of the emission spectra (from 10 K to 300 K), it is clear that the transition centred at around 1050 nm becomes more important and all the bands become broader as increasing the temperature, see Figure 5.4.

UNIVERSITAT ROVIRA I VIRGILI
YTTERBIUM AND ERBIUM DOPEP RbTi1-xMxOPO4 (M=Nb or Ta) CRYSTALS. NEW LASER AND NONLINEAR BIFUNCTIONAL MATERIALS
Alexandra Peña Revellez
ISBN: 978-84-691-0370-8 /DL:T.2188-2007

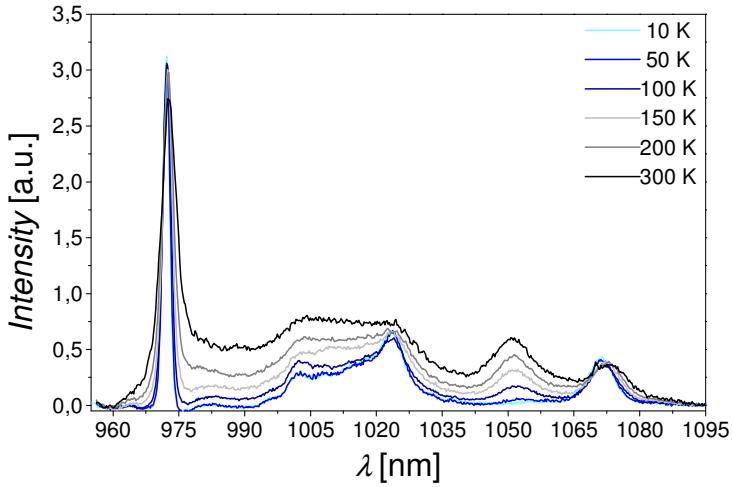

Figure 5.4. Temperature evolution (from 10 K to 300 K) of the emission spectra of $RbTi_{0.95}Ta_{0.03}Yb_{0.02}OPO_4$.

5.3 Absorption of Yb^{3+} and Er^{3+} in $RbTi_{1-x}Nb_xOPO_4$

As ytterbium has already been introduced (see previous section) we focused our attention in erbium. Although Er^{3+} shows five metastable states ($^2H_{9/2}$, $^4S_{3/2}$, $^2F_{9/2}$, $^4I_{11/2}$ and $^4I_{13/2}$) which leads to a broad emission spectral range, the emission transition $^4I_{13/2} \rightarrow {}^4I_{15/2}$ which leads to laser oscillation around 1.55 µm is the most used, mainly for optical communications and in the eyesafe range for lasers, because this particular wavelength matches with the second standard window for long-haul communications, and with strong absorption in the aqueous humor and cornea of the human eye. Additionaly, light sources in the 2.8 µm spectral region, related with the $^4I_{11/2} \rightarrow {}^4I_{13/2}$ transition, are interesting for medical applications and its green emission (induced by up-conversion), $^4S_{3/2} \rightarrow {}^4I_{15/2}$, is interesting for applications such as colour displays or optical data storage. But, single doped Er^{3+} crystals show low absorption cross-sections of the $^4I_{11/2}$ excited state, which limits the laser action around 1.55 µm. This laser action could be achieved in Er^{3+}/Yb^{3+} doped crystals, by using Yb^{3+} as a sensitizer ion of the $^4I_{11/2}$ Er^{3+} level, by pumping Yb^{3+} with diode lasers. The scheme of Er^{3+}/Yb^{3+} laser systems is shown in Figure 5.5.

UNIVERSITAT ROVIRA I VIRGILI
YTTERBIUM AND ERBIUM DOPEP RbTi1-xMxOPO4 (M=Nb or Ta) CRYSTALS. NEW LASER AND NONLINEAR BIFUNCTIONAL MATERIALS
Alexandra Peña Revellez
ISBN: 978-84-691-0370-8 /DL:T.2188-2007

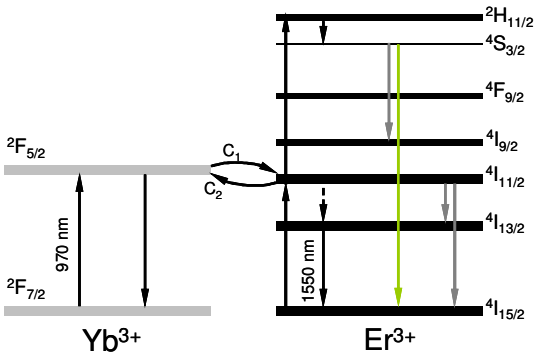

Figure 5.5. Energy transfer and laser schemes in Er^{3+}/Yb^{3+} laser systems.

Up to now, spectroscopic studies of Er^{3+} doped KTP and RTP[75] and $RbTi_{1-x}Nb_xOPO_4$[102] had been performed and Judd-Ofelt theory[129-130] was used to analyse the obtained results. These studies proposed that there are two different erbium sites in the structure, which are due to the erbium substitution of titanium (which occupies two non equivalent positions in the lattice). Both sites have the same symmetry, C_1, and the maximum number of bands for each sublevel (and for each multiplet) would be *(2J+1)/2* for each different site. These observations are going to be checked in the Yb^{3+}/Er^{3+} $RbTi_{1-x}Nb_xOPO_4$ samples.

$RbTi_{1-x}Nb_xOPO_4$ samples were codoped with ytterbium and erbium, achieving the same concentration of ytterbium achieved in mono-doped $Yb:RbTi_{1-x}Nb_xOPO_4$ crystals (≈ 2×10^{20} ions/cm^3) and a lower erbium concentrations (0.25×10^{20} ions/cm^3) than in $Er:RbTi_{1-x}Nb_xOPO_4$.[102] Because of the lower concentration of Er^{3+} achieved in Yb^{3+}/Er^{3+} codoped $RbTi_{1-x}Nb_xOPO_4$ crystals, the observation of all the transitions from the ground state to the different excited states have been more complex and the $^4I_{15/2} \rightarrow {}^4I_{11/2}$ transition could not be observed, as it overlaps with the $^2F_{7/2} \rightarrow {}^2F_{5/2}$ ytterbium transition.

All the absorption spectra were recorded at room temperature and by polarizing light parallel to the ***c*** direction, because, as reported previously for $Er:RbTi_{1-x}Nb_xOPO_4$, it is the most intense absorption.[75] All the transitions below 350 nm will not be observed as RTP is not transparent below this value. From

UNIVERSITAT ROVIRA I VIRGILI
YTTERBIUM AND ERBIUM DOPEP RbTi1-xMxOPO4 (M=Nb or Ta) CRYSTALS. NEW LASER AND NONLINEAR BIFUNCTIONAL MATERIALS
Alexandra Peña Revellez
ISBN: 978-84-691-0370-8 /DL:T.2188-2007

all the other transitions which are in the transparency range of the crystal only nine transitions could be measured; $^4G_{11/2}$, $^2H_{9/2}$, $^4F_{3/2}$, $^4F_{5/2}$, $^4F_{7/2}$, $^2H_{11/2}$, $^4S_{3/2}$, $^4F_{9/2}$, $^4I_{13/2}$, shown in Figure 5.6, and $^2K_{15/2}$ and $^4G_{9/2}$ were identified, but due to the low intensity showed could not been measured. From all these transitions, $^4G_{11/2}$ and $^2H_{11/2}$ are the hypersensitives, showing higher σ_{abs} values. This last one, associated to the $^4I_{15/2} \rightarrow {}^2H_{11/2}$ transition, is responsible for the pink colour of the sample.

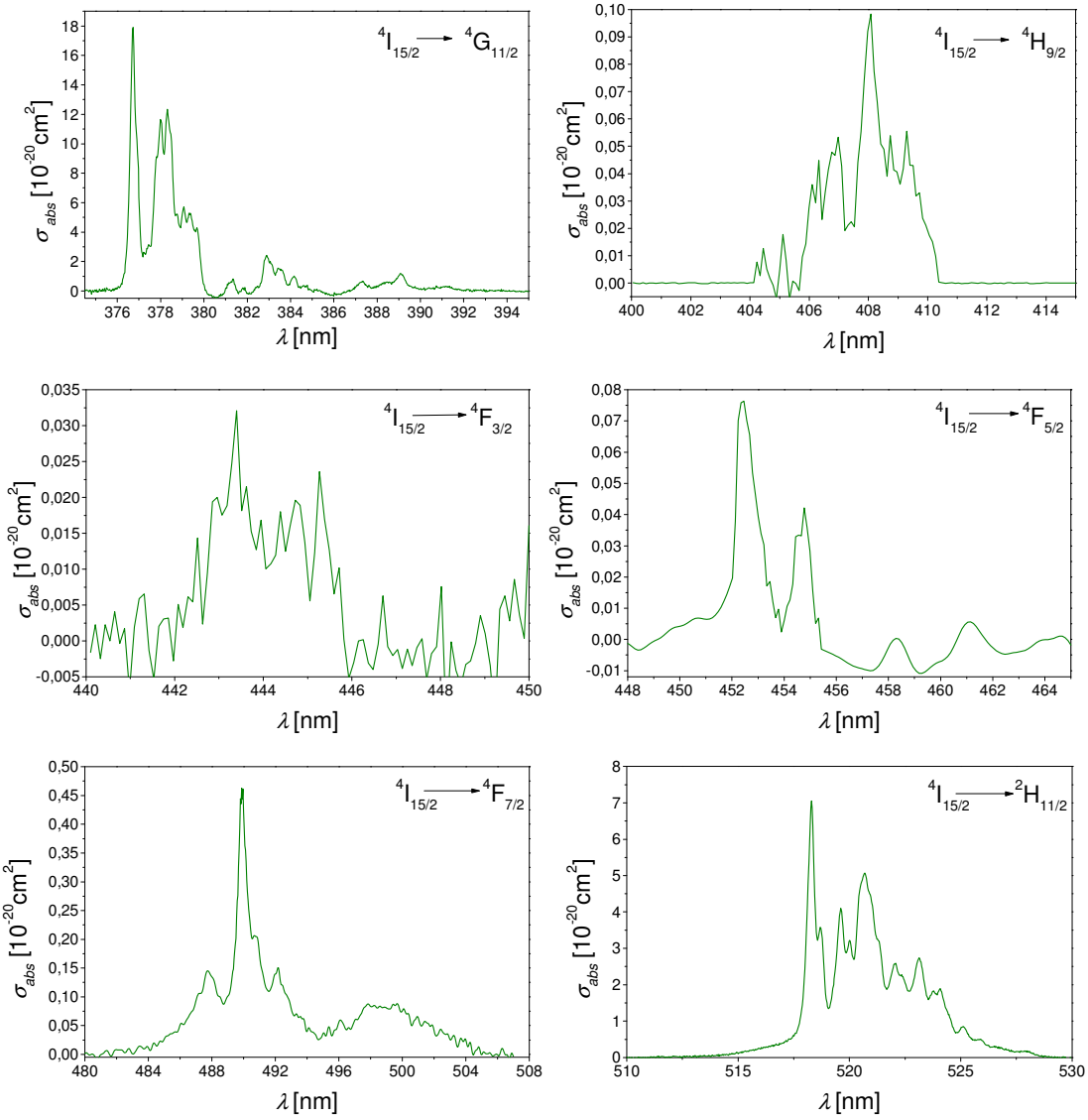

UNIVERSITAT ROVIRA I VIRGILI
YTTERBIUM AND ERBIUM DOPEP RbTi1-xMxOPO4 (M=Nb or Ta) CRYSTALS. NEW LASER AND NONLINEAR BIFUNCTIONAL MATERIALS
Alexandra Peña Revellez
ISBN: 978-84-691-0370-8 /DL:T.2188-2007

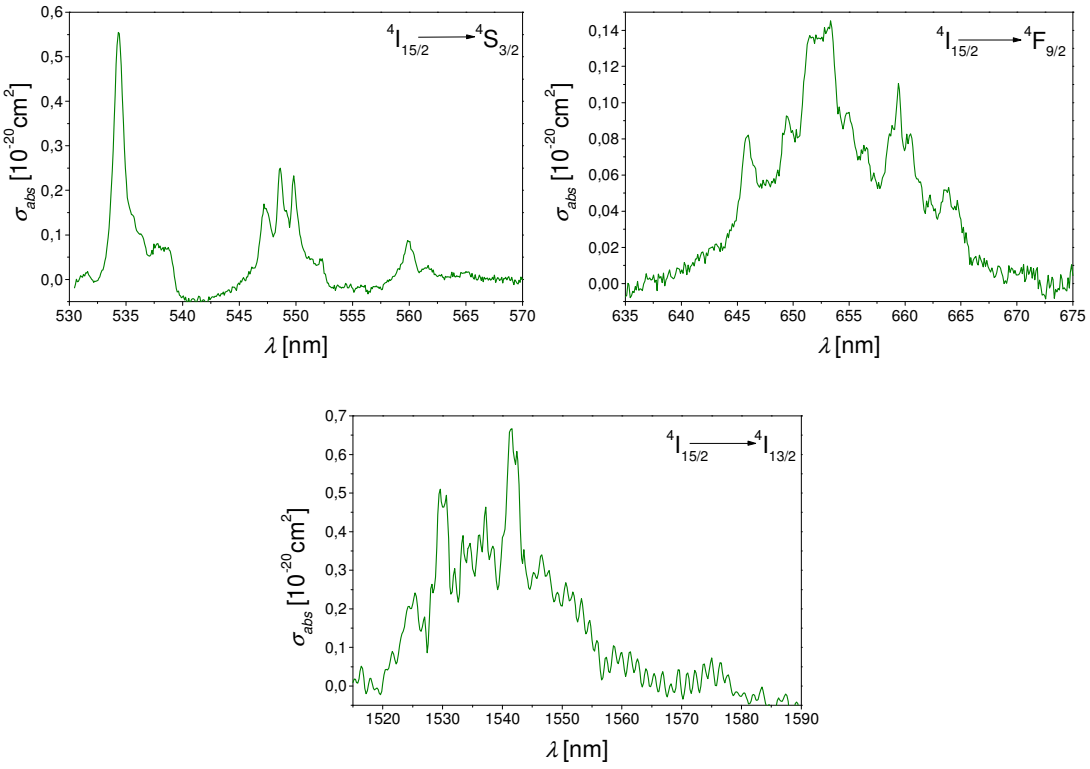

Figure 5.6. Er^{3+} absorption cross sections in Er:Yb:$RbTi_{1-x}Nb_xOPO_4$, recorded at room temperature and with ***E//c***.

The energy positions of the absorption bands of Er^{3+} for each multiplet in RTP and $RbTi_{1-x}Nb_xOPO_4$ are quite similar,[75,131] so it is expected to be quite similar for Yb:$RbTi_{1-x}Nb_xOPO_4$. As we are interested in the emission $^4I_{13/2} \rightarrow {}^4I_{15/2}$ transition, which leads to laser oscillation at around 1.55 μm, we only recorded the spectrum corresponding to the $^4I_{15/2} \rightarrow {}^4I_{13/2}$ transition, at low temperature, see Figure 5.7. The differences in the energy positions of Er^{3+} in Er:Yb:$RbTi_{1-x}Nb_xOPO_4$ when compared to Er:$RbTi_{1-x}Nb_xOPO_4$ and Er:RTP are shown in Table 5.3.

UNIVERSITAT ROVIRA I VIRGILI
YTTERBIUM AND ERBIUM DOPEP RbTi1-xMxOPO4 (M=Nb or Ta) CRYSTALS. NEW LASER AND NONLINEAR BIFUNCTIONAL MATERIALS
Alexandra Peña Revellez
ISBN: 978-84-691-0370-8 /DL:T.2188-2007

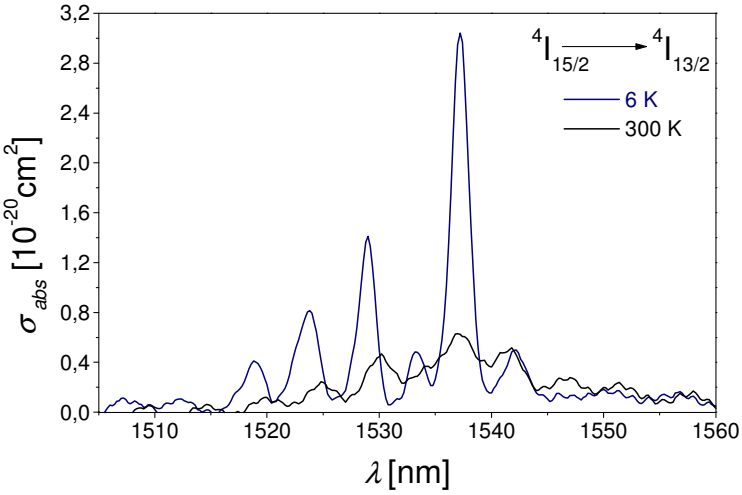

Figure 5.7. Low temperature and room temperature unpolarized absorption spectra of Er^{3+} ($^4I_{15/2} \rightarrow {}^4I_{13/2}$ transition) in Er:Yb:$RbTi_{1-x}Nb_xOPO_4$.

Table 5.3. *Energies of the Stark sublevel of the $^4I_{13/2}$ excited level of Er^{3+} in RTP, $RbTi_{1-x}Nb_xOPO_4$ and $RbTi_{1-x}Nb_xOPO_4$ doped with Yb^{3+}.*

Host	$^{2s+1}L_J$	***Energy*** [cm^{-1}] / ***λ*** [nm]						
RTP	$^4I_{13/2}$	6588	6571	6566	6545	6514	6510	6506
		1518.0	1521.9	1523.1	1528.0	1535.1	1536.0	1537.0
$RbTi_{1-x}Nb_xOPO_4$	$^4I_{13/2}$	6587	6565	6544	6525	6511	6495	6487
		1518.2	1523.2	1528.1	1532.6	1535.9	1539.6	1541.6
$RbTi_{1-x}Nb_xOPO_4$ [(a)]	$^4I_{13/2}$	6584	6562	6540	6529	6522	6505	6485
		1518.8	1523.8	1529.0	1531.6	1533.2	1537.2	1542.1

[(a)] This work

About the obtained room temperature, the absorption spectrum of Yb^{3+} (transition $^2F_{7/2} \rightarrow {}^2F_{5/2}$) in Er:Yb:$RbTi_{1-x}Nb_xOPO_4$ sample, is the same as obtained for Yb:$RbTi_{1-x}Nb_xOPO_4$, see Figure 1 of *paper II*. In the low temperature absorption spectrum, shown in Figure 5.8, two additional peaks appeared at 10204 cm^{-1} (980 nm)* and 10368 cm^{-1} (964.5 nm)* that are related to the Er^{3+} transition $^4I_{15/2} \rightarrow {}^4I_{11/2}$.

UNIVERSITAT ROVIRA I VIRGILI
YTTERBIUM AND ERBIUM DOPEP RbTi1-xMxOPO4 (M=Nb or Ta) CRYSTALS. NEW LASER AND NONLINEAR BIFUNCTIONAL MATERIALS
Alexandra Peña Revellez
ISBN: 978-84-691-0370-8 /DL:T.2188-2007

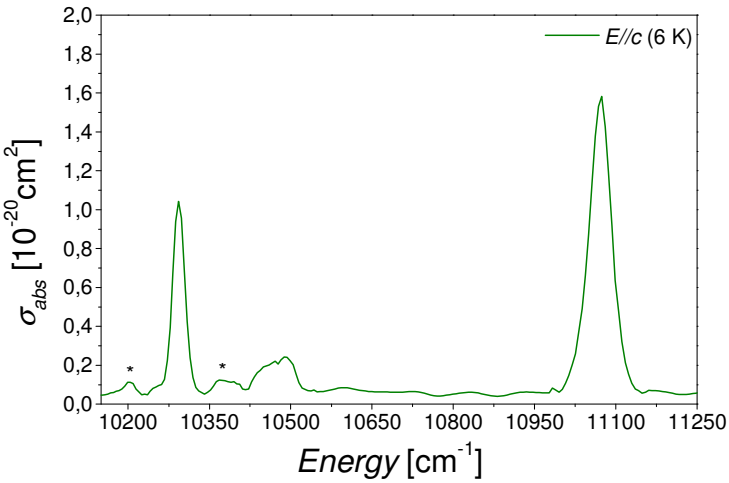

Figure 5.8. Low temperature absorption spectra recorded with ***E//c*** in Er:Yb:$RbTi_{1-x}Nb_xOPO_4$ sample, in the spectral range of $^2F_{7/2} \rightarrow {}^2F_{5/2}$ transition of Yb^{3+} and the $^4I_{15/2} \rightarrow {}^4I_{11/2}$ transition of Er^{3+} (*).

5.4 Emission of Yb^{3+} and Er^{3+} in $RbTi_{1-x}Nb_xOPO_4$

Since now no Er^{3+} visible emission by up-conversion process had been achieved in KTP, RTP or $RbTi_{1-x}Nb_xOPO_4$,[75,83] due to the low absorption efficiency of the $^4I_{11/2}$ level. As the Er^{3+} concentration could not been increased in KTP, RTP or $RbTi_{1-x}Nb_xOPO_4$ crystals grown by the TSSG-SC technique, we grown crystals with Yb^{3+} as a codopand to achieve high absorption efficiency and enhance the Er^{3+} IR emission (≈ 1.55 μm) from the $^4I_{13/2}$ level and obtain up-conversion emission from, for example, the $^4S_{3/2}$ level (≈ 0.55 μm).

All the spectra were performed in a 90º geometry and by pumping the sample at around 900 nm, which matches with one of the maxima of the Yb^{3+} absorption spectrum, as shown in Figure 1 of *paper II*. The emission spectra of Yb^{3+} ($^2F_{5/2} \rightarrow {}^2F_{7/2}$ transition) and Er^{3+} ($^4I_{13/2} \rightarrow {}^4I_{15/2}$ transition) were recorded at low temperature (10 K) and room temperature, to determine the Stark sublevels of the $^4I_{13/2}$ ground state of Er^{3+} and of the $^2F_{7/2}$ ground state of Yb^{3+}, although no significant differences were expected from the Yb^{3+} Stark sublevels previously determined in Yb:$RbTi_{1-x}Nb_xOPO_4$, see Figure 3 of *paper II*. The visible emissions of Er^{3+} ($^2H_{11/2} \rightarrow {}^4I_{15/2}$, $^4S_{3/2} \rightarrow {}^4I_{15/2}$ and $^4F_{9/2} \rightarrow {}^4I_{15/2}$ transitions) were only recorded at room temperature. Figure 5.9 (a) shows the

UNIVERSITAT ROVIRA I VIRGILI
YTTERBIUM AND ERBIUM DOPEP RbTi1-xMxOPO4 (M=Nb or Ta) CRYSTALS. NEW LASER AND NONLINEAR BIFUNCTIONAL MATERIALS
Alexandra Peña Revellez
ISBN: 978-84-691-0370-8 /DL:T.2188-2007

low and room temperature emission spectra of Yb^{3+}, which is characterized by six main lines at low temperature and at room temperature, which are labelled according to the diagram of the Stark sublevels (inset). The extra line that appears, while comparing it with the one obtained for $Yb:RbTi_{1-x}Nb_xOPO_4$, is observed because the laser pump ($\lambda_{pump} \approx 900$ nm) is far from this new line. In Figure 5.9 (b) the Er^{3+} emission spectra of the $^4I_{13/2} \rightarrow {}^4I_{15/2}$ transition is shown, and the main lines are labelled (see inset).

Although not all the bands which appeared in the $^4I_{13/2} \rightarrow {}^4I_{15/2}$ emission spectrum of Er^{3+} were well resolved, identification of the different transitions seems to be consistent, and only one weak band could not be identified.

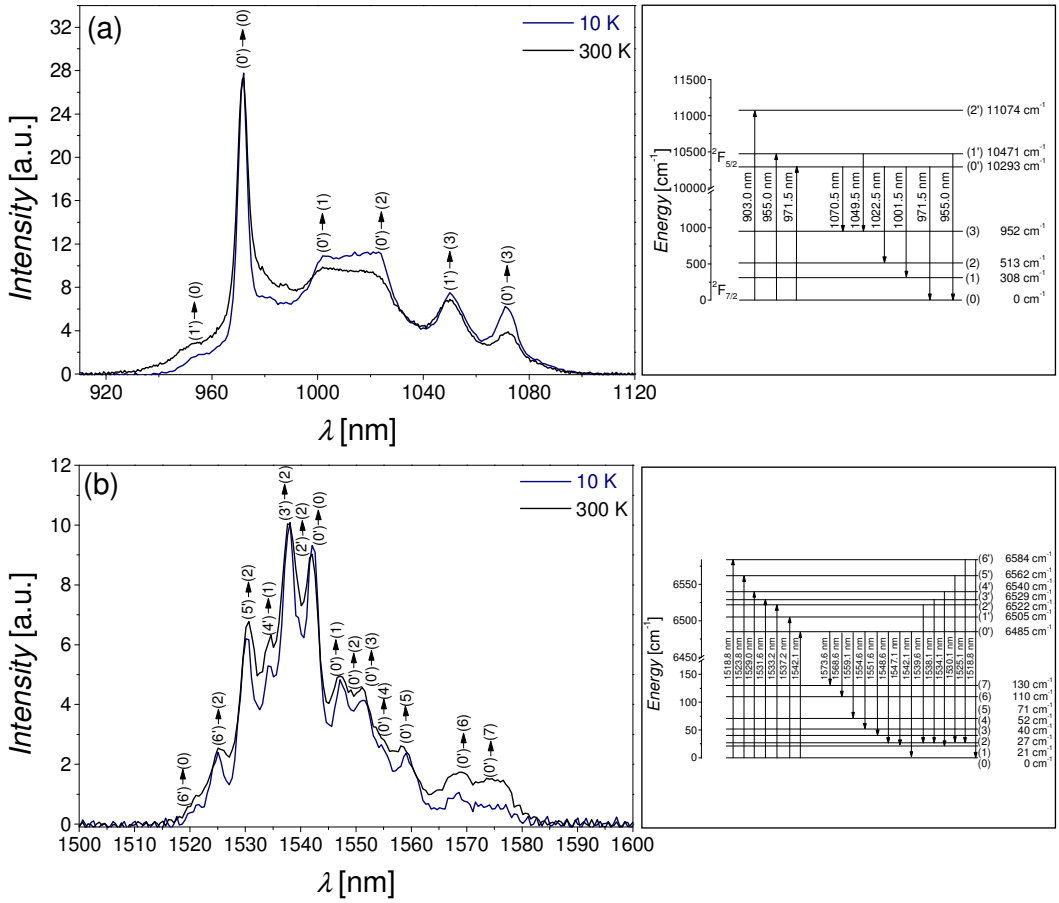

Figure 5.9. (a) $^2F_{5/2} \rightarrow {}^2F_{7/2}$ emission of Yb^{3+} at low and room temperature with all the transition labelled according to the Stark sublevels diagram (right hand), and (b) $^4I_{13/2} \rightarrow {}^4I_{15/2}$ emission of Er^{3+}.

UNIVERSITAT ROVIRA I VIRGILI
YTTERBIUM AND ERBIUM DOPEP RbTi1-xMxOPO4 (M=Nb or Ta) CRYSTALS. NEW LASER AND NONLINEAR BIFUNCTIONAL MATERIALS
Alexandra Peña Revellez
ISBN: 978-84-691-0370-8 /DL:T.2188-2007

Figure 5.10 shows all the Er^{3+} up-conversion emissions, recorded at room temperature, that extend from 500 to 700 nm and as mentioned above comprises the $^2H_{11/2} \rightarrow {}^4I_{15/2}$ and the $^4S_{3/2} \rightarrow {}^4I_{15/2}$, in the green spectral range, and the $^4F_{9/2} \rightarrow {}^4I_{15/2}$, in red spectral range. The band that appears at around 480 nm is due to the presence of Tm^{3+} impurities.

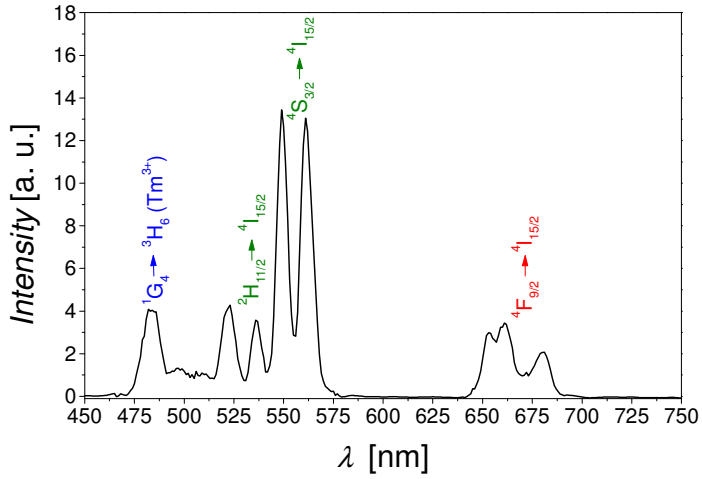

Figure 5.10. Er^{3+} up-conversion emissions, recorded at room temperature, in a $Er:Yb:RbTi_{1-x}Nb_xOPO_4$ crystal.

With these results we can make a scheme, which is shown in Figure 5.11, of the pump and the energy transfer for the generation of the IR (1.55 μm) and visible (500-700 nm) emissions of Er^{3+} in $RbTi_{1-x}Nb_xOPO_4$ doped with Er^{3+} and Yb^{3+} as the sensitizing ion.

So, we have shown that it is possible to enhance IR and visible Er^{3+} emissions by using Yb^{3+} as a sensitizing ion (only one pump wavelength is needed), even though low Er^{3+} concentrations are obtained in the codoped samples. As the Er^{3+} concentration could not be increased in $RbTi_{1-x}Nb_xOPO_4$ single crystals grown by TSSG-SC technique, due to the differences between the Er^{3+} and the Ti^{4+} ionic radii ($r_{Er^{3+}}$ = 0.890 Å; $r_{Ti^{4+}}$ = 0.605 Å),[104] codoping $Er:RbTi_{1-x}Nb_xOPO_4$ with Yb^{3+} is the best way to obtain efficient Er^{3+} emission. Further experiments to evaluate the Er^{3+} lifetime at around 1.55 μm, which should be around 7 ms,[131] and to try to achieve laser operation at around 1.55 μm make the next logical progression in this work.

UNIVERSITAT ROVIRA I VIRGILI
YTTERBIUM AND ERBIUM DOPEP RbTi1-xMxOPO4 (M=Nb or Ta) CRYSTALS. NEW LASER AND NONLINEAR BIFUNCTIONAL MATERIALS
Alexandra Peña Revellez
ISBN: 978-84-691-0370-8 /DL:T.2188-2007

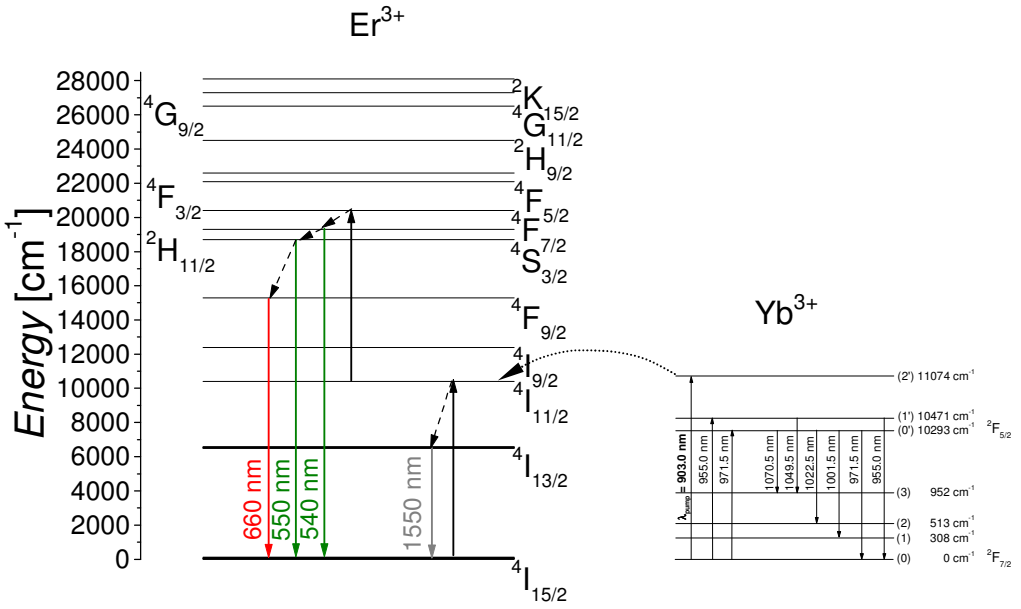

Figure 5.11. Scheme of the pump and the energy transfer from Yb^{3+} to Er^{3+} for the generation of visible and IR emissions of Er^{3+} in Er:Yb:$RbTi_{1-x}Nb_xOPO_4$.

UNIVERSITAT ROVIRA I VIRGILI
YTTERBIUM AND ERBIUM DOPEP RbTi1-xMxOPO4 (M=Nb or Ta) CRYSTALS. NEW LASER AND NONLINEAR BIFUNCTIONAL MATERIALS
Alexandra Peña Revellez
ISBN: 978-84-691-0370-8 /DL:T.2188-2007

UNIVERSITAT ROVIRA I VIRGILI
YTTERBIUM AND ERBIUM DOPEP RbTi1-xMxOPO4 (M=Nb or Ta) CRYSTALS. NEW LASER AND NONLINEAR BIFUNCTIONAL MATERIALS
Alexandra Peña Revellez
ISBN: 978-84-691-0370-8 /DL:T.2188-2007

Chapter 6

Continuous wave laser operation of Yb^{3+} in $RbTi_{1-x}Nb_xOPO_4$

In this chapter some important laser parameters are calculated from spectroscopic data, in order to evaluate Yb:$RbTi_{1-x}Nb_xOPO_4$ as a laser crystal. The results of the Yb^{3+} laser operation in $RbTi_{1-x}Nb_xOPO_4$ at room temperature in continuous-wave (CW) regime are also described. The Yb^{3+} laser operation is observed for the first time, to our knowledge, in a crystal of the KTP family.

UNIVERSITAT ROVIRA I VIRGILI
YTTERBIUM AND ERBIUM DOPEP RbTi1-xMxOPO4 (M=Nb or Ta) CRYSTALS. NEW LASER AND NONLINEAR BIFUNCTIONAL MATERIALS
Alexandra Peña Revellez
ISBN: 978-84-691-0370-8 /DL:T.2188-2007

6.1 Quasi-three-level laser system

At room temperature, Yb^{3+} doped crystals mainly operate as a quasi-three level laser materials. In such systems (see Figure 6.1), the pump and emitting laser levels are energetically close to each other, being Stark levels of the same multiplet ($^2F_{5/2}$ in the case of Yb^{3+}). So, the two-manifold electronic structure of Yb^{3+}, corresponds to the aforementioned scheme for laser operation where inversion is not as easily achieved as in a four-level-laser. In four-level lasers, the lower laser level is practically empty and the pump requirements to achieve threshold are smaller than in quasi-three-level lasers, where the terminating laser level (normally $^2F_{7/2}(3)$) is thermally occupied. Nevertheless, four-level-lasers experience greater thermal load, because of the larger difference between the pump and laser wavelengths, than quasi-three-level lasers.

In Figure 6.1 (a) laser emission starts from the lowest Stark level of the upper multiplet and leads to the highest Stark level of the ground-state. Contribution of laser emissions from higher-located, lower-populated Stark levels of the excited multiplet, have been neglected, but this is taken into account in Figure 6.1 (b) where the laser scheme found for Yb^{3+} in $RbTi_{1-x}Nb_xOPO_4$ is shown.

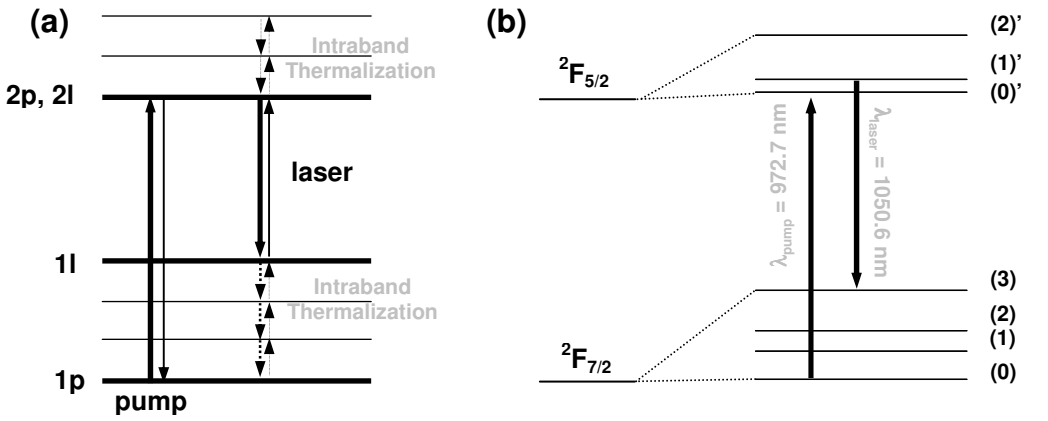

Figure 6.1. (a) Quasi-three-level laser operation, and (b) quasi-three-level scheme of Yb^{3+} in $RbTi_{1-x}Nb_xOPO_4$.

UNIVERSITAT ROVIRA I VIRGILI
YTTERBIUM AND ERBIUM DOPEP RbTi1-xMxOPO4 (M=Nb or Ta) CRYSTALS. NEW LASER AND NONLINEAR BIFUNCTIONAL MATERIALS
Alexandra Peña Revellez
ISBN: 978-84-691-0370-8 /DL:T.2188-2007

The origin of the laser threshold, minimum pump power required for laser emission, is the power loss via fluorescence into a large number of spatial modes. High laser gain (σ_g) and low cavity losses are needed for a low laser threshold. Above threshold, in the CW regime, the inversion density and the gain of a laser are clamped at their threshold values; the round-trip gain of the cavity is equal to the round-trip loss. By increasing the pumping, the laser output power increases but the gain remains fixed.

The efficiency of a laser is often discussed in terms of slope efficiency (η_s), defined as the slope of the curve obtained by plotting the laser output (P_{out}) versus either the absorbed pump power (P_{abs}) or the incident pump power, because the laser output power varies linearly with the pump rate. As shown in Figure 3 of *paper III*, we plotted the P_{out} versus the P_{abs} because seems more realistic since it takes into account the real power that the crystal is making use.

6.2 Parameters of a laser crystal

Values obtained from the spectroscopic characterization, such as absorption and emission cross sections (σ_{abs} and σ_e) as well as the measured lifetime (τ), help to estimate some important laser parameters. Those used to evaluate the potential of a crystal as gain medium are

$$I_{p,sat} = \frac{h\upsilon_{pump}}{\sigma_{abs}(\lambda_{pump})\tau} \;;\; I_{l,sat} = \frac{h\upsilon_{laser}}{\sigma_e(\lambda_{laser})\tau} \qquad \text{eq. 6.1}$$

where $I_{p,sat}$ and $I_{l,sat}$ are the saturation pump and laser intensities, respectively, defined as the intensity values at which the gain decreases one half of their small-signal value in the steady state.

When dealing with a quasi-three-level gain media, with overlapped absorption and emission spectra, these expressions turn into

$$I_{p,sat} = \frac{h\upsilon_p}{\{\sigma_{abs}(\lambda_p)+\sigma_e(\lambda_p)\}\tau} \;;\; I_{l,sat} = \frac{h\upsilon_l}{\{\sigma_{abs}(\lambda_l)+\sigma_e(\lambda_l)\}\tau}. \qquad \text{eq. 6.2}$$

UNIVERSITAT ROVIRA I VIRGILI
YTTERBIUM AND ERBIUM DOPEP RbTi1-xMxOPO4 (M=Nb or Ta) CRYSTALS. NEW LASER AND NONLINEAR BIFUNCTIONAL MATERIALS
Alexandra Peña Revellez
ISBN: 978-84-691-0370-8 /DL:T.2188-2007

Long emission lifetimes (τ), as well as high absorption cross-sections (σ_{abs}) and emission cross-sections (σ_e) at the pump and the laser wavelength respectively, would lead to low saturation intensities.

β_{min} is the minimum fraction of Yb^{3+} ions that must be excited to balance the gain and the ground state absorption at the extraction wavelength (λ_{ext}).

$$\beta_{min} = \frac{\sigma_{abs}(\lambda_{ext=l})}{\sigma_{abs}(\lambda_{ext=l}) + \sigma_{ext=l}(\lambda_{ext=l})} \qquad \text{eq. 6.3}$$

with which we can calculate the minimum pump intensity ($I_{p,min}$) to reach laser threshold, by means of

$$I_{p,min} = \frac{\beta_{min}}{\sigma_{abs}(\lambda_p) - \beta_{min}\{\sigma_{abs}(\lambda_p) + \sigma_e(\lambda_p)\}} \frac{h\upsilon_p}{\tau} \qquad \text{eq. 6.4}$$

This value should be as low as possible in efficient laser materials.

In Table 6.1, the estimated laser parameters of $Yb:RbTi_{1-x}Nb_xOPO_4$ for the three polarizations are listed, which were considered the ideal case of zero cavity losses. With this assumption, the pump threshold from the inversion value for which the gain cross section ($\sigma_g = \beta\sigma_e - (1-\beta)\sigma_{abs}$) reaches zero at some wavelength can be estimated. The gain cross-section (σ_g) reaches zero at the minimum inversion parameter (β_{min}) at the expected laser wavelength (λ_l).

Table 6.1. *Laser parameters calculated from spectroscopic data, using the λ_p and λ_l obtained in the laser operation of $RbTi_{0.95}Nb_{0.03}Yb_{0.02}OPO_4$ (see paper III) along the three principal axes.*

	λ_p (nm)	λ_l (nm)	σ_{abs} (λ_p) ($10^{-20}cm^2$)	σ_e (λ_p) ($10^{-20}cm^2$)	τ (ms)	β_{min} (%)	$I_{p,sat}$ (KW/cm^2)	$I_{p,min}$ (KW/cm^2)
E//a	972.6	1047.0	0.31	0.29	2.2	2.97	15.42	0.95
E//b	972.8	1049.4	0.79	0.77	2.2	2.68	5.94	0.33
E//c	972.8	1050.6	0.33	0.32	2.2	2.55	14.19	0.75

The calculated values using eq. 6.2 and 6.4 are different from those calculated in *paper II* (Table II). To compare these values with those estimated for the non-centrosymmetric hosts where lasing of Yb^{3+} had been achieved up

to now, YAB ($YAl_3(BO_3)_4$),[132] GAB ($GdAl_3(BO_3)_4$),[20] YCOB ($YCa_4O(BO_3)_3$),[133] GdCOB ($GdCa_4O(BO_3)_3$)[53] and LNB ($LiNbO_3$),[57] we should suppose a quasi-four-level system. Although these values have not been calculated in the same way, it seems from spectroscopic data, shown in Table II of *paper II*, that Yb:$RbTi_{1-x}Nb_xOPO$ will be more efficient, or at least of the same order, than Yb^{3+} doped MgO:LNB, GdCOB and YCOB.

6.3 CW laser operation of Yb^{3+} in $RbTi_{1-x}Nb_xOPO_4$

The CW laser radiation from Yb^{3+} in $RbTi_{1-x}Nb_xOPO_4$, was obtained by using a sample with an Yb^{3+} concentration of ≈ 1.9×10^{20} ions/cm^3. The crystal was oriented along the principal optics axes, ***x***, ***y*** and ***z*** and the dimensions along them were 2.95, 2.52 and 3.00 mm, respectively. The faces normal to ***a*** (***x***) and ***b*** (***y***) directions were polished with high optical quality, so that we were able to check the laser activity for each polarization, ***a***, ***b*** and ***c***, in a two propagation configuration, ***a*** and ***b***.

The $RbTi_{0.95}Nb_{0.03}Yb_{0.02}OPO_4$ cube, which was uncoated, was placed in a Z-shaped cavity (see Figure 4 of *paper II* and Figure 2 of *paper III*), under Brewster angle, in order to avoid Fresnel losses. In such a configuration, the cavity losses equal to zero only for the polarization parallel to the reflection plane (*p*), and have high losses for polarization perpendicular to this plane (*s*). To avoid additional losses occurred from the pump, we used the selected pump polarization to be parallel to the laser polarization (*p*).

As pointed out in *paper II* and *paper III*, CW laser operation at room temperature was obtained when the sample was oriented with ***E//b*** and ***E//c*** and propagation along ***a*** axis, and when it was oriented with ***E//a*** and ***E//c*** and propagation along ***b*** axis. Two output couplers were used, 1% and 3%, obtaining laser operation in both cases for ***E//b*** and ***E//c***, but for ***E//a*** it was only obtained by using a T_{oc} = 1%.

While propagating along ***a*** axis, the slope efficiency obtained for an output coupler of 1% was higher, 42.5 %, for ***E//b*** than for ***E//c***, 37.6 %, and so was the output power obtained, 154 mW for ***E//b*** and 115 mW for ***E//c***, this is attributed to the higher gain cross-section (σ_g). In Figure 3 of *paper III* the output power versus the absorbed pump power for output couplers of 1 and 3

% is depicted. In Table III of *paper II* the relevant laser parameters obtained for $RbTi_{0.95}Nb_{0.03}Yb_{0.02}OPO_4$ (pump threshold, slope efficiency and oscillation wavelengths) are listed. Although the output power obtained, under Ti:sapphire pumping, is not too high, it could be increased by either enlarging the crystal length or by increasing the doping level to have more active centers, to increase the absorption. Another way is to increase the pump power by using diode pumping. Moreover, it should be noticed that low laser thresholds have been achieved, because as pointed out in the spectroscopy chapter, the high energies of the Yb^{3+} highest sublevel of the ground state (956 cm^{-1}) facilitates the laser operation in a quasi-three-level laser. This is due to the absence of important electronic population (only 0.76 %) in the aforementioned sublevel of the ground state.

Laser oscillation occurred on the $^2F_{5/2}(1') \rightarrow {}^2F_{7/2}(3)$ transition near 1050 nm, as shown in Figure 6.1, and it shows a tuning range extendable from 1009 to 1081 nm (FWHM of 59 nm) for all three possible polarizations. This tuneable behaviour makes it promising to obtain ultrashort laser pulses.

As it is possible to obtain Type II SHG in the ***ab*** plane, as explained in chapter 4, the tuneable behaviour shown in the IR laser action, might lead to self frequency doubling (SFD) visible light generation from cyan to green. Visible light generation by SFD was observed, up to now, in four ytterbium doped non-centrosymmetric hosts: YAB,[59] YCOB,[51] GdCOB[53] and MgO:LNB.[57]

UNIVERSITAT ROVIRA I VIRGILI
YTTERBIUM AND ERBIUM DOPEP RbTi1-xMxOPO4 (M=Nb or Ta) CRYSTALS. NEW LASER AND NONLINEAR BIFUNCTIONAL MATERIALS
Alexandra Peña Revellez
ISBN: 978-84-691-0370-8 /DL:T.2188-2007

Conclusions

The first main result of this study is the successful growth of single crystals of ytterbium doped $RbTi_{1-x}Nb_xOPO_4$ or $RbTi_{1-x}Ta_xOPO_4$ and erbium/ytterbium doped $RbTi_{1-x}Nb_xOPO_4$. Aditionally, the optical characterizations of the hosts and the spectroscopic characterizations of the active ions indicate that laser action could be obtained from these crystals at ≈ 1 μm, and it was obtained in $Yb:RbTi_{1-x}Nb_xOPO_4$. Laser action at ≈ 1 μm in this material might lead to self-frequency doubling laser action in the visible spectral range.

By studying the crystallization region of RTP in self-flux, when TiO_2 was partially substituted by Ta_2O_5 and Yb_2O_3, we found that the Yb^{3+} concentration achieved was of the same order (≈ 2×10^{20} ions/cm^3) of that obtained by partially substituting TiO_2 by Nb_2O_5 and Yb_2O_3. Both Ta^{5+} and Nb^{5+} could be used to obtain an Yb^{3+} concentration high enough to obtain laser action in crystals of the $KTiOPO_4$ family.

Although the size of the crystals obtained by the TSSG-SC technique was shown to be limited mainly along the ***a*** direction due to the flat morphology along the mentioned direction, this drawback was avoided by using seeds thick in the aforementioned direction.

In addition to RTP, $RbTi_{1-x}Nb_xOPO_4$ and $RbTi_{1-x}Ta_xOPO_4$ show a broad transmission window in thick samples from ≈ 0.350 to 4.5 μm, covering the IR (fundamental) and the visible (second harmonic) ranges.

Experimental results showed that the Yb^{3+} doped $RbTi_{1-x}Nb_xOPO_4$ crystal can be phase matchable for type II second harmonic generation in the ***ab*** plane in the luminescence range of Yb^{3+}, and theoretical simulations showed that it is also possible in the ***bc*** plane. Therefore, $Yb:RbTi_{1-x}Nb_xOPO_4$ is a very promising self frequency doubling crystal.

An enhancement of the Er^{3+} fluorescence at around 1.55 μm in $Er:Yb:RbTi_{1-x}Nb_xOPO_4$ crystals with Yb^{3+} as a sensitizer ion was obtained, which indicates that laser action at around 1.55 μm could be achieved, a wavelength with applications in optical communications. Moreover, Yb^{3+} in $RbTi_{1-x}Nb_xOPO_4$ has generated laser action, and this is the first time that laser generation of

UNIVERSITAT ROVIRA I VIRGILI
YTTERBIUM AND ERBIUM DOPEP RbTi1-xMxOPO4 (M=Nb or Ta) CRYSTALS. NEW LASER AND NONLINEAR BIFUNCTIONAL MATERIALS
Alexandra Peña Revellez
ISBN: 978-84-691-0370-8 /DL:T.2188-2007

Yb^{3+} was achieved in a crystal of the KTP family. The modest output power achieved under Ti:sapphire pumping, which was limited by the Yb^{3+} doping level and the sample size, could be increased by using a diode laser as a pumping source. Laser operation was obtained around 1.050 μm for all three possible polarizations, and with a tuning range extendable from ≈ 1.010 to 1.080 μm, so self frequency doubling visible light generation from cyan to green could be achieved in $Yb:RbTi_{1-x}Nb_xOPO_4$ crystal.

These preliminary laser results indicate that, laser generation of $Yb:RbTi_{1-x}Nb_xOPO_4$ should be thoroughly investigated. In particular, a $Yb:RbTi_{1-x}Nb_xOPO_4$ sphere-shaped crystal should be prepared to further investigate all the self doubling directions.

References

[1] A. L. Schalow, C. H. Townes, "*Infrared and optical masers*", *Physical Review* **112**, *1940* (1958)
[2] T. H. Maiman, "*Stimulated Optical Radiation in Ruby*", *Nature* **187**, *493* (1960)
[3] P. A. Franken, A. E. Hill, C. W. Peters, G. Weireich, "*Generation of optical harmonics*", *Physical Review Letters* **7**, *118* (1961)
[4] S. K. Kurtz, T. T. Perry, "*A powder technique for the evaluation of nonlinear optical materials*", *Journal of Applied Physics* **39**, *3798* (1968)
[5] S. P. Velsko, "*Direct measurements of phase matching properties in small single crystals of new nonlinear materials*", *Soc. Photo-Opt. Instrum. Eng. Conf. Laser Nonlinear Opt. Eng.* **28**, *76* (1989)
[6] B. Boulanger, J. P. Fève, G. Marnier, B. Ménaert, "*Methodology for optical studies of nonlinear crystals: application to the isomorph family $KTiOPO_4$, $KTiOAsO_4$, $RbTiOAsO_4$, $CsTiOPO_4$*", *Pure and Applied Optics* **7**, *239* (1998)
[7] T. Y. Fan, C. E. Huang, B. Q. Hu, R. C. Eckardt, Y. X. Fan, R. L. Byer, R. S. Feigelson, *"Second harmonic generation and accurate index of refraction measurements in flux-grown $KTiOPO_4$"*, *Applied Optics* **26**, *2390* (1987)
[8] J. Jerphagnon, S. K. Kurtz, "*Optical Nonlinear susceptibilities: Accurate Relative Values for Quartz, Ammonium Dihydrogen Phosphate, and Potassium Dihydrogen Phosphate*", *Physical Review B* **1**, *1739* (1970)
[9] B. Boulanger, J. P. Fève, G. Marnier, "*Absolute measurements of quadratic nonlinearities from phase-matched second-harmonic generation in a single KTP crystal cut as a sphere*", *Journal of the Optical Society of America B* **14**, *1380* (1997)
[10] R. G. Smith, K. Nassau, M. F. Galvin, "*Efficient continuous optical second-harmonic generation*", *Applied Physics Letters* **7**, *256* (1965)
[11] T. Y. Fan, G. J. Dixon, R. L. Byer, "*Efficient GaAlAs diode-laser-pumped operation of Nd:YLF at 1.047 μm with intracavity doubling to 523.6 nm*", *Optics Letters* **11**, *204* (1986)
[12] W. P. Risk, T. R. Gosnell, A. V. Nurmikko, *Compact Blue-Green Lasers*, Cambridge University Press, United Kingdom, 2003.
[13] V. G. Dmitriev, G. G. Gurzadyan, D. N. Nikogosyan, *Handbook of Nonlinear Optical Crystals*, Springer-Verlag, United States of America, 1991.
[14] J. A. Giordmaine, R. C. Miller, *Tunable coherent parametric oscillation in $LiNbO_3$ at optical frequencies, Physical Review Letters* **14**, *973* (1965)
[15] A. Authier, *International tables for crystallography; Volume D, Physical properties of crystals,* Kluwer Academic Publishers, The Netherlands, 2003.
[16] A. Brenier, *"The self-doubling and summing lasers: Overview and modeling"*, *Journal of Luminiscence* **91**, *121* (1991)
[17] T. Y. Fan, A. Cordova-Plaza, M. J. F. Digonnet, R. L. Byer, H. J. Shaw, *"Nd:MgO:$LiNbO_3$ spectroscopy and laser devices", Journal of the Optical Society of America B* **3**, *140* (1986)
[18] L. F. Johnson, A. A. Ballman, *"Coherent Emission from Rare Earth Ions in Electro-optic Crystals"*, *Journal of applied physics* **40**, *297* (1969)
[19] V. G. Dimitriev, E. V. Raevskii, N. M. Rubina, L. N. Rashkovich, O. O. Silichev, A. A. Fomichev, *"Simultaneous emission at the fundamental frequency and the second harmonic in an active nonlinear medium: neodymium-doped lithium metaniobate"*, *Sov. Tech. Phys. Lett.* **5**, *590* (1979)

[20] Z. Zhu, J. Li, A. Brenier, G. Jia, Z. You, X. Lu, B. Wu, C. Tu, *"Growth, spectroscopic and laser properties of Yb^{3+}-doped $GdAl_3(BO_3)_4$ crystal: a candidate for infrared laser crystal"*, *Applied Physics B* **86**, *71* (2007)

[21] I. Parreu, M. C. Pujol, M. Aguiló, F. Díaz, X. Mateos, V. Petrov, *"Growth, spectroscopy and laser operation of $Yb:KGd(PO_3)_4$ single crystals"*, *Optics Express* **15**, *2360* (2007)

[22] X. Mateos, V. Petrov, A. Peña, J. J. Carvajal, M. Aguiló, F. Díaz, P. Segonds, B. Boulanger, *"Laser operation of Yb^{3+} in the acentric $RbTiOPO_4$ codoped with Nb^{5+}"*, *Opics Letters* (in press)

[23] A. Brenier, I. V. Kityk, A. Majchrowski, *"Evaluation of Nd^{3+}-doped BiB_3O_6 (BIBO) as a new potential self-frequency laser crystal"*, *Optics Communications* **203**, *125* (2002)

[24] J. Capmany, *"Simultaneous generation of red, green, and blue continuous-wave laser radiation in Nd^{3+}-doped aperiodically poled lithium niobate"*, *Applied Physics Letters* **78**, *144* (2001)

[25] L. M. Dorozhkin, I. I. Kuratev, N. I. Leonyuk, T. I. Timchenko, A. V. Shestakov, *"Optical second harmonic generation in a new nonlinear active medium Nd:YAB" Sov. Tech. Phys. Lett.* **7**, *555* (1981)

[26] B. Lu, J. Wang, H. Pan, M. Jiang, E. Liu, X. Hou, *"Laser self-doubling in neodymium yttrium aluminum borate"*, *Journal of Applied Physics* **66**, *6052* (1989)

[27] I. Schütz, I. Freitag, R. Wallenstein, *"Miniature self-frequency-doubling cw Nd:YAB laser pumped by a diode-laser"*, *Optics Communications* **77**, *221* (1990)

[28] R. E. Stone, R. C. Spitzer, S. C. Wang, *"A Q-Switched Diode-Pumped Neodymium Yttrium Aluminum Borate Laser"*, *IEEE Photonics Technology Letters* **2**, *769* (1990)

[29] H. Hemmati, *"Diode-Pumped Self-Frequency-Doubled Neodymiun Yttrium Aluminum Borate (NYAB) Laser"*, *IEEE Journal of Quantum electronics* **28**, *1169* (1992)

[30] J. Bartschke, R. Knappe, K. J. Boller, R. Wallenstein, *"Investigation of Efficient Self-Doubling Nd:YAB Lases"*, *IEEE Journal of Quantum Electronics* **33**, *2295* (1997)

[31] P. Dekker, Y. Huo, J. M. Dawes, J. A. Piper, P. Wang, B. S. Lu, *"Continuous wave and Q-switched diode-pumped neodymium, lutetium: yttrium aluminium borate lasers"*, *Optics Communications* **151**, *406* (1998)

[32] D. Jaque, J. Capmany, J. Rams, J. García Solé, *"Effects of pump heating on laser and spectroscopic properties of the $Nd:[YAl_3(BO_3)_4]$ self-frequency-doubling laser"*, *Journal of Applied Physics* **87**, *1042* (2000)

[33] A. Cordova-Plaza, T. Y. Fan, M. J. F. Digonnet, R. L. Byer, H. J. Shaw, *"$Nd:MgO:LiNbO_3$ continuous-wave laser pumped by a laser diode"*, *Optics Letters* **13**, *209* (1988)

[34] Z. Li, Q. Fan, F. Zhou, J. Ma, Q. Xue, *"Self frequency doubling of a laser diode array pumped Q-switched NYAB laser"*, *Optical Engineering* **33**, *1138* (1994)

[35] S. Ishibashi, H. Itoh, T. Kaino, I. Yokohama, K. Kubodera, *"New cavity configurations of $Nd:MgO:LiNbO_3$ self-frequency-doubld lasers"*, *Optics Communications* **125**, *177* (1996)

[36] K. Zhang, C. Xie, R. Guo, J. Wang, K. Peng, *"Laser-diode-pumped cw $Nd:MgO:LiNbO_3$ self-frequency-doubling laser around room temperature"*, *Applied Optics* **35**, *3200* (1996)

[37] J. K. Yamamoto, A. Sugimoto, K. Yamagishi, *"Self-frequency doubling in $Nd:Sc_2O_3:LiNbO_3$ at room temperature"*, *Optics Letters* **19**, *1311* (1994)

[38] J. P. Meyn, G. Huber, *"Intracavity frequency doubling of a continuous-wave, diode-laser pumped neodymium lanthanum scandium borate laser"*, *Optics Letters* **19**, *1436* (1994)

[39] V. G. Ostroumov, F. Heine, S. Kück, G. Huber, V. A. Mikhailov, I. A. Shcherbakov, *"Intracavity frequency-doubled diode-pumped $Nd:LaSc_3(BO_3)_4$ lasers"*, *Applied Physics B* **64**, *301* (1997)

UNIVERSITAT ROVIRA I VIRGILI
YTTERBIUM AND ERBIUM DOPEP RbTi1-xMxOPO4 (M=Nb or Ta) CRYSTALS. NEW LASER AND NONLINEAR BIFUNCTIONAL MATERIALS
Alexandra Peña Revellez
ISBN: 978-84-691-0370-8 /DL:T.2188-2007

[40] F. Mougel, F. Auge, G. Aka, A. Kahn Harare, D. Vivien, F. Balembois, P. Georges, A. Brun, *"New green self-frequency-doubling diode-pumped Nd:$Ca_4GdO(BO_3)_3$"*, *Applied Physics B* **67**, *533* (1998)

[41] S. Zhang, Z. Cheng, J. Han, G. Zhou, Z. Shao, C. Wang, Y. T. Chow, H. Cheng, *"Growth and investigation of efficient self-frequency-doubling $Nd_xGd_{1-x}Ca_4O(BO_3)_3$"*, *Journal of Crystal growth* **206**, *197* (1999)

[42] C. Q. Wang, Y. T. Chow, W. A. Gambling, S. J. Zhang, Z. X. Cheng, Z. S. Shao, H. C. Chen, *"Efficient self-frequency doubling of Nd:GdCOB crystal by type-I phase matching out of its principal planes"*, *Optics Communications* **174**, *471* (2000)

[43] A. Brenier, A. Majchrowski, E. Michalski, T. Lukasievicz, *"Evaluation of GdCOB:Nd^{3+} for self-frequency doubling in the optimum phase matching direction"*, *Optics Communications* **217**, *395* (2003)

[44] J. Capmany, V. Bermúdez, E. Diéguez, *"Continuous wave laser radiation at 524 nm from a self-frequency-doubled laser of $LaBGeO_5:Nd^{3+}$"*, *Applied Physics Letters* **72**, *531* (1998)

[45] A. A. Kaminskii, D. Jaque, S. N. Bagaev, K. Veda, J. Garcia Solé, J. Capmany, *"New nonlinear-laser properties of ferroelectric $Nd^{3+}:Ba_2NaNb_5O_{15}$-cw stimulated emission ($^4F_{3/2}\rightarrow{}^4I_{11/2}$ and $^4F_{3/2}\rightarrow{}^4I_{13/2}$), collinear and diffuse self-frequency doubling and summation"*, *Quantum Electronics* **29**, *95* (1999)

[46] A. Ródenas, M. O. Ramirez, D. Jaque, J. Garcia Solé, A. A. Kaminskii, *"Wide infrared and visible tenability from a $Nd^{3+}:Ba_2NaNbO_{15}$ self-frequency-converter disordered laser crystal "*, *Journal of Applied Physics* **99**, *026105* (2006)

[47] J. M. Eichenholtz, D. A. Hammons, L. Shah, Q. Ye, R. E. Peale, M. Richardson, B. Chai, *"Diode-pumped self-frequency doubling in a $Nd^{3+}:YCa_4O(BO_3)_3$"*, *Applied Physics Letters* **74**, *1954* (1999)

[48] Q. Ye, L. Shah, J. Eichenholz, D. Hammons, R. Peale, M. Richardson, A. Chin, B. H. T. Chai, *"Investigation of diode-pumped, self-frequency doubled RGB lasers from Nd:YCOB crystals"*, *Optics communications* **164**, *33* (1999)

[49] C. Tu, M. Qiu, Y. Huang, X. Chen, A. Jiang, Z. Luo, *"The study of a self-frequency-doubling laser crystal $Nd^{3+}:GdAl_3(BO_3)_4$"*, *Journal of crystal Growth* **208**, *487* (2000)

[50] A. Brenier, C. Tu, J. Li, Z. Zhu, B. Wu, *"Spectroscopy, laser operation at 1.3 μm and self-frequency doubling in $GdAl_3(BO_3)_4:Nd^{3+}$"*, *Optics Communications* **200**, *355* (2001)

[51] A. Brenier, Y. Wu, P. Fu, R. Guo, F. Jing, *"Evidence of self-frequency doubling from two inequivalent Nd^{3+} centers in the $La_2CaB_{10}O_{19}:Nd^{3+}$ bifunctional crystal"*, *Journal of Applied Physics* **98**, *123528* (2005)

[52] D. A. Hammons, J. M. Eichenholz, Q. Ye, B. H. T. Chai, L. Shah, R. E. Peale, M. Richardson, H. Qiu, *"Laser action in $Yb^{3+}:YCOB(Yb^{3+}:YCa_4O(BO_3)_3)$"*, *Optics Communications* **156**, *327* (1998)

[53] F. Mougel, K. Dardenne, G. Aka, A. Kahn-Harari, D. Vivien, *"Ytterbium-doped $Ca_4GdO(BO_3)_3$:an efficient infrared laser and self-frequency doubling crystal"*, *Journal of the Optical Society of America B* **16**, 164 (1999)

[54] H. Zhang, X. Meng, P. Wang, L. Zhu, X. Liu, X. Liu, Y. Yang, R. Wang, J. Dawes, J. Piper, S. Zhang, L. Sun, *"Growth of Yb-doped $Ca_4GdO(BO_3)_3$ crystals and their spectra and laser properties"*, *Journal of Crystal Growth* **222**, *209* (2001)

[55] E. Montoya, J. Capmany, L. E. Bausa, T. Kellner, A. Dienig, G. Huber, *"Infrared and sels-frequency doubled laser action in Yb^{3+}-doped $LiNbO_3$:MgO"*, *Applied Physics Letters* **74**, *3113* (1999)

UNIVERSITAT ROVIRA I VIRGILI
YTTERBIUM AND ERBIUM DOPEP RbTi1-xMxOPO4 (M=Nb or Ta) CRYSTALS. NEW LASER AND NONLINEAR BIFUNCTIONAL MATERIALS
Alexandra Peña Revellez
ISBN: 978-84-691-0370-8 /DL:T.2188-2007

[56] J. Capmany, E. Montoya, V. Bermúdez, D. Callejo, E. Diéguez, L. E. Bausá, *"Self-frequency doubling in Yb^{3+} doped periodically poled $LiNbO_3$:MgO bulk crystal"*, *Applied Physics Letters* **76**, *1374* (2000)

[57] E. Montoya, J. A. Sanz-García, J. Capmany, L. E. Bausá, A. Diening, T. Kellner, G. Huber, *"Continuous wave infrared laser action, self-frequency doubling, and tunability of Yb^{3+}:MgO:$LiNbO_3$"*, *Journal of Applied Physics* **87**, *4056* (2000)

[58] L. B. Bausá, M. O. Ramírez, E. Montoya, *"Optical performance of Yb^{3+} in $LiNbO_3$ laser crystal"*, *Physic-Statu-Solidi-A* **201**, *289* (2004)

[59] P. Wang, P. Dekker, J. M. Dawes, J. A. Piper, Y. Liu, J. Wang, *"Efficient continuous-wave self-frequency-doubling green diode-pumped Yb:$YAl_3(BO_3)_4$ lasers"*, *Optics Letters* **25**, *731* (2000)

[60] P. Dekker, J. M. Dawes, J. A. Piper, Y. Liu, J. Wang, *"1.1 W CW self-frequency-doubled diode-pumped Yb:$YAl_3(BO_3)_4$"*, *Optics Communications* **195**, *431* (2001)

[61] P. A. Burns, J. M. Dawes, P. Dekker, J. A. Piper, J. Li, J. Wang, *"Coupled-cavity, single-frequency, tunable cw Yb:YAB yellow microchip laser"*, *Optics Communications* **207**, *315* (2002)

[62] P. Dekker, P. A. Burns, J. M. Dawes, J. A. Piper, *"Widely tunable yellow-green lasers based on the self-frequency-doubling material Yb:YAB"*, *Journal of the Optical Society of America B* **20**, 706 (2003)

[63] M. J. Lederer, M. Hildebrandt, V. Z. Kolev, B. Luther-Davies, B. Taylor, J. Dawes, P. Dekker, J. Piper, H. H. Tan, C. Jagadish, *"Passive mode locking of a self-frequency-doubling Yb:$YAl_3(BO_3)_4$ laser"*, *Optics Letters* **27**, *436* (2002)

[64] L. Ouvrard, M. Troost, *Comptes rendus de l'academie des sciences* **111**, *177* (1890)

[65] I. Tordjman, R. Masse, J. C. Guitel, *Zeitschrift für Kristallographie* **139**, *103* (1974)

[66] F. C. Zumsteg, J. D. Bierlein, T. E. Gier, *"$K_xRb_{1-x}TiOPO_4$: A new nonlinear optical material"*, *Journal of Applied Physics* **47**, *4980* (1976)

[67] Y. S. Liu, D. Dentz, R. Belt, *"High-average-power intracavity second-harmonic generation using $KTiOPO_4$ in an acousto-optically Q-switched Nd:YAG laser oscillator at 5 kHz"*, *Optics Letters* **9**, *76* (1984)

[68] T. A. Driscoll, H. J. Hoffman, R. E. Stone, P. E. Perkins, *"Efficient second-harmonic generation in KTP crystals"*, *Journal of the Optical Society of America B* **3**, *683* (1986)

[69] A. Englander, R. Lavi, M. Katz, M. Oron, D. Eger, E. Lebiush, G. Rosenman, A. Skliar, *"Highly efficient doubling of a high-repetition-rate diode-pumped laser with bulk periodically poled KTP"*, *Optics Letters* **22**, *1598* (1997)

[70] G. D. Stucky, M. L. F. Phillips, T. E. Gier, *"The Potassium Titanyl Phosphate Structure Field: A Model for New Nonlinear Optical Materials"*, *Chemistry of Materials* **1**, *492* (1989)

[71] M. E. Hagerman, K. R. Poeppelmeier, *"Review of the structure and Processing-Defect-Property Relationships of Potassium Titanyl Phoaphate: a strategy for Novel Thin-Films Photonic Devices"*, *Chemistry of Materials* **7**, *602* (1995)

[72] V. Pasikevicius, C. Canalias, F. Laurell, *"Highly efficient stimulated Raman scattering of picosecond pulses in $KTiOPO_4$"*, *Applied Physics Letters* **88**, *041110* (2006)

[73] D. Xue, S. Zhang, *"The origin of nonlinearity in $KTiOPO_4$"*, *Applied Physics Letters* **70**, *943* (1997)

[74] R. Solé, V. Nikolov, I. Koseva, P. Peshev, X. Ruiz, C. Zaldo, M. J. Martín, M. Aguiló, F. Díaz, *"Conditions and possibilities for Rare-Earth doping of $KTiOPO_4$ flux-grown single crystals"*, *Chemistry of Materials* **9**, *2745* (1997)

[75] M. Rico, C. Zaldo, J. Massons, F. Diaz, *"Optical absorption of Er^{3+} in $RbTiOPO_4$ and $KTiOPO_4$"*, *Journal of Physics:Condensed Matter* **10**, *10101* (1998)

[76] C. Zaldo, M. Rico, F. Díaz, J. J. Carvajal, *"Progress in cristal growth and characterization of rare-earth doped non-linear KTP crystals for laser applications"*, *Optical materials* **13**, *175* (1999)

[77] K. M. Wang, W. Wang, P. J. Ding, W. A. Lanford, Y. G. Liu, *"Ion-beam mixing of erbium into potassium titanyl phosphate by mega-electron-volt argon beams"*, *Journal of Applied Physics* **77**, *3581* (1995)

[78] M. J. Martín, C. Zaldo, M. F. Da Silva, J. C. Soares, F. Díaz, M. Aguiló, *"Diffusion of Nd, E rand Nb in potassium titanyl phosphate"*, *Journal of Physics: Condensed Matter* **9**, *L465* (1997)

[79] K. M. Wang, F. Lu, M. Q. Meng, B. R. Shi, D. Y. Shen, Y. G. Liu, D. Fink, *"Depth distribution o frare earth ions implanted into $KTiOPO_4$ determined by the Rutherford backscattering technique"*, *Nuclear Instruments and Methods in Physics research B* **145**, *271* (1998)

[80] K. M. Wang, B. R. Shi, N. cue, Y. Y. Zhu, R. F. Xiao, F. Lu, W. Li, Y. G. Liu, *"Waveguide laser film in erbium-doped $KTiOPO_4$ by pulsed laser deposition"*, *Applied Physics Letters* **73**, *1020* (1998)

[81] M. T. Anderson, M. L. F. Phillips, M. B. Sinclair, G. D. Stucky, *"Synthesis of Transition-Metal-Doped $KTiOPO_4$ and Lanthanide-Doped $RbTiOAsO_4$ Isomorphs that absorb Visible Light"*, *Chemistry of Materials* **8**, *248* (1996)

[82] J. J. Carvajal, R. Solé, Jna. Gavaldà, J. Massons, M. Aguiló, F. Díaz, *" Crystal growth of $RbTiOPO_4$:Nb: a new nonlinear optical host for rare earth doping"*, *Crystal Growth & Desing* **1**, *479* (2001)

[83] J. J. Carvajal, R. Solé, Jna. Gavaldà, J. Massons, M. Aguiló, F. Díaz, *" A new self-doubling material : $RbTiOPO_4$:(Nb,Ln)"*, *Optical Materials* **24**, *425* (2003)

[84] V. K. Yanovskii, V. I. Voronkova, *"Ferroelectric Phase Transitions and Properties of Crystals of the $KTiOPO_4$"*, *Physica Status Solidi A* **93**, *665* (1980)

[85] J. D. Bierlein, F. Ahmed, *"Observation and poling of ferroelectric domains in $KTiOPO_4$"*, *Applied Physics Letters* **51**, *1322* (1987)

[86] N. R. Ivanov, N. A. Tikhomirova, A. V. Grinzberg, S. P. Chumakova, E. I. Eknadiosyants, V. Z. Borodin, A. N. Pinskaya, V. A. Babonskikh, V. A. Dyakov, *Crystallografia Reports* **39**, *593* (1994)

[87] F. Laurell, M. G. Roefols, W. Bindloss, H. Hsuing, A. Suna, J. D. Beirlein, *"Detection of ferroelectric domain reversal in $KTiOPO_4$ waveguides"*, *Journal of Applied Physics* **71**, *4664* (1992)

[88] Z. W. Hu, P. A. Thomas, P. Q. Huang, *"High-resolution x-ray diffraction and topographic study of ferroelectric domains and absolut estructural polarity of $KTiOPO_4$ via anomalous scattering"*, *Physical Review B* **56**, *8559* (1997)

[89] B. Vohnsen, S. I. Bozhevolnyi, *"Near- and far-field second-harmonic imaging of quasi-phase-matching crystals"*, *Journal of Microscopy* **202**, *244* (2001)

[90] M. C. Gupta, W. P. Risk, A. C. G. Nutt, S. D. Lau, *"Domain inversion in $KTiOPO_4$ using electron beam scanning"*, *Applied Physics Letters* **63**, *1167* (1993)

[91] J. J. Carval, R. Solé, Jna. Gavaldà, J. Massons, P. Segonds, B. Boulanger, A. Brenier, G. Boulon, J. Zaccaro, M. Aguiló, F. Díaz, *"Spectroscopic and second harmonic generation properties of a new cristal: Yb-doped $RbTiOPO_4$"*, *Optical Materials* **26**, *313* (2004)

[92] L. T. Cheng, L. K. Cheng, R. L. Harlow, J. D. Bierlein, *"Blue light generation using bulk single crystals of niobium-doped $KtiOPO_4$"*, *Applied Physics Letters* **64**, *155* (1994)

[93] J. J. Carvajal, V. Nikolov, R. Solé, Jna. Gavaldà, J. Massons, M. Rico, C. Zaldo, M. Aguiló, F. Díaz, *"Crystallization region, crystal growth, and characterization of rubidium*

titanyl phosphate codoped with Niobium and lanthanide ions", *Chemistry of Materials* **14**, *3136* (2002)

[94] T. Schweizer, T. Jensen, E. Heumann, G. Huber, *" Spectroscopic properties and diode pumped 1.6 µm laser performance in Yb-codoped Er:$Y_3Al_5O_{12}$ and Er:Y_2SiO_5"*, *Optics Communications* **118**, *557* (1995)

[95] L. K. Cheng, J. D. Bierlein, A. A. Ballman, *"Crystal growth of $KTiOPO_4$ isomorphs from tungstate and molybdate fluxes"*, *Journal of Crystal Growth* **110**, *697* (1991)

[96] J. Pickworth Glusker, K. N. Trueblood, *Crystal structure analysis: A premier*, Oxford University press, New York, 1985.

[97] J. Rodríguez-Carvajal, *Short reference guide for the computer program FULLPROF*, Laboratoire Léon Brillouin, CEA-CNRS, Gif sur Yvette, 1998.

[98] R. A. Young, *The Rietveld method*, International union of crystallography, monographs on crystallography 5, Oxford University Press, Oxford, 1995.

[99] J. L. Pouchou, F. Pichoir, *"Un nouveau modèle de calcul par la microananlyse quantitative par spectrómetrie de rayons X. Partie I: application a l'analyse d'échantillons homogènes"*, *Rech. Aerosp.* **215**, *253* (1984)

[100] G. R. Fowles, *Introduction to modern optics*, Dover publications, New York, 1989.

[101] F. A. Jenkins, H. E. White, *Fundamentals of Optics*, Auckland, McGraw Hill, 1976.

[102] J. J. Carvajal, V. Nikolov, R. Solé, Jna. Gavaldà, J. Massons, M. Rico, C. Zaldo, M. Aguiló, F. Díaz, *"Enhancement of the Erbium concentration in $RbTiOPO_4$ by codoping with Niobium"*, *Chemistry of Materials* **12**, *3171* (2000)

[103] D. Elwell, H. J. Scheel, *Crystal growth from high-temperature solutions*, Academic Press, New York, 1975.

[104] R. D. Shannon, *"Revised effective ionid radii and systematic studies of interatomic distances in halides and chalcogenides"*, *Acta Crysallographica.* **A32**, *751* (1976)

[105] V. I. Voronkova, V. K. Yanovskiĭ, T. Yu. Losevskaya, S. Yu. Stefanovich, S. A. Zverkov, O. A. Alekseeva, N. I. Sorokina, *"Electrical and nonlinear properties of $KTiOPO_4$ single crystals doped with niobium, antimony, and tantalum"*, *Crystallography Reports* **49**, *123* (2004)

[106] W. Liu, H. Y. Shen, G. F. Zhang, D. Y. Zhang, G. Zhang, W. X. Lin, R. R. Zeng, C. H. Huang, *"Studies on the phase-matching condition and the cut-off wavelength of Nb:$KTiOPO_4$"*, *Optics Communications* **185**, *191* (2000)

[107] P. A. Thomas, S. C. Mayo, B. E. Watts, *"Crystal structures of $RbTiOAsO_4$, $KTiO(P_{0.58},As_{0.42})O_4$, $RbTiOPO_4$ and $(Rb_{0.465},K_{0.535})TiOPO_4$, and analysis of pseudosymmetry in crystals of the $KTiOPO_4$"*, *Acta Crystallographica* **B48**, *401* (1992)

[108] J. J. Carvajal, R. Solé, Jna. Gavaldà, J. Massons, F. Díaz, M. Aguiló, *"Phase transitions in $RbTiOPO_4$ doped with Niobium"*, *Chemistry of Materials* **15**, *2730* (2003)

[109] V. K. Yanovskii, V. I. Voronkova, T. Yu. Losevakaya, S. Yu. Stefanovich, S. A. Ivanov, V. I. Simonov, N. I. Sorokina, *"Growth and properties of Nb- or Sn- doped $KTiOPO_4$ crystals"*, *Crystallography Reports* **47**, *S99* (2002)

[110] P. Delarue, C. Lecomte, M. Jannin, G. Marnier, B. Ménaert, *"Behaviour of the non-linear optical material $KTiOPO_4$ in the temperature range 293-973 K studied by X-ray diffractometry at high resolution: alkaline displacements"*, *Journal of Physics: Condensed Matter* **11**, *4123* (1999)

[111] P. Delarue, C. Lecomte, M. Jannin, G. Marnier, B. Ménaert, *"Evolution towards centrosymmetry of the nonlinear-optical material $RbTiOPO_4$ in the range 293-973 K: alkaline displacements and titanyl deformations"*, *Physical Review B* **58**, *5287* (1998)

[112] A. Fragerman, V. Pasikevicius, J. Nordborg, J. Hellström, H. Karlsson, F. Laurell, *"Frequency converters from visible to mid-infrared with periodically poled $RbTiOPO_4$"*, *Applied Physics Letters* **83**, *3090* (2003)

[113] H. Karlsoon, F. Laurell, *"Electric field poling of flux grown $KTiOPO_4$"*, *Applied Physics Letters* **71**, *3474* (1997)

[114] J. J. Carvajal, J. L. García-Muñoz, R. Solé, Jna. Gavaldá, J. Massons, X. Solans, F. Díaz, M. Aguiló, *"Charge self-compensation in the nonlinear optical crystals $Rb_{0.855}Ti_{0.955}Nb_{0.045}OPO_4$ and $RbTi_{0.927}Nb_{0.056}Er_{0.017}OPO_4$"*, *Chemistry of Materials* **15**, *2338* (2003)

[115] Y. S. Oseledchik, A. I. Pisarevsky, A. L. Prosvirnin, V. V. Starshenko, N. V. Svitanko, *"Nonlinear optical properties of the flux grown $RbTiOPO_4$ crystal"*, *Optical Materials* **3**, *237* (1994)

[116] W. Liu, H. Y. Shen, G. F. Zhang, D. Y. Zhang, G. Zhang, W. X. Lin, R. R. Zeng, G. H. Huang, "*Studies on the phase-matching condition and the cut-off wavelength of Nb:$KTiOPO_4$"*, *Optics Communications* **185**, *191* (2000)

[117] J. C. Jacco, G. M. Loiacono, *"Nature of the infrared spectrum in band-edge region of $KTiOPO_4$"*, *Appied. Phyics Letters* **58**, *560* (1991)

[118] M. J. Martín, D. Bravo, R. Solé, F. Díaz, F. J. López, C. Zaldo, *"Thermal reduction of $KTiOPO_4$ single crystals"*, *Journal of Applied Physics* **76**, *7510* (1994)

[119] C. Zaldo, J. Carvajal, R. Solé, F. Díaz, D. Bravo, A. Kling, *"Influence of impurities on the optical damage of $KTiOPO_4$ crystals"*, *Journal of Applied Physics* **88**, *3242* (2000)

[120] J. J. Carvajal, R. Solé, Jna. Gavaldà, J. Massons, M. Rico, C. Zaldo, M. Aguiló, F. Díaz, *"Growth and characterization of $RbTiOPO_4$:Nb crystals as a host for rare earth ions"*, *Journal of Alloys and Compounds* **323-324**, *231* (2001)

[121] P. Galinetto, F. Rossella, E. Giulotto, G. Samoggia, V. Trepakov, L. Jastrabik, P. Syrnkov, S. Kapphan, *"Photoinduced charge transport in $KTaO_3$:Be"*, *Physica Status Solidi c* **2**, *184* (2005)

[122] X. Wang, J. Wang, Y. Yu, R. I. Boughton, *"Growth of cubic $KTa_{1-x}Nb_xO_3$", Journal of Crystal Growth* **293**, *398* (2006)

[123] K. Vivekanandan, S. Selvasekarapandian, P. Kolandaivel, M. T. Sebastian, S. Suma, *"Raman and FT-IR spectroscopic characterisation of flux grown $KTiOPO_4$ and $KRbTiOPO_4$ non-linear optical crystals"*, *Materials Chemistry and Physics* **49**, *204* (1997)

[124] Y. Guillien, B. Ménaert, J. P. Fève, P. Segonds, J. Douady, B. Boulanger, O. Pacaud, *"Crystal growth and refined Sellmeier equations over the complete transparency range of $RbTiOPO_4$"*, *Optical Materials* **22**, *155* (2003)

[125] B. G. Wybourne, *Spectroscopic properties of rare earths*, Wiley, New York, 1965.

[126] C. Görller-Walrand, K. Binnemans, *Handbook on the physics and chemistry o frare earths*, Vol. 25, Chap. 167, Elsevier Science, Amsterdam, 1998.

[127] H. Jiang, J. Wang, H. Zhang, X. Hu, P. Burns, J. A. Piper, *"Spectral and luminiscent properties of Yb^{3+} ions in $YCa_4O(BO_3)_3$ crystal"*, *Chemical Physsics Letters* **361**, *499* (2002)

[128] G. Liu, B. Jacquier, *Spectroscopic properties o frare earth in optical materials*, Springer, China, 2005.

[129] B. R. Judd, *"Optical absorptions intensities of rare-earth ions"*, *Physical Review* **127**, *750* (1962)

[130] G. S. Ofelt, *"Intensities of crystal spectra of rare-earth ions"*, *The Journal of Chemical Physics* **37**, *511* (1962)

[131] J. J. Carvajal, *Growth and characterisation of $RbTiOPO_4$. A New self-frequency doubling crystal*, Tarragona, 2003.

UNIVERSITAT ROVIRA I VIRGILI
YTTERBIUM AND ERBIUM DOPEP RbTi1-xMxOPO4 (M=Nb or Ta) CRYSTALS. NEW LASER AND NONLINEAR BIFUNCTIONAL MATERIALS
Alexandra Peña Revellez
ISBN: 978-84-691-0370-8 /DL:T.2188-2007

[132] P. Wang, J. M. Dawes, P. Dekker, D. S. Knowles, J. A. Piper, B. Lu, *"Growth and evaluation of ytterbium-doped yttrium aluminum borate as a potential self-doubling laser crystal", Journal of the Optical Society of America B* **16**, *63* (1999)
[133] A. Aron, G. Aka, B. Viana, A. Kahn-Harari, D. Vivien, F. Druon, F. Balembois, P. Georges, A. Brun, N. Lenain, M. Jacquet, *"Spectroscopic properties and laser performances of Yb:YCOB and potential of the Yb:LaCOB material", Optical Materials* **16**, *181* (2001)

UNIVERSITAT ROVIRA I VIRGILI
YTTERBIUM AND ERBIUM DOPEP RbTi1-xMxOPO4 (M=Nb or Ta) CRYSTALS. NEW LASER AND NONLINEAR BIFUNCTIONAL MATERIALS
Alexandra Peña Revellez
ISBN: 978-84-691-0370-8 /DL:T.2188-2007

Paper I

Yb:Ta:$RbTiOPO_4$, a new strategy to further increase the lanthanide concentration in crystals of the $KTiOPO_4$ family.

A. Peña, J. J. Carvajal, J. Massons, Jna. Gavaldà, F. Díaz, M. Aguiló

Chemistry of Materials, **19**, *4069* (2007)

UNIVERSITAT ROVIRA I VIRGILI
YTTERBIUM AND ERBIUM DOPEP RbTi1-xMxOPO4 (M=Nb or Ta) CRYSTALS. NEW LASER AND NONLINEAR BIFUNCTIONAL MATERIALS
Alexandra Peña Revellez
ISBN: 978-84-691-0370-8 /DL:T.2188-2007

Chem. Mater. **2007**, *19*, 4069−4076

Yb:Ta:$RbTiOPO_4$, A New Strategy to Further Increase the Lanthanide Concentration in Crystals of the $KTiOPO_4$ Family

A. Peña, J. J. Carvajal, J. Massons, Jna. Gavaldà, F. Díaz, and M. Aguiló*

Física i Cristal·lografia de Materials (FiCMA), Universitat Rovira i Virgili (URV), Campus Sescelades c/ Marcel·lí Domingo, s/n E-43007 Tarragona, Spain

Received March 30, 2007. Revised Manuscript Received May 25, 2007

In this study, we determined the variation of the crystallization region of rubidium titanyl phosphate codoped with tantalum and yterbium at three different molar ratios of Rb_2O, P_2O_5, and TiO_2 in this ternary system. The amount of Yb^{3+} and Ta^{5+} that can substitute for Ti^{4+} without losing the desired phase strongly depends on the amount of TiO_2 in the initial solution. The critical amount of Yb^{3+} increases as the initial solution is richer in TiO_2. Yb:Ta:$RbTiOPO_4$ single crystals have been grown with dimensions and quality enough to perform their optic and spectroscopic characterization. The optical transparency window has been measured for $RbTi_{0.96}Ta_{0.04}OPO_4$ and $RbTi_{0.95}Ta_{0.03}Yb_{0.02}OPO_4$ crystals. Optical absorption and fluorescence of Yb^{3+} in $RbTi_{0.95}Ta_{0.03}Yb_{0.02}OPO_4$ have been recorded at room and low temperatures.

Introduction

$KTiOPO_4$ (KTP) and its isostructural $RbTiOPO_4$ (RTP) are well-known for their high nonlinear optical coefficients. Particularly KTP has been used as a frequency doubler of lasers emitting in the IR spectral range,[1,2] but this application can be extended as well to RTP.

One can assume that when doping with laser-active ions, such as lanthanide (Ln^{3+}) ions, these materials could be used as self-frequency doubling materials. It has been shown that the amount of Ln^{3+} ions with which KTP and RTP can be doped is too low to achieve efficient fluorescence.[3] However, by using a codopant such as Nb^{5+}, which expands the structure and acts as a charge compensator,[4] this amount increases until values high enough to obtain efficient fluorescence are obtained.[5,6] The presence of Nb^{5+} and Ln^{3+} ions with a concentration below 10 at % in RTP has been proven to have little dramatic effect on the NLO properties of the crystal or in the transparency range of the material.[7]

RTP belongs to a structural family with the general formula $ABOXO_4$, with $A = K^+$, Rb^+, Na^+, Cs^+, Tl^+, NH_4^+; $B = Ti^{4+}$, Sn^{4+}, Zr^{4+}, Ge^{4+}, V^{4+}; and $X = P^{5+}$, As^{5+}, which crystallizes in the orthorhombic system with the noncentrosymmetric space group $Pna2_1$ and $Z = 8$. The crystallization region of RTP in its self-flux and in tungstate fluxes has been previously determined.[8] The variation of this crystallization in the self-flux when introducing Nb^{5+} and Ln^{3+} (Er^{3+} and Yb^{3+}) has also been studied.[6] As it has been shown that the use of Nb^{5+} as a codopant enhances the distribution coefficients of lanthanide ions in the RTP matrix, the study of other possible codoping ions could be of interest to further increase the Ln^{3+} concentration.[6] A possible candidate is Ta^{5+}, which can be found in the same group of the periodic table than Nb^{5+} and, as well as this latter ion, has a slightly larger ionic radius ($r_{Ta^{5+}} = 0.640$ Å) than Ti^{4+} ($r_{Ti^{4+}} = 0.605$ Å)[9] and a larger ionic charge. In previous studies, it was shown that Ln^{3+} incorporation in crystals of the structural field of KTP increases when an element with a higher electronic charge and an ionic radius as close as possible to the ion to be substituted is used as codopant.[5] Ta^{5+} may then be a good choice for this purpose.

The Yb^{3+} ion has been chosen as the lanthanide active doping ion in this case, not only because its ionic radius is much closer to the Ti^{4+} than that of other Ln^{3+} ions but also because it is an ion with the same emission range as Nd^{3+}, at around 1 μm, having a much simpler energy level scheme, consisting of only two levels: the ground state ($^2F_{7/2}$) and the excited one ($^2F_{5/2}$). Some effects that lead to a reduction in the laser efficiency in other lanthanide ions, such as excited-state absorption, cross-relaxation, and up-conversion, are not present in this system. Furthermore, because of the closeness between the pumping and the laser wavelengths, there exists a small quantum defect that reduces the thermal loading of the crystals during laser operation. Moreover, the key point of doping RTP crystals (a noncentrosymmetric host) with Yb^{3+} is that Yb^{3+} has no absorption in the visible spectral range, the region in which self-frequency doubling laser action would take place, avoiding the absorption losses

* Corresponding author. E-mail: magdalena.aguilo@urv.cat.

(1) Zumsteg, F. C.; Bierlein, J. D.; Gier, T. E. *J. Appl. Phys.* **1976**, *47*, 4980.
(2) Jacco, J. C.; Loiacono, G. M. *Appl. Phys. Lett.* **1991**, *58*, 560.
(3) Rico, M.; Zaldo, C.; Massons, J.; Díaz, F. *J. Phys.: Condens. Matter* **1998**, *10*, 10101.
(4) Carvajal, J. J.; García-Muñoz, J. L.; Solé, R.; Gavaldà, Jna.; Massons, J.; Solans, X.; Díaz, F.; Aguiló, M. *Chem. Mater.* **2003**, *15*, 2338.
(5) Solé, R.; Nikolov, V.; Koseva, I.; Peshev, P.; Ruiz, X.; Zaldo, C.; Martín, M. J.; Aguiló, M.; Díaz, F. *Chem. Mater.* **1997**, *9*, 2745.
(6) Carvajal, J. J.; Nikolov, V.; Solé, R.; Gavaldà, Jna.; Massons, J.; Aguiló, M.; Díaz, F. *Chem. Mater.* **2002**, *14*, 3136.
(7) Carvajal, J.J.; Solé, R.; Gavaldà, Jna.; Massons, J.; Rico, M.; Zaldo, C.; Aguiló, M.; Díaz, F. *J. Alloys Compd.* **2001**, *323*−*324*, 231.
(8) Carvajal, J. J.; Nikolov, V.; Solé, R.; Gavaldà, Jna.; Massons, J.; Rico, M.; Zaldo, C.; Aguiló, M.; Díaz, F. *Chem. Mater.* **2000**, *12*, 3171.
(9) Shannon, R. D. *Acta Crystallogr., Sect. A* **1976**, *32*, 751.

10.1021/cm070887z CCC: $37.00
Published on Web 07/06/2007

for the generated second harmonic beam. Self-frequency doubling laser action has been achieved in some Yb^{3+}-doped noncentrosymmetric laser hosts, such as YCOB, GdCOB, MgO:LNB, and YAB with a Yb^{3+} concentration of $\sim 1 \times 10^{20}$ atoms/cm^{-3},[10] similar to that obtained in Yb:Nb:RTP crystals.[6] This, added to the recent achievement of IR laser operation in Yb:Nb:RTP crystals,[11] opens up the possibility to obtain self-frequency doubling laser action in the near future in these crystals, and consequently, if the conditions are favorable, also in Yb:Ta:RTP. However, obtaining self-frequency doubling laser action in these crystals is not trivial, as it can be achieved only by type II second harmonic generation (SHG) because of the region in which the original emission from Yb^{3+} ion is produced and the combination of refractive indexes implied in the frequency conversion. This contrasts with self-frequency doubling laser action obtained in other hosts, where type I SHG is the most usual frequency conversion used.

In this paper, we study the crystallization region of Yb:Ta:RTP and the amount of Yb^{3+} reached in each of the solution compositions studied. We have also performed some experiments of growth of Yb:Ta:RTP single crystals with which we have obtained crystals with the desired quality and size to undertake optic and further spectroscopic characterizations, such as room and low temperatures optical absorption and fluorescence. The efficiency of second harmonic generation in powdered samples of Ta:RTP and Yb:Ta:RTP has been evaluated with a KTP powdered sample as reference.

Experimental Section

Yb:Ta:RTP Crystallization Regions. Melt processes cannot be used to grow RTP single crystals and isostructurals because they melt incongruently and concretely at 1343 K in the case of RTP.[12] To begin the study, we chose three solution compositions with different ratios of precursor oxides, $Rb_2O-P_2O_5-(TiO_2 + Ta_2O_5 + Yb_2O_3) = 42.900-35.100-22.000$, $43.125-31.875-25.000$, and $40.800-27.200-32.000$. In every one of these solution compositions, we kept the ratio between Rb_2O and P_2O_5 constant and progressively substituted TiO_2 by Ta_2O_5 or Yb_2O_3 or by a combination of Ta_2O_5 and Yb_2O_3. In each case, we added Ta_2O_5 and Yb_2O_3 until the low-temperature orthorhombic phase of RTP disappeared. Rb_2CO_3 (99%), $NH_4H_2PO_4$ (99%), TiO_2 (99.9%), Ta_2O_5 (99.99%), and Yb_2O_3 (99.9%) were used as initial reagents to prepare the solutions. These reagents were mixed, placed in a 25 cm^3 Pt crucible, and heated until the total bubbling of NH_3, H_2O (coming from $NH_4H_2PO_4$), and CO_2 (coming from Rb_2CO_3) finished. The solutions, with a weight of 15−20 g, were homogenized in a vertical tubular furnace by keeping the temperature constant at around 75 K above the saturation temperature (T_s). To obtain the crystalline phase that crystallizes first as we decreased the temperature, we immersed a Pt wire inside the solution. The crucible was maintained at a position in which an axial gradient of almost 5 K/cm was produced, and we decreased the temperature at a rate of 10 K/h until the crystals nucleated and grew spontaneously on the Pt wire. We applied a slow cooling rate (3 K/h) to obtain a larger amount of small crystals to carry out phase identification by X-ray powder diffraction analysis. The morphological characterization of the as-grown crystals was performed using optical and scanning electron microscopes. Electron probe microanalysis (EPMA) was used to determine the dopant concentration as well as the atomic ratio between the chemical elements that compose the different crystalline phases. After the study of ~30 different solution compositions, the (Ta,Yb):RTP crystallization region in each of these three solution compositions was determined.

X-ray Powder Diffraction. X-ray powder diffraction was used to identify the different crystalline phases we found in the determination of the crystallization region of Yb:Ta:RTP. The characterization was performed in a Siemens D5000 powder diffractometer in a $\theta-\theta$ configuration using the Bragg−Brentano geometry. The diffraction patterns were recorded at $2\theta = 10-70°$, step size = 0.05°, and step time = 3 s.

Single-Crystal Growth. After the crystallization regions were determined, we chose one of those solution compositions, $Rb_2O-P_2O_5-(TiO_2 + Ta_2O_5 + Yb_2O_3) = 40.800-27.200-(29.000+1.000+2.000)$, to grow single crystals of Yb:Ta:RTP big enough for further characterizations, by using the top seeded solution growth−slow cooling (TSSG−SC) method. Crystals were grown in the same tubular furnace used for the determination of the crystallization regions, controlled by an Eurotherm 818P controller/programmer. The solution was prepared as explained before, with a weight of around 30 g and an axial gradient 4−10 K/cm, depending on the experience, adjusted to obtain good-optical-quality crystals, with the bottom of the crucible always hotter than the surface of the solution. All the crystal seeds used in the crystal growth process, except the first one, which was a single crystal of Ta:RTP obtained by spontaneous nucleation on a Pt wire, were of Yb:Ta:RTP composition. Crystal seeds were placed at the end of an aluminum rod with the *c* crystallographic direction perpendicular to the surface of the solution, and the *a* crystallographic direction radial to the rotation movement and centered with the rotation axis. The T_s value was determined accurately by controlling the growth or dissolution of the crystal seed in contact with the surface of the solution. The rotation was kept constant at 60 or 80 rpm during the crystal growth process. The change in the rotation speed was done to check the effect of the rotation on the quality of the crystals obtained. We decreased the temperature around 20 K from T_s at a cooling rate of 0.1 K/h. When the growth process was finished, we removed the crystal from the solution, keeping it over the surface of the solution while we cooled the furnace to room temperature at a cooling rate of 15 K/h.

Dopant Concentration Analyses. To measure the dopant concentrations in the samples, we analyzed Yb:Ta:RTP crystals by EPMA in a Cameca SX50 microprobe analyzer operating in the wavelength-dispersive mode. The sample preparation and the experimental procedure used to determine the concentration of all the different atoms is explained somewhere else.[13]

Second Harmonic Generation. We used the Kurtz method, a powder technique, to qualitatively determine the second harmonic generation (SHG) efficiency of Ta:RTP and Yb:Ta:RTP.[14] The experimental procedure was explained in a previous study.[8]

Transparency Window. In Ta:RTP and Yb:Ta:RTP crystals, we measured the transparency window between 300 and 9000 nm. Plate-shaped crystals perpendicular to the *a* direction and polished to optical quality were used. These plates came from a Ta:RTP crystal grown on a Pt wire and a Yb:Ta:RTP single crystal grown

(10) Brenier, A.; Jaque, D.; Majchrowski, A. *Opt. Mater.* **2005**, *28*, 310.
(11) Mateos, X.; Petrov, V.; Peña, A.; Carvajal, J. J.; Díaz, F.; Aguiló, M.; Segonds, P.; Boulanger, B. *Opt. Lett.* **2007**, in press.
(12) Cheng, L. K.; Bierlein, J. D.; Ballman, A. A. *J. Cryst. Growth* **1991**, *110*, 697.
(13) Carvajal, J. J.; Solé, R.; Gavaldà, Jna.; Massons, J.; Aguiló, M.; Díaz, F. *Cryst. Growth Des.* **2001**, *1*, 479.
(14) Kurtz, S. K.; Perry, T. T. *J. Appl. Phys.* **1968**, *39*, 3798.

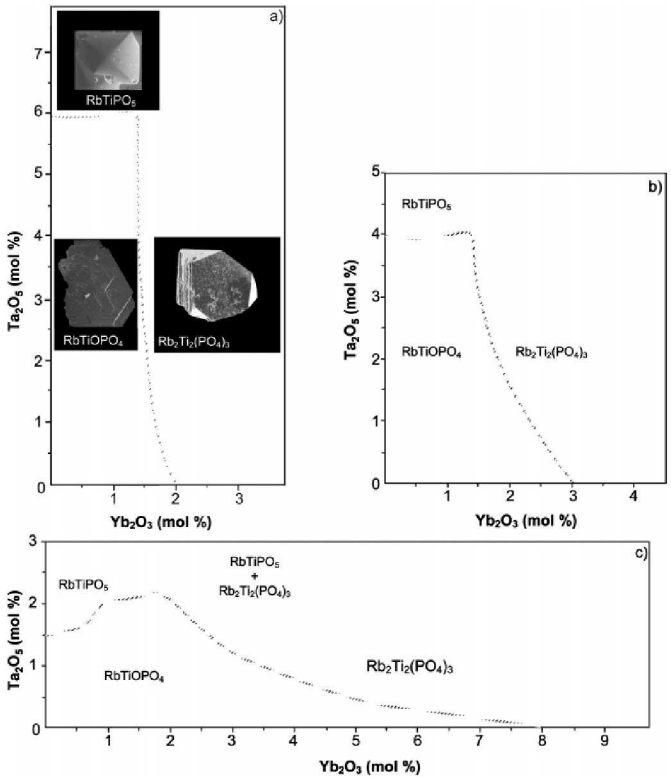

Figure 1. Evolution of the phase diagram of RTP, taking as basis the molar solution compositions of $Rb_2O-P_2O_5-(TiO_2 + Ta_2O_5 + Yb_2O_3)$ (a) 42.900−35.100−22.000, (b) 43.125−31.875−25.000, (c) 40.800−27.200−32.000, where we substituted progressively TiO_2 by Ta_2O_5 and Yb_2O_3, and SEM images of the crystalline phases identified are also shown.

by the TSSG−SC method. The two samples had a thickness of ~300 μm. The optical transparency of the crystals was measured using a Varian Cary 500 scan spectrophotometer in the range 300−3000 nm and using a FT-IR-680 Plus Fourier transformed infrared spectrometer in the range 3000−9000 nm.

Spectroscopic Characterization. The absorption spectra of Yb^{3+} in Yb:Ta:RTP crystals were measured at room and low temperatures using a Varian Cary 500 scan spectrophotometer in the 850−1100 nm range. Low temperatures were reached by using a Leybold RDK-6-320 closed-cycle cryostat. We used a Glan−Taylor polarizer to collect absorption spectra with light polarized along the three crystallographic axes.

Fluorescence measurements were performed by exciting the same sample used in the optical absorption studies, with a 200 mW diode laser emitting at $\lambda = 940$ nm, modulated at 1 kHz. The fluorescence spectra was recorded between 950 and 1100 nm at room and low temperatures in a 90° geometry, with the incident pumping beam in the *ab* plane and the detection recorded in the *bc* plane. The Yb^{3+} fluorescence was dispersed by a 460 mm monochromator (Jobin Ybon-Spex HR460) and detected by a cooled Hamamatsu NIR R5509-72 photomultiplier, which was connected to a lock-in amplifier. Low temperature, 10 K, was reached with a close-cycle cryostat (Oxford CCC1104).

Results and Discussion

Yb:Ta:RTP Crystallization Regions. We studied three solutions with three different molar ratios of $Rb_2O-P_2O_5-TiO_2$, in which we substituted TiO_2 by Ta_2O_5 or Yb_2O_3 or the two of them together and checked the amount of Yb^{3+} and Ta^{5+} allowed in the solution while maintaining the RTP phase, also called critical concentration. We also analyzed how the values of distribution coefficients, K_i, changed for Ti^{4+}, Ta^{5+}, and Yb^{3+}.

Figure 1 shows how the RTP crystallization region evolves as a function of the amount of dopants, Yb^{3+} and Ta^{5+}, in the solution. Figure 1a shows the RTP crystallization region in a solution containing 22 mol % TiO_2 and Rb_2O/P_2O_5 in a ratio of 1.2. Over a 6 at % Ta^{5+} solution, the high-temperature phase of RTP, $RbTiPO_5$,[15] crystallizes, and over 2 at % Yb^{3+} added to the initial solution, the phase which crystallizes is the langbenite, $Rb_2Ti_2(PO_4)_3$, phase.[16] The external morphologies of the three different phases are shown in SEM pictures in Figure 1a. The RTP phase shows a platelike habit similar to that obtained in Nb:RTP crystals,[17] whereas the two other phases show a more isometric habit. Figure 1b shows the Yb:Ta:RTP crystallization region for a

(15) Oseledchik, Y. S.; Belokrys, S. P.; Osadchuk, V. V.; Prosvirnin, A. L.; Selevich, A. F.; Starshenko, V. V.; Kuzemchenko, K. V. *J. Cryst. Growth* **1992**, *125*, 639.
(16) Carvajal, J. J.; Aznar, A.; Solé, R.; Gavaldà, Jna.; Massons, J.; Solans, X.; Aguiló, M.; Díaz, F. *Chem. Mater.* **2003**, *15*, 204.
(17) Carvajal, J. J.; Solé, R.; Gavaldà, Jna.; Massons, J.; Aguiló, M.; Díaz, F. *Cryst. Growth Des.* **2001**, *1*, 479.

Table 1. Distribution Coefficients of Ta^{5+} (K_{Ta}) and Yb^{3+} (K_{Yb}) for RTP Crystals Obtained in the Study of the Variation of the Crystallization Region of RTP When Codoping with Ta^{5+} and Yb^{3+} for Three Different Solution Compositions[a]

solution molar composition: $Rb_2O-P_2O_5-(TiO_2+Ta_2O_5+Yb_2O_3) = 42.900-35.100-22.000$

mol % Ta_2O_5 in solution	mol % Yb_2O_3 in solution: 0	1	2
2	RTP $K_{Ta}= 1.91$; $K_{Yb}= 0.00$	RTP $K_{Ta}= 1.34$ $K_{Yb}= 0.16$	RTP $K_{Ta}= 1.45$ $K_{Yb}= 0.08$; Rb_2
4	RTP $K_{Ta}= 1.16$; $K_{Yb}= 0.00$	RTP $K_{Ta}= 1.09$ $K_{Yb}= 0.16$	
6	RTP $K_{Ta}= 0.80$; $K_{Yb}=0.00$; Rb_5		

solution molar composition: $Rb_2O-P_2O_5-(TiO_2+Ta_2O_5+Yb_2O_3) = 43.125-31.875-25.000$

mol % Ta_2O_5 in solution	mol % Yb_2O_3 in solution: **0**	**1**
2	RTP $K_{Ta}= 1.96$ $K_{Yb}= 0.00$	RTP $K_{Ta}= 2.30$ $K_{Yb}= 0.31$
4	RTP $K_{Ta}= 0.96$ $K_{Yb}= 0.00$	

solution molar composition: $Rb_2O-P_2O_5-(TiO_2+Ta_2O_5+Yb_2O_3) = 40.800-27.200-32.000$

mol % Ta_2O_5 in solution	mol % Yb_2O_3 in solution: 0	1	2	3
1	RTP $K_{Ta}= 1.97$; $K_{Yb}= 0.00$	RTP $K_{Ta}= 1.81$; $K_{Yb}= 0.60$	RTP $K_{Ta}= 1.71$; $K_{Yb}= 0.45$	RTP $K_{Ta}= 1.43$; $K_{Yb}= 0.38$
2	Rb_5	RTP $K_{Ta}= 1.34$; $K_{Yb}= 0.45$	RTP $K_{Ta}= 1.96$; $K_{Yb}= 0.64$; Ru_2	

[a] RTP = $RbTiOPO_4$; Rb_2 = $Rb_2Ti_{2-x}(Yb+Ta)_x(PO_4)_3$; Rb_5 = $RbTiPO_5$.

solution with a 1.4 Rb_2O/P_2O_5 ratio and 25 mol % TiO_2. In this case, the RTP high-temperature phase appeared beyond adding 4 at % Ta^{5+} in the initial solution and the maximum of Yb^{3+} allowed without losing the RTP phase is 3 at %: higher than this value, it appeared again as the langbeinite, $Rb_2Ti_2(PO_4)_3$, phase. Finally, Figure 1c shows the Yb:Ta:RTP crystallization region studied in a solution with a 1.5 Rb_2O/P_2O_5 ratio and a TiO_2 concentration of 32 mol %. The maximum concentrations of dopants that we can introduce in the solution while maintaining the RTP phase are 1.5 at % for Ta^{5+} and 8 at % for Yb^{3+}. So, one can see that for small values of the Rb_2O/P_2O_5 ratio and low concentrations of TiO_2, the critical concentration of Ta^{5+} in solution below which we can still grow the RTP phase reaches a value of 6 at %, the highest of the three molar ratios studied. On the other hand, the highest concentration of Yb^{3+} (8 at %) is reached for large values of the Rb_2O/P_2O_5 ratio and large concentrations of TiO_2.

The differences between the critical amount of Ta^{5+} and Yb^{3+} that are allowed in each crystallization region without losing the RTP phase can be explained in terms of the comparison between the ionic radii in an octahedral environment of Ti^{4+}, Ta^{5+}, and Yb^{3+}, as we expect Ta^{5+} and Yb^{3+} to substitute for Ti^{4+} in the crystalline structure, as with Yb:Nb:RTP crystals.[4] When the amount of Ta^{5+} increased, and because its distribution coefficient is always larger than unity, the solution composition that we get is richer in TiO_2 than the expected one. The quick incorporation of Ta^{5+} ($r_{Ta^{5+}}$ = 0.640 Å) in Ti^{4+} ($r_{Ti^{4+}}$ = 0.605 Å) sites was also observed in KTP.[18] Depending on the initial molar composition of the solution, the amount of codopant allowed could be larger or smaller. In the case of Yb^{3+} ($r_{Yb^{3+}}$ = 0.868 Å), because its distribution coefficient is always smaller than unity, the solution composition is poorer in TiO_2 than the expected one.

The neighboring phases that appeared in all cases were $RbTiPO_5$ and $Rb_2Ti_{2-x}(Yb+Ta)_x(PO_4)_3$. These phases were identified by X-ray powder diffraction and their stoichiometry was deduced from the results obtained by analyzing these crystals by electron probe microanalysis (EPMA). The diffraction patterns obtained were indexed according to the powder diffraction patterns of RTP, (entry 84-2356)[19] and $RbTiPO_5$ (entry 48-0016),[15] both in the database maintained by the Joint Committee for Powder Diffraction Standards (JCPDS), and that of $Rb_2Ti_2(PO_4)_3$.[16] When the amount of Ta_2O_5 in solution is increased, the $RbTiPO_5$ phase, belonging to the cubic system and with space group $Fd\bar{3}m$, crystallized.[15] When the critical concentration of Yb_2O_3 is reached, $Rb_2Ti_{2-x}(Yb+Ta)_x(PO_4)_3$ crystallizes, a langbeinite-type structure belonging to the cubic system and space group $P2_13$.[16]

Table 1 lists the distribution coefficients of Ta^{5+} and Yb^{3+} for the different crystals obtained in the study of the variation of the crystallization region of Yb:Ta:RTP depending on the

(18) Voronkova, V. I.; Yanovskiĭ, V. K.; Losevskaya, T. Yu.; Stefanovich, S. Yu.; Zverkov, S. A.; Alekseeva, O. A.; Sorokina, N. I. *Crystallogr. Rep.* **2004**, *49*, 123.
(19) Kaduk, J. A.; Jarman, R. H. *Z. Kristallogr.* **1993**, *204*, 285.

Table 2. Growth Data of the Crystals of (Yb,Ta):RTP, Using a Solution with a Composition $Rb_2O-P_2O_5-(TiO_2 + Ta_2O_5 + Yb_2O_3)$ = 40.800−27.200−(29.000+1.000+2.000) mol %, Obtained by the TSSG−SC Method

growth experiment	T_s(K)	seed width, *a* (mm)	rotation speed (rpm)	cooling program (cooling range (K)/cooling ramp (K/h))	crystal dimensions ($a \times b \times c$) (mm^3)	crystal weight (g)
1	1209.5		60	4/1 16.5/0.5	$1.84 \times 4.24 \times 3.97$	0.061
2	1208	1.84	60	4/1 27/0.2	$2.46 \times 8.47 \times 7.09$	0.339
3	1205	2.30	60	1/1 17.6/0.1	$2.50 \times 3.53 \times 4.00$	0.100
4	1207	3.00	80	1/1 20/0.1	$3.19 \times 5.73 \times 5.50$	0.182

initial solution composition. These distribution coefficients are defined as

$$K_B = \frac{([B]/[Ti] + [Ta] + [Yb])_{crystal}}{([B]/[Ti] + [Ta] + [Yb])_{solution}}$$

where B = Ti or Ta or Yb. The distribution coefficient K_{Ta}, is almost always larger than unity, but this value tends to decrease when the concentration of Ta^{5+} in the solution is increased. This has also been observed in KTP, where the Ta^{5+} concentration incorporated in the crystal is always higher than the expected when taking into account the Ta^{5+} concentration added in the initial solution.[18] Ta^{5+} ions are expected to replace Ti^{4+} ions in the structure. This could explain why K_{Ta} decreases when the Ta^{5+} concentration in the solution is increased, as the structure becomes saturated in Ta^{5+} and this ion cannot replace Ti^{4+} anymore. K_{Yb} always takes a value smaller than unity because Yb^{3+} has a larger ionic radius than Ti^{4+}. It can be seen in Table 1 that when the Rb_2O/P_2O_5 rate, the amount of TiO_2, and the amount of Ta_2O_5 in the initial solution increase, the value of K_{Yb} slightly increases until it reaches a maximum value of 0.64.

The values of K_{Yb} obtained may be explained in terms of (i) an expansion of the crystal structure due to the incorporation of Ta^{5+} ions that are slightly larger than Ti^{4+} ions, (ii) an expansion of the structure while crystallizing due to an increase in the saturation temperature when the amount of TiO_2 in solution is increased, and (iii) a decrease in the viscosity of the solution when there is a higher Rb_2O/P_2O_5 relation, which would lead to a better degree of homogenization of the solution, increasing the amount of Yb^{3+} ions that could enter into the structure of the growing crystal at the same time.

Top Seeded Solution Growth−Slow Xooling of Yb:Ta:RTP Crystals. Yb:Ta:RTP single crystals were grown by the TSSG−SC method in a solution with a composition $Rb_2O-P_2O_5-(TiO_2+Ta_2O_5+Yb_2O_3)$ = 40.800−27.200-(29.000+1.000+2.000). This composition is placed in the middle of the crystallization region shown in Figure 1c, in a point further from the border between the RTP and $Rb_2Ti_{2-x}(Yb+Ta)_x(PO_4)_3$ phases, which allowed it to obtain a larger concentration of Yb^{3+} in the crystals. The growth conditions are listed in Table 2. We studied how the changes in the speed of rotation, the cooling rate and the cooling interval affected the growth process.

Figure 2 shows a Yb:Ta:RTP crystal obtained following this procedure. In general, the crystals obtained have a flat morphology along the *a* direction. This morphology was previously observed in Nb:KTP[20] and Nb:RTP[13] single crystals. The crystals obtained tended to show some cracks along the *c* direction coming from the crystal seed. The crystals show the same faces as pure RTP: {100}, {011}, {201}, and {110}, listed from the most to the least developed, as can be seen in Figure 2. However, in Yb:Ta:RTP crystals, it should be noticed that the {100} face is much larger than the rest of the faces because the growth rate in the *a* direction is much slower than that in the *b* or *c* directions.To obtain more isometric crystals, we used wider crystal seeds, with dimensions between 1.8 and 3 mm, in the *a* direction, forcing crystal growth along this direction.

All crystal seeds used to grow Yb:Ta:RTP single crystals were placed centered in the rotation axis of the conical platinum crucible, with the wider dimension (the *a* crystallographic direction) in radial direction with respect to the rotation movement and the *c* crystallographic direction perpendicular to the solution surface.

The dimensions of the crystals obtained are listed in Table 2. These dimensions and the weight of the crystals obtained could be increased by enlarging the cooling interval during the growth process. However, the crystals obtained under these conditions had a low optical quality, with small crystals attached to their surface. This is due to spurious nucleation as the crystal that is growing is not able to absorb all the saturation that we are generating in the solution. So, to grow crystals with quality and size enough to carry out further characterizations, when the first additional crystal appears on the surface of the solution and nucleates spontaneously, we removed the main crystal from the solution and decreased the temperature to room temperature before taking the crystal from the furnace. A concentration of Yb^{3+} of 1.6×10^{20} atoms/cm^3 has been obtained in these crystals.

Second Harmonic Generation. The efficiency of the second harmonic generation process, defined as the ratio between the power of the reflected pumping beam generated by a Nd:YAG laser (λ = 1064 nm) and the doubled one generated by the sample (λ = 532 nm), has been measured in RTP samples doped only with Ta^{5+} and in RTP samples doped with Ta^{5+} and Yb^{3+}. The SHG efficiency of a $RbTi_{0.96}Ta_{0.04}OPO_4$ crystal compared to that of KTP is $\eta_{Ta:RTP}/\eta_{KTP}$ = 0.95. For a sample of $RbTi_{0.95}Ta_{0.03}Yb_{0.02}OPO_4$, the efficiency decreases some ($\eta_{(Ta,Yb:RTP)}/\eta_{KTP}$ = 0.80), but the presence of Yb^{3+} in the crystals has a nondramatic effect on the SHG efficiency. This decrease in the efficiency of the second harmonic generation process could be due to a smaller distortion in the TiO_6 octahedra, as proposed by Hagerman

(20) Wang, J.; Liu, Y.; Wei, J.; Jiang, M.; Shao, Z.; Liu, W.; Jiang, S. *Cryst. Res. Technol.* **1997**, *32*, 319.

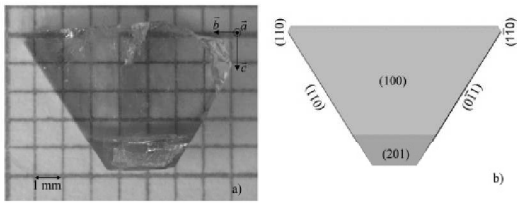

Figure 2. (a) $RbTi_{0.93}Ta_{0.03}Yb_{0.02}OPO_4$ single-crystal grown by the TSSG−SC method on a *c* oriented crystalline seed and (b) scheme of its morphology with the Miller indices of the different faces that appear in the crystal.

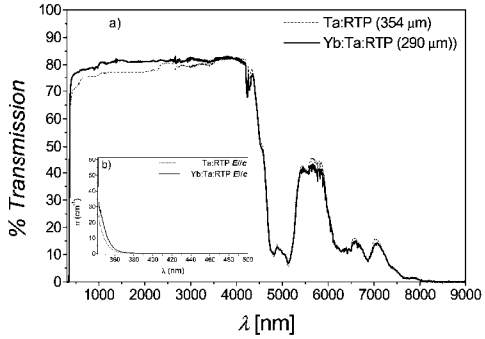

Figure 3. (a) Optical transparency window of $RbTi_{0.96}Ta_{0.04}OPO_4$ (dashed line) and $RbTi_{0.95}Ta_{0.03}Yb_{0.02}OPO_4$ (solid lines) single crystals. (b) Evolution of the cutoff value in the UV region for these crystals.

et al.,[21] or to a decrease in the ionicity in the interactions of the cation framework, as proposed by the extension of the ionic model of second-order susceptibility (χ_{ijk}^2) by Phillips et al.[22] However, no studies on these directions have been performed for the moment in these crystals.

Transparency Window. We have determined the UV and the IR cutoff wavelengths that close the optical transparency window in Ta:RTP and Yb:Ta:RTP samples (Figure 3). The wavelength of the UV cutoff is taken when the optical transmission decays for a factor of $1/e$. For Ta:RTP crystals, with a thickness of 350 μm, the UV cutoff value is located at 340 nm and the IR cutoff is located at ~7500 nm. Similar cutoff wavelengths have been obtained for a Yb:Ta:RTP crystal with a thickness of 290 μm, with the UV cutoff wavelength being located at 342 nm.

It has been previously said that by doping KTP, there exists an enhancement of the susceptibility to optical damage, related to the growth of optical absorption bands close to the UV cutoff.[23,24] We collected the optical absorption of $RbTi_{0.96}Ta_{0.04}OPO_4$ at room temperature in the 350−500 nm range using polarized light parallel to the *c* crystallographic direction and it appears as a band centered around 595 nm, which is similar to those observed in damage or reduced KTP samples.[25] This band is related to the overlapping contribution of $^2T_2 \rightarrow {}^2E$ transition of Ti^{3+} in Ti(1) and Ti-(2) sites of the RTP lattice and disappears after the crystals are annealed at around 800 K for 5 h. If we compare the values obtained for the UV cutoff with those previously reported for $RbTiOPO_4$ (342 nm) and $RbTi_{0.94}Nb_{0.06}OPO_4$ (350 nm),[17] using polarized light parallel to the *c* crystallographic direction, it seems that the UV cutoff of $RbTi_{0.96}Ta_{0.04}OPO_4$ (344 nm) has been red-shifted with respect to that of $RbTiOPO_4$.

This UV cutoff is due to Ti−O electronic transitions, and its value depends on whether tantalum octahedra or only titanium octahedra are present in the structure. As we already know that the UV cutoff for $KTaO_3$ is 365 nm and that by substituting Ta^{5+} by Nb^{5+} in the structure this value increases until 385 nm,[26] the results obtained in our work are in agreement with those previously reported, which is that the cutoff wavelength is smaller in RTP than in Ta:RTP and Nb:RTP.[17]

The bands and peaks that appear in the IR region of the optical transparency window, shown in Figure 3 and centered between 2600 and 2800 nm, are due to the presence of OH^- groups. All the other bands in the spectra between 3300 nm until the end of the spectra (around 8 μm) are combination and overtone bands of the vibrational modes of PO_4^{3-}. The broad and weak band centered at 3400 nm is due to the second overtone of the ν_3, the broad and intense band between 4000 and 5200 nm is the first overtone of ν_3, and the small band at around 5520 nm can be attributed to the first overtone of ν_1. At 6300 nm, the combination band ($\nu_3 + \nu_4$) appears, and at 7500 nm, the band that closes the optical transparency window in the IR region, which corresponds to the combination band ($\nu_1 + \nu_2$), appears. The obtained spectrum is close to that previously obtained by Jacco et al.[2] for KTP, and the bands' assignments have been done with the help of previously published studies.[2,27]

In the spectra of the $RbTi_{0.95}Ta_{0.03}Yb_{0.02}OPO_4$ crystal, the band between 900 and 990 nm corresponds to the Yb^{3+} absorption band associated with the $^2F_{7/2} \rightarrow {}^2F_{5/2}$ transition of Yb^{3+}, which will be studied in more depth in the next section.

Spectroscopic Characterization. We characterized the Yb^{3+} ion in Yb:Ta:RTP crystals spectroscopically. All three possible polarization configurations were studied. The intensity of the spectrum collected with incident light polarized parallel to the *a* axis is much lower than the intensity of the spectrum collected with incident light polarized parallel to the other two axes, showing the same shape of the spectrum collected with light polarized parallel to the *b* direction. To record the spectra in $RbTi_{0.95}Ta_{0.03}Yb_{0.02}OPO_4$, we used a small cube (1.64 × 1.63 × 1.81 mm^3), obtained from the crystal shown in Figure 2. The optical absorption spectra were recorded at room temperature (Figure 4a) with the incident light polarized parallel to the *a*, *b*, and *c* crystallographic axes.

(21) Hagerman, M. E.; Poeppelmeier, K. R. *Chem. Mater.* **1995**, *7*, 602.
(22) Phillips, M. L. F.; Harrison, W. T. A.; Gier, T. E.; Stucky, G. D.; Kulkarni, G. V.; Burdett, J. K. *Inorg. Chem.* **1990**, *29*, 2158.
(23) Martín, M. J.; Zaldo, C.; Díaz, F.; Solé, R.; Bravo, D.; López, F. J. *Radiat. Eff. Defects Solids* **1995**, *136*, 243.
(24) Zaldo, C.; Carvajal, J.; Solé, R.; Díaz, F.; Bravo, D.; Kling, A. *J. Appl. Phys.* **2000**, *88*, 3242.
(25) Martín, M. J.; Bravo, D.; Solé, R.; Díaz, F.; López, F. J.; Zaldo, C. *J. Appl. Phys.* **1994**, *76*, 7510.
(26) Wang, X.; Wang, J.; Yu, Y.; Boughton, R. I. *J. Cryst. Growth* **2006**, *293*, 398.
(27) Vivekanandan, K.; Selvasekarapandian, S.; Kolandaivel, P.; Sebastian, M. T.; Suma, S. *Mater. Chem. Phys.* **1997**, *49*, 204.

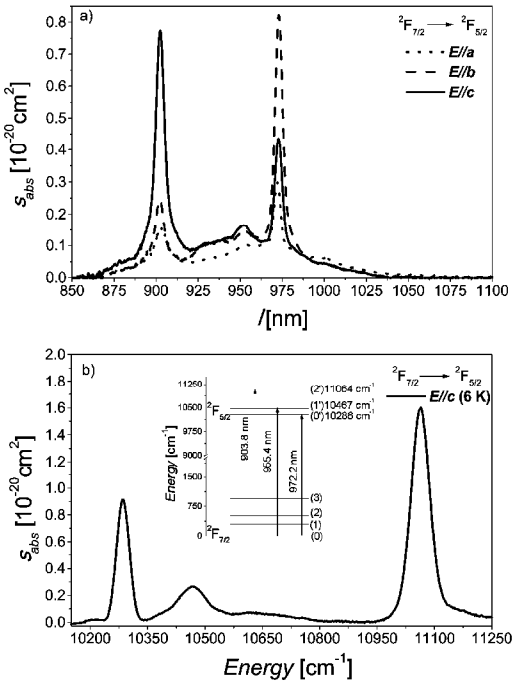

Figure 4. (a) Polarized absorption spectra of the $^2F_{7/2} \rightarrow {}^2F_{5/2}$ transition at room temperature with light polarized parallel to the *a* (dotted line), *b* (dashed line), and *c* (solid line) crystallographic axes in a $RbTi_{0.95}Ta_{0.03}Yb_{0.02}OPO_4$ single crystal, and (b) low-temperature spectrum recorded with light parallel to the *c* crystallographic axis.

The recorded absorption spectra (Figure 4a) show dichroism: when the light is polarized parallel to the *c* crystallographic axis, the most intense peak is located at 903.8 nm, and when it is polarized parallel to the *a* and *b* crystallographic axes, the most intense peak is found at 972.2 nm. The intensity of the peaks as a function of the polarization of the light may vary, but the position or number of peaks are independent of the polarization of the light, as Yb^{3+} has an odd number of electrons in the 4f shell, and then no selection rules exist for the induced electric dipole. The three peaks that appeared in the low-temperature spectra (recorded with light polarized parallel to the *c* axis and shown in Figure 4b) are due to electronic transitions between the ground state ($^2F_{7/2}$) and the three Stark levels of the excited state ($^2F_{5/2}$).

The unpolarized fluorescence spectrum was recorded at room and low temperatures with the same cube used to record the absorption spectra, on a $RbTi_{0.95}Ta_{0.03}Yb_{0.02}OPO_4$ single crystal. The spectrum obtained (see Figure 5), shows four peaks in the low-temperature spectra, and five peaks in the room-temperature spectra, corresponding to the emission from the excited state $^2F_{5/2}$ to the $^2F_{7/2}$ ground state. The most intense peak is centered at 972.2 nm, and it determines the energy of the $^2F_{5/2}(0')$ sublevel because this peak corresponds to the $^2F_{5/2}(0') \rightarrow {}^2F_{7/2}(0)$ electronic transition. A broad band was observed between 1001.7 nm ($^2F_{5/2}(0') \rightarrow {}^2F_{7/2}(1)$) and 1023.2 nm ($^2F_{5/2}(0') \rightarrow {}^2F_{7/2}(2)$). Finally two other peaks of

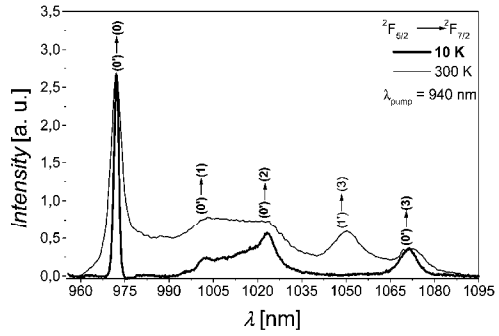

Figure 5. Unpolarized photoluminescence at room and low temperatures of the $^2F_{5/2} \rightarrow {}^2F_{7/2}$ transition for a $RbTi_{0.95}Ta_{0.03}Yb_{0.02}OPO_4$ single crystal after optical pumping at 940 nm with a diode laser.

lower intensity were observed at 1051.1 nm ($^2F_{5/2}(1') \rightarrow {}^2F_{7/2}(3)$) (observed only in the room-temperature spectra) and 1071.5 nm ($^2F_{5/2}(0') \rightarrow {}^2F_{7/2}(3)$).

Both absorption and emission spectra obtained for Yb:Ta:RTP crystals match well, in shape and in position of the peaks with the spectra previously obtained for Yb:Nb:RTP crystals,[28] showing only a slight blue-shift of the peaks in Yb:Ta:RTP crystals. This is important because a broad laser emission around 1 μm can also be obtained in these crystals that may allow for the generation of ultrashort laser pulses and the development of new tunable laser sources.[25]

Conclusions

We obtained Yb:Ta:RTP single crystals doped with enough concentration of Yb^{3+} to get efficient fluorescence at room temperature. When comparing with RTP single crystals codoped with Nb^{5+} and Yb^{3+}, it is interesting to note that using a smaller concentration of Ta^{5+}, instead of Nb^{5+}, in a solution with the same molar composition of precursor oxides, Rb_2O, P_2O_5, and TiO_2, the concentration of Yb^{3+} reached is higher. This is important, as by introducing fewer impurities in the crystal, we get the same Yb^{3+} concentration in the host, minimizing changes in the physical properties of these crystals caused by the presence, at larger concentrations, of these impurities. However, the crystallization region of RTP when using Ta^{5+} as a codopant is much narrower than the crystallization region obtained when using Nb^{5+}. The critical concentration of Ta^{5+} and Yb^{3+} depends on the initial solution composition and the molar concentration of Rb_2O, P_2O_5, and TiO_2. The boundary phases to RTP in these systems are $RbTiPO_5$ above the critical concentration of Ta^{5+}, and $Rb_2Ti_{2-x}(Yb + Ta)_x(PO_4)_3$ above the critical concentration of Yb^{3+}. Spectroscopic studies revealed a strong dichroism that can be useful to optimize the fluorescence response by pumping at different wavelengths for different polarization configurations of the incident light, at around 903 nm when the incident light is polarized along the *c* crystallographic axis, or 973 nm when the incident light is polarized along the *b* crystallographic axis. The same

(28) Carvajal, J. J.; Solé, R.; Gavaldà, Jna.; Massons, J.; Segonds, P.; Boulanger, B.; Brenier, A.; Boulon, G.; Zaccaro, J.; Aguiló, M.; Díaz, F. *Opt. Mater.* **2004**, *26*, 313.

behavior was shown in Yb:Nb:RTP. Also, by comparing the absorption and emission spectra of Yb:Ta:RTP crystals with those obtained on Yb:Nb:RTP crystals,[28] we expect that Yb^{3+} in Yb:Ta:RTP crystals emits with a broad laser emission band at around 1 μm, useful for the generation of ultrashort laser pulses and the development of new tunable laser sources.[11]

Moreover, because of the high SHG process efficiency, even when Yb^{3+} is present in the crystals, Yb:Ta:RTP is a good candidate to be tested as a self-frequency doubling material.

Acknowledgment. This work has been supported by the Spanish government under projects MAT-05-06354-C03-02, MAT-04-20471-E, and CIT-020400-2005-14 and the Catalan government under project 2005SGR658. A.P. thanks to the Spanish government for the personal funding BES-2003-1694.

CM070887Z

UNIVERSITAT ROVIRA I VIRGILI
YTTERBIUM AND ERBIUM DOPEP RbTi1-xMxOPO4 (M=Nb or Ta) CRYSTALS. NEW LASER AND NONLINEAR BIFUNCTIONAL MATERIALS
Alexandra Peña Revellez
ISBN: 978-84-691-0370-8 /DL:T.2188-2007

Paper II

Yb^{3+} spectroscopy in (Nb or Ta):$RbTiOPO_4$ single crystals for laser applications.

A. Peña, J. J. Carvajal, M. C. Pujol, X. Mateos, V. Petrov, P. Segonds, B. Boulanger, F. Díaz, M. Aguiló

Optics Express (submitted)

UNIVERSITAT ROVIRA I VIRGILI
YTTERBIUM AND ERBIUM DOPEP RbTi1-xMxOPO4 (M=Nb or Ta) CRYSTALS. NEW LASER AND NONLINEAR BIFUNCTIONAL MATERIALS
Alexandra Peña Revellez
ISBN: 978-84-691-0370-8 /DL:T.2188-2007

UNIVERSITAT ROVIRA I VIRGILI
YTTERBIUM AND ERBIUM DOPEP RbTi1-xMxOPO4 (M=Nb or Ta) CRYSTALS. NEW LASER AND NONLINEAR BIFUNCTIONAL MATERIALS
Alexandra Peña Revellez
ISBN: 978-84-691-0370-8 /DL:T.2188-2007

Yb^{3+} spectroscopy in (Nb or Ta):$RbTiOPO_4$ single crystals for laser applications

Alexandra Peña,[1] Joan Josep Carvajal,[1] Maria Cinta Pujol, [1] Xavier Mateos, [1,2] Magdalena Aguiló,[1] Francesc Díaz,[1*] Valentin Petrov, [2]Patricia Segonds, [3] and Benoît Boulanger[3]

[1]*Física i Cristal·lografia de Materials (FiCMA), Universitat Rovira i Virgili (URV), Campus Sescelades, c/Marcel·lí Domingo, s/n., E-43007 Tarragona, Spain*

[2]*Max-Born-Institute for Nonlinear Optics and Ultrafast Spectroscopy, 2A Max-Born-Str., D-12489 Berlin, Germany*

[3]*Institut Néel /CNRS – UJF, BP 166, F-38042 Grenoble Cedex 9, France*

**Corresponding author: f.diaz@urv.cat*

Abstract: Single crystals of Yb:$RbTiOPO_4$ codoped with Nb^{5+} or Ta^{5+} were grown by the top seeded solution growth slow-cooling technique. The ytterbium concentration in the crystals varies as a function of the molar ratio of the precursor oxides, and of the codopant, reaching a maximum concentration of 1.9×10^{20} Yb^{3+} ions/cm^3. The broadband emission near 1 μm in absorption and emission spectra at room temperature is due to the large splitting of the Yb^{3+} ground state. The ytterbium $^2F_{5/2}$ level radiative lifetime in Nb:$RbTiOPO_4$ (τ_{rad} = 2.7 ms), was calculated and then compared to the measured fluorescence decay time (2.2 ms), giving an intrinsic quantum efficiency of 81%. To evaluate the potentiality of these crystals for self-frequency doubling, preliminary results of Yb^{3+} laser operation and fundamental wavelength measurements for type-II non-critical second harmonic generation (λ_{NCPM}) are also reported.

OCIS codes: (140.0140) Lasers and laser optics; (140.3580) Lasers, solid-state; (140.5680) Rare earth and transition metal solid-state lasers; (160.4330) Nonlinear optical materials

References and links

1. A. Brenier, D. Jaque, and A. Majchrowski, "Bi-functional laser and non-linear optical crystals" Opt. Mater. **28**, 310-323 (2006)
2. D. A. Hammons, J. M. Eichenholz, Q. Ye, B. H. T. Chai, L. Shah, R. E. Peale, M. Richardson, and H. Qiu, "Laser action in Yb:YCOB (Yb:$YCaOBO_3)_3$)"Opt. Commun. **156**, 327-330 (1998).
3. H. Zhang, X. Meng, P. Wang, L. Zhu, X. Liu, X. Liu, Y. Yang, R. Wang, J. Dawes, J. Piper, S. Zhang, and L. Sun, "Growth of Yb-doped $Ca_4GdO(BO_3)_3$ crystals and their spectra and laser properties" J. Cryst. Growth **222**, 209-214 (2001).
4. L. B. Bausá, M. O. Ramírez, and E. Montoya, "Optical performance of Yb^{3+} in $LiNbO_3$ laser crystal" Phys. Status Solidi A-Appl. Mat. **201**, 289-297 (2004).
5. P. Dekker, J. M. Dawes, J. A. Piper, Y. Liu, and J. Wang, "1.1W CW self-frequency-doubled diode-pumped Yb:$YAl_3(BO_3)_4$ laser " Opt. Commun. **195**, 431-436 (2001).
6. C. Zumsteg, J. D. Bierlein, and T. E. Gier, " K_x $Rb_{1-x}TiOPO_4$: A new nonlinear optical material" J. Appl. Phys. **47**, 4980-4985 (1976).
7. J. Carvajal, V. Nikolov, R. Solé, Jna. Gavaldà, J. Massons, M. Rico, C. Zaldo, M. Aguiló, and F. Díaz, "Enhancement of the Erbium Concentration in $RbTiOPO_4$ by Codoping with Niobium" Chem. Mater. **12**, 3171-3180 (2000).
8. J. Carvajal, V. Nikolov, R. Solé, Jna. Gavaldà, J. Massons, M. Aguiló, and F. Díaz, "Crystallization Region, Crystal Growth, and Characterization of Rubidium Titanyl Phosphate Codoped with Niobium and Lanthanide Ions", Chem. Mater. **14**, 3136-3142 (2002).
9. A. Peña, J. J. Carvajal, J. Massons, J. Gavaldà, F. Díaz, and M. Aguiló, "Yb:Ta:$RbTiOPO_4$, a new strategy for further increase the lanthanide concentration in crystals of the $KTiOPO_4$ family" Chem. Mater. (in press)

ISBN: 978-84-691-0370-8 /DL:T.2188-2007

10. J. J. Carvajal, C. F. Woensdregt, R. Solé, F. Díaz, and M. Aguiló, "Change in the Morphology of $RbTiOPO_4$ Introduced by thePresence of Nb" Cryst. Growth & Des. **6**, 2667-2673 (2006).
11. J. J. Carvajal, J. L. García-Muñoz, R. Solé, Jna. Gavaldà, J. Massons, X. Solans, F. Díaz, and M. Aguiló, "Charge Self-compensation in the Nonlinear Optical Crystals $Rb_{0-855}Ti_{0-955}Nb_{0-045}OPO_4$ and $RbTi_{0,927}Nb_{0-056}Er_{0-017}OPO_4$" Chem. Mater. **15**, 2338-2345 (2003).
12. R. D. Shannon, "Revised effective ionic radii and systematic studies of interatomic distances in halides and chalcogenides", Acta Cryst. A32, 751-767 (1976).
13. J. J. Carvajal, R. Solé, Jna. Gavaldà, J. Massons, P. Segonds, B. Boulanger, A. Brenier, G. Boulon, J. Zaccaro, M. Aguiló, and F. Díaz, "Spectroscopic and second harmonic generation properties of a new crystal: Yb-doped $RbTiOPO_4$" , Opt. Mater. **26**, 313-317 (2004).
14. M. Weber, " Optical Properties of Yb^{3+} and Nd^{3+}-Yb^{3+} energy transfer in $YAlO_3$" Phys. Rev. B **4**, 3153 – 3159 (1971).
15. F. Mougel, K. Dardenne, G. Aka, A. Kahn-Harari, and D. Vivien, "Ytterbium-doped $Ca_4GdO(BO_3)_3$: an efficient infrared laser and self-frequency doubling crystal" J. Opt. Soc. Am. B **16**, 164-172 (1999).
16. A. Aron, G. Aka, B. Viana, A. Kahn-Harari, D. Vivien, F. Druon, F. Balembois, P. Georges, A. Brun, N. Lenain, and M. Jacquet, "Spectroscopic properties and laser performances of Yb :YCOB and potential of the Yb :LaCOB material" Opt. Mater. **16**, 181-188 (2001).
17. P. Wang, J. M. Dawes, P. Dekker, D. S. Knowles, J. A. Piper, and B. Lu, "Growth and evaluation of ytterbium-doped yttrium aluminum borate as a potential self-doubling laser crystal J. Opt. Soc. Am. B **16**, 63-69 (1999).
18. Z. Zhu, J. Li, A. Brenier, G. Jia, Z. You, X. Lu, B. Wu, and C. Tu., "Growth, spectroscopic and laser properties of Yb^{3+}-doped $GdAl_3(BO_3)_4$ crystal: a candidate for infrared laser crystal" Appl. Phys. B **86**, 71-75 (2007).
19. E. Montoya, J. A. Sanz-García, J. Capmany, L. E. Bausà, A. Diening, T. Kellner, and G. Huber, "Continuous wave infrared laser action, self-frequency doubling, and tunability of Yb^{3+}:MgO:$LiNbO_3$" J. Appl. Phys. **87**, 4056-4062 (2000).
20. I. Parreu, M. C. Pujol, M. Aguiló, F. Díaz, X. Mateos, and V. Petrov, "Growth, spectroscopy and laser operation of Yb:$KGd(PO_3)_4$ single crystals" Opt. Express **15**, 2360-2368 (2007).
21. P. Wang, J. M. Dawes, P. Dekker, and J. A. Piper, "Highly efficient diode-pumped ytterbium-doped yttrium aluminum borate laser" Opt. Commun. **174**, 467-470 (2000).

I. Introduction

Solid state laser sources in the visible are of great importance in laser technology because they can be used for several applications such as high density optical storage, laser displays and underwater communications. Furthermore, nonlinear optical materials that can incorporate active ions represent a class of bifunctional crystals where the nonlinear and laser effects take place simultaneously. Up to now the active ion which has been mainly used as a dopant in non-centrosymmetric hosts to obtain self-frequency doubling laser action, was neodymium [1]. Nowadays there is an increasing interest in laser technology to replace neodymium by ytterbium, because both ions operate in the same wavelength range, but ytterbium has a number of advantages mainly related to its simple two-manifold electronic structure. For this purpose non-centrosymmetric hosts such as $YCa_4O(BO_3)_3$ (YCOB),[2] $GdCa_4O(BO_3)_3$ (GdCOB),[3] MgO:$LiNbO_3$ (MgO:LNB)[4] and $YAl_3(BO_3)_4$ (YAB)[5] have been doped with ytterbium and self-frequency doubling laser action in the visible was obtained. The advantages of using ytterbium as doping ion in nonlinear optical materials to obtain a self-frequency doubling laser are that this ion does not exhibit absorption in the green, which means no absorption losses for the generated second harmonic beam, and when broad emission bands exist, some of these materials can produce tunable laser radiation in the visible, extending from the green to the yellow. The broad tunability, when existing, is promising to obtain femtosecond pulses.

$RbTiOPO_4$ (RTP) belongs to the $KTiOPO_4$ (KTP) family of nonlinear optical crystals which crystallize in the orthorhombic system, with the non-centrosymmetric space group $Pna2_1$. RTP, as many of the crystals belonging to the KTP family, is of interest due to its excellent nonlinear and thermo-mechanical properties.[6] Its crystallization region has been previously

UNIVERSITAT ROVIRA I VIRGILI
YTTERBIUM AND ERBIUM DOPEP RbTi1-xMxOPO4 (M=Nb or Ta) CRYSTALS. NEW LASER AND NONLINEAR BIFUNCTIONAL MATERIALS
Alexandra Peña Revellez
ISBN: 978-84-691-0370-8 /DL:T.2188-2007

determined. [7] The variation of the crystallization region in self-flux when introducing niobium and ytterbium, [8] and tantalum and ytterbium [9] has also been investigated.

In this work we study the variation of ytterbium concentration in single crystals of Yb:Nb:RTP and Yb:Ta:RTP obtained by the top seeded solution growth - slow cooling (TSSG-SC) technique using self-fluxes and tungsten-containing fluxes.

We report optical absorption and emission spectra recorded at room and low temperature for Yb:Nb:RTP and Yb:Ta:RTP single crystals, and the corresponding Stark splitting of the Yb^{3+} electronic states which are compared.

Finally, we discuss the continuous-wave laser operation achieved together with experimental results obtained for the fundamental wavelength in type-II non-critical phase-matching (λ_{NCPM}) along the principal axes *x* and *y* for Yb:Nb:RTP, to evaluate the potentiality of these crystals as self-frequency doubling materials.

2. Crystal growth

We grew Yb:Nb:RTP and Yb:Ta:RTP single crystals in self-fluxes and tungsten-containing fluxes by the Top-Seeded-Solution-Growth Slow-Cooling (TSSG-SC) method without pulling. All the growth experiments were performed in a vertical tubular single-zone furnace, where it was placed the crucible in a position that ensures an axial temperature gradient in the solution between 0.15 and 0.6 K/mm, with the surface always colder than any other part of the solution. The determination of the saturation temperature (T_s), which should be made previously to begin the growth process and after the homogenization of the solution, was performed by observing the growth/dissolution of a crystal seed in contact with the surface of the solution. All the crystals were grown onto seeds oriented with the ***c*** crystallographic direction perpendicular to the surface of the solution. During the crystal growth experiments the crystals were submerged in the solution, rotating at a constant velocity. Details on the crystal growth processes, such as the axial gradient or the cooling ramp applied are given in Table 1. Once the end of the cooling ramp, the crystals were slowly removed from the solution and kept some millimeters above the solution surface while cooling the surface down to 298 K at 15 K/h, to avoid any thermal stress.

Table 1. Data associated with ytterbium-doped Nb:RTP and Ta:RTP single crystals grown by the TSSG-SC. A: Growth experiment. B: Solution % molar composition Yb_2O_3:(Nb_2O_5 or Ta_2O_5):TiO_2:Rb_2O:P_2O_5:WO_3. C: Distribution coefficient of ytterbium in RTP. D: Crystal stoichiometry. E: Saturation temperature, K. F: Solution weight, g. G: Axial gradient, K/mm. H: Seed width in *a* direction, mm. I: Cooling program: (cooling range, K)/(cooling ramp, K/h). J: Crystal dimensions (a × b × c), mm^3. K: Crystal weight, g.

A	B	C	D	E	F	G	H	I	J	K
1	0.64:0.96:30.40: 40.80:27.20:0.00	0.38	$RbTi_{0.949}Nb_{0.036}Yb_{0.015}OPO_4$	1195.5	160	0.25	4.8	1/1 4/0.05 9.5/0.02	5.1×10.1×8.2	0.84
2	0.64:0.96:30.40: 40.80:27.20:0.00	0.52	$RbTi_{0.945}Nb_{0.034}Yb_{0.021}OPO_4$	1187.5	160	0.24	5.2	1/1 6/0.05 10/0.03	5.9×16.0×12.7	2.60
3	0.64:*0.32*:31.04: 40.80:27.20:0.00	0.45	$RbTi_{0.949}Ta_{0.033}Yb_{0.018}OPO_4$	1208	32	0.57	2.4	23.2/0.2	2.5×6.6×4.9	0.17
4	0.64:*0.32*:31.04: 40.80:27.20:0.00	0.41	$RbTi_{0.929}Ta_{0.055}Yb_{0.016}OPO_4$	1207	32	0.57	3	1/1 20/0.1	3.2×5.7×5.5	0.18
5	0.45:0.68:21.37: 43.87:23.63: 10	0.37	$RbTi_{0.948}Nb_{0.037}Yb_{0.015}OPO_4$	1144	34	0.18	7	12.6/0.04	7.6×2.9×2.6	0.11
6	0.27:0.41:12.92: 43.82:22.58:20	0.28	$RbTi_{0.956}Nb_{0.031}Yb_{0.011}W_{0.002}OPO_4$	1154	260	0.15	2.5	1/1 19/0.1	3.6×4.0×3.9	0.15

We analyzed the growth conditions of Yb:Nb:RTP and Yb:Ta:RTP crystals grown in self-fluxes and tungsten-containing fluxes. Then we are able to evaluate how the conditions of growth, such as the axial gradient or the cooling program used, and the flux composition used

ISBN: 978-84-691-0370-8 /DL:T.2188-2007

in each case affect the quality of the crystals obtained and the actual ytterbium concentration. The molar ratio of precursor oxides was almost the same for Yb:Nb:RTP and Yb:Ta:RTP crystals grown in self-fluxes. However it was different for Yb:Nb:RTP crystals grown in tungsten-containing fluxes. Crystals of Yb:Nb:RTP and Yb:Ta:RTP were grown in self-fluxes from solution with a molar composition (Yb_2O_3:Nb_2O_5 or Yb_2O_3:Ta_2O_5):TiO_2:Rb_2O:P_2O_5 = x:y:32.00-(x+y):40.80-27.20 (experiments 1 to 4 listed in Table 1). To grow Yb:Nb:RTP crystals in solutions containing WO_3 (experiments 5 and 6 listed in Table 1) the solution composition could not be the same as the previous one used to grow Yb:Nb:RTP crystals from self-fluxes (experiments 1 to 4). This is because when WO_3 is present in the solution the RTP crystallization region shifts to Rb_2O richer regions and becomes narrower. Previously, we also determined how the values of the distribution coefficients of ytterbium in Nb:RTP [8] and Ta:RTP [9] crystals vary as a function of the Rb_2O/P_2O_5 molar ratio and TiO_2 concentration in the initial growth solution. So, to obtain the desired orthorhombic and non-centrosymmetric $Pna2_1$ phase with the highest ytterbium distribution coefficient, while still remaining far enough from the border between RTP and other neighbouring phases, solutions with different molar compositions had to be used in self-fluxes and in tungsten-containing fluxes.

Polished and crack free seeds of almost the same composition of the crystal that was going to be grown were used, since we noticed that the quality of the crystals obtained improved when using this kind of seeds. Moreover the thickness of the seed in the *a* crystallographic direction should be as large as possible, because when doping RTP with Nb^{5+} or Ta^{5+} the crystals show a plate-like habit. We have also shown that using this kind of seeds is a possible way to increase the dimension in the aforementioned direction.[10]

The cooling rate and the cooling interval applied affect the size of the crystals obtained. By applying faster cooling rates spurious nucleation appeared before on the surface of the solution, which means that shorter cooling interval could be applied.

The single crystals obtained were subjected to electron probe microanalysis (EPMA), to determine their chemical composition, as well as the ytterbium distribution coefficient, defined as K_{Yb} = ([Yb]/([Yb]+[Nb or Ta]+[Ti]))$_{crystal}$/([Yb]/([Yb]+[Nb or Ta]+[Ti]))$_{solution}$. These values are listed in Table I. The distribution coefficients obtained, always smaller that unity, can be well understood since ytterbium ions, as other Ln^{3+} ions in the Nb:RTP crystals, [11] are supposed to substitute titanium ions in the structure and the ionic radius of Ti^{4+} (r_{Ti}^{4+}= 0.605 Å) is much smaller than the radius of Yb^{3+} (r_{Yb}^{3+}= 0.868 Å).[12]

As shown in Table 1, the saturation temperature (T_s) tends to increase slightly with increasing TiO_2 content in the solution composition. This rule is not accomplished in the last growth experiment, probably due to a slight change in the solution composition induced by an increase of the solvent evaporation during the homogenization process.

Comparing the first two experiments, grown by using Nb^{5+} as a codopant in self-fluxes and performed with the same solution composition, the difference is related to the cooling interval applied (14.5 K and 17 K respectively) and the seed width used in each case. As mentioned before, the seed width determines the dimension along the *a* crystallographic axis. The crystal dimension in this direction, and the crystal weight were enlarged significantly by using a larger temperature interval in the total cooling program. However, the key of the process seems to be in the second step of the cooling rate program. By increasing the interval of cooling by 2 K at a cooling rate of 0.05 K/h, it was possible to enlarge the last part of the cooling program by 0.5 K, which represents a total enlargement of the cooling program of 2.5 K before spurious nucleation appeared on the surface of the solution. This ensures a better control of the supersaturation during the growth process which provides a larger crystal. This better control of the supersaturation seems to affect positively the ytterbium incorporation in the crystals, as ytterbium distribution coefficient is higher in the second experiment.

The crystals obtained in the third and fourth growth experiments, which were grown by using Ta^{5+} as a codopant, had almost the same weight. However, their dimensions were slightly different, due to the width of the seed in *a* direction used in each case. In this case,

ISBN: 978-84-691-0370-8 /DL:T.2188-2007

also, the introduction of a preliminary step in the cooling program consisting of a 1 K temperature decrease at a rate of 1K/h, and by reducing the cooling rate in the second step have benefits in obtaining a better quality crystal in a smaller cooling interval. The concentration of Ta^{5+} in the crystals has almost doubled, although the ytterbium incorporation remains almost the same.

Although size and weight of the crystals containing Nb^{5+} and Ta^{5+} are not comparable as they were grown in crucibles with different dimensions and with different conditions of seeding, the ytterbium concentration obtained in these four growth experiments does not vary significantly, so both codopants, Nb^{5+} or Ta^{5+}, have more or less the same effect in increasing the concentration of Yb^{3+} in RTP crystals and both can be used for this purpose.

Finally, the addition of WO_3 in the solution, has a beneficial effect, as it decreases the solution viscosity, which allows to grow the crystals at a faster rate and use a smaller axial thermal gradient in the crucible (note that although large axial thermal gradients in the crucible are needed to stir the solution when the viscosity is high, they shift the growth conditions further away from the thermodynamic equilibrium, and thus, from ideal crystal quality). Although this addition of WO_3 does not improve ytterbium incorporation in the crystals, it does not reduce it significantly with respect to crystals grown in self-fluxes.

3. Ytterbium spectroscopy

We studied the polarized optical absorption of ytterbium ion in Nb:RTP and Ta:RTP samples at room and low temperatures. The absorption spectra, recorded between 850 – 1100 nm, were measured using a Varian Cary 500 spectrophotometer and a Glan-Taylor polarizer. The samples, to perform the low temperatures spectra, were cooled with a Leybold RDK-6-320 closed-cycle helium cryostat. Fig. 1 shows polarized absorption spectra recorded at room temperature for Yb:Nb:RTP and Yb:Ta:RTP. The crystallographic axes *a*, *b* and *c* are parallel to the principal optical axes, *x*, *y* and *z* of the dielectric frame, for which $n_x<n_y<n_z$ is fulfilled. Yb^{3+} (which occupies a C_1 symmetry site) has an odd number of electrons in the 4*f* shell. Hence, polarization selection rules for the electronic transitions are not expected. So, the number and position of the peaks are independent of the light polarization, but the intensity may vary. This was confirmed in the recorded polarized absorption spectra (Fig. 1): the most intense peak is the one located near 970 nm, for *E//a* and *b* crystallographic axes, and the one located at ≈ 900 nm for *E//c*. However, the number of peaks and their position is the same for the three orthogonal polarizations.

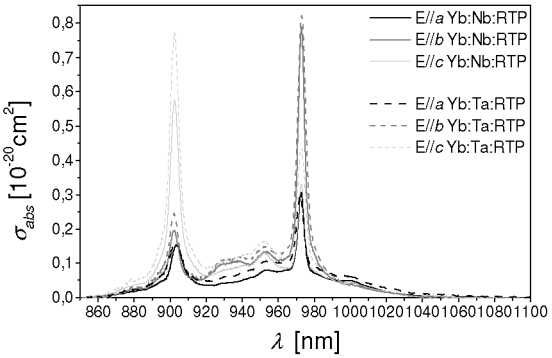

Fig. 1. Yb:Nb:RTP (solid lines) and Yb:Ta:RTP (dashed lines) measured absorption cross-sections at room temperature.

UNIVERSITAT ROVIRA I VIRGILI
YTTERBIUM AND ERBIUM DOPEP RbTi1-xMxOPO4 (M=Nb or Ta) CRYSTALS. NEW LASER AND NONLINEAR BIFUNCTIONAL MATERIALS
Alexandra Peña Revellez
ISBN: 978-84-691-0370-8 /DL:T.2188-2007

As shown in Fig. 1, the main difference between the polarized spectra recorded for Yb:Nb:RTP and Yb:Ta:RTP is that the cross section values obtained for *E//c* (maximum at ≈ 900 nm) and *E//b* (maximum at ≈ 970 nm) are quite different (0.58×10^{-20} cm^2 and 0.79×10^{-20} cm^2, respectively) for Yb:Nb:RTP, while for Yb:Ta:RTP they are much closer (0.77×10^{-20} cm^2 and 0.82×10^{-20} cm^2). Hence, for Yb:Ta:RTP the pump wavelength could be set to ≈ 900 nm or ≈ 970 nm depending on the polarization chosen. The cross section values already published for Yb:Nb:RTP [13] are in good agreement with the results reported in this study.

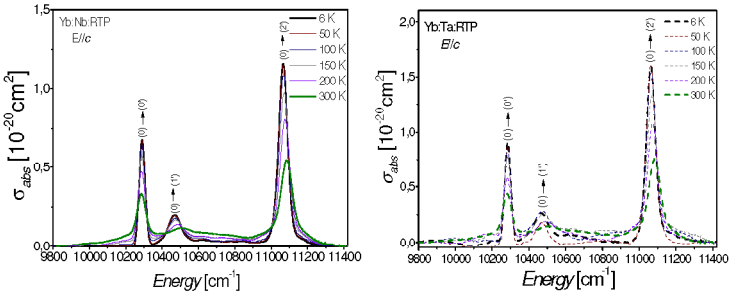

Fig. 2. Temperature evolution of the absorption cross sections of Yb:Nb:RTP (solid lines) and Yb:Ta:RTP (dashed lines) for *E//c*.

In Fig. 2, the evolution of the absorption cross sections from 6 K to 300 K is shown for samples of Yb:Nb:RTP (solid lines) and Yb:Ta:RTP (dashed lines). From the spectra recorded at 6 K we accurately determined the energies of the three Stark sublevels of the $^2F_{5/2}$ multiplet. As shown in the inset of Fig. 3 the energies of the Stark sublevels, do not differ significantly when using niobium or tantalum as a codopant.

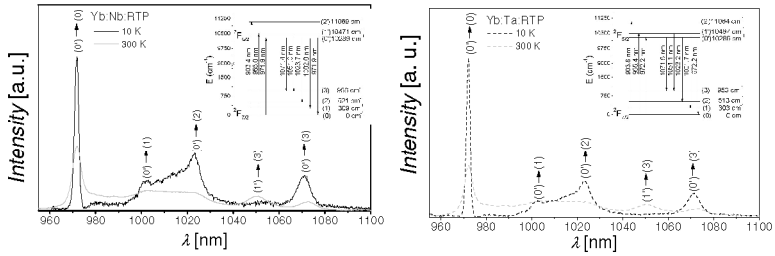

Fig. 3. Room and low temperature emission of Yb:Nb:RTP (solid lines) and Yb:Ta:RTP (dashed lines). Inset: schematic diagram of the Yb^{3+} Stark sublevels and absorption and emission transitions.

The unpolarized fluorescence spectra were recorded between 950 and 1100 nm in a 90º geometry with excitation by a 200 mW diode laser at 940 nm modulated at 1 kHz. The fluorescence was dispersed by a double monochromator (Jobin Ybon-Spex HR460), with a focal length of 0.46 m, and detected by a cooled Hamamatsu NIR R5509-72 photomultiplier which was connected to a lock-in amplifier. To perform the low temperature emission measurements at 10 K a close-cycle helium cryostat (Oxford CCC1104) was used.

From the emission spectra obtained at 10 K the four sublevels of the ground state, $^2F_{7/2}$, were determined (see Fig. 3 inset). An additional peak appears at room temperature, centred at 1051.0 nm in Nb:RTP and at 1051.1 nm in Ta:RTP. It is attributed to a transition between the (1') Stark sub-level of the upper multiplet and the (3) Stark sub-level of the lower multiplet. The large splitting of the Yb ground state, 956 cm^{-1} for Nb:RTP and 953 cm^{-1} for Ta:RTP,

UNIVERSITAT ROVIRA I VIRGILI
YTTERBIUM AND ERBIUM DOPEP RbTi1-xMxOPO4 (M=Nb or Ta) CRYSTALS. NEW LASER AND NONLINEAR BIFUNCTIONAL MATERIALS
Alexandra Peña Revellez
ISBN: 978-84-691-0370-8 /DL:T.2188-2007

results in low (0.76% and 0.75%, respectively) population of the highest $^2F_{7/2}$ sub-level at room temperature. Such high energies of the highest sub-level facilitate the laser operation in a quasi-three level scheme, reducing the laser threshold.

The radiative lifetime value for Yb:Nb:RTP was determined from the spontaneous emission probability (A_{if}) calculated by averaging (over the polarizations) the integrated absorption coefficients using the relationship proposed by Weber [14]

$$\frac{1}{\tau_{rad}} = A_{if} = \left(\frac{g_f}{g_i}\right)\frac{8\pi n^2}{N\lambda^2}\int \alpha(\nu)d\nu \qquad (1)$$

where g_f and g_i are degeneracies of the final and the initial states 4 and 3 respectively. n is the refractive index, N is the ytterbium concentration (which is equal to 1.87×10^{20} ions/cm^3 in this case) and $\alpha(\upsilon)$ is the absorption coefficient at frequency $\upsilon = c/\lambda$. The result is τ_{rad} = 2.7 ms. Comparing it with the fluorescence decay time measured previously, [13] τ_{em} = 2.2 ms, one obtains an intrinsic quantum efficiency of 81%. This fluorescence decay time is of the same order as the one obtained for GdCOB [15] and YCOB,[16] but much larger than in YAB,[17] GAB,[18] MgO:LNB[19] and KGP,[20] as shown in Table 2.

Table 2. Spectroscopic and laser parameters of Yb^{3+} doped non-centrosymmetric laser crystals.

Properties	YAB [15]	GAB [16]	YCOB [17]	GdCOB [18]	MgO:LNB [19]	KGP [20]	Nb:RTP
λ_{ZL} [nm]	981	977	976	976	980	977	971.9
λ_{ext} [nm]	1040	1045	1050	1032	1062	1035	1049.4
λ_{pump} [nm]	975	977	900	902	980	977.1	972.8
σ_{abs} [10^{-20}cm^2]	3.4	3.43	-	0.41	≈1.1	1.17	0.79
σ_{em} [10^{-20}cm^2]	0.8	0.98	0.18	0.55	0.24	0.02	0.27[a]
τ_{em} [ms]	0.68	0.569	2.4 (τ_{rad})	2.6	0.540	1.25	2.2[a]
β_{min}	0.043	0.022	0.06	0.06	0.106	0.05	0.03
I_{sat} [kW/cm^2]	8.8	10.4	42	25.5	33.2	13.9	11.8
I_{min} [kW/cm^2]	0.38	0.23	1.31	1.54	3.51	0.77	0.32
Laser operation							
Laser source	Diode [21]	Diode	Ti:sapphire	Ti:sapphire	Ti:sapphire	Ti.sapphire	Ti:sapphire
λ_{pump} [nm]	976	974	900	902	954	977.1	972.7
P_{th} [mW]	147	800	120	40	312	51	35
η [%]	67	27.4	15	58.8	12.6	53.2	42.5
λ_L [nm]	1040	1043	1060	1056	1064	1017.1	1050.6
T_{oc} [%]	-	2	2	1	0.6	1	1

[a] Value published in ref. 13

The radiative lifetime for Yb:Ta:RTP was also calculated, by using the chromatic dispersion of the principal refractive indices n_x, n_y and n_z of Nb:RTP, because for Ta:RTP the dispersion is unknown (the crystals obtained up to now are not big enough to process prism shaped samples). In any case, as the difference in the n_x, n_y and n_z refractive indices measured at 632.8 nm (by a prism coupler) for the samples used to perform the spectroscopic studies was less than 0.01, the obtained value (τ_{rad} = 2.6 ms) should be very close to the real one.

UNIVERSITAT ROVIRA I VIRGILI
YTTERBIUM AND ERBIUM DOPEP RbTi1-xMxOPO4 (M=Nb or Ta) CRYSTALS. NEW LASER AND NONLINEAR BIFUNCTIONAL MATERIALS
Alexandra Peña Revellez
ISBN: 978-84-691-0370-8 /DL:T.2188-2007

4. Laser operation

The laser set-up scheme (Fig. 4) used to study the laser operation of Yb:Nb:RTP was a standard astigmatically compensated Z-shaped cavity. The pump source was a home-made Ti:sapphire laser (972.7 nm, FWHM < 1 mm, max. 1.8 W), with the beam focused onto the sample, which is inserted under Brewster angle, by a 6.28 cm lens. The estimated Gaussian pump waist in the focus was ≈ 30 μm. The ≈ 150 cm long cavity consisted of two folding mirrors, a rear plane mirror, and a plane output coupler.

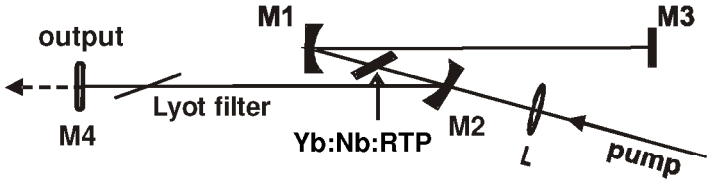

Fig. 4. Laser set-up consisting of two folding mirrors (M1 and M2) with radius of curvature equal to -10 cm, a rear plane reflector (M3), and a plane output coupler (M4) with transmission T_{oc} = 1 or 3%.

We achieved efficient laser operation of Yb:Nb:RTP. The sample used to study the laser operation had dimensions of ≈ 3 × 2.5 × 3 mm^3 ($a \times b \times c$), and was obtained from the growth experiment nº2 (see Table 1). Four of its faces, those normal to the a and b crystallographic directions, were polished.

The main results obtained are summarized in Table 3. As can be seen, the laser wavelength remains almost constant for the three different polarizations ($E//a$, $E//b$ and $E//c$) and the two output couplers (T_{oc} = 1 and 3%). The extremely low laser thresholds obtained are related to the large splitting of the ground state.

Table 3. Relevant laser parameters: threshold (absorbed power P_{th}), slope efficiency (η) and oscillation wavelength (λ_L), of Yb:Nb:RTP in dependence on the polarization and the output coupler used.

Propagation along a axis				
pumping	T_{oc} [%]	P_{th}[mW]	η [%]	λ_L [nm]
$E//b$	1	35	42.5	1050.6
$E//b$	3	88	50.9	1050.6
$E//c$	1	27	37.6	1051.9
$E//c$	3	57	60.1	1050.7
Propagation along b axis				
pumping	T_{oc} [%]	P_{th} [mW]	η [%]	λ_L [nm]
$E//a$	1	39	37.1	1050.8
$E//a$	3	no lasing	no lasing	no lasing
$E//c$	1	18	39.0	1051.7
$E//c$	3	48	45.5	1051.3

ISBN: 978-84-691-0370-8 /DL:T.2188-2007

The tuning behaviour of the laser was also studied by inserting a birefringent filter in the vicinity of the output coupler (M4). The tuning range was almost the same for the three polarizations, extending from 1009 to 1081 nm (the FWHM for *E//b* is 59 nm). This broad tuning range is also related to the large splitting of the ground state. The maximum achievable output power depends not only on the absorption cross section for the corresponding polarization but also on the recycling effect in the quasi-three-level Yb-laser scheme, i.e. on the actual intracavity laser power. Smaller output coupling results in higher intracavity power which compensates the pump bleaching effect increasing the actual crystal absorption. Thus a maximum output power of 154 mW was obtained with T_{OC} = 1%, for propagation along the *a* and polarization along the *b* axes, at an absorbed pump power of 386 mW (optical-to-optical efficiency equal to 40 %).

Table 2 shows some of the spectroscopic as well as estimated and measured laser parameters for the 6 non-centrosymmetric Yb-hosts for which lasing has been demonstrated up to now. To compare these hosts with Nb:RTP, three laser parameters have been calculated. These laser parameters are: β_{min} (the minimum fraction of Yb^{3+} ions that must be excited so that the gain equals the ground-state absorption at λ_{ext} -extraction wavelength), I_{sat} (the pump saturation intensity) and I_{min} (the minimum pump intensity required for transparency to be achieved at the laser wavelength). The equations used to calculate these parameters are listed below:

$$\beta_{\min} = \frac{\sigma_{abs}(\lambda_{ext})}{\sigma_{abs}(\lambda_{ext}) + \sigma_{em}(\lambda_{ext})} \tag{2}$$

where σ_{abs} and σ_{em} are the absorption and the emission cross section values respectively at λ_{ext}.

$$I_{sat} = \frac{hc}{\lambda_{pump}\sigma_{abs}(\lambda_{pump})\tau_{em}} \tag{3}$$

and

$$I_{min} = \beta_{min} I_{sat} \tag{4}$$

I_{min} should be as low as possible for efficient laser materials doped with Yb^{3+}, which means emission cross section as high as possible.

5. Fundamental wavelength for non-critical type-II second harmonic generation

To measure the fundamental wavelength for non-critical type-II SHG (λ_{NCPM}) along the principal optical axes of the dielectric frame, we used a tunable OPO (Continuum Panther) pumped by a Nd:YAG laser (Continuum SLI-10) emitting 5 ns-long (FWHM) pulses between 410 nm and 2.55 μm at a repetition rate of 10 Hz. The OPO wavelength was controlled by a Chromex 250 SM scanning monochromator. The OPO beam was properly focused onto the sample cut as a slab which was stuck on a goniometric head placed in the centre of a goniometric rotation stage. The polished crystal faces were perpendicular to *a* and *b* axes, which were reached successively in normal incidence. An achromatic half-wave plate placed between the laser source and the sample, provided an adjustment of the polarization of the OPO beam to ensure type-II SHG in the *ab* plane of the crystal.

The slab sample used to measure λ_{NCPM} values for type-II SHG of Yb:Nb:RTP in the *ab* plane, comes from the same crystal than the one used to obtain the sample for laser operation. We found λ_{NCPM} = 1118.2 nm at θ = 90º; φ = 0º, corresponding to the *x* or *a* axis, and λ_{NCPM} = 985.4 nm at θ = 90º; φ = 90º, corresponding to the *y* or *b* axis. These data suggest that we have type-II SHG phase-matching directions in the *ab* plane, for wavelength ranging between 985.4 nm and 1118.2 nm. Especially, by choosing the right azimuthal angle φ, type-II SHG phase-matching conditions is possible for a fundamental wavelength matching the laser wavelength at 1050.6 nm which corresponds to a maximum of the laser emission in the crystal provided the associated conversion efficiency is high. Moreover, as the laser tuning

ISBN: 978-84-691-0370-8 /DL:T.2188-2007

range achieved is quite broad, possible deviations of φ as a result of the sample preparation should not be detrimental.

6. Conclusions

We studied the influence of the growth conditions for ytterbium doped RTP crystals codoped with niobium or tantalum using the TSSG-SC technique. The three strategies used to further increase the Yb^{3+} concentration in RTP crystals, codoping with Nb^{5+}, codoping with Ta^{5+}, and growth in W-containing solution, have been successful for this purpose, reaching in all cases similar Yb^{3+} concentrations. A maximum ytterbium concentration of $\approx 2\times10^{20}$ions/cm^3 has been obtained in samples big enough to perform spectroscopic characterizations and study laser operation. From the absorption and the emission measurements in Yb:Nb:RTP and Yb:Ta:RTP the Stark splitting of the two Yb^{3+} electronic states has been determined, and the obtained values are almost the same for the two codopands. The absorption cross section values are in general similar for both hosts, Nb:RTP and Ta:RTP. However, in Yb:Ta:RTP the maximum absorption cross section values obtained for polarizations *E//*b and *E//c* are much closer. Then two different wavelengths (972.2 or 903.8 nm) could be used to pump Yb:Ta:RTP depending on the chosen polarization scheme. Moreover, the Yb^{3+} upper level radiative lifetime in Nb:RTP has been calculated (τ_{rad} = 2.7 ms) and compared with the experimental fluorescence decay time (2.2 ms) recorded at room temperature. Laser operation has been obtained for the first time to our knowledge, in an ytterbium doped crystal belonging to the KTP family. The maximum output power obtained at 1050.6 nm was 154 mW, and the maximum slope efficiency exceeded 60%. Moreover, the broad tuning range achieved (from 1009 to 1081 nm) makes Yb:Nb:RTP promising for mode-locking to obtain ultrashort (femtosecond) laser pulses. Finally, as the laser wavelength for the three possible polarizations is around 1050 nm, self-frequency doubling of the laser action should be possible in Yb:Nb:RTP for a propagation in the *ab* plane at some azimuthal angle φ, leading to a green beam. Future experiments will be devoted to such demonstration.

Acknowledgements

This work has been supported by the Spanish government under projects MAT-05-06354-C03-02, MAT-04-20471-E and CIT-020400-2005-14, the Catalan government under project 2005SGR658 and through the EU project DT-CRYS, NMP3-CT-2003-505580. A. Peña thanks the Spanish government for the personal funding BES-2003-1694.

UNIVERSITAT ROVIRA I VIRGILI
YTTERBIUM AND ERBIUM DOPEP RbTi1-xMxOPO4 (M=Nb or Ta) CRYSTALS. NEW LASER AND NONLINEAR BIFUNCTIONAL MATERIALS
Alexandra Peña Revellez
ISBN: 978-84-691-0370-8 /DL:T.2188-2007

Paper III

Laser operation of Yb^{3+} in the acentric $RbTiOPO_4$ codoped with Nb^{5+}.

X. Mateos, V. Petrov, A. Peña, J. J. Carvajal, F. Díaz, M. Aguiló,
P. Segonds, B. Boulanger
Optics Letters, **32**, *1929* (2007)

UNIVERSITAT ROVIRA I VIRGILI
YTTERBIUM AND ERBIUM DOPEP RbTi1-xMxOPO4 (M=Nb or Ta) CRYSTALS. NEW LASER AND NONLINEAR BIFUNCTIONAL MATERIALS
Alexandra Peña Revellez
ISBN: 978-84-691-0370-8 /DL:T.2188-2007

Laser operation of Yb^{3+} in the acentric $RbTiOPO_4$ codoped with Nb^{5+}

Xavier Mateos,[1,*] Valentin Petrov,[1] Alexandra Peña,[2] Joan J. Carvajal,[2] Magdalena Aguiló,[2] Francesc Díaz,[2] Patricia Segonds,[3] and Benoît Boulanger[3]

[1]*Max-Born-Institute for Nonlinear Optics and Ultrafast Spectroscopy, 2A Max-Born-Strasse, D-12489 Berlin, Germany*
[2]*Física i Cristal·lografia de Materials, Universitat Rovira i Virgili, Campus Sescelades, c/Marcel·lí Domingo, E-43007 Tarragona, Spain*
[3]*Institut Néel/CNRS–UJF, BP 166, F-38042 Grenoble Cedex 9, France*
[*]*Corresponding author: mateos@mbi-berlin.de*

Received February 20, 2007; revised May 3, 2007; accepted May 3, 2007;
posted May 11, 2007 (Doc. ID 80195); published June 25, 2007

We report on continuous-wave lasing of Yb^{3+} at room temperature in the noncentrosymmetric $RbTiOPO_4$ crystal, codoped with Nb^{5+}, for all three possible polarizations. A maximum output power of 154 mW at 1050 nm was obtained for an absorbed power of 386 mW. The highest slope efficiency reached ≈60% and the lowest threshold (with respect to the absorbed power) was 18 mW. The laser was tunable from 1009 to 1081 nm.

OCIS codes: 140.5680, 140.3380, 160.4330, 160.5690.

Self-frequency doubling (SFD) crystals, which convert the fundamental emission to the second harmonic, are important for the development of compact and efficient laser sources in the visible. In the past, the major part of the SFD studies was devoted to the ${}^4F_{3/2} \rightarrow {}^4I_{11/2}$ transition of the Nd^{3+} ion [1]. The Yb^{3+} ion that operates in the same 1 μm spectral range as a quasi-three-level system on the single ${}^2F_{5/2} \rightarrow {}^2F_{7/2}$ transition has a number of advantages including (1) low quantum defect when pumped by InGaAs diodes, i.e., less thermal load; (2) broad absorption bandwidth, i.e., less critical pump wavelength; (3) broad emission bandwidth that allows larger tunability and generation of ultrashort laser pulses; (4) longer lifetime; and (5) absence of undesirable processes such as excited state absorption, upconversion, and nonradiative interaction among excited states. The last advantage is especially relevant to SFD because using Yb^{3+} allows one to avoid absorption losses at the second harmonic.

So far, lasing of Yb^{3+} has been demonstrated only in six acentric hosts, $XAl_3(BO_3)_4$ [2,3] and $XCa_4O(BO_3)_3$ [4,5], where X=Y or Gd, $LiNbO_3$ [6], and $KGd(PO_3)_4$ [7]. The $KTiOPO_4$ (KTP) family of nonlinear optical crystals (orthorhombic, biaxial crystals belonging to the noncentrosymmetric space group $Pna2_1$-point group $mm2$) are well-known materials for frequency conversion, in particular for frequency doubling of Nd^{3+} lasers, with mature growth technology, high nonlinearity, and damage threshold, and they can be poled by electric field to obtain quasi-phase-matching. However, the doping of KTP with trivalent lanthanide ions turned out to be a great challenge and the maximum levels previously achieved for bulk crystals did not exceed a level ranging between 5×10^{17} and 6×10^{18} cm^{-3}, which is too low for laser operation. Recently, on the basis of charge compensation and codoping with Nb^{5+}, the isostructural $RbTiOPO_4$ (RTP) was successfully doped with Yb^{3+} up to $\approx 2 \times 10^{20}$ cm^{-3} (2.2 at.%), preserving the value of the effective nonlinearity [8]. Moreover, the large Stark splitting of the ground state of Yb^{3+} in Nb:RTP (955 cm^{-1}) [8] results in a rather low (0.76%) population of the highest ${}^2F_{7/2}$ sublevel at room temperature. In the present Letter, we report on efficient laser operation of Yb:Nb:RTP, end-pumped by a Ti:sapphire laser. This is, to the best of our knowledge, the first realization of laser generation of Yb^{3+} in a nonlinear crystal belonging to the KTP family. We analyze the polarization dependence and demonstrate extremely broad tunability with a FWHM of 59 nm.

The single crystal of Yb:Nb:RTP used in the present study was grown by a high temperature solution growth method: top-seeded solution growth with slow cooling in a vertical tubular furnace [9]. The solution was prepared by mixing the initial reagents Rb_2CO_3 (99%), $NH_4H_2PO_4$ (99%), TiO_2 (99.9%), Nb_2O_5 (99.9%), and Yb_2O_3 (99.9%) in a 125 cm^3 Pt crucible. The mixture was then heated until total bubbling of NH_3, H_2O, and CO_2, and homogenization of the solution were achieved. The seed used was very thick along the a-axis because when doping RTP with Nb^{5+} the crystals show a platelike habit, and the only way to increase the dimension along the aforementioned direction is using that kind of seed. The crystallographic c-axis of the seed was perpendicular to the surface of the solution, the a-axis was always radial with respect to the rotation, and the seed was offset by ≈5 mm from the rotation axis. Moreover, to facilitate the stirring of the solution, the seed was attached to a special growth device (see [9]), consisting of a Pt turbine rotating together with the crystal seed at 80 rpm. Prior to the crystal growth, the saturation temperature (T_S) was measured by examining the growth and dissolution of the seed. The grown crystals were slowly removed from the solution and kept inside the furnace while cooling it down to room temperature (at 15 K/h) to avoid any thermal stress.

0146-9592/07/131929-3/$15.00

Table 1 shows the relation between the seed size and the obtained crystal size in the a direction. All crystals were grown in a solution with composition $Rb_2O-P_2O_5-(TiO_2+Nb_2O_5+Yb_2O_3)=40.8-27.2-(30.4+0.96+0.64)$ mol% and a weight of 159 g. By comparing the first two experiments, as the seed width increases the crystal size also increases, and so does the crystal weight. In the third experiment, although the seed width was similar, the crystal obtained was smaller than the one obtained in the previous experiment. This was because of the shorter growth time (faster growth rate). Finally, by increasing the cooling interval in the slowest part of the cooling process, we obtained growth conditions that resulted in the larger crystal shown in Fig. 1 from which the sample used for the present laser experiment was extracted.

The laser setup is shown in Fig. 2. The pump beam from a homemade Ti:sapphire laser (FWHM <1 nm, max. 1.8 W) was focused onto the Yb:Nb:RTP sample by a 6.28 cm lens L to a Gaussian waist of $\approx 30\ \mu$m. The ≈ 150 cm long astigmatically compensated cavity consisted of two folding mirrors (M1 and M2), both with a radius of curvature equal to -10 cm, a rear plane mirror, M3, and the plane output coupler, M4, with transmission of 1% or 3%.

The Yb:Nb:RTP sample used (Fig. 1) had dimensions of ≈ 3 mm along the a- and c-axes, and ≈ 2.5 mm along the b-axis, and four of its faces ($\perp a$ and $\perp b$) were polished. The Yb-density in the crystal, measured by EPMA, was 1.9×10^{20} cm^{-3}. The sample was inserted under Brewster angle between the two folding mirrors and no special cooling was applied.

The input–output characteristics of the Yb:Nb:RTP laser are summarized in Fig. 3 for the three possible polarizations and propagation along the a-axis (a) and b-axis (b). The pump wavelength was 972.1 nm ($E\|a$ and $E\|c$) and 972.7 nm ($E\|b$). In all cases the pump spectral width was much narrower than the FWHM of the corresponding absorption lines (3.6, 4.1, and 3.7 nm for polarization parallel to the a, b, and c-axes, respectively).

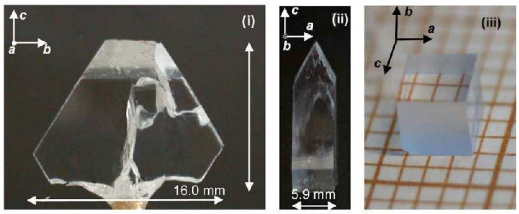

Fig. 1. (Color online) Yb:Nb:RTP crystal grown by the TSSG-SC method with a c-oriented seed (i, ii) and sample used in the laser study (iii).

The highest absorption cross-section is for $E\|b$ (see [8]) with maximum absorption for propagation along the a-axis. In this case, a maximum output power of 154 mW at 1050.6 nm was obtained using an output coupler with $T=1\%$, for an absorbed pump power of 386 mW. The corresponding slope efficiency was $\eta=42.5\%$. and the threshold (absorbed power) was $P_{th}=35$ mW.

The performance of the laser for $E\|c$ and propagation direction along the a- and b-axes was very similar although the sample thickness was different. For propagation along the b-axis, the slope efficiency reached $\eta=60.1\%$ for $T=3\%$, while propagation along the a-axis resulted in an output power of 115 mW with $T=1\%$, for an absorbed pump power of 323 mW.

For $E\|a$ and propagation along the b-axis, generation was obtained only in the case $T=1\%$ and the slope efficiency was lower compared with $E\|b$ and $E\|c$, presumably because of the smaller gain cross-section.

The laser wavelength was basically the same for the three polarizations and the two output couplers, i.e., the maximum of the gain curve remains unchanged. The extremely low laser thresholds are related to the large splitting of the ground state.

With lasing interrupted, the absorption of the sample was bleached at the maximum incident pump power of 1.8 W. Under lasing conditions the absorption was still quite low (13% for $E\|a$, 25-20% for $E\|b$, and 15%–20% for $E\|c$ depending on the output cou-

Table 1. Yb:Nb:RTP Single Crystal Growth

Exp.	T_S [K]	Seed Dimensions ($x\times y\times z$) [mm]	Axial Gradient [K/cm]	Cooling Range [K]	Cooling Ramp [K/h]	Crystal Dimensions ($x\times y\times z$) [mm]	Crystal Weight [g]
1	1195.5	3.65×1.5×5	2	0.1	1		
				4	0.05		
				9	0.02	4.97×14.40×11.80	1.8148
2	1195.0	4.77×1.5×5	2	0.1	1		
				4	0.05		
				9	0.02	5.46×13.99×11.46	1.9945
3	1187.0	4.90×1.5×5	2.4	1	1		
				6	0.05		
				7.5	0.03	5.28×12.53×11.18	1.5172
4	1187.5	5.20×1.5×5	2.4	1	1		
				6	0.05		
				10	0.03	5.95×16.04×12.69	2.6029

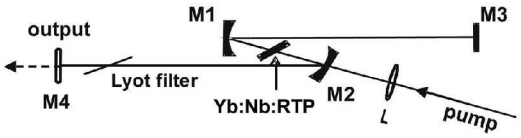

Fig. 2. Experimental setup of the Yb:Nb:RTP laser.

pler used) and remained almost constant with increasing pump power. This is a consequence of the low Yb-ion density in the crystal and the relatively low absorption cross-sections. However, in the lasing state, the intracavity power in the three-level Yb-system increases the pump saturation intensity, and this balances the bleaching effect.

The tuning behavior of the laser was studied inserting a birefringent filter in the vicinity of the output coupler, Fig. 4. The obtained linewidth was below our resolution of 0.5 nm. The broadest tuning range was obtained for $E \| b$ although all three curves look quite similar. The FWHM is 59 nm, which is an indication of the potential of Yb:Nb:RTP for generation of ultrashort (femtosecond) laser pulses. Such a broad tuning range and the relatively low wavelengths that were obtained are also related to the large splitting of the ground state: the three peaks in Fig. 4 correspond to transitions from the two lowest sublevels of the upper multiplet to the two highest sublevels of the lower multiplet [8].

We experimentally determined the fundamental wavelength for noncritical type II second harmonic

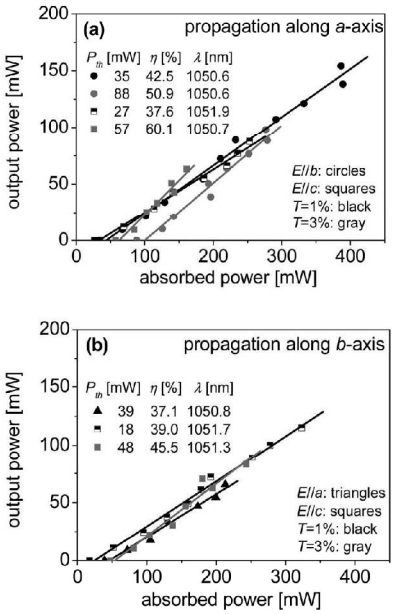

Fig. 3. Input-output characteristics of the Yb:Nb:RTP laser for different output coupling (T) and polarization (E): P_{th}: threshold absorbed power, η: slope efficiency, λ: oscillation wavelength.

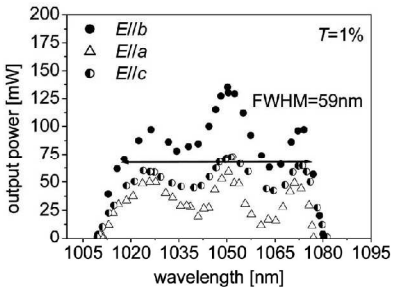

Fig. 4. Wavelength tunability of the Yb:Nb:RTP laser with a two-plate intracavity Lyot filter for the three polarizations. In the case of $E \| c$ the propagation is along the a-axis.

generation and obtained 1120 and 985 nm for the propagation along the a- and b-axes, respectively. These results are very similar to those published for Nb:RTP [10]. Since the laser wavelength found for Yb:Nb:RTP is within the above range, in principle SFD operation should be possible at some intermediate propagation direction in the a–b plane. Work is in progress to achieve this.

In conclusion, we achieved continuous-wave laser operation of Yb^{3+} at room temperature in orthorhombic Nb:RTP around 1050 nm for all three possible polarizations, which guarantees that this also will be possible along any phase-matching direction of second harmonic generation.

This work was supported through the European Union project DT-CRYS, NMP3-CT-2003-505580, and by the Catalan government by Project 2005SGR658 and the Ministerio de Educación y Ciencia of the Spanish government, under Projects MAT-05-06354-C03-02, MAT-04-20471-E, and CIT-020400-2005-14.

References

1. A. Brenier, J. Lumin. **91**, 121 (2000).
2. P. Dekker, P. A. Burns, J. M. Dawes, and J. A. Piper, J. Opt. Soc. Am. B **20**, 706 (2003).
3. Z. Zhu, J. Li, B. Alain, G. Jia, Z. You, X. Lu, B. Wu, and C. Tu, Appl. Phys. B **86**, 71 (2007).
4. A. Aron, G. Aka, B. Viana, A. Kahn-Harari, D. Vivien, F. Druon, F. Balembois, P. Georges, A. Brun, N. Lenain, and M. Jaquet, Opt. Mater. **16**, 181 (2001).
5. H. Zhang, X. Meng, P. Wang, L. Zhu, X. S. Liu, X. M. Liu, Y. Yang, R. Wang, J. Dawes, J. A. Pipper, S. Zhang, and L. Sun, J. Cryst. Growth **222**, 209 (2001).
6. L. E. Bausá, M. O. Ramírez, and E. Montoya, Phys. Status Solidi A **201**, 289 (2004).
7. I. Parreu, M. C. Pujol, M. Aguiló, F. Díaz, X. Mateos, and V. Petrov, Opt. Express **15**, 2360 (2007).
8. J. J. Carvajal, R. Solé, Jna. Gavaldà, J. Massons, P. Segonds, B. Boulanger, A. Brenier, G. Boulon, J. Zaccaro, M. Aguiló, and F. Díaz, Opt. Mater. **26**, 313 (2004).
9. J. J. Carvajal, V. Nikolov, R. Solé, Jna. Gavaldà, J. Massons, M. Rico, C. Zaldo, M. Aguiló, and F. Díaz, Chem. Mater. **12**, 3171 (2000).
10. J. J Carvajal, P. Segonds, A. Peña, J. Zaccaro, B. Boulanger, F. Díaz, and M. Aguiló, J. Phys. Condens. Matter **19**, 116214 (2007).

UNIVERSITAT ROVIRA I VIRGILI
YTTERBIUM AND ERBIUM DOPEP RbTi1-xMxOPO4 (M=Nb or Ta) CRYSTALS. NEW LASER AND NONLINEAR BIFUNCTIONAL MATERIALS
Alexandra Peña Revellez
ISBN: 978-84-691-0370-8 /DL:T.2188-2007

UNIVERSITAT ROVIRA I VIRGILI
YTTERBIUM AND ERBIUM DOPEP RbTi1-xMxOPO4 (M=Nb or Ta) CRYSTALS. NEW LASER AND NONLINEAR BIFUNCTIONAL MATERIALS
Alexandra Peña Revellez
ISBN: 978-84-691-0370-8 /DL:T.2188-2007

Paper IV

Scanning probe microscopies applied to the study of the domain wall in a ferroelectric crystal.

J. Canet-Ferrer, L. Martín-Carrón, J. Martínez-Pastor, J. L. Valdés, A. Peña, J. J. Carvajal, F. Díaz

Journal of Microscopy, **226**, *133* (2007)

UNIVERSITAT ROVIRA I VIRGILI
YTTERBIUM AND ERBIUM DOPEP RbTi1-xMxOPO4 (M=Nb or Ta) CRYSTALS. NEW LASER AND NONLINEAR BIFUNCTIONAL MATERIALS
Alexandra Peña Revellez
ISBN: 978-84-691-0370-8 /DL:T.2188-2007

Journal of Microscopy, Vol. 226, Pt 2 May 2007, pp. 133–139
Received 27 September 2006; accepted 17 January 2007

Scanning probe microscopies applied to the study of the domain wall in a ferroelectric crystal

J. CANET-FERRER*, L. MARTÍN-CARRÓN*, J. MARTÍNEZ-PASTOR*, J. L. VALDÉS*, A. PEÑA†, J. J. CARVAJAL† & F. DIAZ†
**Institut de Ciència dels Materials de la Universitat de València, E-46071 Valencia, Spain*
†Laboratori de Física i Cristalografia de Materials, Universitat Rovira i Virgili, E-43005 Tarragona, Spain

Key words. AFM, chemical etching, domains, ferroelectric, near field, $RbTiOPO_4$.

Summary

Scanning near-field optical microscopy is capable of measuring the topography and optical signals at the same time. This fact makes this technique a valuable tool in the study of materials at nanometric scale and, in particular, of ferroelectric materials, as it permits the study of their domains structure without the need of chemical etching and, therefore, not damaging the surface (as will be demonstrated later). We have measured the scanning near-field optical microscopy transmission, as well as the topography, of an $RbTiOPO_4$ single crystalline slab, which exhibits two different of macroscopic ferroelectric domains. A chemical selective etching has been performed to distinguish between them, obtaining areas with a noticeable roughness (C^- domain) in comparison with the original flat aspect of the other ones (C^+ domain). The effects of the selective chemical etching have been quantified in topographic images obtained by means of our fibre tip probe, and have been compared to topographic images obtained by Atomic Force Microscopy, with a better resolution. The near-field optical transmission images recorded have been obtained under different excitation wavelengths. These images are modulated by the light scattering due to the grains at the rough surface, which depends on the excitation wavelength used. In addition, they show a significant optical contrast due to the variations of the dielectric constant on the proximity of the ferroelectric domain wall.

Introduction

In the last century, optical microscope's resolution reached its limit, which is given by the wavelength of the light, used for illumination. Several techniques, like electronic, tunnel effect or scanning probe microscopies (SPMs), were proposed as novel alternatives to observe the nanoworld (Paeleser & Moyer 1996). SPM, required a great deal of technological development, so microscopes based on this concept could not be built since the end of 1980s, when the atomic force microscopy (AFM) appeared (Binnig & Quate 1986; Martin *et al.*, 1987). At that moment, new research lines were opened, given that SPM instruments obtained improved images of the surface of a vast kind of samples by local measurement of different physical properties (Kwak *et al.*, 2000; Cefali *et al.*, 2003). These measurements revealed important differences in electro-optical and mechanical properties between macroscopic and nanometre systems. Thus, most experiments already performed in the field of materials science have been reproduced at the nanometre scale providing new information. Furthermore, a great number of dielectric materials, which exhibited difficulties when imaged by electronic microscopy, can now be studied at the nanometre scale by means of SPM techniques. The scanning near-field optical microscope (SNOM) is one of these novel techniques, which, with a resolution limited by the probe parameters, allows the microscope user to obtain the sample's near-field features and the topography images simultaneously (Paeleser & Moyer 1997; Kawata *et al.*, 2002; Lewis *et al.*, 2003).

$RbTiOPO_4$ (RTP) is a ferroelectric material at room temperature, isostructural with potassium titanyl phosphate, which shows interesting non-linear optical properties (Guillien *et al.*, 2003). Doping with lanthanide, the photoluminescence of the ion and the non-linear optical properties of the material can be merged (Carvajal *et al.*, 2003a, b). The structure and ferroelectric domain inversion of RTP have been studied by means of some SPM techniques (Jiang *et al.*, 2000; Rosenman *et al.*, 2003a, b; Rosenwaks *et al.*, 2005), as high-voltage SPM

Correspondence to: Joseph Canet Ferrer. Tel: +34 96 354 3267; fax: +34 96 354 3633; e-mail: Jose.Canet-Ferrer@uv.es

or AFM. In this work, we present a SNOM study of a RTP sample showing two macroscopic ferroelectric domains.

Experimental set-up and sample description

We have obtained high-resolution topography images of the sample surface by using a commercial AFM (Nanotec Electronica, Madrid, Spain) working in non-contact tapping mode. The 256×256 pixel scanning images were acquired by using a piezoelectric tube ($17.5 \times 17.5 \times 3\ \mu m^3$). We used a Nanosensors PointProbePlus tip with an elastic constant $k = 40$ N/m, a tip radius of 10 nm and a resonance frequency around 150 kHz. It is located on a Nanotec standard head for AFM mounted with a 659-nm Schäffer–Kirchoff laser. The cantilever is illuminated by the laser and its deflection is controlled by collecting the light reflection on a four-quadrant photo-detector.

The basis of our SNOM (attoSNOMIII from Attocube Systems AG, München, Germany) is similar to that described above for the non-contact mode AFM, but the standard probe is replaced by monomode optical fibre shaped as tip by flourhidric acid (FH) etching and coated with aluminium. The head of this SNOM is based on a 32.7-kHz tuning-fork quartz (see the diagram in Fig. 1). The control of the SNOM has been possible by adapting a commercial electronic feedback (also from Nanotec Electronica), in order to manage the electric signal of the quartz, and register the optical signal during a scan. For this experiment, the SNOM is used in illumination configuration under a constant gap mode (Fig. 1). The light coupled to the fibre probe was delivered through a 2×2 fibre beam splitter,

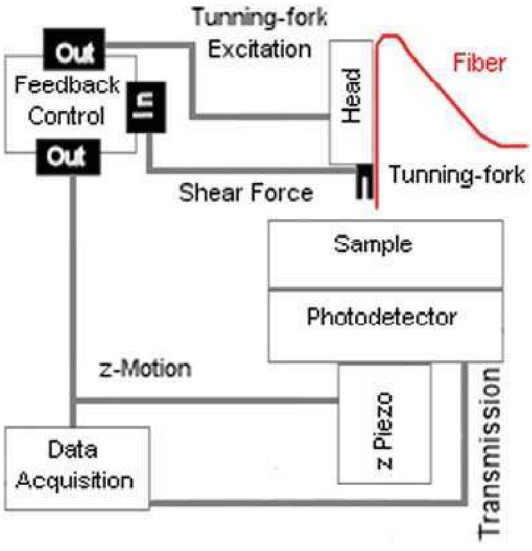

Fig. 1. SNOM illumination configuration scheme.

whose inputs are connected to two diode lasers working at 660 and 980 nm. In this way, a given zone of the sample surface can be consecutively scanned twice by only switching off one of the two lasers. The mechanical stability of our instrument is very high and the same zone of the sample surface (covering up to $10.5 \times 10.5\ \mu m^2$) can be scanned during several hours without appreciable changes. The *xyz* motion is done by piezoelectric inertial motors, whose steps can be controlled within the range of 10–100 nm. It allows us to move across the ferroelectric domain wall several hundreds of micrometres with a high precision. Furthermore, the piezoelectric ceramics of the *xy* motors are used to perform the scan. Finally, an extra *z*-piezoceramics is used to correct the tip-sample distance by the feedback electronics. The transmitted light was collected by a germanium detector, whose signal is incorporated to the main electronic board after it is conveniently amplified by a low-noise trans-impedance pre-amplifier.

A chemical selective etching with a mixture of KOH : KNO_3 at 350 K has been performed on the sample studied here, in order to reveal the different domains present in the RTP slab, oriented, cut and polished from an as-grown single crystal. The sample surface roughness analysis has been performed by AFM. Several islands of the opposite domain are observed into the dominating macroscopic ferroelectric domains. Some of them present irregular shapes, as round or triangular, which may be produced either by an inefficient etching, due to the viscosity of the mixture, or some thermal and chemical gradients.

The domain walls have been imaged with our SNOM instrument, obtaining both topographic and optical information using different wavelengths (660 and 980 nm). Previous SNOM studies in ferroelectric materials analyze the optical near-field images of polarized domains and domain wall and study their evolution under applied electric field (Yang *et al.*, 1999), the variations in their dielectric constant and patterns of microwave loss (Yu *et al.*, 1997), or they perform an optical characterization of channel waveguides (Caccavale *et al.*, 2000). One of the main differences in our measurements is the possibility of combining both the topographic and optical images of the same sample area.

The average (statistical) domain wall profiles, measured in SNOM-topography images along hundreds of micrometres, are in agreement with the crystallographic predictions. The simultaneously measured SNOM-transmission images exhibit interesting features: the near-field images of the C^- zones with sub-wavelength roughness and the effect of this roughness on the C^+ images close to the interface between both domains. Nevertheless, the most important effect is the optical contrast at the domain wall.

Results and discussion

Crystals of the potassium titanyl phosphate family may present two 180° inverse ferroelectric domains normal to the

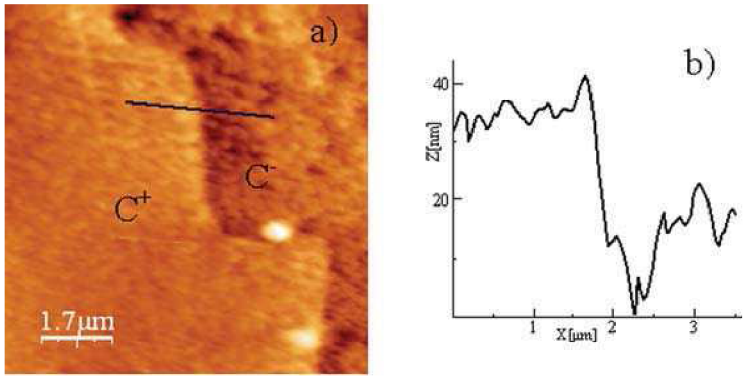

Fig. 2. AFM Topography images of the zigzag shape exhibited by the domain wall (a), the different rough domains can be easily observed. The C^- zone are extremely attacked by the chemical agent whereas the C^+ one maintains its flat surface, (b) as a result a step around 50 nm is formed along the entire domain wall.

directions [0 0 1] and [0 0 −1] (i.e. C^+ and C^-). The domain wall in crystals that present both domains has been observed to describe a characteristic zigzag profile reproducing angles higher than 90° and close to 135°, formed by a combination of wall segments running along the [1 1 0], [−1 1 0], [1 0 0] and [0 1 0] main growing directions (Hu *et al.*, 1997). The selective chemical etching has been performed during 30 min on the RTP single crystalline cut and polished slab oriented along the (0 0 1) direction. The selective etchant attacks the C^- surface with a greater rate than to the C^+ one and, consequently, a step is formed at the interface between both domains. AFM images have been obtained to quantify the effects of the chemical attack. Figure 2a shows an AFM image of the border between two zones of different roughness. Here, we can distinguish the rougher surface associated to the C^- zone at the right-hand side of the image, in comparison to the flat aspect of the C^+ one (left-hand side of the image). Approximately, half of the sample is occupied by the C^+ domain and the other half by the C^- domain. It is crossed from side to side by a visible (after etching) domain wall. The interface between the two zones corresponds to where the domain wall is located. Here, a step of around 40 nm high is formed due to the chemical action, as can be seen in Fig. 2b.

Figure 3a shows a C^+ micro-domain into a C^- domain area and Fig. 3b shows a C^- micro-domain into a C^+ domain area together with their respective height profiles (as insets). The C^+ micro-domains typically present polygonal forms with angles arising from the combination of the [1 1 0], [−1 1 0], [1 0 0] and [0 1 0] crystallographic directions. On the opposite, the C^- micro-domains that are located into a C^+ domain area are smaller than the C^+ ones described above and have a rounded shape, with no apparent angles. Moreover, the height of the step in these structures (C^- into C^+), is smaller than either the domain wall crossing the sample or the step associated to the other kind of defects (C^+ into C^-). These geometric differences can be attributed to differences in the (anisotropic) etching efficiency when C^- is occupying smaller or bigger areas.

Figure 4 shows the topography and transmission SNOM images of a zone near the one shown in Fig. 3. These images have been recorded under slightly different scanning conditions ($10.5 \times 10.5\ \mu m^2$, 256×256 pixels, 25 min/image), when compared to the previous ones recorded with AFM ($12 \times 12\ \mu m^2$, 256×256 pixels, 5 min/image), mainly due to the smaller frequency resonance of the quartz fork. In Fig. 4a we show a SNOM topography image of a typical small portion of the domain wall. Once more, the two zones with a different roughness (i.e. the C^+ and C^- ferroelectric domains) can be clearly distinguished. The main difference with AFM images is the resolution: better for AFM. In both cases, the resolution is approximately limited by the tip radius (10 nm for AFM and 100 nm for SNOM). The resolution in the SNOM optical transmission images depends on the probe aperture used, which is not very different from the tip radius in our case. The SNOM transmission images obtained at excitation wavelengths of 660 and 980 nm are shown in Figs 4b and c, respectively. We basically observe the step between ferroelectric domains in Fig. 4b, when using visible light, whereas most of the surface details are reproduced in Fig. 4c, when using a wavelength of 980 nm. In this case, a resolution comparable to the topography image is reached. These images evidence the strong dependence of the near-field signal on the wavelength. In fact, the optical contrast in a near-field optical transmission experiment depends on the relation between the wavelength and the tip-sample distance (Kawata *et al.*, 2002). In both images we have used the same constant gap conditions, below 20 nm. This gap is only a small fraction of the wavelength, giving rise to better resolution

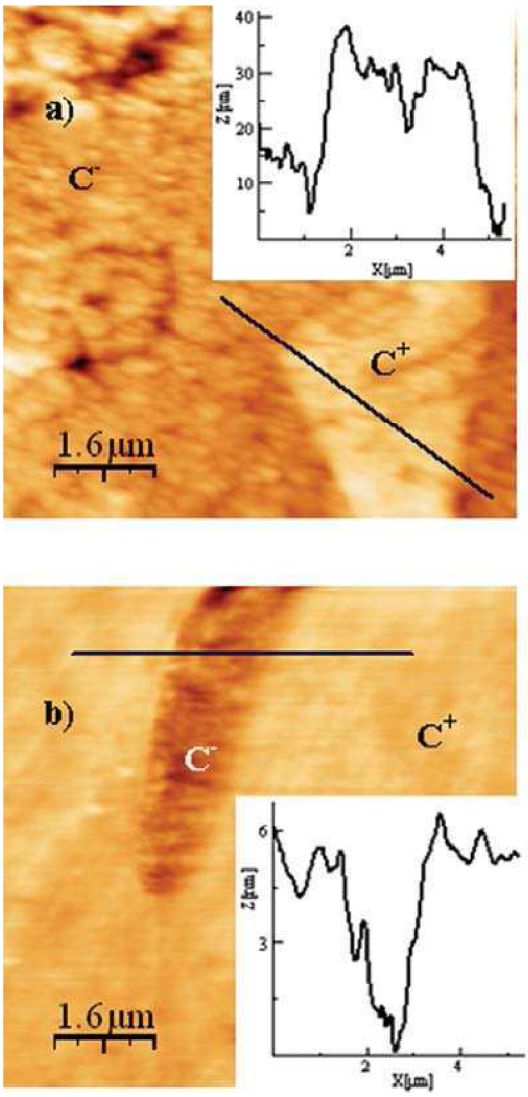

Fig. 3. The topographic features (AFM measurements) observed in (a) and (b) are C^+ nanodomains into the C^- zone and C^- nanodomains in C^+ one, respectively. In the insets, the profile reveal the different etching intensity suffered in each zone.

when the wavelength is appreciably longer than the surface roughness.

In the optical images the domain wall step appears accompanied by a strong optical contrast at the interface. This kind of contrast depends on the wavelength used to record the image and it is not observed in other topographical features. Furthermore, the optical signal registered at 660 nm is slightly affected by topographical features in comparison with the 980 nm one, as can be observed in the profile of the protrusion in Figs 4d–f. However, the optical contrast that is correlated with the step is observed under both illumination wavelengths with similar resolution and transmitted light (see Figs 4g–i). From these results, we can conclude that the strong contrast observed at the domain wall must be mainly attributed to an optical origin, rather than to a topological one. In particular, it may be due to the increment of the refractive index produced by the strain at the domain wall (Chaib *et al.*, 2002). Due to this strain, the dielectric constant changes abruptly at the domain walls, although it does not affect the features a few micrometers away, like at the protrusion in Fig. 4, or the grooves shown in Fig. 5.

An accurate analysis of several SNOM transmission images recorded at 980 nm has been undertaken in order to distinguish between the contribution to the light transmission due to the step, as a topographic defect at the sample surface, and the purely optical contrast associated to the dielectric constant pining up at the domain wall. We have compared protrusions of mean heights between 70 and 130 nm and mean diameters between 1 and 4 μm (similar to the defect observed in Fig. 4). These features present optical contrasts in the range between 60 and 150 mV. This great deviation in the averages means that the optical contrast depends strongly on the protrusion height, but in general, it also depends on the width and shape of the protrusion. For this reason, other defects on the surface of our sample have been investigated to compare with the domain wall. They consist of grooves about tens of micrometers long and 1–2 μm wide, thus having a geometry similar to the step but slightly higher. These grooves have been produced during the manipulation of the sample after polishing. When we measure a groove between 70 and 120 nm deep (Figs 5a and c), an optical contrast between 50 and 90 mV (Figs 5b and d) is obtained, relative to an average transmitted signal of around 2 V. The value (in mV) of the contrast in the optical signal is similar for protrusions and grooves, although the standard deviation is larger in the case of protrusions due to their irregular shape. From these results, we should expect the height of the domain wall to induce an optical contrast in the order of around 1 mV/nm. The profile shown in Fig. 4g corresponds to a zone of the domain wall with a height of around 30 nm and hence a topographical optical contrast of 30 meV should be expected in Fig. 4i. However, optical contrasts as high as 120 and 140 mV are measured in the images registered at 660 and 980 nm, respectively, as shown in Figs 4 h and i.

As a result, the magnitude of the optical contrast at domain ferroelectric walls makes possible to reproduce the results without a previous chemical attack, as we have reported in a previous work developed in other ferroelectric materials having periodic or quasi-periodic domain structures (Canet-Ferrer *et al.*, 2006). Nevertheless, in as-grown RTP,

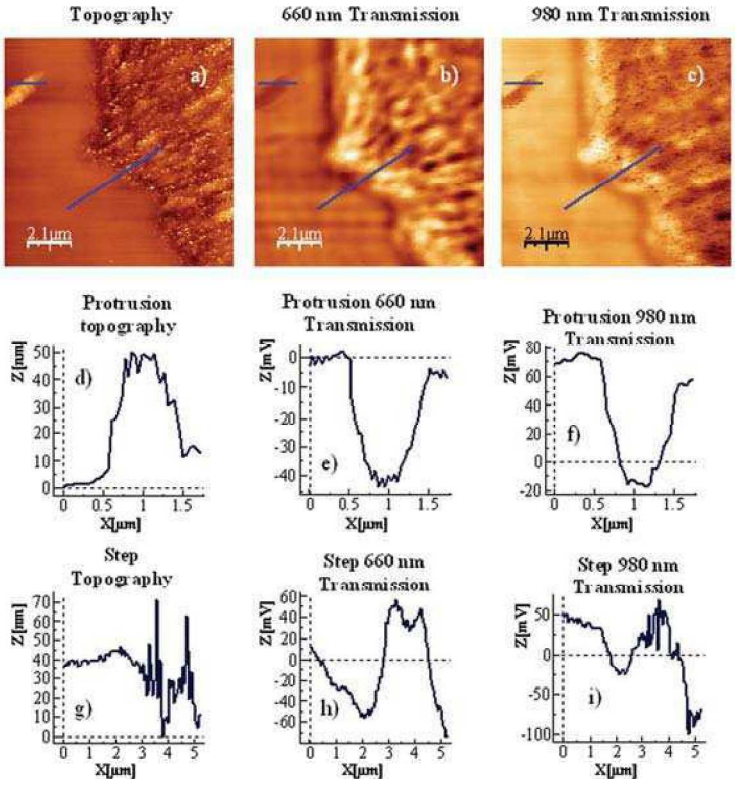

Fig. 4. Typical domain border SNOM images accompanied by their profiles: on top the lateral resolution can be observed in topographic images (a), whereas transmission images dependence on wavelength can be observed by comparison of (b) and (c) (660 nm and 980 nm). The grey lines marked in the images corresponds to the profiles plotted in the next figures: the protrusion plots are located in the middle (d), (e) and (f) and the step ones are in the bottom (g), (h) and (i).

where the domains are very large, the etching technique has been necessary to locate the domain wall between domains.

Conclusions

A RTP single crystal with two different macroscopic ferroelectric domains has been studied by AFM and SNOM techniques. We have quantified the effect of the selective chemical etching performed in the sample surface to distinguish the domains by AFM characterization. One of the ferroelectric domains, C^-, exhibits an appreciable roughness due to the etching process, whereas the second domain, C^+, maintains its original flat aspect. The domain wall between these domains presents a step usually smaller than 50 nm height that could also be observed in SNOM topography images. From SNOM optical images, having a lateral resolution better than 80 nm, we have determined that the changes produced in the transmission measurements are due to different effects, like the dielectric constant variations at the interface between domains and the light scattering at the interface step. The optical and topological effects can be distinguished by comparison of 660 and 980 nm transmission images of small grains and grooves since the topography features are slightly observed in the first ones.

Acknowledgments

We acknowledge 'Ministerio de Educación y Ciencia' of Spain for financial support under the projects MAT2002-4603-C05-02 and MAT2005-06354-C03-02 and 'Generalitat Valenciana' for the group support 'grupos05/75'. LM-C also wants to acknowledge 'Ministerio de Educación y Ciencia' of Spain for financial support under the program 'Juan de la Cierva'.

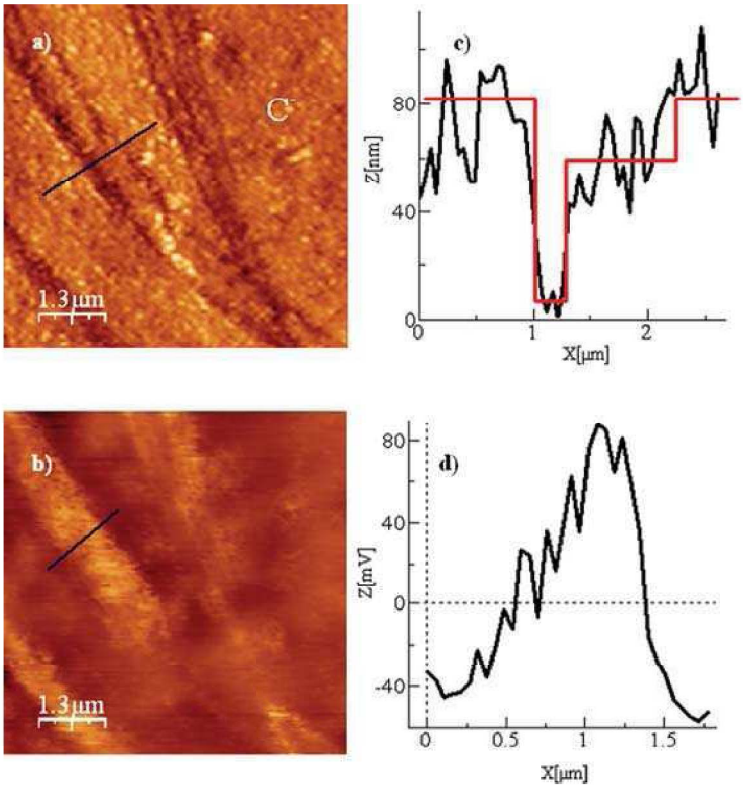

Fig. 5. Protrusions on the RTP C^{-} surface after polish. On the left-hand side can be seen the topography and transmission images (a) and (b), respectively). A profile of one of the grooves is shown in the right-hand side (c and d), in this case the resolution of topography is higher but the optical contrast value (in mV) is comparable with the height of the protrusion (in nanometres).

References

Binnig, G. & Quate, C.F. (1986) Atomic force microscope. *Phys. Rev. Lett.* **56**, 930–933.

Caccavale, F. *et al.* (2000) Correlation between optical and compositional properties of Ti:$LiNbO_3$ channel optical waveguides. *J. Appl. Phys.* **87**, 1007–1011.

Canet-Ferrer, J. *et al.* (2006) Scanning probe microscopy applied to the study of domain walls in a ferroelectric $KNbO_3$ Crystal. *Bol. Soc. Esp. Ceram y Vidrio* **45**, 218 222.

Carvajal, J. *et al.* (2003a) Growth and structural characterization of $Rb_2Ti_{1.01}Er_{0.99}(PO_4)_3$. *Chem. Mater.* **15**, 204–211.

Carvajal, J. *et al.* (2003b) A new self-doubling material: $RbTiOPO_4$(Nb, Ln). *Opt. Mater.* **24**, 425–430.

Cefali, E. *et al.* (2003) A versatile multipurpose scanning probe microscope. *J.Microsc.* **210**, 262–268.

Chaib, H. *et al.* (2002) Theoretical study of ferroelectric and optical properties in the 180° ferroelectric domain wall of tetragonal $BaTiO_3$. *Phys. Stat. Sol. (b)* **233**, 250–262.

Guillien, Y. *et al.* (2003) Crystal growth and refined Sellmeier equations over the complete transparency range of $RbTiOPO_4$. *Opt. Mat.* **22**, 155–162.

Hu, Z.W. *et al.* (1997) High-resolution x-ray diffraction and topographic study of ferroelectric domains and absolute structural polarity of $KTiOPO_4$ via anomalous scattering. *Phys. Rev. B* **56**, 8559–8565.

Jiang, Q. *et al.* (2000) Ferroelectricity, conductivity, domain structure and poling conditions of rubidium titanyl phosphate. *J. Phys. D* **33**, 2831–2836.

Kawata, S. *et al.* (2002) *Nano-Optics*. Springer-Verlag, Berlin, Heidelberg.

Kwak, K.J. *et al.* (2000) Near field fluorescence imaging and simultaneous observation of surface potential. *J. Microsc.* **202**, 413–419.

Lewis, A. *et al.* (2003) Near-Field Optics: from Subwavelenght Illumination to Nanometric Shadowing. *Nature Biotech.* **21**, 1378–1386.

Martin, Y. *et al.* (1987) Atomic force microscope-force mapping and profiling on a sub 100-A scale. *J. Appl. Phys.* **61**, 4723–4729.

Paeleser, M.A. & Moyer, P.J. (1996) *Near-field optics: Theory, instrumentation, and applications*. John Wiley& sons, Inc.

Rosenman, G. *et al.* (2003a) Submicron ferroelectric domain structures tailored by high-voltage scanning probe microscopy. *Appl. Phys. Lett.* **82**, 103–105.

Rosenman, G. *et al.* (2003b) Nanodomain engineering in $RbTiOPO_4$. *Appl. Phys. Lett.* **82**, 3934–3936.

Rosenwarks, Y. *et al.* (2005) Ferroelectric domain engineering using atomic force microscopy tip arrays in the domain breakdown regime. *Appl. Phys. Lett.* **86**, 012909–012911.

Yalin, Lu *et al.* (1997) Non-destructive imaging of dielectric-constant profiles and ferroelectric domains with a scanning tip microwave near-field microscope. *Science* **276**, 2004–2006.

Yang, T.J. *et al.* (1999) Direct observation of pinning and bowing of a single ferroelectric domain wall. *Phys. Rev. Lett.* **82**, 4106–4109.

UNIVERSITAT ROVIRA I VIRGILI
YTTERBIUM AND ERBIUM DOPEP RbTi1-xMxOPO4 (M=Nb or Ta) CRYSTALS. NEW LASER AND NONLINEAR BIFUNCTIONAL MATERIALS
Alexandra Peña Revellez
ISBN: 978-84-691-0370-8 /DL:T.2188-2007

Paper V

Structural and optical properties of $RbTiOPO_4$:Nb crystals.

J. J. Carvajal, P. Segonds, A. Peña, J. Zaccaro, B. Boulanger, F. Díaz, M. Aguiló

Journal of Physics: Condensed Matter, **19**, *116214* (2007)

UNIVERSITAT ROVIRA I VIRGILI
YTTERBIUM AND ERBIUM DOPEP RbTi1-xMxOPO4 (M=Nb or Ta) CRYSTALS. NEW LASER AND NONLINEAR BIFUNCTIONAL MATERIALS
Alexandra Peña Revellez
ISBN: 978-84-691-0370-8 /DL:T.2188-2007

IOP PUBLISHING JOURNAL OF PHYSICS: CONDENSED MATTER

J. Phys.: Condens. Matter **19** (2007) 116214 (15pp) doi:10.1088/0953-8984/19/11/116214

Structural and optical properties of $RbTiOPO_4$:Nb crystals

J J Carvajal[1], P Segonds[2], A Peña[1], J Zaccaro[3], B Boulanger[2], F Díaz[1] and M Aguiló[1,4]

[1] Física i Cristal.lografia de Materials (FiCMA), Universitat Rovira i Virgili, Campus Sescelades, c/Marcel.lí Domingo, s/n, E-43007-Tarragona, Spain
[2] Laboratoire de Spectrométrie Physique, Université Joseph Fourier and Centre National de la Recherche Scientifique BP 87, 38402 St Martin d'Hères Cedex, France
[3] Laboratoire de Cristallographie, Centre National de la Recherche Scientifique, 25 Avenue des Martyrs BP 166, 38042 Grenoble Cedex 09, France

E-mail: magdalena.aguilo@urv.net

Received 2 November 2006, in final form 8 February 2007
Published 5 March 2007
Online at stacks.iop.org/JPhysCM/19/116214

Abstract

When dealing with crystals showing self-frequency conversion properties, $RbTiOPO_4$ doped with Nb^{5+} (RTP:Nb) is a better matrix than RTP for hosting luminescent ions in higher concentration. Therefore, we investigated the structural and the non-linear optical properties of RTP:Nb and RTP crystals for comparison. We used a new crystal growth process for RTP:Nb, which provides isometric inclusion- and crack-free crystals. Structural studies show that Nb^{5+} ions are located in Ti positions only, which is confirmed by optical absorption and polarized Raman scattering studies. Moreover, the transparency domain of RTP:Nb is affected in the UV edge and in the IR region by the presence of Nb^{5+} ions. Finally, we found that the fundamental wavelengths of type II angular non-critical phase-matching for second-harmonic generation along the x and y principal axes are smaller in RTP:Nb than in RTP, approaching those of KTP.

1. Introduction

In the past ten years, the literature has widely reported efficient non-linear crystals of the isostructural titanyl phosphate family $MTiOPO_4$ (where M = Na, K, Rb, Cs, Ag, NH_4, or Tl). The most attractive have been $KTiOPO_4$ (KTP) crystals, which are used in numerous laser devices due to their efficient and thermally stable non-linear optical properties for frequency conversion. For example, KTP is a privileged crystal for the second-harmonic generation (SHG) of the wavelength around 1 μm, emitted by neodymium- and ytterbium-based lasers [1]. KTP is also phase-matched for sum- and difference-frequency generation over wavelengths

[4] Author to whom any correspondence should be addressed.

ranging from the visible to the infrared, and it is used for optical parametric amplification (OPA) and optical parametric oscillation (OPO) generating 1.58 μm for eye-safe applications [2]. However, the occurrence of photochromic damage limits the use of KTP in high-power devices.

$RbTiOPO_4$ (RTP) is another compound of the isostructural titanyl phosphate family $MTiOPO_4$. Although RTP was the first known derivative of KTP [3], it has not been intensively studied because the crystal growth as well as the linear and non-linear properties of this material are very close to those of KTP. However, the photochromic damage threshold of RTP—1.8 times higher than that of KTP [4]—makes it more suitable for high-power applications. RTP is also of prime interest for quasi-phase-matched interactions, since thick samples of periodically poled RTP have been designed [5].

Furthermore, crystals with non-linear optical properties for frequency conversion, and doped with lanthanide (Ln^{3+}) photo-luminescent ions, can show self-frequency conversion properties. In previous studies, we reported that RTP is a good matrix for hosting luminescent Ln^{3+} ions at a higher concentration than that obtained in KTP [6]. When RTP is codoped with Nb^{5+} ions (RTP:Nb) it is even a better matrix for hosting Ln^{3+} ions, as their concentration increases and reaches a value high enough to produce an efficient laser emission [7]. This is attributed to the fact that the incorporation of Nb in these crystals expands the cell parameters of the structure of RTP, favouring the incorporation of a larger ion in the structure, as is the case for Ln^{3+}. Nb^{5+} also acts as a charge compensator when Ln^{3+} ions substitute Ti^{4+} in the structure, which stabilizes the electroneutrality of the crystals, allowing a higher concentration of Ln^{3+} ions to be incorporated in the crystals [8].

In the present work we investigate changes caused by the presence of Nb^{5+} ions in the structure and in the optical properties of RTP. In particular, this paper is devoted to $Rb_{0.955}Ti_{0.955}Nb_{0.015}OPO_4$, labelled from now as RTP:Nb, which is a representative example of these changes. First, we report crystal growth and structure studies of RTP:Nb. Secondly, we present polarized light absorption spectra and Raman spectroscopy studies. Finally, we report non-linear optical properties of RTP:Nb including refractive index measurements as a function of the wavelength, and direct measurements of non-critical phase-matching angles for second-harmonic generation (SHG). All the investigated properties of RTP:Nb are discussed in comparison to RTP and KTP.

2. Crystal growth

Because of its incongruent melting, conventional growth techniques from the melt cannot be used for the growth of RTP:Nb crystals. Instead, they were grown by using the TSSG (top-seeded solution growth) slow-cooling method. We considered the Rb_2O–P_2O_5–TiO_2–Nb_2O_5 self-flux system using a molar% composition of 40.8–27.2–31.0–1.0. By using self-flux growth we take advantage that only constituents of the crystal formula are used and then no other impurities are introduced. Moreover, cracks were avoided by using crystal seeds with the same composition as that of the crystal being grown. However, we previously reported that doping with Nb strongly affects the morphology of RTP crystals: they grow as thin plates along the a axis, reducing significantly the dimensions of the sample along this crystallographic direction [9]. Fortunately, this effect could be compensated by using a seed with an a-axis dimension thicker than the two others [10]. Then, grown crystals are more isometric, but their a-axis dimension is almost the same as that of the crystal seed. With this method, inclusion- and crack-free RTP:Nb crystals were grown with a 4.5 atom% Nb concentration, and with typical dimensions of 5 mm $\times$ 5 mm $\times$ 5 mm corresponding to the $a \times b \times c$ axes of the crystallographic frame respectively. One as-grown RTP:Nb crystal is depicted in figure 1(a) and the Miller indices of its natural faces are given in figure 1(b).

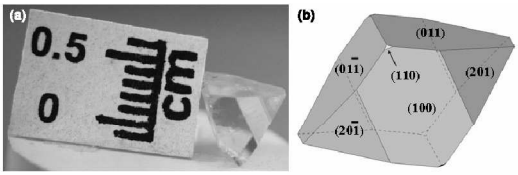

Figure 1. (a) Single crystal of RTP:Nb grown using the acentric crystal growth system described in [9]. It uses crystal seeds of 5.0 mm × 1.5 mm × 3.0 mm in $\boldsymbol{a} \times \boldsymbol{b} \times \boldsymbol{c}$ directions. (b) Miller indices of the natural faces of the RTP:Nb single crystal shown in figure 1(a) on a schematic representation of the theoretical morphology of a RTP:Nb crystal obtained with the shape utility.

The chemical composition of RTP:Nb was determined from the refinement of the structure by single-crystal x-ray diffraction, which is reported in the following section. It corresponds to a stoichiometric formula of $Rb_{0.955}Ti_{0.955}Nb_{0.045}OPO_4$.

3. Structure

We refined the crystal structure of $Rb_{0.955}Ti_{0.955}Nb_{0.045}OPO_4$, labelled as RTP:Nb. These studies were performed at room temperature, by using x-ray diffraction analysis on an as-grown single crystal. The crystal structure was solved by Patterson synthesis and refined by full-matrix least squares using the SHELXS97 utility [11]. We found that RTP:Nb crystallizes in the orthorhombic crystal system with the space group of symmetry $Pna2_1$. The unit cell parameters have the following values: $\boldsymbol{a} = 12.947$ (3) Å, $\boldsymbol{b} = 6.498$ (3) Å, $\boldsymbol{c} = 10.579$ (7) Å, and $Z = 8$. Then, parameter $\boldsymbol{a}$ is smaller, parameter $\boldsymbol{b}$ is slightly larger and parameter $\boldsymbol{c}$ is clearly larger than the corresponding ones in the structure of RTP [12]. This result follows the general trend in the evolution of the cell parameters in RTP when doped with Nb [13].

The structure of the compounds of the titanyl phosphate family $MTiOPO_4$ generally consists of two crystallographically independent TiO_6 octahedra, which are distorted and linked together by sharing corners, forming helical chains oriented along the $\boldsymbol{c}$ axis. These chains are further bridged by PO_4 tetrahedra, in such a way that a three-dimensional network is created. Then, large structural cages are formed in the free spaces left by TiO_6 and PO_4 polyhedra. These spaces are occupied by a monovalent cation (Rb in our case) that is arranged in two non-equivalent crystallographic positions [12].

We also found in RTP:Nb typical long and short Ti–O bonds located in helical chains of TiO_6 octahedra. However, in this crystal the short distances are shorter and the long distances are longer than the corresponding ones in RTP [12]. Then, the distortion of the TiO_6 octahedra in RTP:Nb is larger than that of RTP, which is expected to have implications for the non-linear optical properties [14]. We also found that Nb only substitutes one of the two available Ti crystallographic positions in the unit cell of RTP:Nb structure. In our opinion, this preference has an electrostatic reason rather than a steric one, because the distances between Ti and Rb are shorter for one of the Ti sites compared with the other. This prevents the substitution of Ti^{4+} by a cation with a larger electrical charge, as is the case for Nb^{5+}, and it is self-compensated electrically by the creation of vacancies for monovalent cation Rb. Note that this feature was observed in KTP:Nb [15, 16].

Finally, the structure of RTP:Nb is the enantiomorphic image of RTP. This means that the atomic positions in this structure correspond to those of RTP by the reflection in a mirror plane located at almost a quarter of the cell parameter along the $\boldsymbol{c}$ axis. This observation has

Table 1. UV transmission cut-off wavelengths, $\lambda_{\text{cut-off}}$, in nanometres, given at a 1/e-factor from the maximum value of the transmittance for RTP and RTP:Nb.

Crystal	$E \parallel b$ $\lambda_{\text{cut-off}}$	$E \parallel c$ $\lambda_{\text{cut-off}}$	Maximum value of the transmittance (%)
RTP	338	342	89.0
RTP:Nb	345	350	85.8

also already been reported in the structure of KTP:Nb when compared to that of KTP [15, 16]. Then, we can assert that similar trends occur in the structure of RTP and KTP when doped with Nb^{5+} ions.

4. Transmission spectra

Generally, the transparency domain for KTP isostructurals ranges between 0.35 and 4.5 μm [17], and due to the anisotropic nature of this family of crystals polarized light transmission spectra are recorded [18]. We performed such studies in RTP and RTP:Nb crystals cut as slabs polished to optical quality and with their input and output faces oriented perpendicularly to the *a* axis. All the RTP and RTP:Nb slabs were 1 mm thick, but we also cut 50 μm thick slabs for studies of the IR band edge. The linear polarization of the incident beam was oriented along the *b*- and *c* axis successively. The measurements were carried out between 0.1 and 3.0 μm by using a Cary 500 spectrophotometer and between 3.0 and 9.0 μm by using a Midac Prospect Fourier-transform IR (FTIR) spectrometer. A Glan–Thompson quartz polarizer was used in the Cary 500 spectrophotometer to record polarized light spectra. With the Midac Prospect FTIR spectrometer, we studied unpolarized light spectra in N_2 atmosphere, avoiding the adsorption of water vapour from the atmosphere on samples.

With the Cary 500 spectrophotometer, we first recorded absorption spectra of RTP:Nb in the visible, before and after annealing at 773 K during 3 h in air. We observed two broad absorption bands centred at 594 and 639 nm that disappear after annealing, and that may be related to the presence of Ti^{3+} which oxidizes to Ti^{4+} during annealing [19]. This means that the substitution of Ti^{4+} by Nb^{5+} is compensated by two different mechanisms: (i) the creation of Rb vacancies as we have already reported in the previous section and (ii) the presence of Ti^{3+} in the structure.

The ultraviolet (UV) absorption edge in the isostructural titanyl phosphate family $MTiOPO_4$ is generally attributed to the absorption of light by the Ti–O subgroups [17]. We recorded low-resolution transmission spectra in RTP:Nb and in RTP for comparison and took special care to record the polarized light transmission and optical absorption spectra at the UV band edge, to study the effects of substitution of Ti by Nb in their structure. They are shown in figures 2(a) and (b), for RTP:Nb and RTP, respectively, and table 1 gives the UV cut-off wavelengths determined at a 1/e-factor from the maximum value of the transmittance. Our data show that the maximum value of transmittance is 5% higher for RTP than that of RTP:Nb, and it is higher with light linearly polarized parallel to the *b* axis rather than to the *c* axis in both crystals. We can also see from figures 2(c) and (d) and table 2 that the value of the cut-off wavelength, $\lambda_{\text{cut-off}}$, is larger in RTP:Nb for both polarization schemes, which is in agreement with the reported values of $\lambda_{\text{cut-off}}$ around 400 nm in $KNbO_3$ [20] and around 350 nm in KTP [17].

With the FTIR spectrometer we studied IR unpolarized transmission spectra from 2.6 to 9.0 μm that are reported in figures 3(a) and (b) for RTP and RTP:Nb respectively. Such spectra generally show a band edge, which is caused by the first and second overtones of the two bond

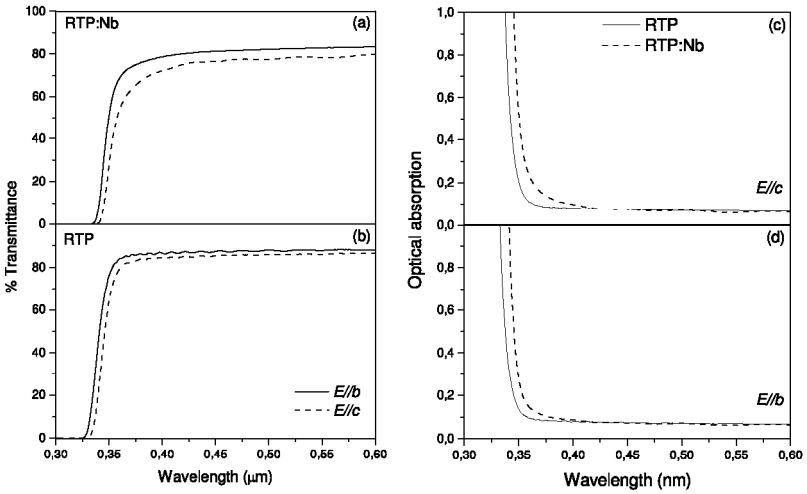

Figure 2. Transmission spectra of RTP:Nb (a) and of RTP (b) measured as a function of the wavelength in the UV region for a propagation along the ***a*** axis and for the linear polarization parallel to the ***b*** axis (solid line) and to the ***c*** axis (dashed line). Optical absorption spectra of RTP (solid line) and of RTP:Nb (dashed line) measured as a function of the wavelength in the UV region for a propagation along the ***a*** axis for the linear polarization parallel to the ***c*** axis (c) and for the linear polarization parallel to the ***b*** axis (d).

Table 2. Position of the absorption bands in the IR region marked out in wavelengths and in wavenumbers and their assignment for RTP:Nb.

Position		
Wavelength (μm)	Wavenumber (cm^{-1})	Assignation
2.8	3475	Tensions of H_2O with H-bonds
3.4	2900	Second overtone ν_3 of PO_4
4.6–5.2	2153–1907	First overtone ν_3 of PO_4
5.4–5.8	1709–1835	First overtone ν_1 of PO_4
5.9–6.9	1463–1690	Combination bands ($\nu_3 + \nu_4$) of PO_4
7.6–8.1	1227–1511	Combination bands ($\nu_1 + \nu_2$) of PO_4

stretching ν_3 and ν_1 vibrations of the PO_4 tetrahedra [17]. The value of this IR absorption edge has been reported to depend on the thickness for KTP crystals [17]. By recording the transmission spectra in two samples of RTP with different thicknesses (1 mm and 50 μm), we corroborated these results as shown in figure 3(a). Comparing the transmission spectra in the IR region between 50 μm thick RTP:Nb and RTP crystals (see figures 3(a) and (b)) we found similar slopes and no shifting of the vibrational bands in this region when Nb is introduced in the RTP crystal. This observation corroborates that Nb only substitutes Ti positions in the RTP:Nb structure, as was expected from the results of x-ray diffraction [8].

Table 2 gives the position of the absorption bands in microns and in cm^{-1}, as well as their assignment for RTP:Nb, between 2 and 8 μm. The internal vibrations of a regular PO_4 tetrahedron have been defined as non-degenerate ν_1, double degenerate ν_2 and triply degenerate

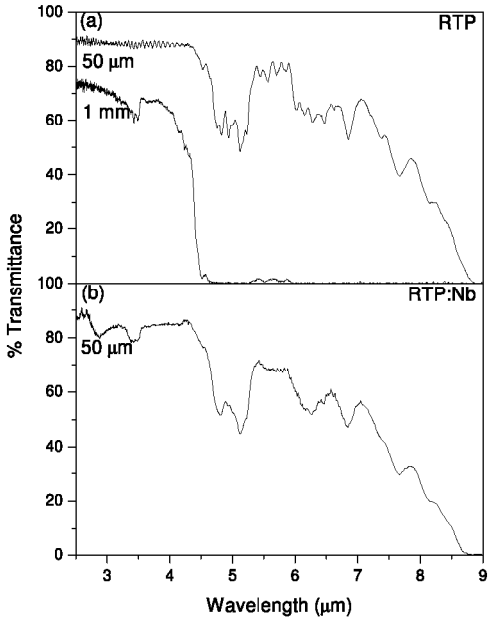

Figure 3. (a) IR unpolarized transmission spectra from 2.6 to 9 μm for RTP as a function of the wavelength for two thicknesses of RTP slabs. (b) IR unpolarized transmission spectra from 2.6 to 9 μm for a 50 μm thick RTP:Nb slab.

ν_3 and ν_4 modes [21]. When the PO_4 tetrahedron is slightly deformed, the degeneracy of the ν_2, ν_3 and ν_4 modes breaks, generating a higher number of bands than in the regular PO_4 tetrahedron [22]. We found that this is the case for RTP and RTP:Nb since the first overtone of the ν_3 consists of six peaks located between 4.6 and 5.2 μm (1907 and 2153 cm^{-1}), as shown in figures 3(a) and (b). Note that their wavelength (wavenumber) is longer (smaller) than the ones in KTP [17]. This is probably due to the difference in the bond distance between P and O when comparing RTP or RTP:Nb to KTP [12]. In the range between 5.4 and 5.8 μm (1709 and 1835 cm^{-1}) a series of bands in RTP and a broad band in RTP:Nb crystals have been observed (see figures 3(a) and (b)) that can be related to the first overtone of the ν_1 vibration of the phosphate group [17]. Furthermore, several bands appear at longer wavelengths for both crystals. They may correspond to a combination of bands derived from the sum or difference of two or more fundamental vibrations of the PO_4 group [17]. For example, the groups of bands ranging between 5.9 and 6.9 μm (1430 and 1690 cm^{-1}) match with the summation of $(\nu_3 + \nu_4)$ vibrations and the groups of bands centred at 7.6 and 8.1 μm (1225 and 1300 cm^{-1}) match with the summation of $(\nu_1 + \nu_2)$ vibrations. Then, the two distorting ν_2 and ν_4 vibrations of the PO_4 tetrahedron, whose fundamental modes are expected to appear between 20 and 25 μm, can interact with the ν_1 and ν_3 vibrations, generating new bands in the IR region where the band edge is observed. Finally, while no bands attributed to OH^- are observed in RTP, one appears at 2.8 μm (3475 cm^{-1}) in RTP:Nb. OH^- bands are generally attributed to the adsorption of

water from the environment by the crystal, which seems to indicate that the RTP:Nb crystals are a little more hygroscopic than pure RTP crystals.

5. Raman analysis

The literature has already reported an extensive polarized Raman scattering study of KTP [23], leading to chemical and structural information of the crystal, including bondings. No such information about RTP:Nb or RTP has been published yet. It is given in this section from a detailed analysis of spontaneous Raman scattering measurements. For this study RTP:Nb and RTP crystals were cut as a slab with dimensions of around 2 mm $\times$ 2 mm $\times$ 2 mm and with six faces polished and oriented perpendicularly to the three crystallographic axes $\boldsymbol{a}$, $\boldsymbol{b}$ and $\boldsymbol{c}$. Since RTP and RTP:Nb structures crystallize in the orthorhombic system, the $\boldsymbol{a}$-, $\boldsymbol{b}$- and $\boldsymbol{c}$-axes correspond to the x-, y- and z-axes of the dielectric frame respectively. Spontaneous Raman scattering measurements were performed in a back-scattering configuration and by using a Jobin-Yvon T64000 spectrometer coupled with an Olympus metallographic microscope. The excitation beam was provided by the green light of an Ar^+ laser emitting at $\lambda = 514.5$ nm with a power of about 3.9 mW. The same polarization of the Raman radiation was always assured on the first window of the monochromators by using a half-wave plate after the analyser. Then we can compare the different intensities among the different polarization configurations of the recorded spectra.

We investigated spontaneous Raman polarized spectra for different scattering configurations at room temperature, in order to involve phonons propagating along different directions in RTP:Nb and in RTP for comparison. To classify the different observed vibrations, we have to take into account that the Raman active irreducible representations of the vibrational optic phonon modes in the $mm2$ orthorhombic group must include A_1, A_2, B_1 and B_2 symmetry representations [23]. Figure 4 shows the recorded spectra belonging to the $x(yy)\bar{x}$, $x(yz)\bar{x}$ and $x(zz)\bar{x}$ scattering configurations, corresponding to the A_1, B_2 and A_1 symmetry representations, respectively. These spectra involve phonons propagating along the [100] direction. Figure 5 shows the polarized spectra belonging to the $z(xx)\bar{z}$, $z(xy)\bar{z}$ and $z(yy)\bar{z}$ scattering configurations and corresponding to A_1, A_2 and A_1 symmetry representations respectively. They involve phonons propagating along the [001] direction. Phonons propagating along the [010] direction have not been shown for the sake of brevity and because of the similarities observed with phonons propagating along the [100] direction. Tables 3 and 4 give the positions of the principal modes of vibration marked out in wavenumbers, as well as a classification of the strength of their intensity and their assignment for this configuration in RTP and RTP:Nb for comparison.

The recorded Raman spectra have revealed a complicated structure with about 100 peaks of very different intensities for both RTP and RTP:Nb samples due to the complexity of their crystallographic structure. Moreover, we observed a general broadening of the lines in RTP:Nb compared to RTP, which was previously observed in other compounds and assigned to an inhomogeneous structure [24]. By comparing the Raman spectra of RTP and RTP:Nb crystals given in figures 4, and 5, and from the analysis of the position of the principal modes of vibrations given in tables 3 and 4, we can distinguish between modes involving mostly the TiO_6 group or the PO_4 or Rb^+ groups. Indeed, as we reported in the previous sections, Nb substitutes Ti in the structure, and modes corresponding to the TiO_6 group are the only ones affected by this substitution. The most intense structures in all the spectra, located around 203, 265 and 693 cm^{-1}, arise from vibrations involving the TiO_6 octahedra. The ν_1 mode, a symmetric Ti–O stretching vibration [23], is the most intense peak in the region of the high-frequency modes, located at around 693 cm^{-1}. The high intensity associated with this band in RTP

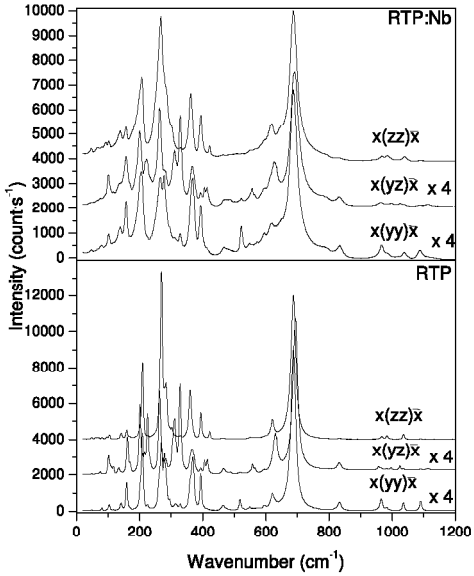

Figure 4. Raman spectra recorded at room temperature for RTP and in RTP:Nb as a function of the wavenumber in the back-scattering geometry for the $x(yy)\bar{x}$, $x(yz)\bar{x}$ and $x(zz)\bar{x}$ configurations. The $x(yy)\bar{x}$ and the $x(yz)\bar{x}$ configurations have been enhanced fourfold for a better comparison with the $x(zz)\bar{x}$ configuration.

reveals a highly ordered structure. As the intensity is maintained for RTP:Nb crystals, the non-homogeneity observed by the broadening of the bands does not affect the order of the structure, as observed in other analogues to KTP [25]. Peaks with the highest intensities, appearing around 280 and 700 cm^{-1}, have been reported in KTP, making it an excellent candidate for stimulated Raman converters or oscillators [23]. Therefore, we expect that such peaks observed in RTP and RTP:Nb from figures 4 and 5 lead to the same properties in these samples. The ν_2 mode, which is a pure bond stretching vibration, occurs at a lower energy and appears between 616 and 633 cm^{-1}, depending on the polarization. The ν_4 mode, considered as a combination of stretching and bending vibrations, appears with peaks between 311 and 330 cm^{-1} depending on the polarization scheme. The ν_5 Raman mode, an interbond angle bending vibration, is located at around 265 cm^{-1} in all the spectra. Finally, the line observed in all the spectra near 205 cm^{-1} belongs to the ν_6 mode, the other bond angle bending vibration of the structure. This mode is silent in a perfect TiO_6 octahedron [23]. In our case, however, it is activated by the distortion of the TiO_6 group in the structure. The fact that we have two crystallographically different positions for Ti in the structure [8] means that the two different TiO_6 octahedra have different Ti–O bond distances. This may be responsible for the multiple lines observed for the different vibrational modes [26]. The general shift to shorter wavenumbers in RTP:Nb, when compared to RTP, proves that Ti is substituted by a heavier ion, which is the case for Nb.

When phonons propagated along the [100] direction (see figure 4), a band was observed as a shoulder at 788 cm^{-1} for RTP:Nb crystals which has been assigned to the vibration of the Nb–O–Ti group [27]. The absence of a band corresponding to NbO_4 groups, normally located

Table 3. Position of the principal modes of vibration (cm^{-1}) recorded on the polarized spontaneous Raman scattering spectra for RTP and RTP:Nb crystals at room temperature in the $x(yy)\bar{x}$, $x(yz)\bar{x}$ and $x(zz)\bar{x}$ configurations. The intensity of the bands is expressed as vs (very small), s (small), medium (m), strong (st) and very strong (vst). When the band could not be resolved, it is indicated as sh (shoulder).

$RbTiOPO_4$			$Rb_{0.955}Ti_{0.955}Nb_{0.045}OPO_4$			
$x(yy)\bar{x}$	$x(yz)\bar{x}$	$x(zz)\bar{x}$	$x(yy)\bar{x}$	$x(yz)\bar{x}$	$x(zz)\bar{x}$	Assignation
81 vs		81 vs			81 vs	Polar vibrations Rb–O
105 s		105 vs			105 vs	
			138 s	138 sh	138 s	Translational modes Rb
143 s		143 s				
			158 m	158 m	158 m	Displacement of octahedra
160 m	160 m	160 m				
	202 st			202 st		ν_6 TiO_6
			205 st		205 st	
211 st		211 st				
	215 s					
				224 m		
228 s	228 m	228 sh				
	265 st		265 st	265 st	265 vst	ν_5 TiO_6
311 s	311 m		311 vs	311 m		ν_4 TiO_6
329 s	329 st	329 s	329 s	329 st	329 vs	
		362 st			362 st	Octahedra sharing corners
			368 st	368 m		
370 st	370 m					
395 m	395 s	395 st	395 m	395 s	395 st	ν_2 PO_4
		423 s			423 s	
465 s	465 s	465 s	465 s	465 s	465 s	ν_4 PO_4
519 m	519 vs					
			523 m	523 vs		
549 s	549 vs		549 s		549 vs	
				556 s		
	558 s					
	567 s					
574 vs			574 vs			
			618 m		618 m	ν_2 TiO_6
621 s	598 s	621 m				
				627 m		
	631 m					
688 vst		688 vst	688 vst		688 vst	ν_1 and ν_3 TiO_6
				691 vst		
	694 vst					Nb–O–Ti vibration
			788 sh	788 sh	788 sh	ν_1 PO_4
833 s	833 s	833 s	833 s	833 s	833 s	ν_3 PO_4
	907 vs			907 vs		
	1025 s			1025 vs		
1037 s		1037 s				
			1040 m		1040 s	
1091 s	1091 m		1091 m	1091 vs		
	1114 vs			1114 vs		

at 815 cm^{-1} [28], reinforces the fact that Nb ions only substitute Ti in the structure. The fully symmetric ν_1 vibration of PO_4 [26] is observed at around 833 cm^{-1} in all configurations.

Table 4. Position of the principal modes of vibration (cm^{-1}) recorded on the polarized spontaneous Raman scattering spectra for RTP and RTP:Nb crystals at room temperature in the $z\,(xx)\,\bar{z}$, $z\,(xy)\,\bar{z}$ and $z\,(yy)\,\bar{z}$ configurations. The intensity of the bands is expressed as vs (very small), s (small), medium (m) and strong (st). When the band could not be resolved, it is indicated as sh (shoulder).

$RbTiOPO_4$			$Rb_{0.955}Ti_{0.955}Nb_{0.045}OPO_4$			
$z(xx)\bar{z}$	$z(xy)\bar{z}$	$z(yy)\bar{z}$	$z(xx)\bar{z}$	$z(xy)\bar{z}$	$z(yy)\bar{z}$	Assignation
80 st	80 s		80 m			Polar vibrations Rb–O
104 st	104 st	104 m	104 st	104 st	104 m	
142 m		142 m	142 m		142 s	Translational modes Rb^+
161 s	161 m	161 st	161 s	161 m	161 st	Displacement of the octahedra
203 sh		203 sh			203 sh	ν_6 TiO_6
211 m	211 s	211 st	211 m	211 s	211 st	
	224 vs	224 s				
262 s		262 m	262 s		262 m	ν_5 TiO_6
	265 s				265 st	
313 m	313 m	313 st	313 m	313 m	313 st	ν_4 TiO_6
		330 m			330 m	
367 m	367 s	367 st	367 m	367 m	367 vst	Octahedra sharing corners
393 m	393 s	393 st	393 m	393 s	393 st	ν_2 PO_4
417 st	417 s	417 s				
			419 s	419 s		
476 st	476 vs	476 sh				ν_4 PO_4
			480 st	480 s	480 sh	
490 m	490 s	490 st			490 st	
518 st	518 s	518 st				
			523 st	523 m	523 st	
549 st	549 s	549 st	549 st	549 s	549 st	
		573 s			573 m	
627 m	627 vs	627 m	627 m	627 s	627 m	ν_2 TiO_6
	693 s	693 m		693 m	693 st	ν_1 PO_4
833 m	833 vs	833 st	833 m	833 vs	833 st	
	994 s					
				996 s		ν_3 PO_4
1006 m		1006 m				
			1011 m		1011 m	
					1023 s	
	1080 vs	1080 st		1080 s	1080 st	
1115 s		1115 m				
			1117 s		1117 m	

The ν_2 mode appears centred at around 394 cm^{-1} or at around 420 cm^{-1} according to the configuration, due to the two different structural positions of P in the framework. The ν_3 triply degenerate modes are located between 1000 and 1100 cm^{-1} and the ν_4 ones between 450 and 575 cm^{-1}. All these vibrations do not normally shift when Nb is incorporated into the crystal.

If we compare our study to the previous studies of Kugel *et al* [23], it seems reasonable to complete the internal mode picture with an analysis involving collective and coupled mode propagation in the crystal lattice. The structures lying between 138 and 188 cm^{-1} consist of a vibration in which the whole octahedron is displaced relative to the lattice. These bands tended to shift to shorter wavenumbers when Nb was present in the crystals when phonons propagated along [100] and [010] directions. Other bands involving polar vibrations between Rb^+ and the neighbouring oxygen ions are seen at around 80 and 104 cm^{-1}. Finally, the translational modes associated with Rb^+ are seen at around 140 cm^{-1}. Although a certain shifting of these bands

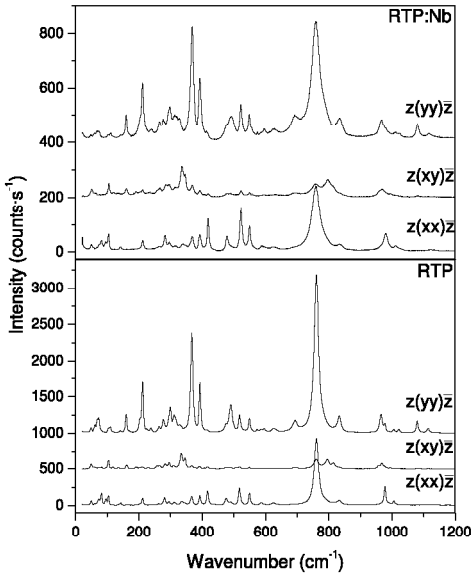

Figure 5. Raman spectra recorded at room temperature for RTP and in RTP:Nb as a function of the wavenumber in the back-scattering geometry for the $z(xx)\bar{z}$, $z(xy)\bar{z}$ and $z(yy)\bar{z}$ configurations.

to shorter wavenumbers is observed in some of the configurations, we think that this effect is more related to the presence of Rb^+ vacancies in the RTP:Nb structure [8] than to a possible substitution of Rb^+ by Nb^{5+}. The low frequency of the external lattice modes, involving Rb^+ below 200 cm^{-1}, shows the weakness of the bonds between Rb and the neighbouring ions, which are essentially ionic, as reported in the literature for tungstate and molybdate crystals [26].

6. Nonlinear optical properties for frequency conversion

We have shown that RTP:Nb and RTP crystallize in the orthorhombic crystal system with the space group of symmetry $Pna2_1$. As already said, the axes of the crystallographic frame a, b and c correspond to the axes of the dielectric frame x, y and z, respectively. The knowledge of the dispersion equations of the magnitudes of the three principal refractive indices, i.e. $n_x(\lambda)$, $n_y(\lambda)$ and $n_z(\lambda)$, in the whole transparency range of a crystal is of prime importance for the complete study of its non-linear optical properties. Indeed, the phase-matching directions for sum- or difference-frequency conversion depend on the ratios between the three principal refractive indices, $\frac{n_x}{n_y}(\lambda)$, $\frac{n_y}{n_z}(\lambda)$ and $\frac{n_x}{n_z}(\lambda)$ [29]. We implemented the minimum-deviation technique on prisms generally used for the determination of the dispersion equations of the three principal refractive indices. For the study of a new material, this method uses two oriented prisms and has been combined in the present study with polarized light sources emitting only in the visible and near infrared. We cut two oriented prisms of RTP:Nb and RTP with their medians parallel to the x axis and to the y axis in the x–z and y–z principal planes, respectively.

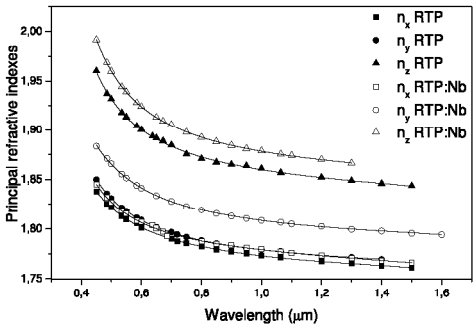

Figure 6. The three principal refractive indices as a function of the wavelength measured at room temperature in the visible and the IR regions for RTP (full figures) and RTP:Nb (open figures). The solid lines refer to the fit of all the recorded data simultaneously which is reported in this study.

Then the study of the different refractive indices relies only on a change of the polarization parallel to the x, y and z axes, successively by keeping the beam in normal incidence on the median of each of the two prisms. The three principal refractive indices n_x, n_y and n_z were measured at room temperature to an accuracy of 5×10^{-4} and as a function of the wavelength in the 0.4–1.5 μm range, by using a narrow linewidth BMI VEGA optical parametric oscillator pumped by a BMI SAGA Nd:YAG laser. The recorded data are given in figure 6 for RTP:Nb and RTP. It shows significant changes in the refractive index values between RTP:Nb and RTP: n_x is almost independent of the doping with Nb^{5+} ions, n_y and n_z significantly increase in RTP:Nb compared to RTP. Such results have been also reported in KTP:Nb compared to KTP [30]. Moreover, our data are in agreement with the literature for RTP [31, 32]. Then the $(n_z - n_x)$ birefringence is enhanced in RTP:Nb when compared to RTP. Such an increase in birefringence has been attributed to the change in the position of the UV band edge to longer wavelengths when Nb is present in KTP crystals [30]. We assume that it is the same between RTP:Nb and RTP since we reported in section 4 the same behaviour of their UV band edge. The increase of the birefringence in RTP:Nb with respect to RTP makes possible the use of these crystals for frequency doubling of light at wavelengths shorter than the one that can be doubled by RTP. This hypothesis will be confirmed later on in this paper by measuring the type II angular non-critical phase-matching (NCPM) fundamental wavelength for SHG. Note that the $(n_z - n_y)$ birefringence is smaller in RTP:Nb when compared to RTP, in opposition with what happens between KTP:Nb and KTP. This is unexpected, so we assume that it may be related to the accuracy of the measurements.

The best fit of all the recorded data simultaneously leads to the determination of three dispersion equations reliable in the scanned transparency domain only of the studied crystal. They can be used to calculate the phase-matching angles of any wavelength of this domain which are generated by sum- and difference-frequency generation. For RTP:Nb and RTP, the recorded data were simultaneous fitted with the following form of the Sellmeier equation, including one UV pole and one IR correction term:

$$n_i^2 = A_i + \frac{B_i \lambda^2}{\lambda^2 - C_i} - D_i \lambda^2 \tag{1}$$

where i stands for x, y or z and λ is in microns. We got from the fit a set of four parameters, A_i, B_i, C_i and D_i, which are listed in table 5 for RTP:Nb and RTP respectively.

Table 5. Room-temperature Sellmeier and thermo-optic coefficients of RTP and RTP:Nb.

Principal refractive index	A_i	B_i	C_i (μm^2)	D_i (μm^{-2})	$\partial n/\partial T$ (K^{-1})
			RTP		
n_x	1.6795	1.4281	0.0325	0.0119	5.6×10^{-5}
n_y	2.0360	1.0883	0.0437	0.0090	9.1×10^{-5}
n_z	2.2864	1.1280	0.0562	0.0188	6.6×10^{-5}
			RTP:Nb		
n_x	2.4753	0.6664	0.0578	0.0180	4.7×10^{-5}
n_y	1.1320	2.0885	0.0278	0.0096	7.7×10^{-5}
n_z	2.2619	1.2069	0.0594	0.0168	9.2×10^{-5}

We also studied the change of the three principal refractive indices as a function of the temperature within the 293–473 K range in both crystals. We used a microfurnace with temperature control, heating the samples homogeneously, and an He Ne laser emitting at $\lambda = 0.6328$ μm. Then we could deduce the values of the thermo-optic coefficients that are given in table 5. As we can see, they are of the same order of magnitude for RTP and RTP:Nb. Moreover, they are similar to those of KTP [29]. The thermo-optic coefficients are almost isotropic for both crystals, which means that the birefringence of the crystals does not change with the temperature.

Finally, the type II angular non-critical phase-matching (NCPM) fundamental wavelength for SHG was measured along the principal axes. The laser source was a tunable OPO (Continuum Panther) pumped by an Nd:YAG laser (Continuum SLI-10) emitting 4 ns long (FWHM) pulses between 410 nm and 2.55 μm at a repetition rate of 10 Hz. The wavelength of the OPO was controlled by a Chromex 250 SM scanning monochromator. The laser beam was focused in normal incidence on RTP and RTP:Nb crystals cut as slabs with two faces oriented perpendicularly to the x and y axes of the dielectric frame. An achromatic half-wave plate was used to adjust the polarization of the incident beam to ensure type II NCPM SHG. We measured the corresponding fundamental wavelength λ_{NCPM}, that verifies the following relation:

$$n_\alpha\left(\frac{\lambda_{\mathrm{NCPM}}}{2}\right) = \frac{n_\alpha\left(\lambda_{\mathrm{NCPM}}\right) + n_z\left(\lambda_{\mathrm{NCPM}}\right)}{2} \tag{2}$$

where $n_\alpha = n_y$ for a propagation along the x axis, and $n_\alpha = n_x$ for a propagation along the y axis. The experimental values of λ_{NCPM} given in table 6 decrease when Nb is present in the crystals, getting closer to that of KTP, i.e. 1079.1 and 994 nm in x and y directions, respectively [33]. For RTP, our measurements were compared with success with calculated values deduced from relation [2] by using previously published equations [31, 32]. The agreement between our measurements and calculated values deduced from relation [2] by using relation [1] and table 5 is not so good. This is due to the few data available around 1.1 μm for the refractive index measurements shown in figure 6. As a consequence, such a disagreement remains for RTP:Nb. All these data are shown in table 6. We also measured the SHG conversion efficiency of RTP:Nb and RTP along these two directions and found the same order of magnitude as that of RTP. Since these two samples crystallize in the same orthorhombic system with the same group space, we suggest that the magnitudes of the non-zero elements of their second-order electric susceptibility tensor should be close.

Table 6. Fundamental wavelengths of type II angular non-critical phase-matching for SHG in RTP and RTP:Nb. They were measured and calculated along the x and y axes respectively.

	Measurements (this work)	Calculations (this work)	Calculations (reference [32])	Calculations (reference [31])
		x axis		
RTP	1144 ± 0.5	1125.1 ± 0.1	1145.8 ± 0.1	1148.6 ± 0.1
RTP:Nb	1101 ± 0.5	1319.5 ± 0.1	No equations	No equations
		y axis		
RTP	1030 ± 0.5	1053.8 ± 0.1	1033.3 ± 0.1	1029 ± 0.1
RTP:Nb	984 ± 0.5	983.6 ± 0.1	No equations	No equations

7. Conclusions

Transparent, crack- and inclusion-free isometric $Rb_{0.955}Ti_{0.955}Nb_{0.045}OPO_4$ crystals have been grown using the TSSG method and crystal seeds with millimetric dimensions. The structure of the crystals labelled as RTP:Nb was refined, which was confirmed by transmission spectra. Moreover, the edge in the UV region is shifted to longer wavelengths in RTP:Nb when compared to RTP. This suggests that Nb substitutes Ti positions in the structure. This is confirmed by the fact that the IR and polarized Raman bands corresponding to the PO_4 tetrahedra are not shifted when Nb is present in the crystals, while bands involving vibrations of the TiO_6 octahedra are shifted when Nb is present in the crystals. Finally, the chromatic dispersion curves were measured and used to calculate the fundamental wavelengths corresponding to the type II angular non-critical phase-matching for second-harmonic generation (SHG), λ_{NCPM}. They were compared with success to measured values of λ_{NCPM}, which decrease in RTP:Nb when compared to RTP, approaching that of KTP. The associated conversion efficiencies remain of the order of that of RTP, leading to RTP:Nb as a new very good non-linear crystal.

Acknowledgments

This work was supported by CICyT of the Spanish Government under MAT-2005-06354-C03-02, MAT-2004-20471-E and CIT-020400-2005-14, and by CIRIT of the Catalonian Government under 2005SGR658.

References

[1] Bierlein J D and Vanherzeele H 1989 *J. Opt. Soc. Am.* B **6** 622–33
[2] Chung J and Siegman A E 1993 *J. Opt. Soc. Am.* B **10** 2201–10
[3] Masse R and Grenier J C 1971 *Bull. Soc. Fr. Minéral. Cristallogr.* **94** 437–9
[4] Oseledchik Y S, Pisarevsky A I, Proscirnin A L, Starshenko V V and Svitanko N V 1994 *Opt. Mater.* **3** 237–42
[5] Karlsson H, Laurell F and Cheng L K 1999 *Appl. Phys. Lett.* **74** 1519–21
[6] Zaldo C, Rico M, Díaz F and Carvajal J J 1999 *Opt. Mater.* **13** 175–80
[7] Carvajal J J, Solé R, Gavaldà J, Massons J, Aguiló M and Díaz F 2003 *Opt. Mater.* **24** 425–30
[8] Carvajal J J, García-Muñoz J L, Solé R, Gavaldà J, Massons J, Solans X, Díaz F and Aguiló M 2003 *Chem. Mater.* **15** 2338–45
[9] Carvajal J J, Nikolov V, Solé R, Gavaldà J, Massons J, Rico M, Zaldo C, Aguiló M and Díaz F 2000 *Chem. Mater.* **12** 3171–80
[10] Carvajal J J, Woensdregt C F, Solé R, Díaz F and Aguiló M 2006 *Cryst. Growth Des.* **6** 2667–73

[11] Sheldrick G M 1997 *SHELXS97. A Computer Program for Crystal Structure Determination* University of Göttingen, Germany
[12] Thomas P A, Mayo S C and Watts B E 1992 *Acta Crystallogr.* B **48** 401–7
[13] Carvajal J J, Solé R, Gavaldà J, Massons J, Díaz F and Aguiló M 2003 *Chem. Mater.* **15** 2730–6
[14] Zumsteg F C, Bierlein J D and Gier T E 1976 *J. Appl. Phys.* **47** 4980–5
[15] Thomas P A and Watts B E 1990 *Solid State Commun.* **73** 97–100
[16] Losevskaya T Y, Alekseeva O A, Yanovskii V K, Voronkova V I, Sorokina N I, Simonov V I, Stefanovich S Y, Ivanov S A, Eriksson S and Zverkov S A 2000 *Crystallogr. Rep.* **45** 739–43
[17] Jacco J C and Loiacono G M 1991 *Appl. Phys. Lett.* **58** 560–2
[18] Hansson G, Karlsson H, Wang S and Laurell F 2000 *Appl. Opt.* **39** 5058–69
[19] Martín M J, Bravo D, Solé R, Díaz F, López F J and Zaldo C 1994 *J. Appl. Phys.* **76** 7510–8
[20] Zysset B, Biaggio I and Gunter P 1992 *J. Opt. Soc. Am.* B **9** 380–6
[21] Herzberg G 1975 *Infrared and Raman Spectra of Polyatomic Molecules* (New York: Van Nostrand)
[22] Jacco J C 1986 *Mater. Res. Bull.* **21** 1189–94
[23] Kugel G E, Bréhat F, Wyncke B, Fontana M D, Marnier G, Carabatos-Nedelec C and Mangin J 1988 *J. Phys. C: Solid State Phys.* **21** 5565–84
[24] Voronko V K, Sobol A A, Ushakov S N and Tsybal L I 2000 *Inorg. Mater.* **36** 947–53
[25] Bushiri M J and Nayar V U 2001 *J. Non Linear Opt. Phys. Mater.* **10** 345–54
[26] Basiev T, Sobol A A, Voronko Y K and Zverev P G 2000 *Opt. Mater.* **15** 205–16
[27] Balachandran U and Eror N G 1982 *J. Mater. Sci. Lett.* **1** 374–6
[28] Blasse G 1973 *J. Solid State Chem.* **7** 169–71
[29] Dmitriev V G, Gurzadyan G G and Nikogosyan D N 1991 *Handbook of Nonlinear Optical Materials* (Berlin: Springer)
[30] Cheng L T, Cheng L K, Harlow R L and Bierlein J D 1994 *Appl. Phys. Lett.* **64** 155–7
[31] Oseledchik Y S, Pisarevsky A I, Prosvirnin A L, Lopatko V N, Kholodenkov L E, Titov F F, Demidovich A A and Shkadarevich A P 1990 *Proc. Conf. on Lasers Optics* (Leningrad: Leningrad University Press)
[32] Guillien Y, Ménaert B, Fève J P, Segonds P, Douady J, Boulanger B and Pacaud O 2003 *Opt. Mater.* **22** 155–62
[33] Boulanger B, Fève J P, Marnier G and Ménaert B 1998 *Pure Appl. Opt.* **7** 239–56

UNIVERSITAT ROVIRA I VIRGILI
YTTERBIUM AND ERBIUM DOPEP RbTi1-xMxOPO4 (M=Nb or Ta) CRYSTALS. NEW LASER AND NONLINEAR BIFUNCTIONAL MATERIALS
Alexandra Peña Revellez
ISBN: 978-84-691-0370-8 /DL:T.2188-2007